University of Sheffield

Department of Civil and Structural Engineering

BEHAVIOUR OF BURIED PIPELINES SUBJECTED TO EXTERNAL LOADING

by

Paul Chi Fai Ng

BEng

Thesis submitted to the University of Sheffield

for the Degree of Doctor of Philosophy

November 1994

SUMMARY

Differential ground movement is the most important cause of flexural failure in pipelines. To improve the understanding of the behaviour of buried pipelines subjected to differential ground movement, British Gas has conducted a number of field tests on its own pipeline system. The results of two pipe loading tests, axial and lateral push tests, have been reported. A simple 2-D finite element model is proposed to simulate the axial push test and the results shown to be satisfactory when compared with the field test. The results of the lateral push test were used for the validation of a two stage analysis technique, developed by British Gas, for the modelling of laterally loaded pipelines. Stage 1 uses a 2-D plane strain finite element analysis to predict the restraining effect of the soil as a function of pipe displacement. These predictions are then used in stage 2 which models the lateral behaviour of the pipe using an elastic beam on elastic foundation program. The elastic beam on elastic foundation program has been modified to include the effects of plastic behaviour of the pipe material, change in shape of the cross-section and shear deformation in the pipe. The introduction of a modified interface element into the FE program significantly affects the prediction of the pressure-displacement relationship of the pipe. Different soil models have been used to represent the backfill in the FE analyses and different interface conditions between the soil and pipe and between the backfill and natural ground assumed. The results show that the tensile stress developed at the back of the pipe significantly affect the predicted pressure-displacement relationship. The analyses using the Non-linear elastic model and the Elasto-plastic model together with interface elements around the pipe and along the trench or a no tension procedure give satisfactory agreement to the field data. A parametric study has been carried out using the above 2-D FE model. The influence of the relative strength between natural ground and backfill, trench width and angle of the trench sides has been studied. On the basis of the parametric study, present empirical relationships have been extended by including the effects of the existence of a backfill trench in the prediction of the pressure-displacement relationship of a laterally loaded pipe.

ACKNOWLEDGEMENTS

The research presented in this Thesis was carried out at the University of Sheffield under the supervision of Dr I. C. Pyrah and Dr W. F. Anderson, and Mr G. Leach at British Gas Engineering Research Station (ERS). The research was financially supported by a British Gas Research Scholarship and by the Overseas Research Students Awards Scheme.

The Author would like to express his sincere gratitude to his supervisors for their invaluable help, guidance and encouragement during the development of the research.

The Author is also grateful to Dr S. R. Ali for his interest and assistance throughout the research. Special thanks also go to Dr S. J. Wheeler for his supervision during the first year of the research and sound advice in the initial stage of the work.

The Author would like to express his gratitude to all members of the geotechnics group at the University of Sheffield for the useful discussions and comments. Special thanks and appreciation are extended to the staff at the ERS, particularly Mr E. Middleton for providing the data of the field tests and constructive comments.

The laboratory tests were performed at ERS Soils Laboratory for which the Author is thankful to the laboratory staff. The Author must also thank British Gas for providing the computer hardware and software for performing the numerical analyses, and the printing facilities to produce the Thesis. Thanks also go to Mr D. Reay and Mr B. Bellwood at the Gas Research Centre of British Gas for ensuring continuous financial support throughout the award period.

Finally, the Author wishes to thank his family and friends for their endless support and encouragement throughout the period of study in the UK. Without them, this Thesis may never have been completed.

TABLE OF CONTENTS

LIST OF TABLES

LIST OF FIGURES

LIST OF SYMBOLS

A_p	Cross-sectional area of a pipe element
A_s	Cross-sectional area of pipe to resist shear
A_1, A_2	Constants
C	Depth of cover above the pipe
C_c	Compression index
C_s	Swelling index
C_0, C_1, C_2	Factors to calculate ultimate oblique pressure
D	External diameter of the pipe
[D]	Stiffness matrix
E	Young's modulus of soil
E'	Empirical modulus of soil reaction
E_p	Young's modulus of pipe material
E_s	Young's modulus of soil
E_2	Young's modulus of pipe material after yielding
F_{ac}	Factor to correct F_{ch} to take into account the slope angle of the trench sides
F_{ay}	Factor to correct the prediction of y_u to take into account the slope angle of the trench sides
F_{ch}	Factor to correct N_{ch} to take into account the influence of trench width and R_c
G	Shear modulus of soil
G_p	Shear modulus of pipe material
G_s	Specific gravity of soil particles
H	Depth of trench
H_e	Vertical extent of failure surface
I_p	Second moment of area of pipe
I_{pc}	Second moment of area of pipe cross-section
J	Yield criterion
J	Constant
K	Bulk modulus
K	Coefficient of *in situ* horizontal soil stress
K_a	Active stress coefficient
K_n	Modulus in the normal direction $(= k_n \times t)$

K_{nsep}	Normal modulus during separation
K_s	Modulus in the shear direction $(= k_s \times t)$
K_{sres}	Residual modulus in the shear direction
K_0	Coefficient of earth pressure at rest
L	Length of trench
L	Length of interface element
L	Total length of a pipeline/beam
$\{\mathbf{L}\}$	Column vectors of the loading intensity
M	Bending moment
M_p	Plastic moment
M_y	Yield moment
N_{cd}	Vertically downward bearing capacity factor for cohesive soil
N_{ch}	Horizontal bearing capacity factor for cohesive soil
N_{cu}	Vertically upward bearing capacity factor for cohesive soil
N_{qd}	Vertically downward bearing capacity factor for frictional soil
N_{qh}	Horizontal bearing capacity factor for frictional soil
N_{qu}	Vertically upward bearing capacity factor for frictional soil
N_γ	Vertically downward bearing capacity factor for frictional soil
P	Lateral pressure
P_{cr}	Critical external pressure to cause buckling of pipe
P_u	Ultimate lateral soil pressure on pipe
P_{uob}	Ultimate oblique soil pressure on pipe
P-y	Lateral pressure-displacement relationship
Q	Vertical soil pressure
Q_{ud}	Ultimate vertical soil pressure (downward)
Q_{uu}	Ultimate vertical soil pressure (upward)
Q-z	Vertical pressure-displacement relationship
R	Mean radius of pipe
R_c	Ratio of the shear strength between natural ground and backfill
R_{disp}	Ratio between maximum pipe displacement with shear deformation and maximum pipe displacement without shear deformation
R_f	Factor less than 1
R_{strain}	Ratio between maximum pipe strain with shear deformation and maximum pipe strain without shear deformation
R_u	Ultimate axial soil resistance per unit area of the pipe
R_ψ, R_R, R_K	Correction factors for bearing capacity factors to determine P_u and Q_u used by Rowe & Davis (1982a, b)

S_r	Degree of saturation
V	Shear force
W	Width of trench
X	Total movement of a buried pipe
Z	Depth of soil to pipe centre
a	Constant
b	Constant
c	Cohesion intercept of soil
c	Shear strength of soil
c_i	Cohesion intercept of soil/structure interface
c_u	Undrained shear strength of soil
d	Inner diameter of the pipe
e	Void ratio
f	Shape factor
g	Shear coupling parameter
i	Coefficient of inclination
i_d	Inclination factor for $90° \leq \beta \leq 180°$
k	Spring constant for effective soil spring
k_{ai}	Initial tangent stiffness of axial spring
k_a	Axial spring stiffness
k_e	Empirical modulus of soil reaction
k_h	Horizontal spring stiffness
k_{ho}	Coefficient of subgrade reaction measured by DMT
k_i	Initial stiffness of P-y curve
k_n	Normal stiffness of interface element at contact mode
k_{ns}, k_{sn}	Stiffness for coupling between shear and normal behaviour
k_{nt}	Normal stiffness of interface element at separation mode
k_s	Shear stiffness of interface element
k_{si}	Subgrade reaction for a 1ft² plate
k_{vd}	Vertically downward spring stiffness
k_{vu}	Vertically upward spring stiffness
l	Length of an element in finite difference approximation
p	Mean total stress $\left(=\frac{1}{3}(\sigma_1+\sigma_2+\sigma_3)\right)$
p	Lateral loading
p_u	Ultimate lateral soil resistance force

p-y	Lateral load-displacement relationship
q	Deviator stress $(= \sigma_1 - \sigma_3)$
q	Axial load on pipe
q_e	External radial pressure to the pipe
q_i	Internal pressure of the pipe
q_{ud}	Ultimate vertical soil force (downward)
q_{uu}	Ultimate vertical soil force (upward)
r_u	Ultimate axial soil resistance force
t	Wall thickness of pipe
t	Thickness of interface element
u_n	Normal displacement of interface element
u_p	Lateral pipe displacement
$\{u_p\}$	Column vector of pipe displacement
u_s	Lateral soil displacement
u_s	Shear displacement of interface element
u_v	Shear deformation
v_p	Axial displacement of pipe
v_s	Axial displacement of soil
x	Distance along pipe longitudinal axis
x	Axial displacement of pipe
x_u	Ultimate axial displacement (when reaches r_u)
x_1, x_2, x_3, x_4	Different components of the movement of a buried pipe towards an excavation
y	Distance from the point to neutral axis of pipe
y	Lateral displacement of pipe
y_u	Ultimate lateral displacement (when reaches P_u)
z	Vertical displacement of pipe
z_{ud}	Ultimate downward vertical displacement (when reaches Q_{ud})
z_{uu}	Ultimate upnward vertical displacement (when reaches Q_{uu})
M	Slope of critical state line
α	Adhesion factor
β	Angle of thrust measured from pipe crown
γ	Soil density
γ'	Effective soil density
γ_{oct}	Octahedral shear strain

$\gamma_{12}, \gamma_{23}, \gamma_{31}$	Principal shear strains
δ	Friction angle between soil and pipe surface (or the structural material)
δ	Small increment or change
$\delta\varepsilon^p$	Plastic strain increment vector
ε	Strain
ε_s	Shear strain
ε_s^p	Plastic shear strain
ε_v	Volumetric strain
ε_v^p	Plastic volumetric strain
ε_{yi}	Yield strain of pipe
$\varepsilon_1, \varepsilon_2, \varepsilon_3$	Principal strains
θ	Angle measured from pipe crown
μ	Friction factor
μ_0, μ_1	Influence terms to determine the vertically downward spring stiffness
ν	Poisson's ratio of soil
ν_p	Poisson's ratio of pipe material
ν_s	Poisson's ratio of soil
σ_e	Equivalent uniaxial stress
σ_n	Normal stress
σ_n'	Effective normal stress
σ_{nav}	Average normal stress
σ_{ntlim}	Limiting adhesion of the interface element in normal direction
σ_x	Longitudinal stress
σ_y	Hoop stress
σ_{yi}	Yield stress of pipe
σ_z	Radial stress
$\sigma_1, \sigma_2, \sigma_3$	Principal stresses
τ	Shear stress
τ_{lim}	Limiting shear stress
$\tau_{12}, \tau_{23}, \tau_{31}$	Principal shear stresses
ϕ	Friction angle of soil
ϕ'	Drained (effective stress) friction angle of soil
ω	$= \beta / 90°$

CHAPTER 1

INTRODUCTION

1.1. Background

Pipelines are a safe and economical means of transporting gas, water, sewage and other fluids. They are usually buried in the ground to provide protection and support and the construction techniques involve either conventional trenching and backfilling, or trenchless methods such as microtunnelling. Pipelines are generally designed on the basis of the flow requirements and the operating pressure. For buried pipelines, additional design requirements are needed such as the maximum and minimum cover depth, the trench geometry and backfill properties.

Many of the existing distribution systems, including gas, water and sewer, are located at shallow depths beneath roads in urban areas and many of the pipes are very old (see Section 1.2). Many of these pipes are already near the limit of their current strength and only a relatively small increase in stress could initiate failure. Large amounts of money are being invested annually in repair and replacement of these pipelines. Such activities inevitably produce some undesirable ground movement and consequent damage to other underground services as well as to highway pavements and overlying structures. Earlier studies at the City University (see Symons, 1980), the report of the inquiry into serious gas explosions (King, Clegg & Walters, 1977) and many other incidents all suggest that differential ground movement is the most important cause of flexural failure in cast iron pipes.

Pipeline failures not only cost unnecessary remedial works, but in some circumstances may lead to gas explosions, resulting in loss of human life. Records show that about 1/3 of the gas explosions in the UK are caused by gas escaping from broken pipes (Herbert & Leach, 1990). To minimize the risk of any accident, injury and material loss, it is necessary to understand how buried pipelines respond to external loading and to be able to predict their behaviour.

1.2. The Distribution System of British Gas

In 1980, the gas and water distribution systems in the UK comprised over 500,000km of buried pipeline with a value based on replacement costs of the order of £15,000 – 20,000 million (Symons, 1980), thus the present day cost would be even higher. The distribution system of British Gas consists of approximately 232,000km of mains in four principal materials — grey cast iron, ductile iron, steel and polyethylene (Herbert & Leach, 1990). Extensive research has lead to the use of better pipe materials having higher strength, higher ductility and improved resistance to corrosion.

Approximately 117,400km of cast iron mains are still operating in the current distribution system of British Gas and approximately 14% of them are aged over 80 years (Herbert & Leach, 1990). Corrosion is a major problem for these old cast iron pipes. Most failures of pipelines are associated with this category of pipe.

Gas mains in the cast iron population generally fall into the 3" – 48" (75 – 1200mm) size range with most of them being the smaller diameters. Approximately 90% of the current cast iron system comprises mains smaller than 12" (300mm) diameter.

Jointing of the cast iron system includes rigid turned and bored, semi-rigid lead/yarn and flexible rubble gasket joints. The lead/yarn joints in particular can be susceptible to leakage when pipes are disturbed by ground movement.

Operating pressure in the distribution system can be classified as:

Low pressure:	0 – 75 mbar (1 bar = 100kN/m²)
Medium pressure:	75 mbar – 2 bar
Intermediate pressure:	2 – 7 bar

High pressure pipes (over 7 bar) are only used in the high pressure transmission system, which consists of over 17,000km of mains (Fearnehough & Middleton, 1992). The operating pressures in the low and medium pressure cast iron systems do not lead to significant in-service stresses to the pipe. On the other hand, the operating pressure in the high pressure system is a major consideration for the design of the pipe.

1.3. Research on Buried Pipeline Behaviour

A significant amount of work on the design of rigid and flexible pipes and conduits has been carried out since the early part of the century. The earlier investigations, carried out mainly at the Iowa State University in the USA, and the Building Research Station and Transport and Road Research Laboratory in the UK, concentrated on the performance of pipes of circular cross-section subjected to uniform loading under plane strain conditions.

Until recently, very little work had been carried out to determine the performance required to ensure that the pipelines would not fail when subjected to different loading conditions. The load is mainly due to differential ground displacement caused by adjacent excavation and construction work, traffic, pneumatic moling, pipe bursting, soil swelling/shrinking, piling and ground subsidence (see Section 2.3).

To ensure a realistic and acceptable analysis it is important that any significant interaction process between the pipe and the soil is recognised and represented in the calculations. This necessitates the identification, experimental investigation and theoretical modelling of the principal modes of soil/pipe interaction under appropriate loading conditions leading to a gradual improvement of the modelling of buried pipelines.

Initial work on buried pipeline behaviour in response to differential loading along the length of the pipeline utilised research into the design and performance of laterally loaded piles and anchor plates due to the lack of direct fundamental work. More recently, investigations carried out over the last decade have included *in situ* pipe loading tests, investigations into stress-strain behaviour of pipe backfill materials and numerical modelling.

Extensive full scale pipe loading experiments under controlled conditions and normal field conditions have been performed in the UK by British Gas, the Water Research Centre and by the Transport and Road Research Laboratory (Needham & Leach, 1987).

The prediction of magnitude and distribution of ground movements and the restraint provided by the soil require sophisticated stress analysis techniques using a suitable stress-strain relationship for the soil. Large scale laboratory work has been carried out at the British Gas Engineering Research Station and at the University of Sheffield to provide information on the deformation characteristics of both natural ground and backfill at shallow depths, which are often unsaturated (*e.g.* Goodwin, 1991). Soil models have also been developed to describe the behaviour of the unsaturated backfill material (*e.g.* Ali, 1993a) and both this and the laboratory work is continuing.

Numerical techniques have been developed by British Gas that can be used to model the behaviour of buried pipelines subjected to differential ground displacements. The numerical method uses a two stage analysis technique. Stage 1 uses a finite element program to predict the restraining effect of the soil as a function of pipe displacement. These

predictions are then used in stage 2 which models the lateral behaviour of the pipe using an elastic beam on elastic foundation program:

Figure 1.1 summarizes the important factors that govern the behaviour of a buried pipeline and the role of soil/pipe interaction of particular importance to the Gas Industry.

1.4. Objectives and Scope of the Research

In 1988 a series of full-scale loading tests on an existing transmission pipeline were performed at a site in Staffordshire in the UK. At the same time a geotechnical site investigation was carried out to measure the properties of the soil in the vicinity of the pipeline.

The purpose of this research is to investigate the use of numerical techniques to predict the behaviour of the pipeline when subjected to lateral loading. The predicted results are then compared with the field test results to assess the predictive technique.

The principal objectives of the present research are:

i. To understand the interaction between pipe and soil under different kinds of ground movement, and to identify the important factors that govern the interaction.

ii. To process the data for the full scale pipe loading tests and perform stress path tests on soil samples to determine the material properties of the backfill and surrounding natural ground for use in the later validation of the predictive method.

iii. To develop a simple predictive method which uses a 2-D finite element analysis to model the axial push test.

iv. To validate the existing predictive method, developed by British Gas, for modelling laterally loaded pipelines with the results of the full scale *in situ* lateral push test.

v. To improve the predictive method for modelling laterally loaded pipelines by carrying out modifications to the interface element used in the 2-D finite element analysis and to the elastic beam on elastic foundation program.

vi. To perform a parametric study using the improved predictive method to examine the influence of several factors in the prediction of *P-y* curves, including the relative strength between the natural ground and the backfill, the width of the trench and the angle of the sides of the trench.

vii. To use the results from the parametric study to extend the present empirical relations by including the effects of the existence of a backfill trench in the quick prediction of *P-y* curves.

This thesis is composed of nine chapters. Following this brief introduction to the problem of buried pipelines, Chapter 2 reviews various aspects of the modelling of buried pipelines A case history involving both axial and lateral pipe loading tests and the results of three stress path tests on soil samples from the test site are presented in Chapter 3. Chapter 4 examines the behaviour of three kinds of interface element for use in 2-D FE analysis and describes modifications to the CRISP90 interface element. Chapter 5 presents a simplified 2-D FE model to simulate the axial push test whilst modifications for the elastic beam on elastic springs program are presented in Chapter 6. Chapter 7 presents results using the two stage analysis technique to model the lateral push test and the results of the parametric study. The material presented in the previous chapters is discussed in Chapter 8 and Chapter 9 presents the main conclusions of the research and suggests possible future work.

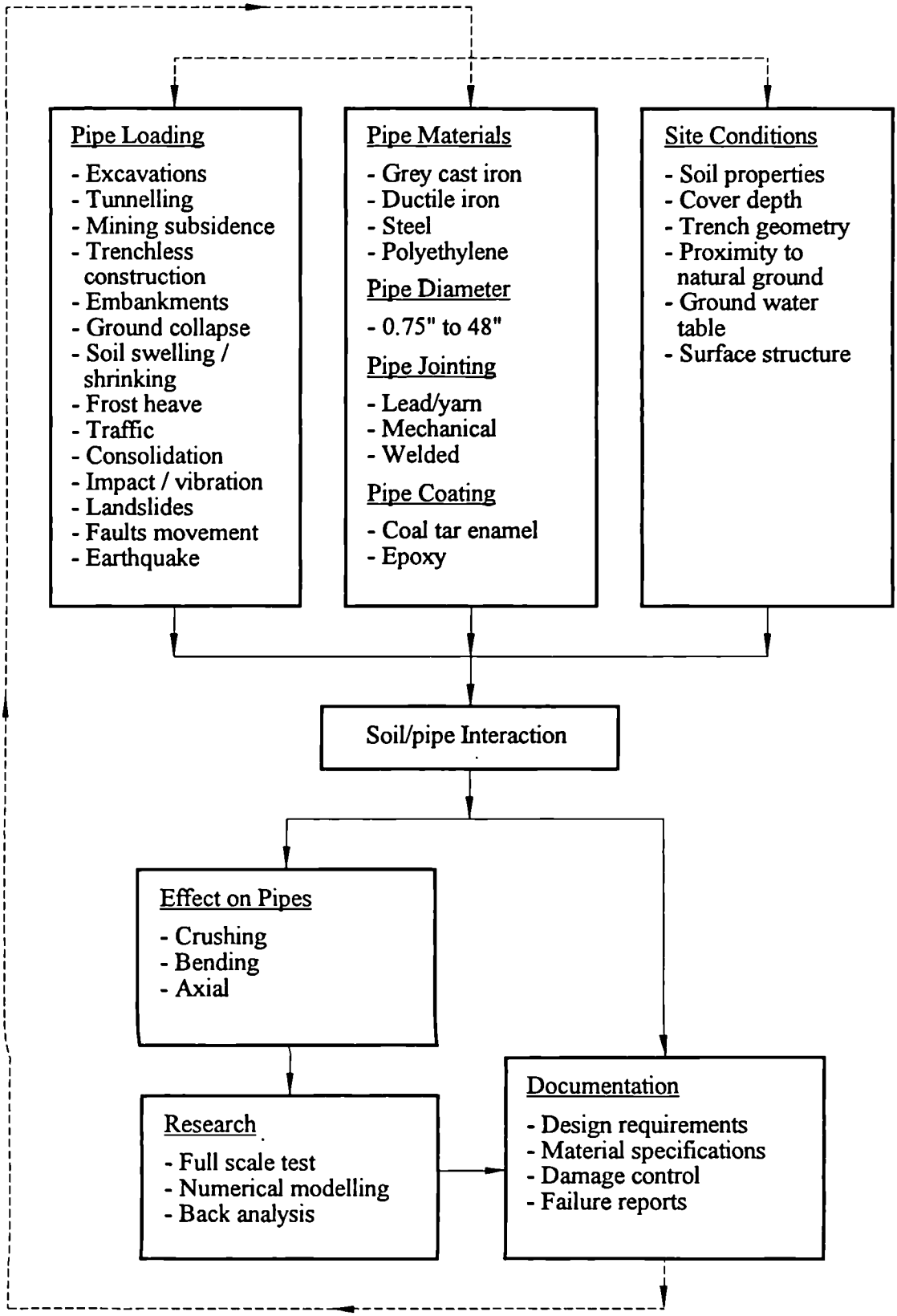

Fig. 1.1. Factors that govern the behaviour of buried pipelines and the role of soil/pipe interaction within the gas industry (after Mercer, 1987).

CHAPTER 2

REVIEW OF MODELLING OF BURIED PIPELINE

2.1. Introduction

In examining the soil/pipeline interaction problem, a number of facets of the problem need to be considered:

i. the modelling of the interaction between the soil and buried pipeline;
ii. the modelling of the mechanical behaviour of the pipeline;
iii. the modelling of the mechanical response of the soil surrounding the pipeline;
iv. the modelling of the mechanical response of the soil/pipeline contact surface;
v. the geometry and orientation of the pipeline;
vi. the probable variations in the properties of the soil strata and backfill materials, if present, and the general features of the terrain in which the pipeline is located;
vii. an estimation of the *in situ* stress state and loading acting on the pipeline.

Due to the complexity of the problem, analytical techniques using numerical methods have been developed to model the behaviour of buried pipelines. The analytical techniques should be able to take into account the above factors and be flexible enough for general application to a wide range of pipe loading situations.

The subsequent sections will give more insight into the above factors that govern the soil/pipeline interaction problem, and review the numerical methods that may be used to model the problem.

2.2. Modes of Pipe Deformation and Their Stress-Strain Relationships

2.2.1. Introduction

The behaviour of cylindrical pipes is covered by many classic text books, for example Timoshenko & Goodier (1970). Young (1989) presented a large number of elastic stress-strain formulae for a variety of structural elements, and the formulae for thin-walled cylindrical pipe have been used in the subsequent sections.

2.2.2. Stresses On Pipe Wall

The three principal stresses in a cylindrical pipe are defined in Fig. 2.1; the stress σ_x, acting in a direction parallel to the axis of the pipe barrel, is termed the longitudinal stress, the stress σ_y, acting in the circumferential direction, is called the circumferential or tangential stress and the stress σ_z, acting in the radial direction and varying through the thickness of the pipe wall, is termed the radial stress.

For thin walled pipes, where the ratio of the mean radius of the pipe R and the wall thickness of the pipe t is more than 10 (*i.e.* $R/t > 10$), the stresses σ_x and σ_y are practically uniform throughout the thickness of the wall and are the only important ones present, the radial stress σ_z are usually negligibly small (Young, 1989).

2.2.3. Crushing – Ring Bending

A tangential stress σ_y and a bending moment M are induced by a crushing mode of deformation in which the original circular cross-section becomes oval under the action of external loading. The deformed shape and distribution of tangential stress and bending

moment in a pipe wall due to a point load and a uniformly distributed load are shown in Fig. 2.2.

2.2.4. Uniform Radial Internal Pressure

The operating (internal) pressure of the pipe may induce significant hoop (tangential) stress in the pipe wall and the pipe will undergo uniform radial expansion as illustrated in Fig. 2.3. In the case of uniform radial external pressure, the effect on the pipe will be the reverse.

2.2.5. Axial Extension / Compression

A uniform axial extensive or compressive stress will produce a uniform axial tensile or compressive strain in the pipe wall along the longitudinal axis as illustrated in Fig. 2.4.

2.2.6. Longitudinal Bending

Bending of a straight pipe will impose a curvature on the longitudinal axis, with the fibres on the convex side lengthening (subjected to tensile stress) and fibres on the concave side shortening (subjected to compressive stress). Assuming that plane sections remain plane, the fibre strains and stresses are proportional to the distance from the neutral axis; for a uniform and symmetric cross-section this corresponds to the longitudinal axis of the pipe. The longitudinal stress σ_x at any point is given by: $\sigma_x = My/I_p$, where M is the applied bending moment, y is the distance of the point to the neutral axis and I_p is the second moment of area of the pipe cross-section (see Fig. 2.5); and $\sigma_x = \pm MD/2I_p$ at the extreme fibres, where D is the external diameter of the pipe.

In the simple theory of bending of beams it is assumed that no appreciable distortion of the cross-section takes place so that there is no displacement of material either toward or away

from the neutral axis. Ford & Alexander (1977), however, pointed out that when a thin-walled pipe is subjected to bending, movement of the fibres towards the neutral axis does occur. The flattening of the cross-section redistributes the stresses with those near the extreme fibres being reduced and the fibres nearer to the neutral axis being more highly stressed. Finite element benchmark tests on a straight thin walled pipe of circular cross-section loaded in pure bending, demonstrated this ovalization behaviour (Prinja & Clegg, 1993). This effect must be consider when the curvature is very sharp, *i.e.* when the radius of curvature is less than ten times the diameter of the pipe. The effect is less important, and usually not be considered, for large radii of curvature and small diameter pipes.

2.2.7. Equivalent Uniaxial Stress

The above sections describe the individual stress components which exist in a pipeline subject to different loading conditions. In order to assess the allowable working stress on the pipe, it is convenient to define a resultant stress or equivalent uniaxial stress σ_e combining all the different stress components mathematically (Middleton & Henderson, 1994). Hucka, Blair & Kimball (1986) suggested the use of distortion energy theory to determine the value of σ_e where:

$$\sigma_e = \sqrt{\sigma_x^{\,2} + \sigma_y^{\,2} - \sigma_x \sigma_y} \qquad (2.1)$$

The σ_e can be used to define the yield criteria of the pipe under combined longitudinal and tangential stresses (Middleton, Carvill & Johnson, 1990), when the effect of the two stresses are treated separately (see also Section 6.7.2).

2.3. Pipe Loading

2.3.1. Introduction

The following sections examine a range of loading conditions that buried pipelines can experience as a result of soil/pipe interaction caused by nearby ground loading/unloading. Although the determination of these loadings is out of the scope of this research, some of them have been briefly mentioned for completeness. In addition to these loadings, the pipeline may already be subjected to some initial stresses such as hoop tension and longitudinal contraction caused by internal pressure, axial stress as a result of temperature change and ring bending due to overburden pressure and the pipe laying process. The existing stress state of a steel pipeline can be determined directly by a technique known as the "centre hole drilling" method (Fearnehough & Middleton, 1992) and these stresses should be added to the additional stresses arising from any subsequent loading.

It should be noted that the response of a pipeline due to a wide spread (extensively distributed) loading along its length and a concentrated load are slightly different because of different restraints offered by the pipe sections that are not loaded. For example, for a wide spread load, the unloaded "end sections" of the pipe offer less restraint to the central loaded section of the pipe than for a concentrated load. Thus the pipe is freer to move horizontally, vertically or to rotate, and in addition to the movement in the direction of the applied load there may be a significant component at right angle. For a concentrated load the movement, in the main, will be limited to the direction of the application of the load.

2.3.2. Adjacent Deep Excavation

Trenches for other utility services and excavations for building developments (*e.g.* basement construction), induce ground movement; the magnitude and extent of which will be determined by the excavation geometry, the ground conditions and construction technique.

Pipelines within the zone of influence of an excavation, either running parallel with the excavation or crossing it, will be subjected to loading as illustrated in Fig. 2.6.

Chard & Symons (1982) and Chard, Symons, Toombs & Nagarkatti (1983) have carried out carefully controlled field work on ground movements adjacent to trenching. The ground movement under typical construction conditions for a deep trench were studied by Toombs, McCaul & Symons (1982).

The presence of a temporary trench support system usually reduces the ground movement when compared with an unsupported trench. The deformations can be divided into "short term" and "long term" for excavations in saturated clay. Crofts, Menzies & Tarzi (1977) suggested that the total movement X of a buried pipe towards an excavation consists typically of four components of movement each dependent on a particular stage of the construction sequence. The total movement can be expressed as:

$$X = x_1 + x_2 + x_3 + x_4 \tag{2.2}$$

where x_1 to x_3, are the movement due to the unsupported vertical face of the trench, movement to bring the face of the trench into contact with the support and deflection of the supports as a result of mobilization of the full support of the propping system retaining the trench sides. These short term deformations should be added to the long term deformation, x_4, associated with the consolidation/compression of the backfill used to reinstate the trench.

The paper suggested some approximate equations, based on empirical relationships and field measurement, to estimate each of the four components. The approach was later discussed by Symons (1978) and O'Rourke (1978), where modifications and refinements have been suggested.

Field monitoring of the response of a pipeline to ground movements caused by trenching was carried out by Carder, Taylor & Pocock (1982) and by Carder & Taylor (1983). Their

results showed that the greatest permanent bending moment in the pipe occurred near the ends of a trench running parallel to the pipe due to the restraint of the natural ground to the pipe movement (see Fig. 2.6a).

2.3.3. Soft Ground Tunnelling

The excavation of a tunnel leads to a release of stresses in the soil resulting in movement of the surrounding material towards the opening. The magnitude of the movement depends on the tunnel construction technique. This produces a permanent ground displacement field above the completed tunnel and a transient displacement wave that moves with the tunnel heading. Figure 2.7 illustrates the ground and pipe deformation produced by the tunnelling process for a pipeline crossing the axis of the tunnel.

In traditional methods to predict the ground movement, the shape of the settlement trough above soft ground tunnelling can be approximated as a normal probability curve (Bickel & Kuesel, 1982). By assuming the soil undergoes no volume change, Attewell & Woodman (1982) suggested that the form of the settlement trough over a tunnel can be approximated by the cumulative effect of a dome-shaped sink hole over a point source representing the tunnel. The shape of the sink hole is based on a mathematical treatment of the problem without regard to the soil properties. The approach also assumes the vertical settlement profile perpendicular to the line of a tunnel to be a normal probability curve. They concluded that the approach is only an approximation, both because of the assumptions made and the local variations on site.

On the basis of empirical observation of tunnel construction, O'Reilly & New (1982) derived a technique for computing ground movement towards the excavation. Rogers & O'Reilly (1991) used this technique to predict ground movement during tunnelling. Reasonably good agreement has been obtained between the measured and predicted results, despite the limitations of the model.

Rowe, Lo & Kack (1983) suggested a theoretically based method for predicting settlement at the surface and at various depths. An important aspect of this approach is the introduction of a "gap parameter", which takes into account the ground loss as a function of strength and deformation behaviour in both elastic and plastic stages, physical dimension of the gap between lining and soil, and workmanship. Lee, Rowe & Lo (1992) developed a numerically based procedure for the estimation of "gap parameter" which can be used to predict the resulting ground deformations using the 2-D finite element method or an empirical correlation. In a subsequent paper, Rowe & Lee (1992) used the numerical procedure to predict settlements above tunnels constructed in soft ground and evaluated the method with fourteen case histories. Reasonable agreement was obtained and they suggested that the procedure can be used for preliminary design purposes.

2.3.4. Ground Subsidence Due To Mining Activities

The method of mining varies with location and country; methods such as room-and-pillar method and the long wall total extraction method are widely used in the UK. Usually the room-and-pillar method will not induce surface subsidence except by pillar failure. Unlike the room-and-pillar method, however, the longwall total extraction method for coal involves the movement of a locally supported working face advancing ahead of the extracted area. After extraction of the coal the roof collapses and closure of the worked area produces surface subsidence. The subsidence profile consists of an established settlement area with little differential movement over the extracted area and a transient subsidence wave moving above the working face. The ground displaces downwards and towards the centre line of the removed coal panel (see Fig. 2.8).

Coal mining activity has already affected about 100km of the British Gas high pressure transmission system. If remedial action is not taken at the appropriate time the pipeline can distort and buckle because of induced bending and axial compression stresses, or even fail

completely as a result of fracture of the girth welds which join each pipe-section together (Fearnehough & Middleton, 1992).

Traditional prediction of the maximum subsidence involves use of the Subsidence Engineer's Handbook (National Coal Board, 1975). For example, Hucka *et al* (1986) used the Handbook to predict the subsidence profile, strain and slope along a buried pipeline crossing over a coal mine, and then used this data directly to predict the maximum pipeline stress intensities (*i.e.* no soil/pipe interaction).

2.3.5. Trenchless Construction of Underground Utility Services

The trenchless construction methods of underground utility services, such as off-line percussive moling techniques, pipejacking, microtunnelling, and pipe bursting techniques for the on-line replacement of existing pipelines, involves the creation or enlargement of a linear cylindrical void in the ground by forced soil displacement. The ground surface, and other services within the zone of influence, are subjected to ground loading as illustrated in Fig. 2.9.

An example of the influence of a pipe bursting operation on an adjacent buried gas main was presented by Herbert & Leach (1990). The results of the field study showed that when the pipe bursting machine passes the gas main, the strain level due to longitudinal bending built up rapidly. Significant recovery of the strain occurred when the machine moved away. This transient peak and decay to a residual value is a typical observed response of pipelines subjected to the ground displacements produced by the pipe bursting process.

Rogers & O'Reilly (1991) used the incompressible flow technique suggested by Sagaseta (1987) to predict the soil movement around a pipe bursting trial in sand. By assuming zero movement at the invert (the outward displacements around the pipe are all upward), good agreement has been obtained between the measured displacements and predicted results.

2.3.6. Embankments / Spoil Heaps

Embankment construction, or the temporary placement of waste materials over an existing pipeline, can provide additional loading on the buried pipeline due to the increased overburden pressure (total stress), this can lead to differential ground movement below and beyond the side slopes of the fill area as illustrated in Fig. 2.10.

2.3.7. Collapse of Voids in the Ground

Large voids may occur naturally in the ground or they may be caused by the erosion of fine sand or silt by ground water percolating into a fractured drain or sewer. These voids are usually undetected until a collapse occurs. The effect on the pipe is similar to mining subsidence described in Section 2.3.4.

2.3.8. Soil Swelling / Shrinking

The variations of ground water level in a saturated soil and changes of suction in an unsaturated soil near the ground surface can cause ground movements at utility service depths, especially in expansive and collapsible soil. Differential movement may occur due to variations in soil type and soil properties.

2.3.9. Frost Heave

The action of frost heave in soils usually occurs in the cold regions, for example, Alaska and Siberia, which have a mean annual temperature less than 0°C. The soil in these regions is usually frozen and it is called the permafrost. Exploitation of oil and gas in these regions (*e.g.* Alaska) requires the construction of pipelines from these Arctic areas to the southern populated area. The gas pipelines are usually buried and the gas is transported below

freezing temperature, thus avoid the thawing of permafrost soil. In the zones of shallow and discontinuous permafrost, the chilled pipe would lead to the freezing of previously unfrozen soils. A thicker and thicker ring of frozen soil and ice lenses would form slowly around the pipe in frost susceptible soil. Consequently, frost heave would be induced. A pipeline passing through different soil regions may experience differential heave thus induce stresses onto the pipe.

Williams (1986) used the Trans-Alaska pipeline as an example to explain the problem associated with pipeline construction on permafrost, with particular attention to the frost heave problem. Nixon (1987) also provided an extensive review on this subject. A physical model of frost heave was proposed by Gilpin (1980) and the model was extended to the two-dimensional plane strain case for predicting heave beneath a pipeline by Nixon (1992). Figure 2.11 shows the "active" ice lenses which cause the heave are present at the interface between frozen and unfrozen soil. He compared the predictive results with two pipeline test sections on site and satisfactory agreement was obtained. The magnitude of the heave is a function of soil properties, temperature profiles and time.

2.3.10. Traffic Loading

Pipes beneath roads are subjected to the effects of static and dynamic vehicle loading. Deterioration of the pavement structures can lead to a loss of the load spreading ability of the pavement and a concentration of loading over a buried pipe. Figure 2.12 illustrates the response of a pipeline due to a single surface wheel load. Needham & Leach (1987) summarized the findings of a series of tests carried out by British Gas which examined the effect of static and dynamic wheel loading, applied through undamaged and damaged road structures, on instrumented pipes with different support conditions.

2.3.11. Consolidation of Made Ground / Fill Material

Newly placed fill material may experience consolidation settlement due to the dissipation of excess pore water pressure built up in the filling process. Variation of the components making up the fill and poor compaction can cause differential settlement which will result in soil loading on pipelines laid across the area.

2.3.12. Ground Impact / Vibration and Piling

Dynamic consolidation of fill, blasting, pneumatic moling, piling using forced displacement piles, building demolition and some biophysical exploration techniques involving dynamic loading of the ground, may produce ground loading to nearby buried pipelines by permanent ground movement and transient loading due to propagated shock waves.

2.3.13. Landslides / Unstable Ground

Instability in natural slopes, slopes formed by excavation and slopes of embankments and earth dams may cause mass movement of soil from high points to low points. The most important forces to cause the instability are gravitational and seepage forces. Pipelines within the zone of movement can experience very high stresses and fracture may occur due to large movements.

2.3.14. Discontinuous Ground Movement

Discontinuous ground movement may be caused by fault movement. Routes of pipelines usually avoid the crossing of faults but in situations that the pipeline crossing the fault cannot be avoided, special care should be taken. Faults may be activated by deep mining

operations (Middleton & Henderson, 1994). Figure 2.13 shows the double curvature caused by a downward fault movement.

2.3.15. Earthquake

Buried pipelines are often damaged when a strong earthquake causes severe ground disturbance. A rapidly developing research area, known as lifeline earthquake engineering, is concerned with the planning, design, construction, operation and maintenance of pipeline systems under seismic hazards. Onshore seismic hazards that can offset pipelines include:

i. ground failures, which include faulting, landslides, lateral spreading, liquefaction, densification and ground cracks;
ii. tectonic uplift and subsidence;
iii. vibratory ground motion.

The ASCE Committee on Gas and Liquid Fuel Lifelines has produced a monograph, entitled "*Guidelines for the Seismic Design of Oil and Gas Pipelines Systems*" (ASCE, 1984). This provides a brief discussion of the above seismic hazards.

2.4. Soil Models

2.4.1. Introduction

Soil behaviour is very difficult to predict when compared with other engineering materials such as steel and concrete. This is because soil is a multi-phase material consisting mainly solid particles, water and air (or sometimes oil and gas may be present). These make the

components of soil very complex. Soil properties can also have large variation across the field.

To describe the behaviour of soil, many conceptual models have been developed. All of them are the simplifications of real soil behaviour and concentrated on some particular aspect. Some of the models are relatively simple (*e.g.* linear elastic), but some of them are very complex (*e.g.* non-linear plasticity model). However, there is no unique model yet developed that is valid for all geologic materials under all loading and physical conditions (Desai, 1982); this is still true today.

A number of soil models will be described in the subsequent sections. The Elastic-perfectly Plastic and Modified Cam clay models are available in the finite element software CRISP90 (Britto & Gunn, 1990) and the Non-linear Elastic and Elasto-plastic models were developed by British Gas Engineering Research Station (Ali, 1993b and Leach, 1986 respectively). These models will be used to represent the backfill material in the 2-D FE analysis for predicting a pressure-displacement relationship of pipe in Chapter 7 such that the suitability of each soil model in representing backfill material can be examined.

2.4.2. Elastic-Perfectly Plastic Model

When the stress reaches the limiting yield stress, yielding of the material will occur. The yield condition can be specified as Von Mises, Tresca, Drucker-Prager or Mohr-Coulomb. For all stresses below such yield a linear elastic relationship is assumed which is described in terms of two elastic constants, Young's Modulus E and Poisson's ratio ν. CRISP90 allows these constants vary linearly with depth.

2.4.3. Modified Cam Clay Model

This is a plasticity model developed by Roscoe & Burland (1968), which was based on the original Cam clay model (Schofield & Wroth, 1968 and Atkinson & Bransby, 1978). The model incorporates the "Critical State Theory" for soil. It gives a reasonably good qualitative description of the stress-strain behaviour of saturated clayey soil and is a good conceptual model for understanding soil stress-strain behaviour. The parameters for the model must be in terms of **effective stress**. Detailed description of the model can be found in the book by Wood (1990).

2.4.4. Non-Linear Elastic Model

This is a non-linear elastic stress-strain model (*K-G* model) developed in British Gas suitable for modelling the behaviour of loose granular (frictional) material that the strength is increase with increasing mean stress. The stress-strain relationship is dictated by two piecewise linear curves which describe the changes in shear modulus G (deviator stress/mean total stress (q/p) against total shear strain ε_s), and bulk modulus K (mean total stress p against total volumetric strain ε_v) of the soil up to failure, as shown in Fig. 2.14. No plastic straining of soil is permitted in the model although this would only be observed in an unloading situation. For monotonic loading the elastic non-linearity simulates plastic strain hardening behaviour. Detailed description of the model was presented by Ali (1993b).

2.4.5. Elasto-Plastic Model

This is an elasto-plastic stress-strain model developed in British Gas suitable for modelling unsaturated backfill soil. The total strain in the model is separated into elastic and plastic strains. The elastic component of the stress-strain relationship is controlled by the elastic

properties E and ν. The plastic behaviour is described by two piecewise linear curves: one relates deviator stress q to plastic shear strain ε_s^p and the other relates plastic volumetric strain ε_v^p to plastic shear strain ε_s^p, as shown in Fig. 2.15. The yield surface is dictated by the starting q value of the curve in Fig. 2.15a. Below this q value the soil is elastic. The relationship in Fig. 2.15a also provides the hardening parameter of the soil. The normality condition is applied in the flow rule (determined from the relationship between ε_v^p and ε_s^p in Fig. 2.15b) such that the plastic strain increment vector $\delta\varepsilon^p$ is normal to the plastic potential. Detailed description of the model was presented by Leach (1986).

2.4.6. Determination of Soil Parameters

No matter how rigorously a soil model has been developed, it needs some "good quality" parameters to represent the soil behaviour. The soil parameters are usually determined by performing laboratory tests on soil samples recovered from the site. The samples may be "disturbed" or "undisturbed", depending on the method for recovery. Conventional triaxial compression, consolidation and direct shear tests have been some of the common tests perform in a laboratory. *In situ* or field tests are also commonly used such as plate bearing and pressuremeter tests. Although these tests can provide useful data for some practical problems, they are usually restricted to a particular stress path and loading condition The stress path method, due to Lambe (1967), can be used to provide a more realistic estimation of the parameters, in which the actual stress paths of a number of critical elements of the problem are estimated and laboratory triaxial tests are performed as closely as possible along the same stress path, subjected to the appropriate state of stress and stress increment. The stress path tests described in Section 3.3.2 were based on this method.

The stress paths during incremental loading followed by different elements in the discretized mass can be different. Desai (1977) found that only a few elements follow the stress path in a conventional triaxial test and most other elements do not conform with the laboratory

stress path. He also found that the stress-strain behaviour of the same soil was different for three different paths; hence, the material parameters were different for different paths. This ties in with the fact that soil is an elasto-plastic, anisotropic, heterogeneous and history-dependent material. It should be noted that, however, in the real geotechnical situations, the stress paths are usually very complex and uncertain. It is very difficult to qualitatively assess or even reproduce those stress paths in a laboratory testing apparatus.

2.5. Modes of Soil / Pipe Interaction

2.5.1. Introduction

The behaviour of a buried pipe is significantly different from a free standing pipe because of the interaction between the soil and the pipe. When external loading acts on a buried pipe, the actual magnitude and distribution of the soil pressure around the pipe is difficult to estimate accurately and is related to the depth of burial, depth of water table, geometry of the site, pipe stiffness and mechanical properties of the soil. The complete definition of the soil/pipe system also requires specification of the load transfer conditions at the soil/pipe interface. For real situations, the pipe and soil are unbonded in the outward direction (*i.e.* no tensile load can be transferred normal to the pipe wall), tangential load conditions may vary between non-slippage and full slippage but normally non-slippage until a prescribed stress is reached .

The loadings described in Section 2.3 generate different forms of soil/pipe interaction, some being major and some being secondary. Table 2.1 summarizes the likely major and secondary soil/pipe interactions for different loadings. It should be noted that the influence of pipe diameter and the pipe cross-sectional stiffness have not been considered in Table 2.1, and it should be used as a rough guide only.

2.5.2. Diametric Deflection

The vertical load acting on a pipe is very much influenced by the arching action of the surrounding soil. For rigid pipes, the deformation of the pipe crown is generally very small when compared with the soil deformation (settlement) on either side of the pipe. This differential settlement of the soil gives rise to the concentration of load on the pipe crown and this is called the negative arching effect of soil (see Fig. 2.16a). The horizontal stresses caused by pipe deformation remain practically unchanged in this case (there are some changes of horizontal stresses due to the soil arching). For flexible pipes, soil arches will be formed around the pipe due to the large downward deflection of the pipe crown, thus reducing the external load imposed on the pipe. This is called positive arching action (see Fig. 2.16b). In addition to the downward deflection of the crown, the two sides of the pipe also deflect, in this case horizontally outwards. This will generate lateral passive resistance in the soil resulting in an increase of the horizontal stresses.

Chua & Lytton (1989) presented typical radial soil pressure distributions for a rigid pipe (concrete) and a flexible pipe (HDPE, high density polyethylene) as shown in Fig. 2.17. It demonstrates the influence of pipe distortion and soil arching on the stress distribution around the pipe.

2.5.3. Axial Soil / Pipe Interaction

The ground movement acting horizontally and parallel with the longitudinal axis of a pipe may create a soil/pipe interaction if the axial stiffness of the pipeline permits it to resist the deformation of the ground.

The relative soil/pipe movement is usually concentrated in a narrow annular zone where shear failure and slippage occurs at the soil/pipe interface. The relative movement decreases rapidly away from the pipe surface, as illustrated in Fig. 2.18.

2.5.4. Longitudinal Bending

If a very flexible pipe passes through a soil displacement field, it will follow the ground displacement profile exactly. For a more rigid pipe, the bending stiffness of the pipe will provide a certain restraint to the pipe displacement which will be different to that of the soil. The loading along the pipe may vary according to the relative displacement between the soil and the pipe, reaching a maximum value where the soil adjacent to the pipe is brought to complete failure.

The maximum restraint that can be offered by the soil may be influenced by the direction in which ground movement takes place (upward, downward and lateral movements). Settlement of the soil past a pipe will impose soil loading from the material above the pipe (soil is moving downward relative to the pipe). Excessive relative movement between the soil and the pipe will produce tensile and shear failure in the overlying soil leading to the development of a soil wedge over the pipe rather than complete failure of the surrounding soil (see Fig. 2.19).

Conversely, if the soil is moving upward relative to the pipe, restraint will be provided by the passive resistance of the underlying soil. The soil resistance will increase with the displacement of the pipe reaching a maximum value when the surrounding soil has been brought to complete failure (see Fig. 2.20).

Horizontal movement of the ground in a direction perpendicular to the longitudinal axis of the pipe may produce a similar effect as upward movement of the soil. Horizontal passive resistance is produced by the soil in front of the pipe. If the depth of burial is too shallow, wedge failure of the soil may occur in front of the pipe, as shown in Fig. 2.21.

2.6. Modelling of Soil / Pipe Interaction

2.6.1. Diametric Deflection

2.6.1.1. Traditional Methods

A large amount of effort was concentrated on the diametric deflection of a pipe in the early research into soil/pipe interaction. The "Iowa Formula" developed at the Iowa State University, USA, due to Spangler (*e.g.* Spangler, 1956) forms the basis of the conventional design method for buried pipes. The Iowa formula has the form:

$$\text{Ring deflection} = \frac{\text{Vertical pressure at pipe crown} \times \text{Bedding constant}}{\text{Pipe stiffness term} + \text{Lateral soil stiffness term}}$$

The design method is based on an assessment of the performance (deformation and buckling load) of the circular pipe cross-section under uniform loading extending the length of the pipeline. Once an estimation of the vertical pressure on a pipe is made, a simple analysis can be performed to determine the deflection of the pipe ring. In the case of a flexible pipe, account is taken of the mobilization of passive lateral soil resistance to outward deflections of the pipe spring lines.

The pipe ring also needs to be checked for buckling. One of the commonly used buckling formulae of a circular pipe, reported by Cheney (1976), is:

$$P_{cr} = 2\sqrt{k \cdot R \cdot \frac{E_p I_{pc}}{R^3}} \tag{2.3}$$

where P_{cr} is the critical external pressure, k is the spring constant for the effective soil spring, R is the radius of the pipe, E_p is the Young's modulus of the pipe and I_{pc} is the second moment of area of unit length of the pipe cross-section.

When Cheney uses the experimental results by Allgood, Ciani & Lew (1968) to compare with Eq. (2.3), however, the formula departs from the general trend of the data and is

unconservative. Cheney derived a new formula based on the derivation of the differential equations for the buckling of a thin ring supported by radially directed springs and then applied this to a long thin-walled cylindrical pipe. By comparing the new formula with the test results by Allgood *et al* (1968), Cheney proposed the following design formula:

$$\frac{P_{cr}}{E_p t^3/R^3} = \frac{0.130}{\left(1-\nu_p^{\,2}\right)^{\frac{1}{3}}\left(1-\nu_s^{\,2}\right)^{\frac{2}{3}}}\left(\frac{E_s}{E_p t^3/R^3}\right)^{\frac{2}{3}} \tag{2.4}$$

where E_s is the Young's modulus of the soil, ν_p is the Poisson's ratio of the pipe, ν_s is the Poisson's ratio of the soil and t is the wall thickness of cylindrical pipe.

Gumbel & Wilson (1981) used first principles to describe the buried pipe/soil system and included the effect of *in situ* stresses; the method also allows representation of the soil as a two-dimensional elastic continuum. They developed a series of design charts to determine the ring deflection and buckling load that can be used in practice.

Cheney (1991) studied more details of the local buckling of pipe in an elastic continuum. A graphical solution method has been developed in which he stated that the solution represented an upper bound of the buckling of soil-surrounded pipes that may also be affected by local imperfections in the pipe walls and internal residual stresses.

2.6.1.2. Beam on Elastic Foundation Approach

Although the traditional method described in Section 2.6.1.1 can provide a simple method to determine the behaviour of the pipe, it is limited to some idealized support conditions and the loadings are only by the overburden pressure and surcharge at the surface. A more general approach is needed for more complex loading and support conditions. Hetényi (1946) presented a solution for a single concentrated radial force acting on a circular ring in contact with springs representing elastic soil support as shown in Fig. 2.22. The soil springs can only take compressive force and no tensile force is allowed. This analytical solution has been implemented into a computer program (Nath, 1987) which also adopted the

assumption of superposition. The program can be used to analyse the effect of multiple concentrated radial loads applied to an elastic ring. This approach allows design to be based on an estimated radial loading distribution, the stiffness of the pipe, and the stiffness of the supporting soil adjacent to the pipe (the radial springs).

2.6.1.3. Finite Element Method

The finite element (FE) method provides a comprehensive tool for predicting the detailed performance of buried structures. It can take into account the non-linear soil behaviour, bedding details, slippage between soil and structure, and any desired geometric shape can be analysed during construction, service and ultimate conditions.

Moore (1988) used the finite element method to examine the buckling strength of flexible metal tubes deeply buried in elastic ground. He considered four different tube geometries: circle, ellipse, square and rectangle, and used straight beam-column elements to represent the cross-section of the tube and 8-noded isoparametric elements to represent the elastic soil in a 2-D plane strain condition. He found that modelling one half of the system was better than one quarter of it because the buckling deformations are harmonic in nature. As the structure becomes more flexible the harmonic number increases from 2 (corresponding to elliptical deformations) to 3, 4 and so on. The boundary conditions for the analysis of one quadrant are such that only even numbered harmonics can be accommodated. Both odd and even harmonics are covered if one half is modelled. The errors associated with modelling one half and one quarter of the buried tube diminish and become negligible when the flexural stiffness of the structure is low relative to the surrounding ground. He suggested that one should model half the system with a small number of elements when the structure is stiff, but only one quarter of the problem with a large number of elements when the tube is more flexible.

2.6.2. Axial Extension / Compression

2.6.2.1. One-Dimensional Bar Element Approach

In this approach the surrounding soil is totally ignored and the pipe is represented by a number of 1-D 2-noded structural bar elements. The element is subjected to axial forces at each node producing axial nodal deflections. The axial force is generated by shear stresses due to the relative soil/pipe movement acting on the outside surface of the bar element (pipe). The derivation of the load and stiffness matrix of a single 2-noded bar element for modelling longitudinal extension/compression was described by Needham & Leach (1987). They also described another method based on the principle of consistent deformations.

2.6.2.2. Beam on Elastic Foundation Approach

This is another one-dimensional approach similar to the above method, but using Winkler type elastic beam on elastic foundation approach. The basic differential equation for the axial soil/pipe interaction, assuming elastic behaviour, is:

$$E_p A_p \frac{d^2 v_p}{dx^2} + q = 0 \tag{2.5}$$

where A_p is the cross-sectional area of the pipe, v_p is the axial displacement of the pipe due to axial loading q (force/unit length) and x represents distance along the longitudinal axis.

For the case of the axial loading produced by a soil displacement field, *i.e.* the shear stress developed at the outer skin of the pipe due to relative soil/pipe displacement:

$$q = \pi D k_a \left(v_s - v_p \right) \tag{2.6}$$

where k_a is the stiffness of axial spring representing the surrounding soil (see Section 2.7 for details of how to determine k_a) and v_s is the axial soil displacement.

Solution to Eq. (2.5) can be solved by the finite difference method. For a typical element i the second order differential quantity can be approximated by:

$$\frac{d^2 v_p(i)}{dx^2} = \frac{v_p(i-1) - 2v_p(i) + v_p(i+1)}{l^2} \tag{2.7}$$

where l is the length of an element.

Section 2.6.3.1 shows more details of using finite difference method to solve the elastic beam on elastic foundation approach.

2.6.2.3. Finite Element Analysis

Relatively few applications of the finite element method have been used to model the axial extension/compression behaviour. This is because the 3-D nature of the problem (both non-uniform distribution of the radial pressure and the geometry) leads to expensive 3-D analysis. However, it is possible to simplify the analysis by assuming an equivalent uniform pressure distribution and treat the problem in a 2-D analysis (either axisymmetry or plane strain). The simplified 2-D model can substantially reduce the computational effort and gives reasonably good predictions. Details of the model are presented in Chapter 5.

2.6.3. Longitudinal Bending

2.6.3.1. Beam On Elastic Foundation Approach

One of the numerical methods for the modelling of a soil/pipe system subjected to transverse ground movement is to represent the pipe as an elastic beam in contact with discrete elastic springs representing the soil (Winkler, 1867). The springs are mounted transverse to the pipe axis to represent load transfer associated with ground movement acting perpendicular to the longitudinal axis of the pipe. Vertical and horizontal springs are needed to deal with the respective components of the ground movement. In the original Winkler model, the behaviour of the spring (soil) is assumed to be independent of the neighbouring springs. Although this assumption is not strictly true, experimental results indicate that it is sufficiently accurate for practical purposes (Poulos & Davis, 1980), and is

a closer representation of soil behaviour than the other extreme of complete continuity provided by the assumption of an elastic solid as the support medium. Regan (1982) conducted full scale experiments on a pipeline buried in polystyrene beads (idealized soil) and subjected to differential displacement. His experimental results have proved the validity of the beam on elastic foundation approach for polystyrene beads and he concluded that the approach can also be used for real soils.

Pipeline response to a soil displacement pattern is illustrated in Fig. 2.23. The pipe translates from its original position taking up a longitudinal bending profile dictated by the soil displacement profile, spring characteristics and flexural stiffness of the pipe. The pipe is usually assumed to act as a thin strip whose behaviour is governed by the simple theory of bending of a straight beam:

$$E_p I_p \frac{d^4 u_p}{dx^4} + p = 0 \tag{2.8}$$

where p is the lateral loading intensity (force/unit length), u_p is the deflection of the beam due to longitudinal bending and x represents distance along the longitudinal axis.

For the case of the loading intensity produced by soil displacement:

$$p = k_h D(u_s - u_p) \tag{2.9}$$

where k_h is the lateral spring stiffness (sometimes referred to the coefficient or modulus of subgrade reaction, see Section 2.7 for details of how to determine k_h), D is the outer diameter of the pipe and u_s is the soil displacement perpendicular to the pipe longitudinal axis.

Solution to the Eq. (2.8) may be obtained either analytically or numerically. Hetényi (1946) provides analytical solutions to the problem for the case of constant k_h. For non-linear distributions of k_h, solutions are most conveniently obtained by a numerical finite-difference method (*e.g.* Palmer & Thompson, 1948). The essence of the approach is to replace the fourth order differential quantity in Eq. (2.8) by a numerical approximation written in terms

of unknown pipe displacements u_p. For a typical element i (referring to Fig. 2.24) the differential quantity can be approximated by:

$$\frac{d^4u_p(i)}{dx^4} = \frac{u_p(i-2)-4u_p(i-1)+6u_p(i)-4u_p(i+1)+u_p(i+2)}{l^4} \tag{2.10}$$

The approximation can be applied to elements 4 to $n-4$. For the first three and last three elements, the approximations are dependent on the boundary conditions at the two ends. The final equation is of the form:

$$\{\mathbf{L}\} = [\mathbf{D}]\ \{u_p\} \tag{2.11}$$

where $\{\mathbf{L}\}$ is the column vector of the loading intensity, $[\mathbf{D}]$ is the stiffness matrix of finite difference coefficients and $\{u_p\}$ is the column vector of unknown pipe displacements. The elastic beam on elastic foundation program "WOMOD", described in Chapter 6, is based on this numerical method.

Another numerical method has also been widely used is based on a 1-D 2-noded structural beam element with a soil spring at each node to represent the soil restraint. The derivation of the stiffness matrix for a 1-D beam element was described by Needham & Leach (1987). The stiffness matrix for a beam element subjected to 3-D loading was presented by Koike, Imai & Kaneko (1992).

2.6.3.2. Finite Element Analysis – Soil / Pipe Continuum

The longitudinal bending behaviour of a buried pipe in contact with soil and subjected to some arbitrary soil displacement pattern can be modelled in a finite element analysis, in which the process creating the loading and the pipeline effect (soil/pipe interaction) can be simulated in the same analysis.

A three-dimensional stress analysis model is necessary where the geometry of the site, the geometry of the pipe, any variation of soil properties and any other utilities near by can be modelled in the analysis. This type of analysis is currently of limited use due to the

necessity to refine the mesh in areas of stress concentration particularly in the pipe wall area. An acceptable refined mesh in 3-D would involve many elements and be expensive to solve, especially with a non-linear soil model.

An alternative approach is to ignore the geometric dimensions of the pipe and represent it as a number of dimensionless beam elements with the same flexural stiffness (E_pI_p) as the pipe which is placed along the centre line of the longitudinal axis of the pipe (Nath, 1983). This approach can reduce the size of the analysis, but fails to represent the dimensions of the pipe and the consequential soil/pipe interaction. The effect could be very significant for large diameter pipes.

2.7. The Pressure-Displacement Relationship for the Soil Springs in the Elastic Beam on Elastic Foundation Approach

2.7.1. Introduction

The elastic beam on elastic foundation approach described in Section 2.6.2.2 for modelling axial extension/compression and Section 2.6.3.1 for longitudinal bending modes of soil/pipe interaction was found to be the most economic and reasonably accurate method. This method requires pressure-displacement relationships for the springs to represent soil restraint and different methods will be reviewed in this section. Figure 2.25a shows the idealized three-dimensional soil restraint represented by soil springs in three components: axial, transverse horizontal and transverse vertical. The pressure-displacement relationships are non-linear as shown in Fig. 2.25b and geometry, soil material dependent and coupled.

To quantify the relationship may require a full scale field test of existing pipelines. In situations where full scale testing is not feasible, it may be necessary to resort to other approaches such as non-linear stress analysis, the use of elastic solutions, published empirical methods, indirect field tests, centrifuge modelling tests and scaled model tests.

2.7.2. Full Scale Field Testing

Field loading tests on existing buried pipelines can provide information on the pressure-displacement behaviour of the soil for the particular site geometry and soil strength, and takes into account the influence of construction method and workmanship. Extensive full scale pipe loading experiments have been conducted by British Gas (Needham & Leach, 1987).

By applying load in different directions, the pressure-displacement relationship of the soil in different directions can be determined. Pipe lifting tests (corresponding to the settlement or downward movement of the soil relative to the pipe) provide the information on soil restraint from the overburden soil; downward pushing tests (corresponding to the upward movement of the soil relative to the pipe) can determine the soil restraint of the underlying soil; lateral pushing/pulling tests can determine the lateral soil restraint to the pipe. Herbert & Leach (1990) presented some typical Q-z curves obtained from pipe lifting tests for cohesive and granular soil. A relative soil/pipe movement of 20 – 30mm was needed to generate a limiting pressure on the pipe.

Although these full scale loading tests provide useful information on the pressure-displacement relationships of the soil which also take into account the soil/pipe interactions, they are limited to the particular site geometry and soil properties, and very expensive to carry out.

2.7.3. Empirical Relations

2.7.3.1. Axial Soil/Pipe Movement

The axial restraint by the soil spring represents the surface resistance along the pipeline. This interaction is similar to the skin friction or shaft resistance of piles. The ultimate axial soil resistance per unit length of the pipe r_u for a fully buried pipeline can be expressed as (ASCE, 1984):

$$r_u = 0.5\pi D\gamma' Z(1+K_0)\tan\delta \qquad \text{(for sand)} \qquad (2.12)$$

$$r_u = \pi D\alpha c_u \qquad \text{(for clay)} \qquad (2.13)$$

where δ is the interface friction angle between soil and pipeline and α is the adhesion factor. Alternatively, the ultimate axial soil resistance per unit area of the pipe R_u can be used ($R_u = r_u/\pi D$). It should be noted that in most practical situations the loading considered is relatively short term, thus undrained conditions are applicable to clay, and for this reason c_u is used in Eq. (2.13) (and later in Eqs 2.19, 2.22 and 2.25).

The ultimate axial displacement x_u is typically 2mm to 5mm for dense to loose sand and 5mm to 10mm for stiff to soft clay. A bilinear *r-x* curve can be estimated by assuming an axial displacement of, say, 5mm to reach the maximum axial resistance, hence the stiffness for the axial spring equals:

$$k_a = \frac{r_u}{0.005\pi D} \qquad \text{(kN/m²/m)} \qquad (2.14)$$

A hyperbolic formulation has been suggested by Clough and Duncan (1971) to model the non-linear variation of k_a:

$$k_a = \left[1 - \frac{R_f \tau}{\sigma_n' \tan\delta}\right]^2 k_{ai} \qquad (2.15)$$

where k_{ai} is the initial tangent stiffness of the axial spring and R_f is a factor less than 1.

The term "$0.5\pi D\gamma' Z(1+K_0)$" of Eq. (2.12) represents the average effective normal stress acting along the area of contact between the soil and pipeline. It should be noted that, however, this average normal stress only applies for at-rest conditions. In the situation where lateral soil pressures are imposed on the pipeline by relative soil/pipe displacement, the average normal stress is much higher than in the at-rest condition, thus much higher axial stress (or strain) can be developed on the pipeline (ASCE, 1984).

The value of δ may be related to the friction angle of the surrounding soil ϕ:

$$\delta = \mu\phi \tag{2.16}$$

where μ is the friction factor.

Values of μ may vary from 0.3 to 1.0 depending on the characteristics of the interface between the pipe surface material and the soil in contact with it. Table 2.2 summarizes the friction factor μ for a variety of materials reported by other research workers.

Pipelines that have been wrapped or roughened may have μ close to 1.0 especially for soft wrapping and fine-grained materials in which full interlocking of the soil particles and the texturing can be achieved. For bare metal pipelines buried for many years, μ may also be close to 1.0 due to the oxidation of the pipe such that soil particles become cemented and bonded to the metal. If the pipeline surface is treated and coated with a smooth, relatively hard, and weathering resistant material, then the friction between the soil/pipe interface could be reduced substantially, resulting in a μ value of 0.5 to 0.7 (ASCE, 1984).

For pipelines buried in clay, the adhesion factor α is generally determined from the results of shaft resistance of pile load tests. It has been shown that α is a function of c_u, and reduces with increasing c_u (Tomlinson, 1957, Woodward, Lundgren & Boitano, 1961, ASCE, 1984 and Trigg & Rizkalla, 1994). Figure 2.26 shows the recommended pipeline adhesion factor relationship from ASCE (1984) and the experimental value of α from *in situ*

push-out tests on steel pipe performed by NOVA corporation of Alberta (Trigg & Rizkalla, 1994). However, the coating material of the pipe has not been mentioned.

2.7.3.2. Lateral Soil/Pipe Movement

Audibert & Nyman (1977) and Needham & Leach (1987) provide comprehensive literature reviews of published information on the lateral soil spring stiffness k_h (or the coefficients of subgrade reaction), a term to describe the slope of the pressure-displacement relationship of a pipe pushed into the reacting soil. Most of the earlier empirical formulations for the spring stiffness were constant although some of them do take into account the influence of overburden pressure. Table 2.3 summarizes some of the formulations to determine the value of the coefficient of horizontal subgrade reaction for longitudinal bending.

For better representation of the behaviour of the soil spring, a non-linear pressure-displacement relationship (the *P-y* curve) should be used. On the basis of model tests on the lateral displacement of buried pipes in loose and dense sand, Audibert & Nyman (1977) suggested a technique for the prediction of a non-linear *P-y* curve for a laterally loaded pipe buried in sand. The proposed equation was in a hyperbolic form:

$$P = \frac{y}{a + by} \tag{2.17}$$

where P is the pressure on the pipe, y is the displacement of the pipe, $a = \frac{0.145 y_u}{P_u}$, $b = \frac{0.855}{P_u}$, y_u is the pipe displacement at failure and P_u is the ultimate pressure on the pipe.

Trautmann & O'Rourke (1985) performed model tests and suggested a similar hyperbolic *P-y* curve, with slightly different values for the constants a and b, for buried pipes in sand subjected to lateral force. They also suggested that the *P-y* curve may be simplified by representing it as a bilinear relationship having a secant slope defined at 70% of the maximum force, as recommended by Thomas (1978). Other researchers have also proposed formulations for the non-linear *P-y* curve and these are summarized in Table 2.4. Some

other researchers suggested *P-y* curves involving the estimation of the strain at one-half the maximum deviator stress in undrained triaxial test, for example Matlock (1970) and Dunnavant & O'Neill (1989), but these are not discussed in here.

The results of the pipe loading test by Audibert & Nyman (1977) suggested that y_u for loose sand was approximately $0.060Z$, $0.041Z$, $0.030Z$ and $0.025Z$ for pipe diameter D = 25.4mm, 61.0mm, 114.3mm and 254.0mm respectively (Z is the depth of soil to the centre of pipe). For dense sand, y_u for the four pipe diameters are $0.036Z$, $0.026Z$, $0.022Z$ and $0.019Z$ respectively. Trautmann & O'Rourke (1985) found that y_u was about $0.13Z$, $0.08Z$ and $0.03Z$ for loose, medium and dense sand respectively. For stiff to soft clay, $y_u = 0.03Z$ to $0.05Z$ (ASCE, 1984).

Methods to determine the ultimate pressure P_u (or $p_u = P_u \times D$) have been suggested by many researchers. For example Audibert & Nyman (1977) suggested the use of Brinch-Hausen bearing capacity factor, N_{qh} (Hansen, 1961); Randolph & Houlsby (1984) provided analytical solution to P_u based on plasticity theory and some others based on the behaviour of anchor plates (*e.g.* Rowe & Davis, 1982a, b). The general equations to determine P_u are:

$$P_u = \gamma Z N_{qh} \quad (\text{or } p_u = \gamma Z N_{qh} D) \quad \text{(for sand)} \tag{2.18}$$

$$P_u = c_u N_{ch} \quad (\text{or } p_u = c_u N_{ch} D) \quad \text{(for clay)} \tag{2.19}$$

Tables 2.5 and 2.6 summarize the formulations to determine P_u proposed by other researchers for granular and cohesive soils respectively, with source of reference.

2.7.3.3. Upward Movement of Pipe

On the basis of laboratory pipe lifting tests in sand, Trautmann, O'Rourke & Kulhawy (1985) suggested that the non-linear pressure-upward displacement relationship (*Q-z* curve) can be expressed in a hyperbolic form:

$$Q = \frac{z}{\frac{0.07 z_{uu}}{Q_{uu}} + \frac{0.93 z}{Q_{uu}}} \tag{2.20}$$

The ultimate upward displacement z_{uu} was found to be in the range from $0.005Z - 0.015Z$ for dense to loose sand and they suggested a value of $0.01Z$ could be used in most applications. ASCE (1984) suggested the range for z_{uu} from $0.1Z - 0.2Z$ for stiff to soft clay.

The general equations to determine the ultimate soil pressure Q_{uu} are:

$$Q_{uu} = \gamma Z N_{qu} \quad (\text{or } q_{uu} = \gamma Z N_{qu} D) \quad (\text{for sand}) \tag{2.21}$$

$$Q_{uu} = c_u N_{cu} \quad (\text{or } q_{uu} = c_u N_{cu} D) \quad (\text{for clay}) \tag{2.22}$$

Trautmann, O'Rourke & Kulhawy (1985) summarized some of the formulations proposed by other research workers to determine the value of N_{qu} and they are shown in Table 2.7.

For pipelines buried in cohesive soil, Rowe & Davis (1982a) suggested a graphical relationship between the dimensionless factor $N_{cu}(= Q_{uu}/c_u D)$ and the Z/D ratio as shown in Fig. 2.33. The results were based on finite element analysis results of anchor plate buried in cohesive soil subjected to uplift force.

2.7.3.4. Downward Movement of Pipe

For the downward direction of motion, the pipeline is usually assumed to act as a strip footing having cylindrical shape. Needham & Leach (1987) summarized some early formulations to determine the downward linear spring stiffness k_{vd} and these are shown in Table 2.8.

The downward ultimate soil resistance q_{ud} can be determined by conventional bearing capacity theory, as suggested by ASCE (1984):

$$q_{ud} = c N_{cd} D + \gamma' Z N_{qd} D + 0.5 \gamma D^2 N_\gamma \tag{2.23}$$

where N_{cd}, N_{qd} and N_{γ} are bearing capacity factors for horizontal strip footings, vertically loaded in the downward direction (see Fig. 2.34).

For the particular case of cohesionless granular soil, the equation becomes:

$$q_{ud} = \gamma' Z N_{qd} D + 0.5 \gamma D^2 N_{\gamma} \tag{2.24}$$

and for the case of undrained loading in clays, the equation becomes:

$$q_{ud} = c_u N_{cd} D \tag{2.25}$$

On the basis of plasticity theory for a rigid pipe resting on purely cohesive soil of infinite depth, Murff, Wagner & Randolph (1989) found that the upper and lower bounds of the ultimate downward resistance for a pipe halfway embedded in soil to be:

Smooth pipe: $q_{ud} = 4.0 - 5.56 c_u D$ (2.26a)

Rough pipe: $q_{ud} = 5.4 - 5.92 c_u D$ (2.26b)

The ultimate downward displacement z_{ud} is generally considered to be $0.1D$ to $0.15D$ for both sand and clay (ASCE, 1984).

A bilinear elasto-plastic relationship can be obtained by the value of q_{ud} and z_{ud}, or using the spring stiffness values presented in Table 2.8. No hyperbolic Q-z relationship been suggested so far, but the finite element analysis results presented by Needham & Leach (1987) showed that the pressure-displacement relationship for downward and lateral movement of pipe were quite close, suggesting that the hyperbolic equations for laterally loaded pipe (Table 2.4) may be used for downward movement of pipe.

2.7.3.5. Oblique Movement of Pipe

When the relative soil/pipe movements have both horizontal and vertical components, *i.e.* oblique movements, the full 3-D beam on springs model (Fig. 2.25) has to be used. However, due to the complexity of the 3-D model, a simplified approach can be used to

resolve the horizontal and vertical components of soil restraints transverse to the pipe into an oblique soil spring corresponding to the resultant direction of soil movement. O'Rourke & Tawfik (1987) reported an analytical approach proposed by Nyman (1982, 1984) to determine the response of the equivalent oblique soil spring. The ultimate oblique pressure P_{uob} is obtained from the equation:

$$P_{uob} = i(P_u - Q_{uu}) + Q_{uu} \tag{2.27}$$

where i is the coefficient of inclination:

$$i = \left(\frac{0.25\omega}{1.0 - 0.75\omega}\right) \qquad (\text{for } 0° \le \beta \le 90°) \tag{2.28}$$

$$i = C_0 + C_1\omega + C_2\omega^2 \qquad (\text{for } 90° \le \beta \le 180°) \tag{2.29}$$

where $\omega = \beta/90°$, β is the angle of thrust measured from the pipe crown, $C_0 = i_d - 8.0$, $C_1 = 14.0 - 2i_d$, $C_2 = i_d - 5.0$ and the factor $i_d = \dfrac{Q_{ud} - Q_{uu}}{p_u - Q_{uu}}$.

ASCE (1984) suggested that the ultimate oblique displacement can be interpolated between the ultimate horizontal displacement and the ultimate vertical (upward or downward as it may apply) displacement. Nyman (1982) suggested the values of $0.015Z$ to $0.025Z$ for dense to loose materials for the ultimate oblique displacement.

2.7.4. Non-Linear Stress Analysis

The pressure-displacement relationship can also be determined by non-linear finite element analysis. With the FE mesh set up to the particular geometry and boundary conditions, together with suitable soil model and appropriate soil properties to represent the soil, the relationships at different directions can be determined. Ng (1993) used 2-D plane strain analysis to obtain the lateral soil restraint to a buried pipe using different soil models (see Section 3.4 for more details). Yin, Paulin, Clark & Poorooshasb (1993) also obtained the *p-y* curve for a laterally loaded pipe using 2-D FE analysis. They compared the numerical results with centrifuge test data by Rizkalla, Poorooshasb & Clark (1992) and the empirical

relations by Hansen (1961) and Rowe & Davis (1982b). They found that the FE analysis gave reasonably good predictions of the centrifuge test data while the empirical methods under-predicted the *p-y* curve.

Needham & Leach (1987) presented typical results of numerical analysis that predicted the soil restraint for a pipe moving in different directions. They found that the soil resistance for the pipe moved down into the soil was significantly higher than in the pipe lifting situation. The result for horizontal restraint was between the two cases but in closer agreement with the downward mode of pipe movement than with the upward mode.

The advantage of using non-linear stress analysis is that once the FE mesh has been set up, the soil restraint in different directions can easily be obtained. Parametric studies can also be performed by varying the soil properties and the site geometry without too many difficulties. This kind of numerical analysis is relatively inexpensive when compared with full scale or model testing, but good quality input parameters are needed to obtain realistic results. Moreover, the soil/pipe interaction must be considered in the analysis (*e.g.* the possible slippage and gap formation between the pipe and soil).

2.8. Interface Between Pipe and Soil

2.8.1. Introduction

The performance and behaviour of buried structures can be strongly influenced by soil/structure interaction. One aspect of this involves the properties and load transfer characteristics of the soil/structure contact surfaces. The proper modelling of the soil/structure interface is very important if numerical methods are applied to obtain solutions to this type of problem, and this is shown in Chapter 7.

In conventional continuum implementations of the finite element method, compatibility is enforced between adjacent elements. Soil/structure interfaces can therefore only be represented as fully bonded. In reality, however, the interface behaviour is more complex. Relative slip often takes place at the interface between two different materials when the bond strength is exceeded. If tensile stress starts to develop across a soil/structure interface, separation is likely to occur and a gap will form. To model these interface characteristics in the finite element method, special "interface elements" have been developed to account for the relative motions and associated deformation modes. Applications of interface elements can be found in a wide range of geotechnical problems, including piling (Brown & Shie, 1990, 1991 and Cheung, Lee & Zhao, 1991), shallow foundations (Sekiguchi, Rowe, Lo & Ogawa, 1992, Ruffier & Mahler, 1988 and Zaman, 1985), rock joints (Goodman, Taylor & Brekke, 1968, Werner, Bellmann, Niedermeyer, Bauer & Rahn, 1988 and Wang & Garga, 1993), arch dam/abutments (Hohberg & Bachmann, 1988), retaining walls (Clough & Duncan, 1971), buried pipes (Schweiger & Haas, 1988 and Bolzoni, Cuscunà & Perego, 1993) and reinforced embankments on soft ground (Kwok, 1987 and Russell, 1992a).

2.8.2. Behaviour of Soil / Structure Interface and Interface Element

The behaviour of soil/structure interfaces can be separated into shear and normal behaviour. Typical results from direct shear tests (Desai & Nagaraj, 1988), illustrated in Fig. 2.35, show interface slip at a limiting shear stress and the interface closure in compression and separation under a small tensile stress. These stress-strain relationships are usually idealized as elastic-perfectly plastic and linear elastic respectively for the mathematical formulation of the interface element. The transition of normal stiffness from the bonded to debonded state can involve a gradual reduction with stress from a high to low value. However, most idealizations adopt the debonded state (separation) of the element as soon as the normal stress changes to tensile.

There are usually five modes of behaviour for an interface element:

i. Non-slip — The element is behaving elastically with a normal stiffness k_n and shear stiffness k_s.

ii. Slip — When the shear stress reaches the bond strength, may be governed by Mohr-Coulomb relationship, large relative displacement (slip) occurs and the shear stiffness k_s is reduced to zero.

iii. Unloading — If unloading occurs, the shear stiffness is restored to the original value.

iv. Separation — If the normal stress becomes tensile, the normal stiffness is reduced to zero and the shear stress and shear stiffness are also reduced to zero.

v. Rebonding — If separation has occurred and during some later increment the interface re-contacts (normal stress becomes compressive) then the original normal and shear stiffness is restored.

The modes (i) to (iii) are regarded as shear behaviour and the element is in compression. The modes (iv) and (v) are regarded as normal behaviour. These five modes of behaviour are illustrated graphically in Fig. 2.36.

2.8.3. Types of Interface Element and Their Constitutive Relationship

2.8.3.1. Zero Thickness Element

The zero thickness element, first proposed by Goodman, Taylor & Brekke (1968), was the earliest type of interface element and is still commonly used today. The element is characterized by its thickness equals to zero so that the corresponding nodes on the two longer sides of the element can have the same co-ordinates and without introducing any singularity in their formulation. The element was developed initially for the use of modelling the relative displacement along a joint between two intact rock masses. The

element stiffness is expressed in terms of normal and shear components. The original formulation was for a 4-noded rectangular element with a linear displacement field.

Zienkiewicz, Best, Dullage & Stagg (1970) recommended the use of a continuous isoparametric element with a simple non-linear material property for shear and normal stresses, assuming uniform strain in the thickness direction. However, numerical difficulties may arise from ill-conditioning of the stiffness matrix due to very large off-diagonal terms or very small diagonal terms which are generated by these elements in certain cases. It was recommended that the ratio between the stiffnesses of the interface and adjacent element should not be greater than 1000.

Ghaboussi, Wilson & Isenberg (1973) presented exact explicit stiffness matrices for an interface element in 2-D cases. They proposed a formulation which was derived by considering relative displacement between surrounding elements (top and bottom of the interface element) as an independent degree-of-freedom. The merit of the formulation was demonstrated by Wilson (1977) with a simple numerical example. The instabilities due to the diagonal terms in the stiffness matrix were eliminated and the accuracy of solution was greatly improved.

Although the interface elements proposed by Zienkiewicz *et al* (1970) and Ghabonssi *et al* (1973) have a finite thickness, from the point of view of stiffness formation its nodes were assumed to coincide with its mid-section. The actual thickness of the element is only used when computing the element properties. Therefore, the elements are still grouped into the category of zero-thickness element.

The deformations of interface elements are cause by normal stress σ_n (acting perpendicular to the length) and shear stress τ (acting parallel to the length) as shown in Fig. 2.37. The normal behaviour is often idealized as linear elastic controlled by normal stiffness k_n and the shear behaviour is idealized as elastic-perfectly plastic (see Fig. 2.35). The elastic portion is

described by shear stiffness k_s up to the limiting shear strength τ_{lim} which is defined by Mohr-Coulomb yield criterion:

$$\tau_{lim} = c + \sigma_n \tan\phi \tag{2.30}$$

where c is the cohesion intercept and ϕ is the angle of friction.

For 2-D analysis, the stress and strain of the interface element in the elastic region is related through the material property matrix:

$$\begin{Bmatrix} \sigma_n \\ \tau \end{Bmatrix} = \begin{bmatrix} k_n & k_{ns} \\ k_{sn} & k_s \end{bmatrix} \begin{Bmatrix} u_n \\ u_s \end{Bmatrix} \tag{2.31}$$

where u_n is the normal displacement, u_s is the shear displacement and k_{ns} and k_{sn} are the stiffnesses for coupling between shear and normal behaviour.

For the simplest non-dilatant case (no volume change due to shear strains) shear and normal components of deformation are uncoupled:

$$\begin{Bmatrix} \sigma_n \\ \tau \end{Bmatrix} = \begin{bmatrix} k_n & 0 \\ 0 & k_s \end{bmatrix} \begin{Bmatrix} u_n \\ u_s \end{Bmatrix} \tag{2.32}$$

For the dilatant case, normal displacement and shear force can be coupled together or vice versa, or use can be made of a strain hardening plasticity model for the stress-strain relation.

Some similar kinds of interface elements have been proposed recently. Beer (1985) proposed an interface element of zero thickness with an isoparametric formulation similar to Ghabonssi *et al* (1973). Both 2-D and 3-D elements have been formulated and the 3-D element can be used with shell and solid elements.

Kwok (1987) and Russell (1992a) have implemented an interface element of the type proposed by Goodmen *et al* (1968) to the finite element program CRISP84 (see Section 4.3 for the behaviour of this interface element) to model the soil/reinforcement interface in reinforced embankments on soft ground. Kwok (1987) performed a number of numerical

analyses to test the interface element; some of the results were compared with analytical solutions and the agreements were satisfactory.

Britto & Gunn (1990) have implemented an 8-noded interface element into the finite element program CRISP90. However, the two mid-side nodes along the narrow dimension are dummy nodes and not used in the analysis, even though these are assigned numbers (see Fig. 4.1). From the formulation point of view, it is essentially a 6-noded element with linear strain variation along the longer sides and constant strain along the narrow sides. The element can have coinciding double-nodes for the longer sides similar to the para-linear interface element proposed by Zienkiewicz *et al* (1970). They recommended that the ratio of the length and thickness of the element should be within the range of 10 and 100. The behaviour of the CRISP90 interface element is described in Section 4.3. Modifications to this interface element were made in Section 4.4 in order to use it in the modelling of a laterally loaded pipe in Chapter 7.

2.8.3.2. Thin-Layer Element

The thin-layer element was proposed by Desai (1982) and Desai, Zaman, Lightner & Siriwardane (1984). The behaviour of the interface is described through suitable 2-D elements for which a small (but different from zero) thickness is assumed. Particular constitutive relationships are used for the thin-layer element that allow for the various deformation modes of the interface. For the plain strain and isotropic condition, and also assuming the shear and normal response are uncoupled, the elastic constitutive matrix of the interface can be given as:

$$\begin{bmatrix} A_1 & A_2 & 0 \\ A_2 & A_1 & 0 \\ 0 & 0 & G \end{bmatrix} \tag{2.33}$$

where $A_1 = \dfrac{E(1-\nu)}{(1+\nu)(1-2\nu)}$, $A_2 = \dfrac{E\nu}{(1+\nu)(1-2\nu)}$ and G = shear modulus.

The performance of the thin-layer element can be influenced by the thickness of the element. If the thickness is too large in comparison with the length, the thin-layer element will behave essentially as a solid element. If the thickness is too small, computational difficulties may arise. Desai *et al* (1984) performed parametric studies to compare the performance of the element with different thickness values and recommended the length/thickness ratio should be between 10 to 100.

Schweiger & Hass (1988) implemented a similar thin-layer element as Desai *et al* (1984) into their FE program. An independent shear modulus was introduced to allow large relative displacements in the elastic range without causing numerical difficulties.

2.8.3.3. Conventional Element

Conventional quadrilateral elements, with either minor or no modification have been used to model the soil/structure interface, especially the slip behaviour at the interface. The constitutive relationships for the element can be found in many standard text books (*e.g.* Zienkiewicz & Taylor, 1989).

In the past, if the aspect ratio (length/thickness of the element) of a conventional quadrilateral element was too high, then numerical problems might occur. Following the advance of computer hardware, this problem has been overcome by higher precision Pande & Sharma (1979) used modified 8-noded quadrilateral elements with relative displacement as an independent parameter to model the slip behaviour at an interface and compared the results with normal 8-noded elements. They obtained almost identical results for the two kinds of element up to a very high aspect ratio (over 10000) on high precision machines (48-bit) without numerical ill-conditioning. They also showed that on smaller word length computers (24-bit), an aspect ratio of up to thousands could be used without creating any numerical problems.

Griffiths (1985) also used conventional 8-noded quadrilateral elements to model slip phenomena at an interface. He found that for aspect ratios up to 100, the element behaviour was satisfactory, but for higher ratios up to 1000, a much tighter convergence tolerance was needed for the interactive method to model the non-linearity. He concluded that 8-noded quadrilateral elements may be used as a first approximation for an analysis and the justification of the needs of special interface elements.

Griffiths (1987) modelled a smooth interface using modified quadrilateral elements by introducing an extra degree-of-freedom at the nodes along the interface. The directions of the degree-of-freedom were also transformed such that their orientations were parallel and perpendicular to the interface direction. He analysed some examples by considering two extreme cases of perfectly rough and perfectly smooth conditions at the interface. The results were compared with closed form solutions and good agreement was obtained. He also demonstrated that in some cases, where the results between the two extreme cases are not great, the use of specialized interface elements may be unnecessary.

Hohberg & Bachmann (1988) compared the elastic performance of a thin conventional quadrilateral element and a zero thickness interface element. When the thickness of the conventional element diminished to zero and the spatial components decoupled ($\nu = 0$), the behaviour of the conventional element approached the zero thickness element and both elements can be used to model slippage at an interface.

2.8.4. Evaluation of Material Parameters for Interface Element

One of the major difficulties in using these interface elements is the adoption of material parameters. For thin-layer and conventional elements, the material parameters usually needed are the Young's Modulus E and Poisson's ratio ν. These parameters may be found using conventional laboratory tests (*e.g.* triaxial compression test). The parameters for zero-thickness elements, normal stiffness k_n and shear stiffness k_s, can be obtained from a

direct shear box test in which the bottom portion contains the material of the structure and the top portion of the soil. k_n can be found from the measurement of vertical deformation under the applied normal load (σ_n/u_n), and k_s is evaluated as a tangent modulus from the shear stress-displacement curve (τ/u_s) of the direct shear box test prior to interface slip. Typical results and idealization of the stress-strain behaviours are shown in Fig. 2.35.

It should be noted that the shear and normal stiffnesses are expressed in units of force per unit volume (kN/m³), and do not represent any real physical soil property. They are convenient mathematical parameters describing the rate of change of soil pressure with displacement (kN/m²/m) or shear stress with displacement.

It is possible to link the normal modulus K_n (= $k_n \times t$) and shear modulus K_s (= $k_s \times t$) to E and ν by using Hooke's law, so that:

$$\begin{aligned} K_n &= \frac{E(1-\nu)}{(1+\nu)(1-2\nu)} \\ K_s &= \frac{E}{2(1+\nu)} \end{aligned} \quad \text{or} \quad \begin{aligned} k_n \times t &= \frac{E(1-\nu)}{(1+\nu)(1-2\nu)} \\ k_s \times t &= \frac{E}{2(1+\nu)} \end{aligned} \tag{2.34}$$

and

$$\begin{aligned} E &= \frac{(3K_n - 4K_s)K_s}{K_n - K_s} \\ \nu &= \frac{K_n - 2K_s}{2(K_n - K_s)} \end{aligned} \quad \text{or} \quad \begin{aligned} \frac{E}{t} &= \frac{(3k_n - 4k_s)k_s}{k_n - k_s} \\ \nu &= \frac{k_n - 2k_s}{2(k_n - k_s)} \end{aligned} \tag{2.35}$$

where t is the chosen thickness of the interface element.

Appendix A shows the derivation of the above relationships. By using these equations, one can use either a direct shear box test or conventional laboratory tests (*e.g.* triaxial compression test) to determine the material parameters for all kinds of interface element.

The normal stiffness for zero-thickness elements is often assigned a very high value (Hird & Russell, 1990) based on the assumption that the structural and geological media do not overlap at the interface. For thin-layer and conventional elements, it is more appropriate to

assign the same properties as the geological material because the elements are often being modelled as part of the geological material.

Desai (1977) pointed out that there are some limitations for the direct shear box test to evaluate the material parameters. For example, in the direct shear test, the direction of critical stress can be inclined to the direction of shearing and the maximum shear stress can be greater than the measured shear stress parallel to the axis of shear box. Moreover, the distribution of shear stress may not be uniform. To overcome these problems, Desai proposed a modified simple ring shear device to obtain the material parameters. Desai, Drumm & Zaman (1985) developed a new device for cyclic testing of large size interfaces between structural and geologic materials and rock joints.

2.9. Modelling of Buried Pipeline Subjected to External Loading

2.9.1. Introduction

It is very important to design new pipelines and check the existing pipeline performance in response to differential ground loading along the pipeline length. Initial work on this problem has utilised the research information on the design and performance of laterally loaded piles and anchor plates due to the lack of direct fundamental work.

The method of modelling usually employs the elastic beam on elastic foundations approach. More recently, when more powerful computers are available, it is feasible to perform 3-D finite element analysis to model the problem. The following sections will describe how other researchers have used the above methods to model their particular problems.

2.9.2. Related Research on Laterally Loaded Piles

The behaviour of laterally loaded piles are in many ways similar to laterally loaded pipes and the research information can be used as guidance. The traditional method of designing laterally loaded pile is by using *p-y* curves (load-displacement relationships) derived from field tests, model tests, or by empirical relationships. More recently, centrifugal model tests and the finite element method have been used extensively to investigate the behaviour and performance of laterally loaded piles.

Yan & Byrne (1992) performed a model test on a single vertical pile under monotonic lateral pile head loading. They found that the experimental *p-y* curves were highly non-linear and stress dependent. Georgiadis, Anagnostopoulous & Saflekon (1992) carried out centrifugal tests to examine the behaviour of laterally loaded piles in sand. They concluded that the depth-variable non-linear soil characteristics should be taken into account. From their test results, they proposed that the non-linear characteristics of soil (*p-y* curve) can be represented by a hyperbolic function (see Table 2.4).

To numerically model the behaviour of the pile, a conventional beam on elastic foundation model has been used extensively. For example, Georgiadis *et al* (1992) used this model together with their proposed hyperbolic function to represent the spring stiffness. Good agreement was obtained with their centrifugal test results. They also compared some earlier *p-y* curves suggested by other researchers, but the results showed that these earlier relationships all under-predicted the pile displacement, indicating that the *p-y* curves were too stiff.

The conventional beam on elastic foundation model has been modified by Georgiadis & Butterfield (1982) for modelling laterally loaded piles, in which non-linear shear coupling was introduced between the non-linear soil springs so that any displacement of a spring generates displacement of the neighbouring springs. The loading intensity in Eq. (2.9) therefore becomes:

$$p = k_h D(u_s - u_p) - g\frac{d^2(u_s - u_p)}{dx^2} \tag{2.36}$$

where g is the shear coupling parameter which can be determined from two independent plate loading tests.

Puswewala, Rajapakse, Domaschuk & Shields (1993) modelled laterally loaded piles in ice as a beam on a spring-dashpot system by introducing a secondary creep rate relationship in the conventional beam on elastic foundation model to account for the continuous deformation (creep) of ice under load.

Three-dimensional finite element analysis has been used by Brown & Shie (1990, 1991) to study the performance of a laterally loaded pile. Non-linear characteristics of the soil response were considered and the soil/pile interface has been modelled as a frictional interface. A gap was formed on the trailing side of the pile and slippage occurred around the pile. They concluded that an appropriate finite element model of the laterally loaded pile problem must include provisions for slippage and gapping at the soil/pile interface. The frictional resistance at the interface also contributed a significant portion to the soil resistance. The back-calculated *p-y* curves of the pile were not particularly sensitive to the friction coefficient used at the interface, as long as frictional behaviour was provided.

Chen & Poulos (1993) pointed out that the conventional finite element method may in some cases require a great number of elements to properly simulate the far-field behaviour although the main interest lies within the near-field. They suggested the use of combined infinite and finite element method. The infinite elements were used to simulate the far-field behaviour of the soil medium, while standard finite elements were used to model the pile and the soil immediately surrounding it. The combined infinite and finite element method was found to provide a more accurate and efficient technique for solving problems involving unbounded domains than the conventional finite element method. Good agreement was obtained between numerical results and analytical solutions. Their parametric study showed

that for a single rigid pile loaded laterally in a purely cohesive soil, the ultimate lateral soil resistance was mainly governed by the pile adhesion and the properties of the soil/pile interface.

Anagnostopoulous & Georgiadis (1993) studied the behaviour of a pile subjected to simultaneous axial and lateral loading. In current practice, piles are independently analysed for axial and lateral loading. They performed model tests to investigate experimentally any possible effects of lateral loading on axial pile displacements and stress as well as the influence of axial loads on the lateral pile response. They found that the lateral load increased significantly the axial pile displacement but caused a small reduction of the axial pile stresses near the ground surface, and the effect of axial loading on the lateral pile response was rather limited. They suggested that the interaction between axial and lateral pile response can be studied with a 3-D non-linear finite element analysis.

2.9.3. Related Research on the Behaviour of Anchor Plates

The design methods developed by Rowe & Davis (1982a, b) for buried anchor plates have been used by many researchers to predict soil restraint against uplift loading and lateral disturbance of buried pipes in sand and clay. Dickin (1988) performed a parametric study on the stress-displacement behaviour of rectangular buried anchor plates and buried pipes in centrifugal test equipment. The test results showed that distinct similarities exist between the general behaviour of the plates and pipes and comparisons have been made to the design method suggested by Ovesen & Stromann (1972) and Rowe & Davis (1982a, b). Although some discrepancies existed, Dickin suggested the design theories for vertical anchor plates may be applied to laterally loaded buried pipes. The design method together with the non-linear *P-y* curve (Table 2.4) and the elastic beam on elastic foundation method provides a simple approach to model the behaviour of a buried pipeline subjected to lateral loading.

2.9.4. Trenching

A 3-D elastic finite element study has been carried out by Nath (1983) in which the pipeline was modelled by dimensionless beam elements in contact with continuum brick elements representing the soil. The study examined the influence of geometric and material properties on the bending moments induced in buried pipes running parallel with the trench.

Kyrou & Kalteziotis (1985) performed parameteric studies using 3-D elastic finite element analysis to investigate some aspects of the adverse effect of trench excavation induced ground movements on an adjacent buried pipeline. The pipe was modelled using 2-noded elastic beam elements having compatible nodal displacements with the surrounding soil. The soil, assumed to be fully saturated clay and behaving as an incompressible elastic material, was represented by 8-noded brick elements.

Their results showed that maximum horizontal and vertical movement of the ground increase as *L/H* ratio (Length/Depth of trench) increases from zero to approximately 2 and thereafter remain almost constant (plane strain condition). They stated that for a short trench the pattern and magnitude of movement is governed by the restraining effect of the ends of trench. For longer excavations the magnitude of movement in the central portion of the trench is governed by the restraint provided by the bottom of the excavation. The *W/H* ratio (Width/Depth of trench) also influences the general ground movement patterns. The horizontal movements at the excavation end have been shown to increase as the excavation width increases and the deformation gradients decrease significantly. Therefore narrower trenches are likely to affect more adversely nearby shallow buried pipelines. The numerical results have been compared with field measurement data from Symons (1980) and Symons, Chard & Carder (1981). Similar ground displacement patterns were observed.

These 3-D FE analyses, however, all failed to represent the dimension of the pipe and the consequential soil/pipe interaction.

2.9.5. Pipe Bursting

Herbert & Leach (1990) presented a stress analysis procedure to determine the stresses of a gas pipe crossing above a proposed on-line replacement in a perpendicular alignment. The first step was to estimate the ground displacement components along the axis of the crossing pipe by a 2-D plane strain FE analysis simulating the on-line replacement process. The second step is to determine the relationships between soil restraint and movements of the crossing pipe. Several methods can be used as described in Section 2.7. In this particular case, 2-D FE analyses were used. The final step is to quantify the effect of the ground movement on the crossing pipe, using the elastic beam on elastic foundation approach. The crossing pipe was represented by an elastic beam in contact with springs representing the soil and subjected to the soil displacement loading predicted in step one. The predicted longitudinal bending strain profile was compared to the recorded distribution on site and good agreement was obtained.

2.9.6. Frost Heave

Selvadurai (1988) presented a coupled finite element-boundary element scheme which can be used for linear elastostatic modelling of soil/pipe interaction. He presented numerical results to several soil/pipe interaction problems which resulted from loadings by the overburden soil mass, lateral ground movement and ground swelling from frost heave. Although the model is highly simplified, it illustrated the manner in which the flexural stresses and displacements in the pipeline are influenced by the depth of embedment and the relative stiffness of the soil/pipe system.

Rajani & Morgenstern (1992) analysed a beam buried in a homogeneous and isotropic, elastic and non-linear viscous medium using the Winkler type beam on elastic foundation model. The model has been used to analyse the time-dependent movement of a buried pipeline subjected to frost heave.

Rajani & Morgenstern (1993) presented a simple analytical formulation for a beam on an elastic-plastic foundation which can be used to model the vertical uplift behaviour of a pipeline due to frost heave. The solutions developed for an anchor plate by Rowe & Davis (1982a) were incorporated with the analytical formulation to obtain an approximate 3-D solution. The approximate solution was compared with a 3-D finite element solution for a shell pipe embedded in an elastoplastic medium which indicated that the simplified solution of a beam on elastoplastic foundation is a practical alternative for analysing the uplift behaviour of shallow pipelines. The results were presented in the form of non-dimensional charts that permit hand calculations and rapid verification of structural design of pipelines.

2.9.7. Wave Propagation

O'Rourke & Ayala (1993) summarized some of the earlier empirical methods to assess the seismic damage to pipelines due to wave propagation. They expanded the data set used by Barenberg (1988) and established a refined empirical relation between seismic wave propagation damage to cast iron pipe and peak horizontal particle velocity.

2.9.8. Landslide

Rajani, Robertson & Morgenstern (1993) have developed an approximate 3-D analytical solution for transverse landslide movement. The design method accounts for the embedment and breakaway conditions behind the pipeline, and makes use of the capacity factor N_{ch} (Fig. 2.30) developed by Rowe & Davis (1982a). Non-dimensional load-displacement and moment-displacement relationships were developed and presented in the form of charts. By assuming a pipe displacement value, the corresponding maximum moment and stress in the pipeline can be calculated. The solution was extended to longitudinal landslide case by Trigg & Rizkalla (1994).

O'Rourke & Nordberg (1992) also presented analytical solutions to predict the behaviours of buried pipelines subjected to permanent longitudinal and transverse ground deformations, but in highly idealized situations such that the pipe displacement profile follows exactly the ground displacement profile (*i.e.* no soil/pipe interaction considered), also the method for transverse ground deformation is only applicable to the case where the width of ground deformation is much greater than the length of a pipe segment (wide spread type loading). The solutions are therefore should be used as a first approximation only.

2.9.9. Fault Movement

Kennedy, Chow & Williamson (1977) analysed the behaviour of a shallow buried pipe in cohesionless soil subjected to large fault displacement using an extended and refined version of the analytical procedure developed by Newmark & Hall (1975). The simplified analysis procedures take into account the lateral, horizontal and axial movement of the pipe relative to the soil. Kennedy *et al* found that the axial stiffness of the pipe is essentially independent of curvature of the pipe while bending stiffness decreases substantially. On this basis, they claimed that for large fault movement, where the pipe strain is often very large, the forces on the pipe are supported by axial tension in the pipe acting through longitudinal curvature of the pipe rather than by developing bending moment. From these assumptions they have ignored the bending stiffness of the pipe and the pipeline is conservatively analysed as if it has axial stiffness only.

Wang & Yeh (1985) presented an analysis procedure for buried pipelines applicable to fault movement. Their formulations included the effect of bending rigidity of the pipe, a shear force at the point of inflection of the curved pipe crossing the fault zone, a boundary condition related to a semi-infinite beam on an elastic foundation at some distance away from the fault zone, effect of axial force and bending moment interaction and effect of large deformation. The problem has been solved by iterative procedures and a series of

parametric analyses have been performed to study the influence of fault movement, crossing angle, soil/pipe friction angle, buried depth and pipe diameter effects on the design of buried pipelines. Their procedure has been extended by Vougioukas & Carydis (1992) to include the compression effect on the pipeline. The model is applicable to simulate both horizontal and vertical fault movements, either for strike slip or reverse strike slip faults. Parametric studies have been performed to examine the influence of parameters such as angle of pipe crossing the fault, geometric characteristics of the pipe *etc.*

Trautmann, O'Rourke & Kulhawy (1985) showed an idealized model for a pipeline affected by soil displacement that occurs during normal faulting or at the edge of a subsidence basin. The beam on elastic foundation model was used where the pipeline has been modelled by a number of beam elements and spring-slider elements were used to represent elastoplastic soil restraint in the vertical and longitudinal directions.

Yeh (1988) studied the landslide effect to buried pipelines. The proposed analysis models used the concepts of the beam on elastic foundation and the ultimate passive soil pressure to represent horizontal soil resistance to the pipe movement. He considered two failure mechanisms: one a small movement region, and the other a large movement region He concluded that the combined (coupled) effects of axial pipe force and the bending moment occurring along the pipe segment near the sliding region are significant, and neglecting the additional bending moment caused by the eccentricity of the axial pipe force within the transition zone, may lead to a non-conservative design of pipeline buried through a fault zone.

Selvadurai & Pang (1988) performed 3-D FE analysis to investigate the interaction between a buried pipeline and the surrounding soil which was induced by a discontinuous vertical ground movement. The pipeline was modelled as a cylindrical shell by 8-noded superparametric shell elements and the soil mass was modelled by 20-noded isoparametric brick elements having ideal elastic-plastic behaviour. The interface between the pipeline

shell and the surrounding soil was modelled as rough (fully bonded). They considered a plane of asymmetry existed at the fault thus only half of the problem was modelled. However, the results of numerical analysis and a field test have shown that the soil restraint above the pipe is significantly weaker than beneath the pipe due to the existence of the free surface (Herbert & Leach, 1990). The full soil-pipe system should be considered for vertical fault movement instead of only half of it. Their results indicated that the maximum flexural moment at the transition zone was altered by the yielding response of the cohesive soil and the relative stiffness of the soil/pipeline system.

Bolzoni, Cuscunà & Perego (1993) performed experimental laboratory tests and finite element simulations of a pipe buried in a clay bed and crossing a fault line. The pipe was modelled as a shell beam assuming perfect soil/pipe adhesion and the bending and axial effects were treated separately. By comparing the numerical and experimental results, they concluded that the finite element model was apt to reproduce, with an acceptable level of accuracy, the state of stress in the pipeline, provided that the following were taken into account: the plastic behaviour for both the soil and the pipeline, the behaviour of soil/pipe interface and the geometric non-linearity.

2.10. Summary

The modes of pipe deformation and their stress-strain relationships have been reviewed. The different loading conditions that cause such deformations and stresses on a pipeline have also been discussed. It should be noted that the loading condition considered in this research is closer to a wide spread type loading, because this loading condition is more likely encountered in the field and relates directly to the Hilderstone field tests (Chapter 3). Four soil models that are available have been described. Of those available with the FE program CRISP90 these were considered to be those most able to model the soil

encountered in the field tests and in the field generally. They will be used in Chapter 7 to model the backfill material such that the merits/limitations of each model can be examined. Different modes of soil/pipe interaction due to external loading acting on a buried pipeline and methods that model these interactions have been reviewed. For an axially loaded pipeline, simple 1-D models were often used. However, these models cannot include the essential influence of the surrounding soil such as volume changes due to shear dilation and contraction. Whilst a 3-D FE model is more appropriate, it is very expensive to use. For this reason, a 2-D FE model is proposed in Chapter 5 which is a simplified version of a 3-D model and is more sophisticated than the 1-D models. For a laterally loaded pipeline, 3-D FE analysis was found to be the most sophisticated method. However, it is too expensive to be used regularly. On the other hand, the elastic beam on elastic foundation approach is an economic and reasonably accurate method that has been widely used in practice. The elastic beam on elastic foundation approach requires a pressure-displacement relationship for the springs to represent soil restraint. Different methods to quantify the relationship have been reviewed. Most traditional (empirical) methods cannot take into account the existence of a backfill trench although, in practice, most pipelines are laid in an excavated trench which is then backfilled with other material. It was found that non-linear finite element analysis is the most cost effective and accurate method for predicting the *P-y* relationship. To model soil/pipe interaction properly in a FE analysis, special interface elements have to be used. The behaviour of different kinds of interface element have been reviewed. More detailed tests on these interface elements are reported in Chapter 4. The behaviour of laterally loaded piles and anchor plates are in many ways similar to laterally loaded pipelines and research in these two areas has been reported and discussed. Finally, different methods that have been used by other researchers for modelling the behaviour of buried pipelines in their particular problems have been reviewed. It was found that the methods can be grouped into three categories: analytical solutions, 3-D FE analysis and beam on elastic foundation approach. As mentioned earlier, for the analytical solutions, certain assumptions to the soil behaviour, geometries and loading conditions have to be

made to simplify the problem. Moreover, the behaviour of the soil/pipe contact surface and the existence of backfill trench cannot be taken into account. For 3-D FE analysis, although it is the most sophisticated method, it is still of limited use due to the high operational cost. The beam on elastic foundation approach is therefore the most cost effective and reasonably accurate method to predict the behaviour of buried pipelines. Modifications will be made in Chapter 6 to the classical elastic beam on elastic foundation approach to improve the modelling of the pipe. The method will be used in Chapter 7 to simulate a lateral push test on a pipeline (Chapter 3). A 2-D FE model with interface elements will be used to predict the pressure-displacement relationship of the pipe due to the reasons mentioned earlier.

Pipe Loading	Soil/Pipe Interaction		
	Diametric Deflection	Axial Soil/Pipe Interaction	Longitudinal Bending
Deep excavation	Secondary	Secondary	Major
Soft ground tunnelling	Secondary	Major	Major
Mining subsidence	Secondary	Major	Major
Embankments	Major	Secondary	Major
Ground collapse	Secondary	Major	Major
Soil swelling/shrinking	Secondary	Secondary	Major
Frost heave	Secondary	Secondary	Major
Traffic load	Major	Secondary	Secondary
Consolidation	Secondary	Secondary	Major
Ground impact	Secondary	Secondary	Major
Landslides	Secondary	Major	Major
Discontinuous Ground movement	Secondary	Major	Major
Earthquake	Secondary	Major	Major

Table 2.1. Soil/pipe interactions due to different loadings.

Reported by	Original results from	Materials	Value of μ	Comments
ASCE (1984)	Kulhawy, Trautmann, Beech, O'Rourke & McGuire (1983)	Sand/Smooth steel Sand/Rough steel	0.5 – 0.7 0.7 – 1.0	
ASCE (1984)	Trautmann & O'Rourke (1983)	Sand/Smooth Formica	0.6	Indicate the μ value between sand and plastic pipelines.
Leach & Row (1991)	Leach & Row (1991)	Clayey sand & gravel/ Coal tar enamel coated surface Clayey sand & gravel/ Epoxy coated surface	0.74 0.48	The soil used was a typical backfill material and the coal tar enamel and epoxy are two typical pipe coating materials.
Wilson-Fahmy, Koerner & Sansone (1994)	Wilson-Fahmy, Koerner & Sansone (1994)	Concrete sand/Polymer	0.62 – 0.76	The polymer is the material used for making geogrids indicate the μ value of plastic pipelines.
Orman (1994)	Orman (1994)	Coarse-grained drainage sand/Smooth HDPE Coarse-grained drainage sand/Roughened HDPE Fine-grained silt/Smooth HDPE Fine-grained silt/ Roughened HDPE	0.63 – 0.67 0.67 – 0.73 0.36 – 0.43 1.0	

Table 2.2. Value of the friction factor μ for a variety of materials.

Reported by	Original results from	Proposed formulation	Comments
Audibert & Nyman (1977) / Needham & Leach (1987)	See Audibert & Nyman (1977)	$k_h = \frac{2E'}{D}$ Quoted E' values are (in kN/m^2): 1600–2480 (sandy clay loam, untamped) 3460–5380 (sandy clay loam, tamped) 2410–8270 (sand) 4630 (well graded gravel, untamped) 43440 (graded crushed gravel, compacted) 55020 (crushed sandstone, compacted)	The reported E' values are secant values for an unknown amount of deflection.
Audibert & Nyman (1977) / Needham & Leach (1987)	See Audibert & Nyman (1977)	$k_h = \frac{2k_eC}{1.5D}$ where C is the depth of cover above the pipe. Quoted k_e values are (in kN/m^3): 410–1090 (loose sand) 1090–3260 (medium sand) >3260 (dense sand)	Proposed formula for dry or moist granular soil only. k_e values are halved for submerged sands.
Audibert & Nyman (1977) / Needham & Leach (1987)	See Audibert & Nyman (1977)	$k_h = \frac{k_eZ}{D}$ Quoted k_e values are (in kN/m^3): 1170–3530 (loose sand) 3530–11670 (medium sand) 11670–23350 (dense sand)	Proposed formula for dry or moist granular soil only. k_e values are approximately halved (0.6) for submerged sands.
Audibert & Nyman (1977) / Needham & Leach (1987)	See Audibert & Nyman (1977)	$k_h = \frac{2E_s}{1.5D}$	Proposed formula for cohesive soil only. E_s is the soil Young's Modulus from triaxial compression test.
Needham & Leach (1987)	Crofts *et al* (1977)	Empirical k_h values (in kN/m^3): k_h Clay Sand 4000 very soft to soft (c_u<40kN/m^2) very loose to loose 8000 firm (40<c_u<75) medium dense 16000 stiff (75<c_u<150) dense 32000 very stiff or hard (>150) very dense	The results are secant values for an unknown magnitude of displacement.
Pyke & Beikae (1984)	Pyke & Beikae (1984)	k_h (in kN/m^3) ν_s $2.3E_s/D$ 0 $2.0E_s/D$ 0.33 $1.8E_s/D$ 0.5	For laterally loaded pile surrounded by an infinite elastic medium, but allows separation from the back of the pile.
Habibagahi & Langer (1984)	Habibagahi & Langer (1984)	$k_h = \sigma_n / y\left(a + \sqrt{Z/D}\right)$ a is a constant for any given horizontal displacement y and angle of internal friction of soil. For $\phi = 30°$: a y (mm) 5 2.54 9 6.35 12 12.7 15 25.4	Equation based on field load test data for dry to moist granular soils.

Table 2.3. Proposed formulations to determine horizontal spring stiffness k_h for granular and cohesive soils.

Reported by	Original results from	Proposed formulation	Comments
Needham & Leach (1987)	Audibert & Nyman (1977)	$P = \frac{y}{\frac{0.145y_u}{P_u} + \frac{0.855y}{P_u}}$	Model test on laterally loaded pipe in sand.
Trautmann & O'Rourke (1985)	Trautmann & O'Rourke (1985)	$P = \frac{y}{\frac{0.17y_u}{P_u} + \frac{0.83y}{P_u}}$	Full scale laboratory test on laterally loaded pipe in sand.
Georgiadis, Anagnostopoulous & Saflekon (1992)	Georgiadis, Anagnostopoulous & Saflekon (1992)	$P = \frac{y}{\frac{1}{k_i} + \frac{y}{P_u}}$ where k_i is the initial stiffness of the P-y curve.	Centrifugal test on laterally loaded pile in sand.
Gabr, Lunne & Powell (1994)	Gabr, Lunne & Powell (1994)	$P = P_u \tanh\frac{K_{ho}(Z \text{ or } D)}{P_u} y$ where k_{ho} is the coefficient of subgrade reaction (force/ length^3) measure by DMT.	Data from dilatometer tests (DMT) for laterally loaded pile.

Table 2.4. Proposed non-linear P-y curve formulations for lateral soil/pipe movement.

Reported by	Original results from	Proposed formulation	Comments
Needham & Leach (1987)	Audibert & Nyman (1977)	$P_u = \gamma Z N_{qh}$ where γ = soil density For value of N_{qh}, see Fig. 2.27.	N_{qh} is determine from Brinch-Hausen bearing capacity factor (Hansen, 1961) for granular soil.
Trautmann & O'Rourke (1985)	Rowe & Davis (1982b)	$P_u = \gamma Z N_{qh} R_\psi R_R R_K$ where N_{qh} is the basic capacity factor as shown in Fig. 2.28. R_ψ is the correction factor for dilatancy of sand. R_R is the correction factor for pipe roughness. R_K is the correction factor for effect of *in situ* stress state K_0 and may be taken as 1 for practical purpose.	Based on finite element results on friction soil. For smooth plate anchor and assumes no soil dilatancy, the three correction factors R_ψ, R_R and R_K are equal to 1.0.
ASCE (1984) / Trautmann & O'Rourke (1985)	ASCE (1984) / Trautmann & O'Rourke (1985)	$P_u = \gamma Z N_{qh}$ The values of N_{qh} are show in Fig. 2.29.	Results from full scale laboratory test on laterally loaded pipe in sand.
Wilson-Fahmy, Koerner & Sansone (1994)	Jewell (1991)	$P_u = \gamma Z N_{qh}$ where N_{qh} = bearing capacity factor: $N_{qh} = \tan\left(\frac{\pi}{4} + \frac{\phi}{2}\right)\exp\left[\left(\frac{\pi}{2} + \phi\right)\tan\phi\right]$	From pullout test for geogrid. Formula give the ultimate bearing resistance of the transverse ribs.

Table 2.5. Proposed formulations to determine the ultimate pressure for laterally loaded pipe in sand.

Reported by	Original results from	Proposed formulation	Comments
Needham & Leach (1987)	Reese (1958)	$\frac{p_u}{c_u D} = 2 + \frac{\gamma Z}{c_u} + 2\sqrt{2}\frac{Z}{D}$ (2 at G.L. to 12 at $3D$)	For laterally loaded pile in cohesive soil.
Gabr, Lunne & Powell (1994)	Matlock (1970)	$p_u = c_u N_{ch} D$ where $N_{ch} = 3 + \frac{\sigma_n'}{c_u} + J\frac{Z}{D}$ (3 at G.L. to max. 9) $J = 0.5$ for soft clays of Gulf of Mexico and 0.25 for stiffer clays.	Based on the behaviour of laterally loaded piles in soft clay.
Poulos & Davis (1980)	Poulos & Davis (1980)	$\frac{p_u}{c_u D} = 3 + \frac{\gamma Z}{c_u} + 0.5\frac{Z}{D}$ (3 at G.L. to max. 9)	Based on the behaviour of laterally loaded pile in cohesive soil.
Rowe & Davis (1982a)	Rowe & Davis (1982a)	$\frac{p_u}{c_u D} = N_{ch} = 2$ to 11.5 For the value of N_{ch}, see Fig. 2.30.	Based on finite element results of a smooth anchor plate buried in cohesive soil. Results provided in graphical forms and depend on depth of embedment and the state of breakaway at back of pipe.
Randolph & Houlsby (1984)	Randolph & Houlsby (1984)	Smooth pipe: $\frac{p_u}{c_u D} = 9.14$ Rough pipe: $\frac{p_u}{c_u D} = 11.94$ For shallow depth ($Z<3D$): $\frac{p_u}{c_u D} = 2 + \frac{\gamma Z}{c_u} + 1.5\frac{Z}{D}$ For cavity expansion: $\frac{p_u}{c_u D} = 7 + \frac{\gamma Z K_0}{c_u}$	Based on plasticity theory for a rigid disc buried in cohesive soil of infinite depth.
ASCE (1984)	ASCE (1984)	$p_u = c_u N_{ch} D$ where $N_{ch} = 2.8$ to 7.8 (see Fig. 2.27 for the value).	N_{ch} is determine from Brinch-Hausen bearing capacity factor (Hansen, 1961) for cohesive soil.

Table 2.6. Proposed formulations to determine the ultimate pressure for laterally loaded pipe in clay.

Reported by	Original results from	Proposed formulation	Comments
Trautmann, O'Rourke & Kulhawy (1985)	See Trautmann, O'Rourke & Kulhawy (1985)	$N_{qu} = \frac{\exp(2K_a \tan\phi Z/D) - 1}{2K_a \tan\phi Z/D}$ where K_a is the active stress coefficient.	Failure surface reaches ground surface (complete projection condition for buried pipes).
Trautmann, O'Rourke & Kulhawy (1985)	See Trautmann, O'Rourke & Kulhawy (1985)	$N_{qu} = K \tan\phi \frac{Z}{D} + 1 - \frac{\pi D}{8Z}$ where K is the coefficient of *in situ* horizontal soil stress.	Vertical slip surface model. Assumes failure surfaces reach ground surface. Choice of K should reflect density and compaction of soil.
Trautmann, O'Rourke & Kulhawy (1985)	See Trautmann, O'Rourke & Kulhawy (1985)	$N_{qu} \doteq 0.95 \tan\phi \frac{Z}{D} + 1$	Failure surface reaches ground surface (shallow conditions for strip footings).
Trautmann, O'Rourke & Kulhawy (1985)	See Trautmann, O'Rourke & Kulhawy (1985)	$N_{qu} = \left(\frac{2Z}{D} - \frac{H_e}{D}\right)\left(\frac{H_e}{Z}\right)(0.95\tan\phi) + 1$ where H_e is the vertical extent of failure surface, given empirically as: ϕ = 30 35 40 45; H_e/D = 4 5 7 9	Failure surface does not reach ground surface (deep conditions for strip footings).
Trautmann, O'Rourke & Kulhawy (1985)	See Trautmann, O'Rourke & Kulhawy (1985)	N_{qu} given empirically as: ϕ = 30 35 40; N_{qu} = 5.0 7.0 9.7	Limiting deep condition for strip footings.
Trautmann, O'Rourke & Kulhawy (1985)	See Trautmann, O'Rourke & Kulhawy (1985)	N_{qu} is equal to the breakout factor for cylinder depends on ϕ and Z/D ratio:	Based on shallow cavity expansion model assuming plane strain conditions. Failure surface reached ground surface.
Rowe & Davis (1982b)	Rowe & Davis (1982b)	$Q_{uu} = \gamma Z N_{qu} R_\psi R_R R_K$ where N_{qu} is the basic capacity factor as shown in Fig. 2.31. R_ψ is the correction factor for dilatancy of sand. R_R is the correction factor for pipe roughness. R_K is the correction factor for effect of *in situ* stress state K_0 and may be taken as 1 for practical purpose.	Based on finite element results on friction soil. For smooth plate anchor and assumes no soil dilatancy, the three correction factors R_ψ, R_R and R_K are equal to 1.0.
Trautmann, O'Rourke & Kulhawy (1985)	Trautmann, O'Rourke & Kulhawy (1985)	Suggested values of N_{qu} are shown in Fig. 2.32.	N_{qu} is determine from the results of full scale laboratory pipe lifting test in sand.

ϕ	Z/D = 1.0	1.5	2.5	5.0
30	1.08	1.45	2.03	3.30
40	1.19	1.61	2.30	3.83
50	1.25	1.70	2.44	4.12

Table 2.7. Proposed formulations to determine the dimensionless factor for the ultimate pressure for upward movement of pipe in sand.

Reported by	Original results from	Proposed formulation	Comments
Needham & Leach (1987)	Terzaghi (1955)	$k_{vd} = \frac{0.203 k_{si}}{D}$ where k_{si} is the subgrade reaction for a 1ft² plate.	
Needham & Leach (1987)	Vesic (1961)	$k_{vd} = \frac{0.65}{D} \sqrt[12]{\left(\frac{E_s D^4}{E_p I_p}\right)} \frac{E_s}{\left(1-\nu_s^2\right)}$	
Needham & Leach (1987)	Janbu, Bjerrum & Kjaernsli (1956)	$k_{vd} = \frac{E_s}{\mu_0 \mu_1 D}$ where μ_0 and μ_1 are influence terms depend on the cover depth and pipe diameter.	The product $\mu_0\,\mu_1$ for deformation beneath the pipe is typically 0.75, corresponding to a pipe of infinite length with burial depth of $2D$. Therefore: $k_{vd} \approx \frac{1.3 E_s}{D}$

Table 2.8. Proposed formulations to determine the linear springs stiffness for the downward movement of pipe.

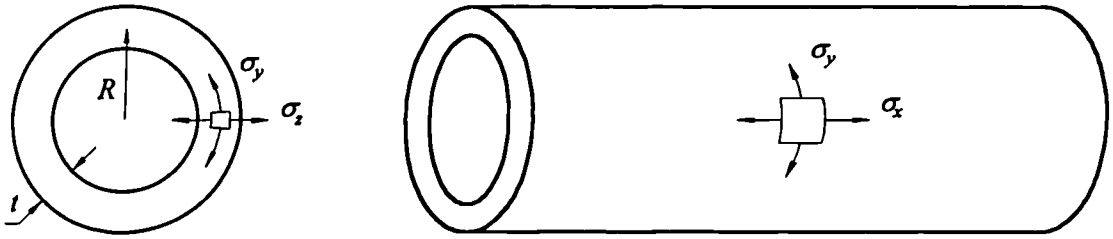

Fig. 2.1. Principal stresses of a cylindrical pipe.

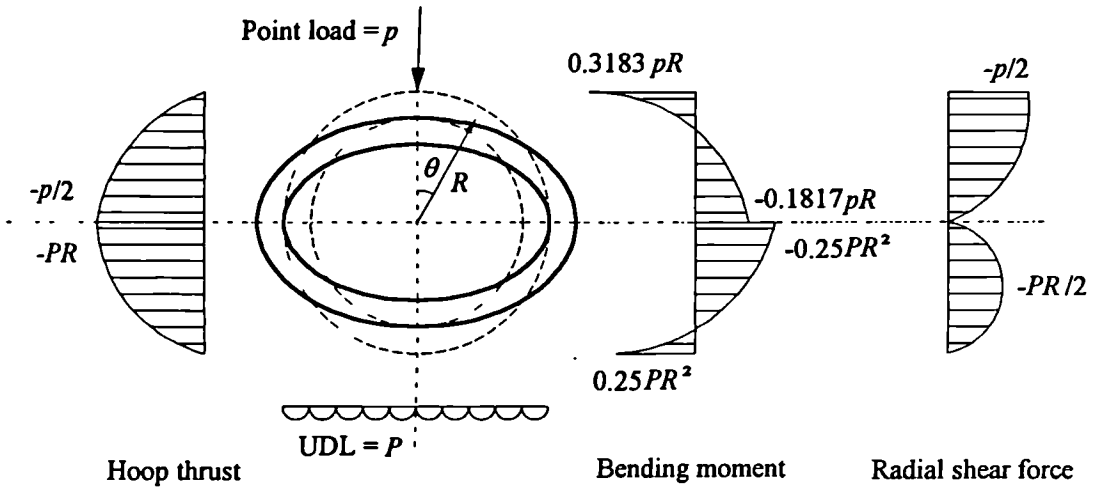

Fig. 2.2. Deformation and stresses in a pipe induced by crushing.

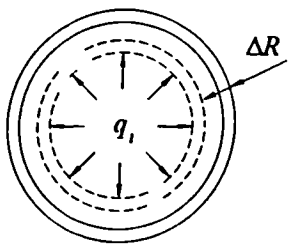

Fig. 2.3. Deformation and stresses in a pipe induced by uniform radial internal pressure.

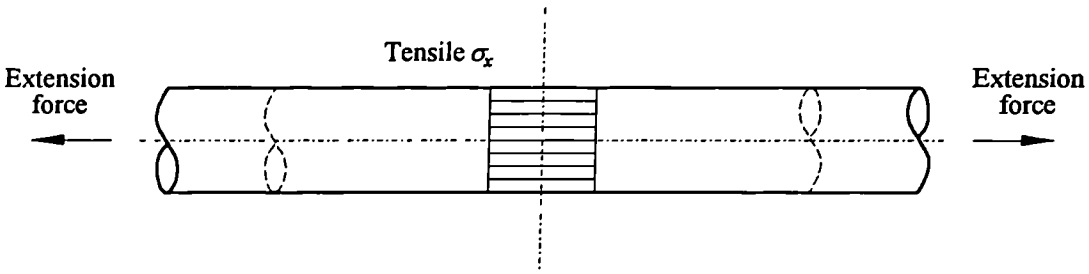

Fig. 2.4. Deformation and stresses in a pipe induced by longitudinal extension.

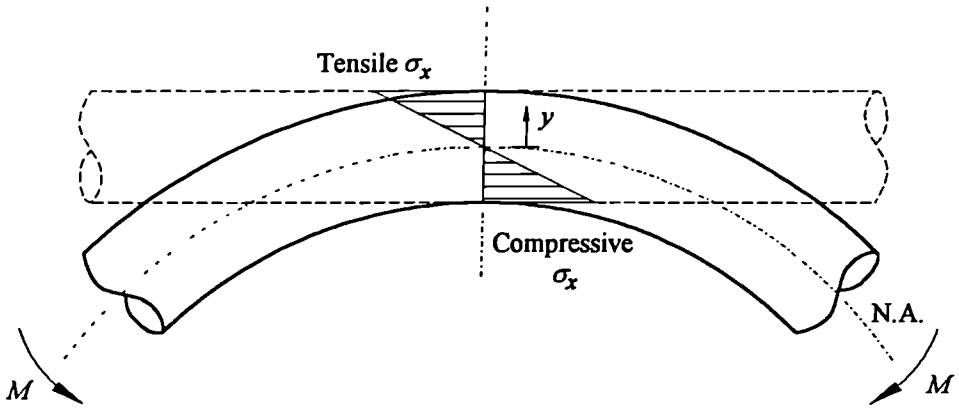

Fig. 2.5. Deformation and stresses in a pipe induced by longitudinal bending.

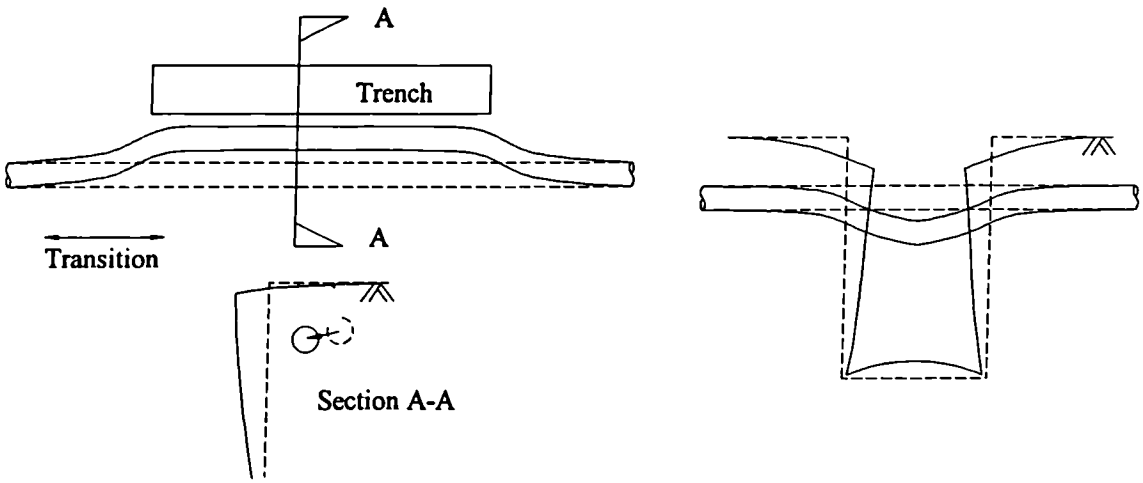

(a) Pipe parallel to trench

(b) Pipe crossing trench

Fig. 2.6. Ground and pipe deformation due to trench excavation.

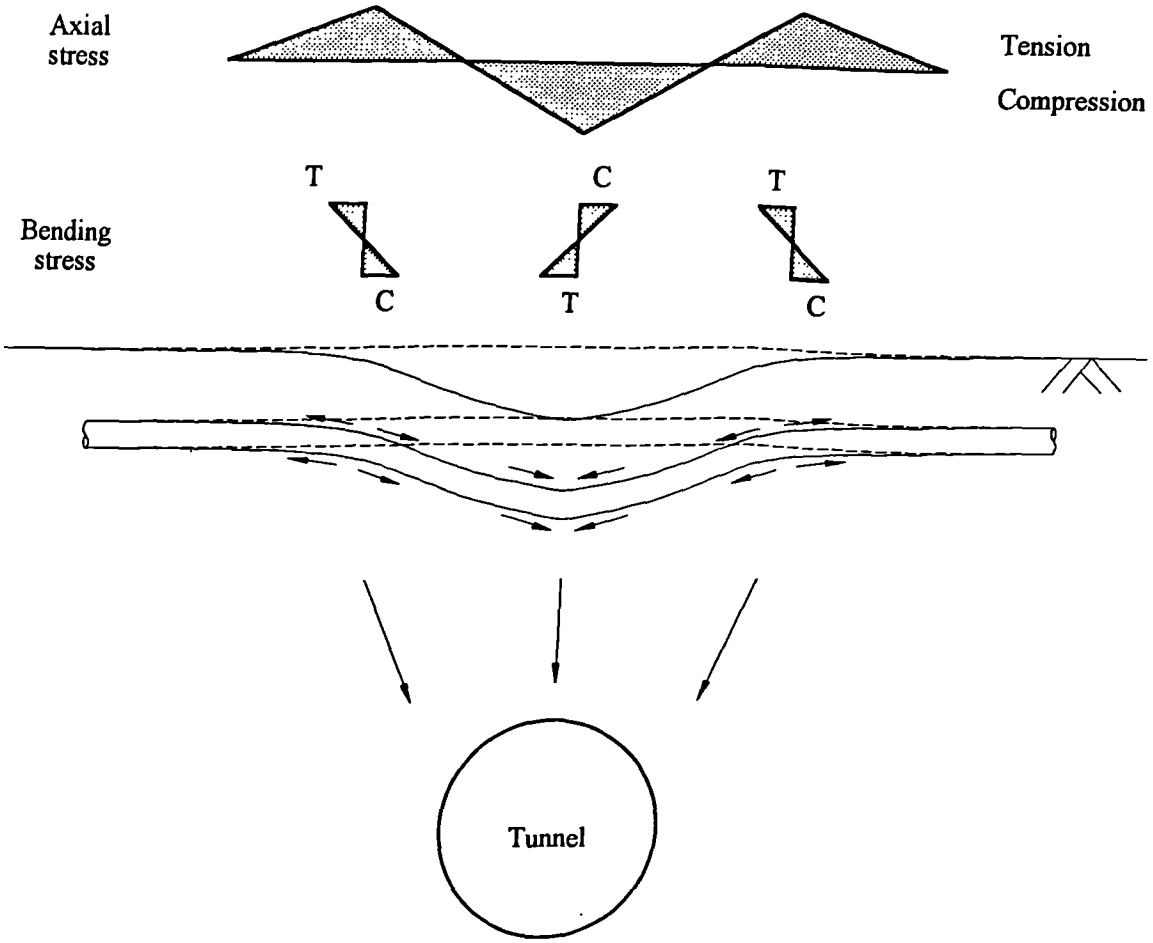

Fig. 2.7. Ground and pipe deformation due to soft ground tunnelling.

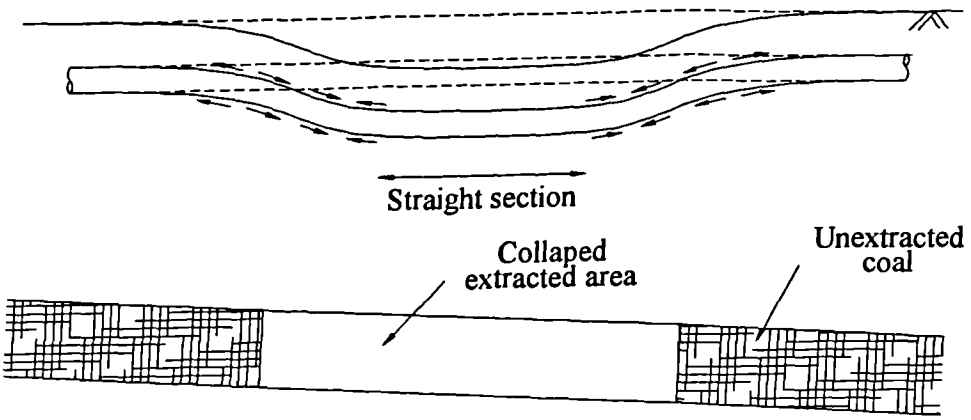

Fig. 2.8. Ground and pipe deformation due to longwall coal mining.

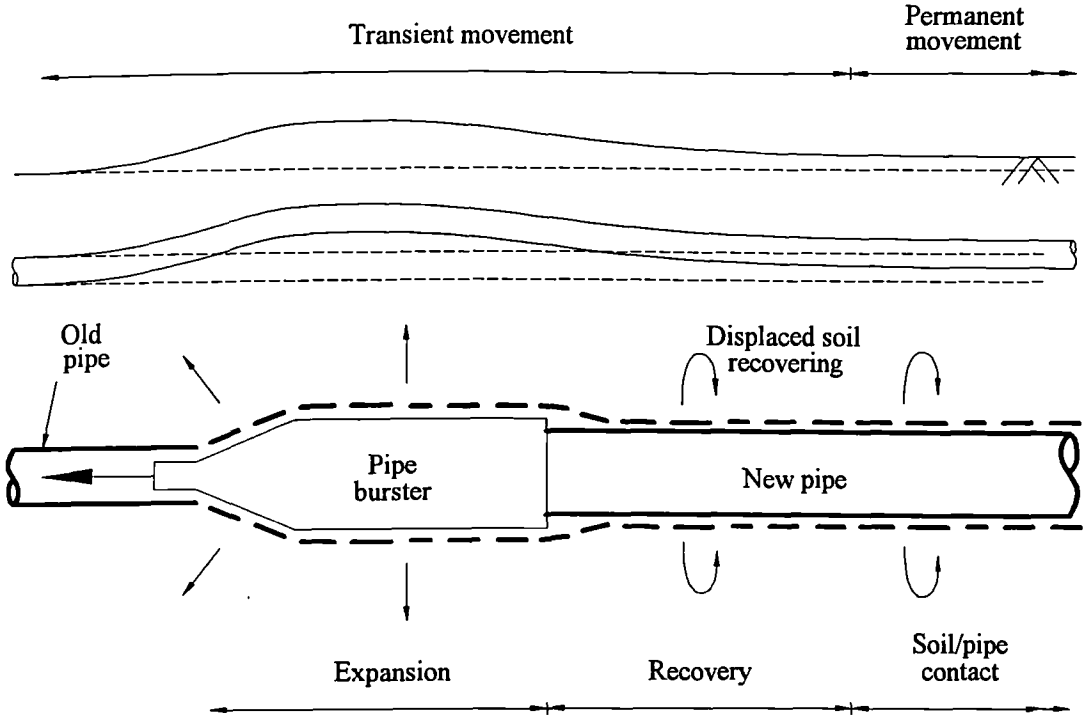

Fig. 2.9. Ground and pipe response along the line of pipe bursting.

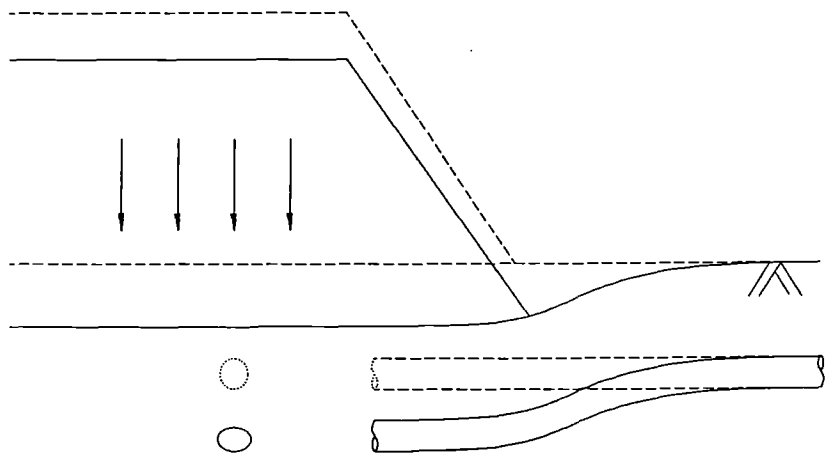

Fig. 2.10. Ground and pipe deformation due to embankment construction.

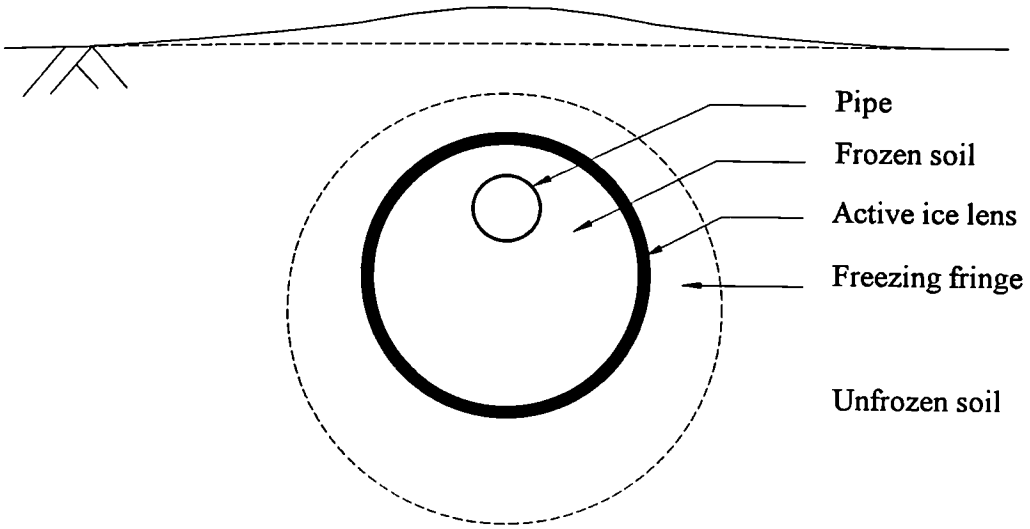

Fig. 2.11. Ground heave caused by active ice lenses (after Nixon, 1992).

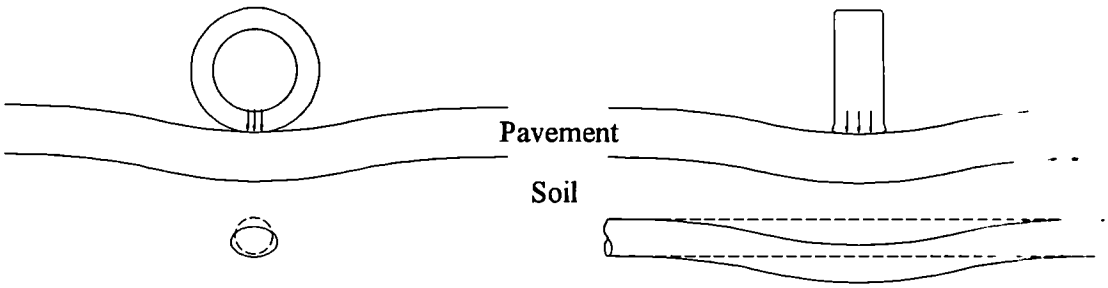

Fig. 2.12. Ground and pipe deformation due to traffic loading.

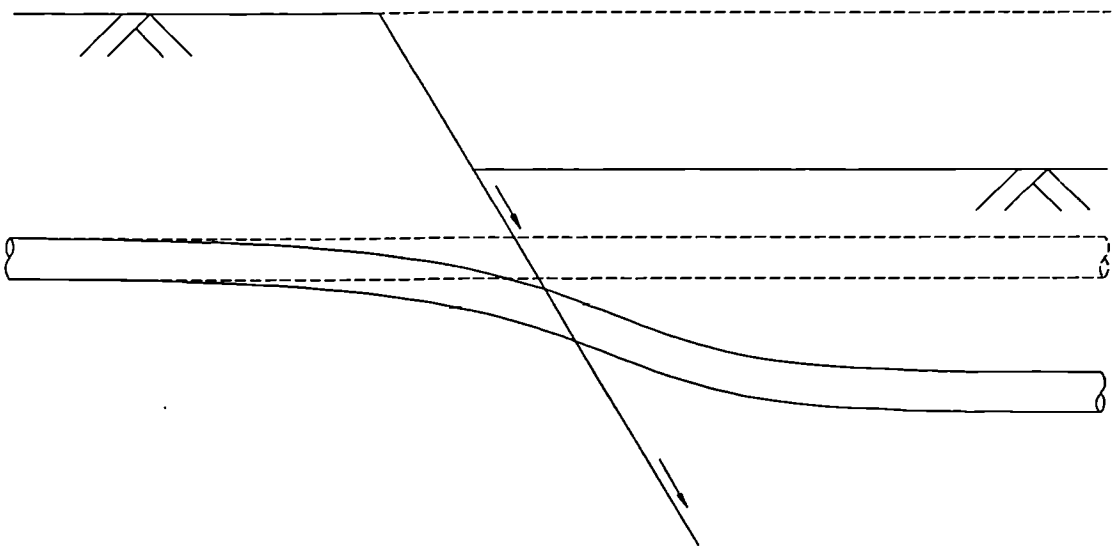

Fig. 2.13. Ground and pipe deformation due to fault movement.

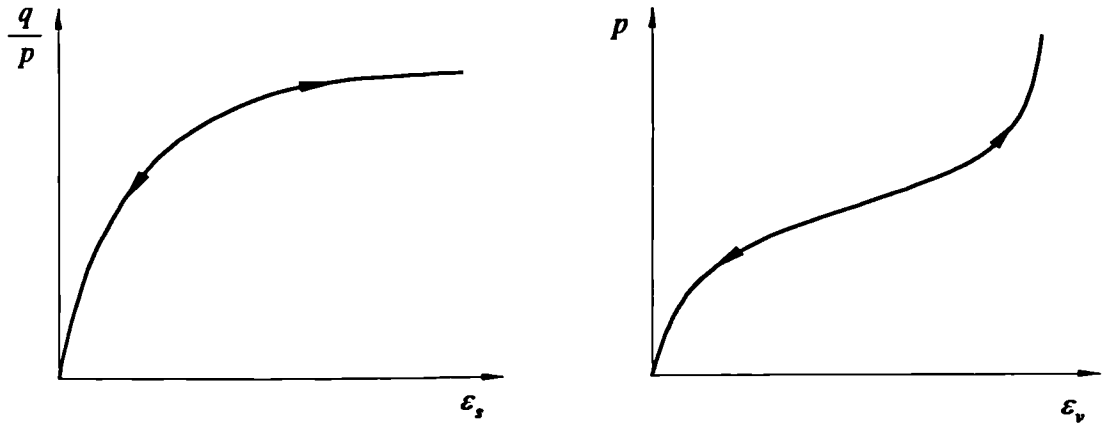

(a) (b)

Fig. 2.14. Stress-strain relationships of the British Gas Non-linear Elastic model.

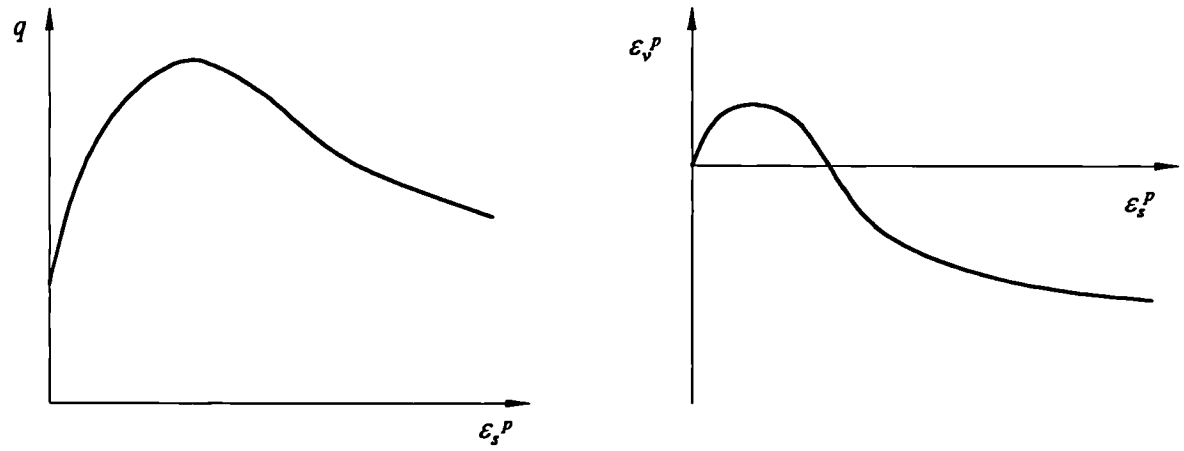

Fig. 2.15. Stress-strain relationships of the British Gas Elasto-plastic model.

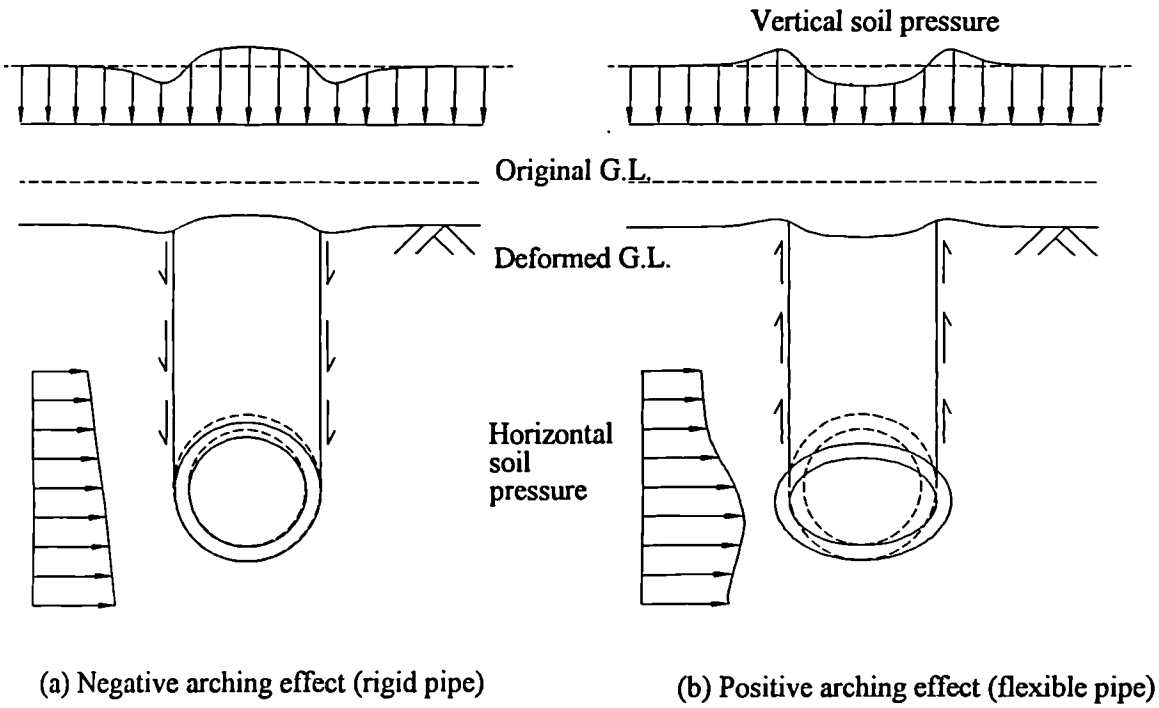

Fig. 2.16. Load distribution and ground settlement profile due to negative and positive arching effect.

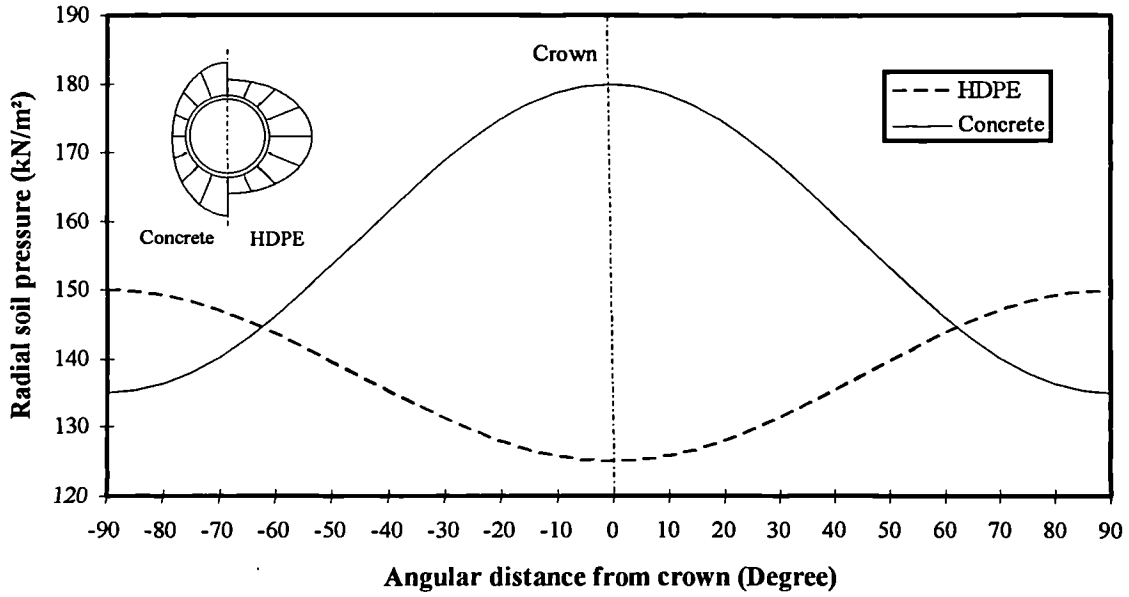

Fig. 2.17. Typical radial stress distribution of rigid and flexible pipe due to overburden pressure (after Chua & Lytton, 1989).

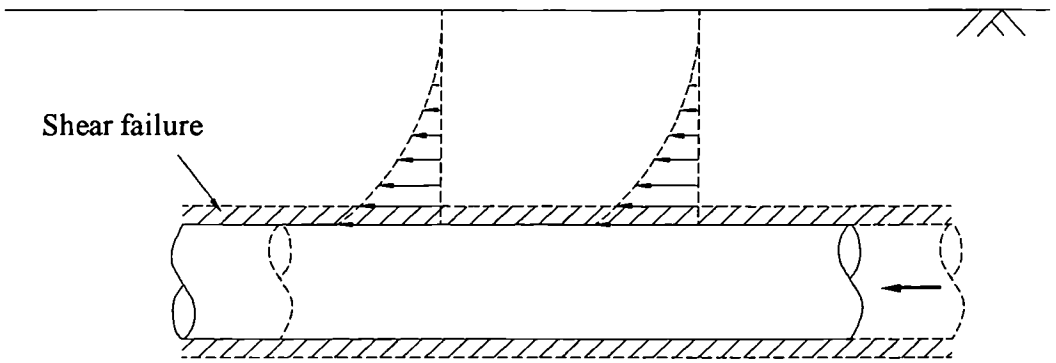

Fig. 2.18. Ground behaviour due to axial pipe movement (after Herbert & Leach, 1990).

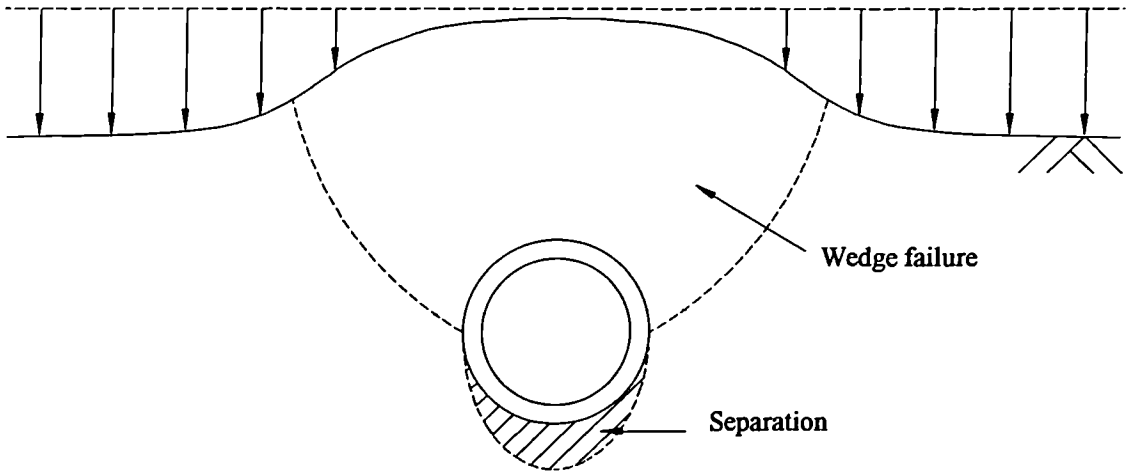

Fig. 2.19. Ground behaviour due to settlement around stationary pipe.

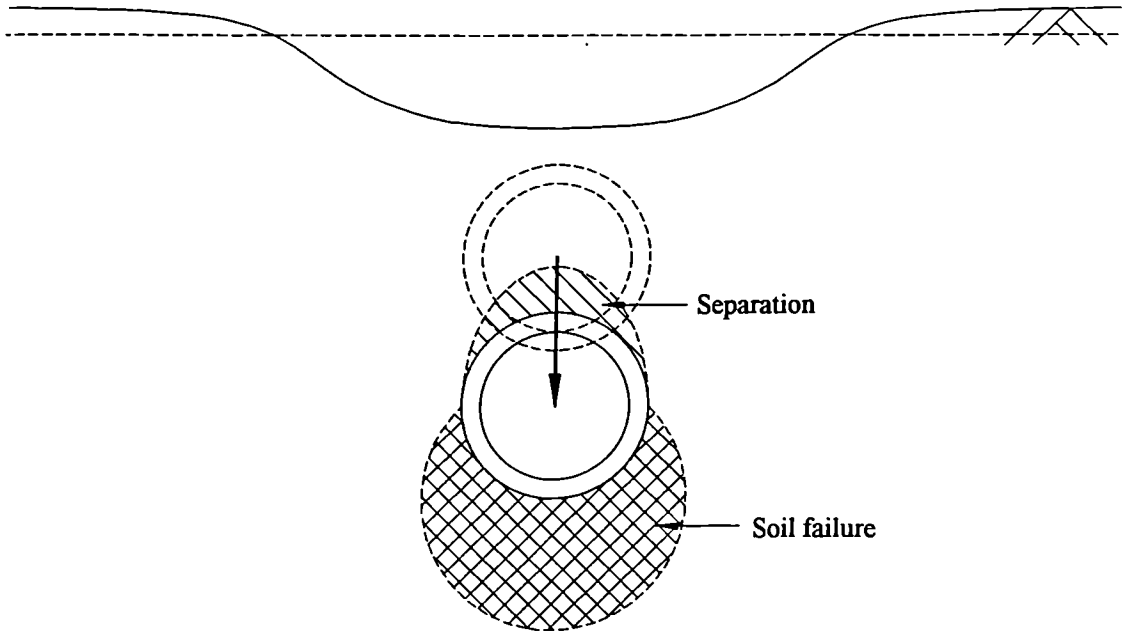

Fig. 2.20. Ground behaviour due to downward pipe movement.

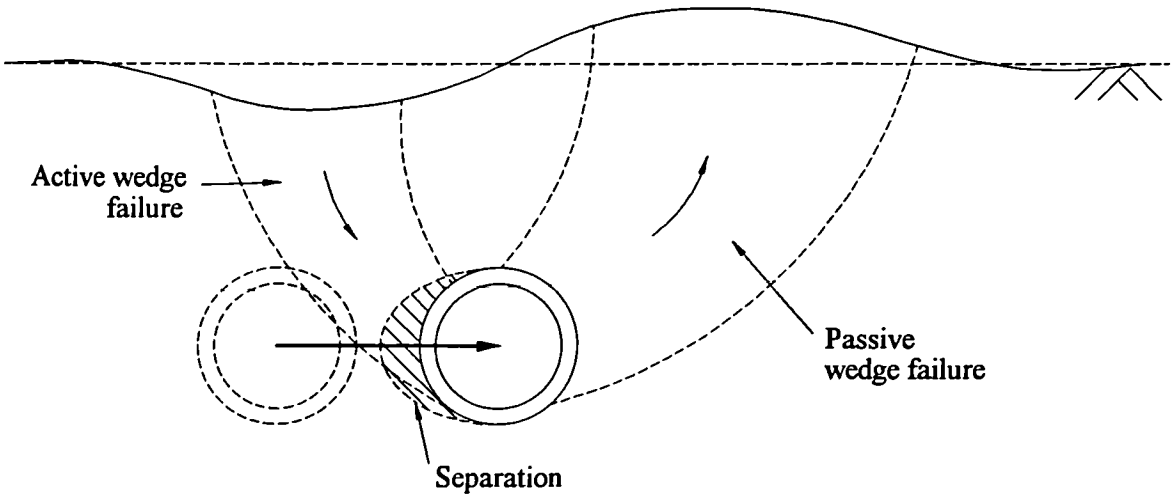

Fig. 2.21. Ground behaviour due to horizontal pipe movement.

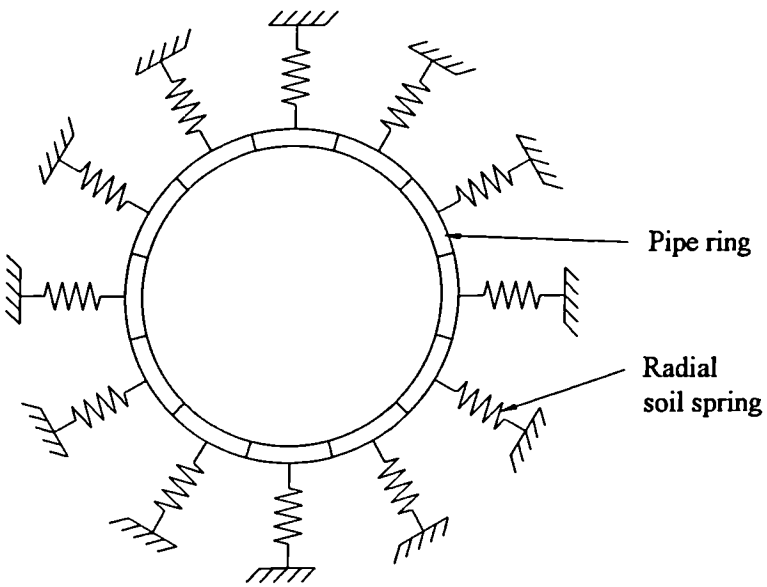

Fig. 2.22. Circular ring on springs model for buried pipeline.

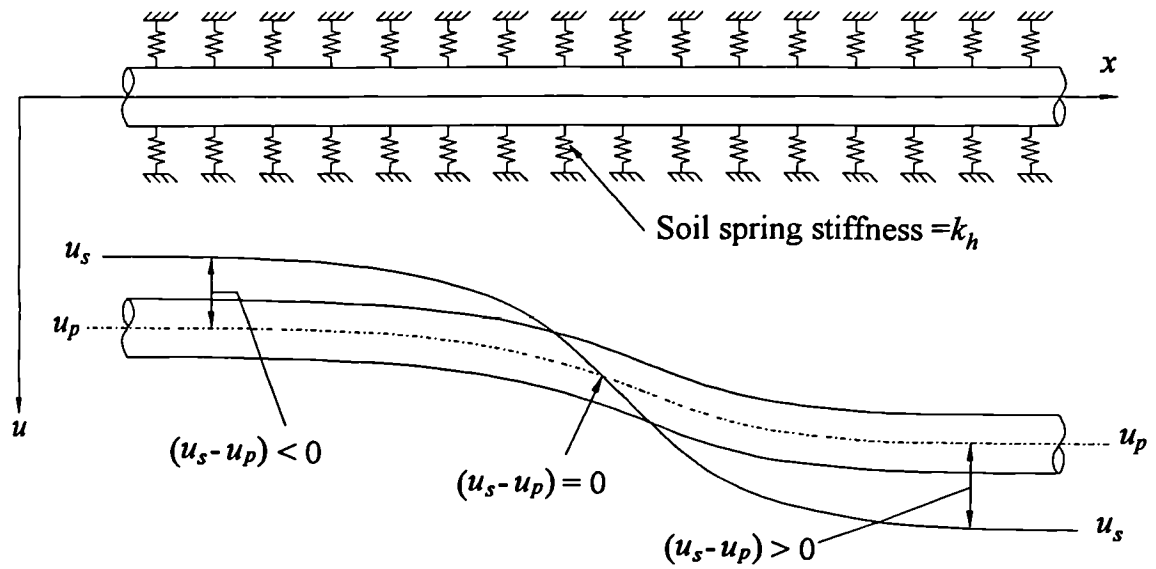

Fig. 2.23. Longitudinal bending of pipe due to soil displacement loading.

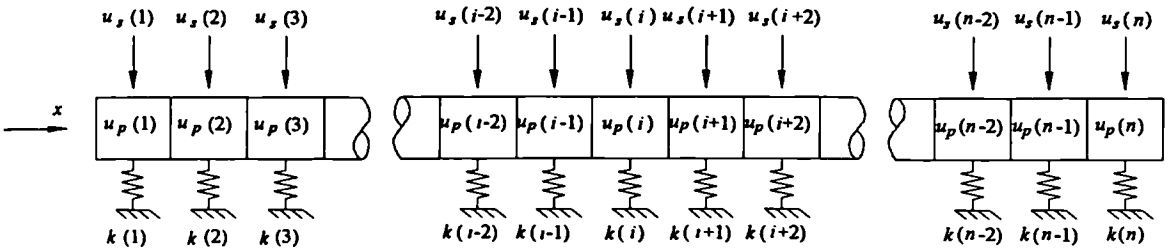

Fig. 2.24. Subdivision of pipeline for finite difference approach.

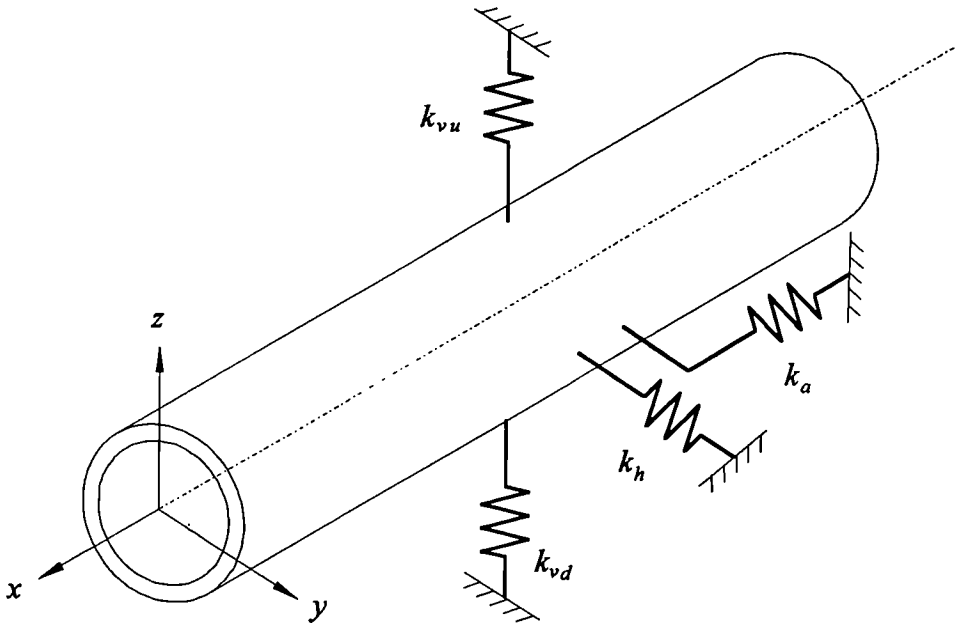

(a) Idealized 3-D beam on elastic foundation model

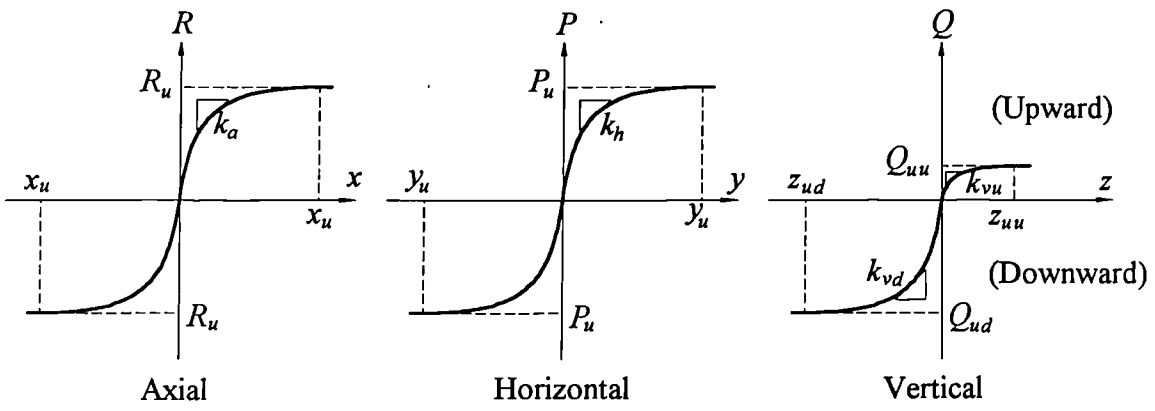

(b) Typical load-deformation relationship for the soil springs

Fig. 2.25. Idealized three-dimensional soil spring model to represent the actual soil restraint (after ASCE, 1984).

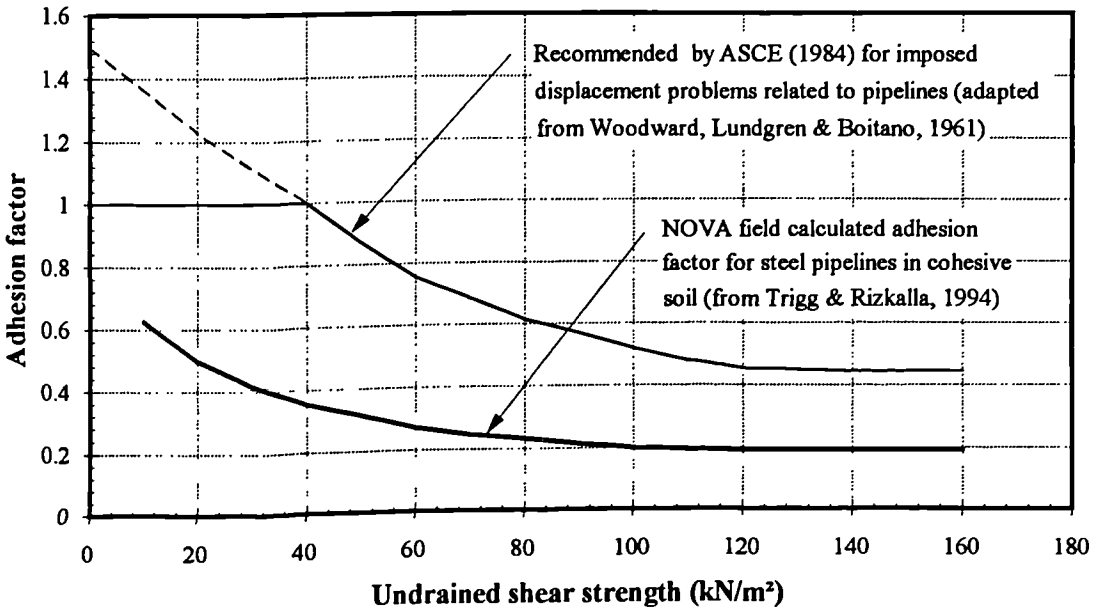

Fig. 2.26. Adhesion factor as a function of undrained shear strength of soil (after ASCE, 1984 and Trigg & Rizkalla, 1994).

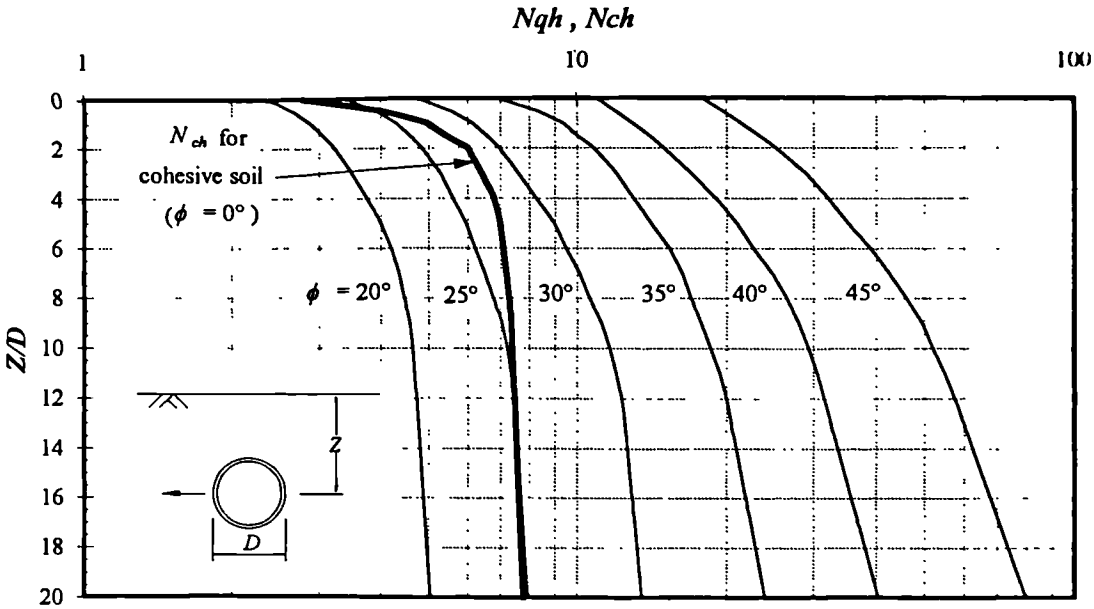

Fig. 2.27. Horizontal bearing capacity factors as a function of embedment ratio for pipelines buried in sand and clay with different values of ϕ based on Hansen (1961) (after ASCE, 1984).

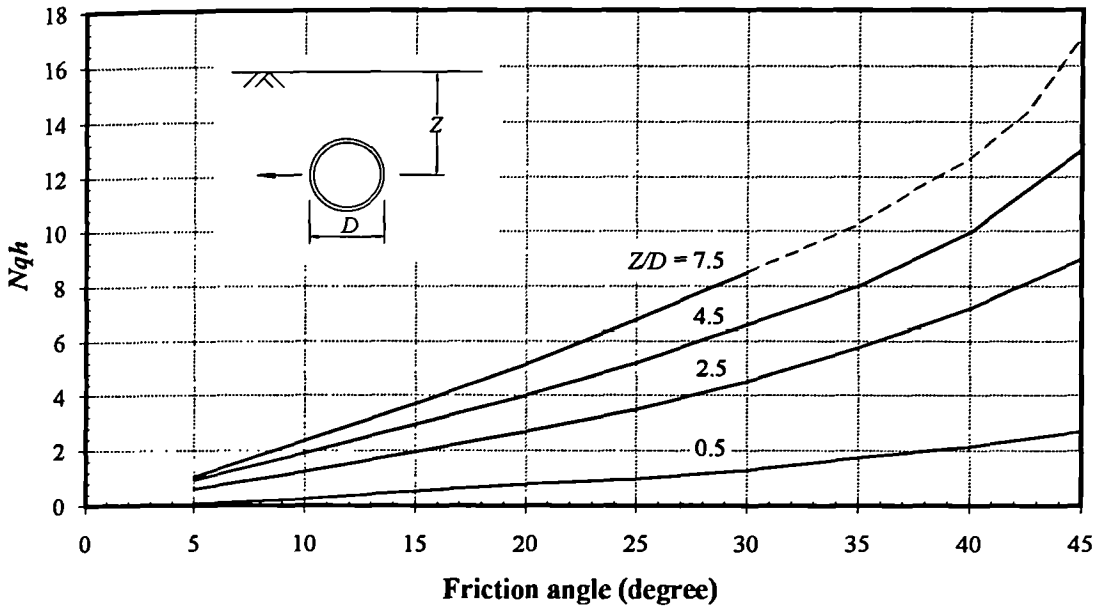

Fig. 2.28. Variation of bearing capacity factor N_{qh} with ϕ (after Rowe & Davis, 1982b).

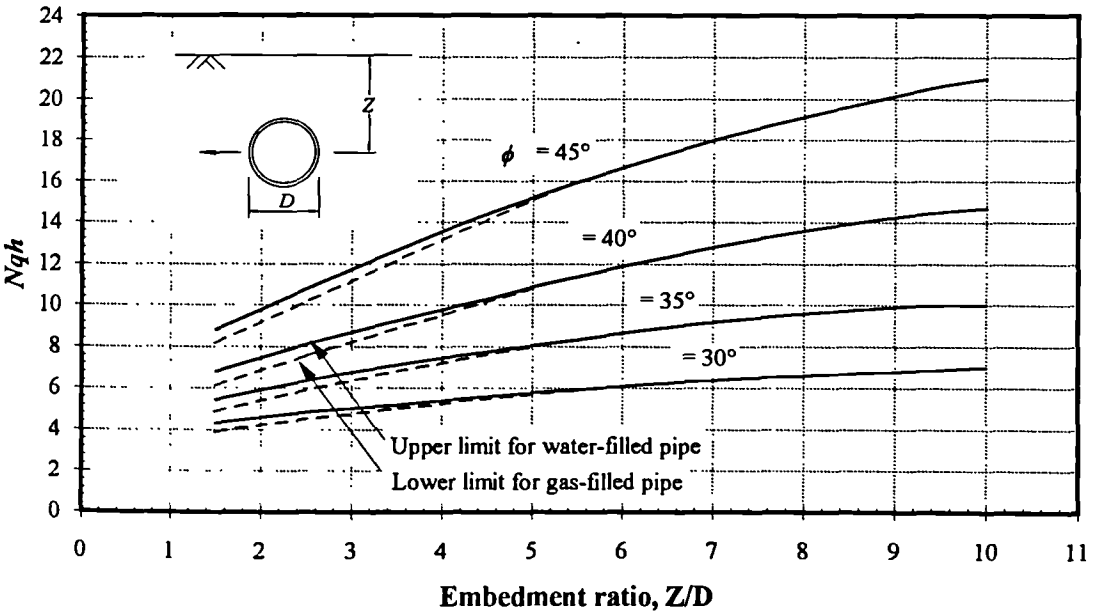

Fig. 2.29. Variation of horizontal bearing capacity factor for sand with embedment ratio (after ASCE, 1984).

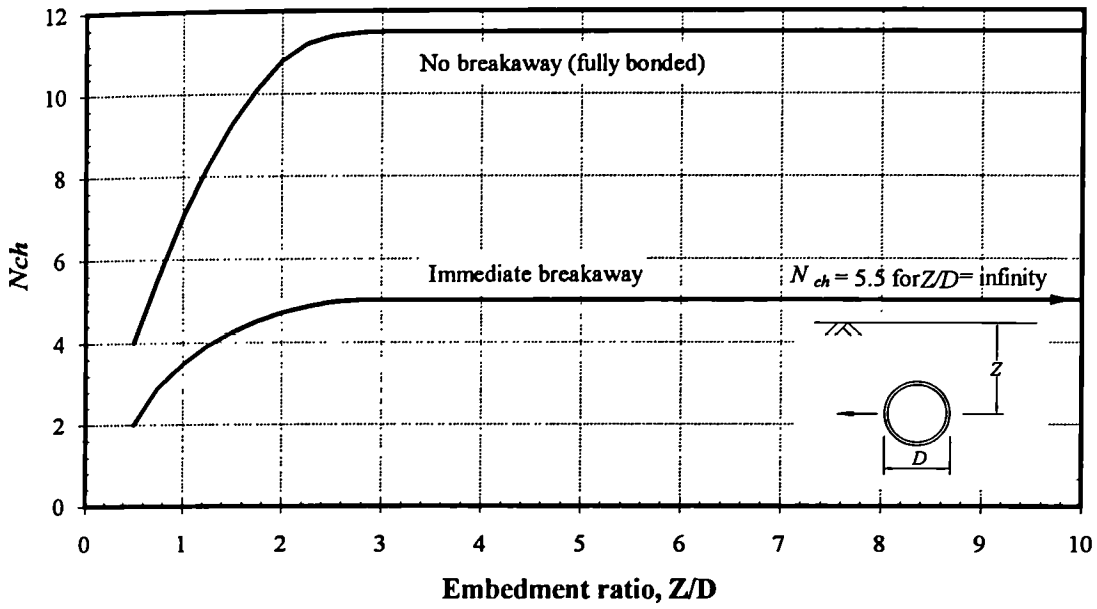

Fig. 2.30. Variation of the bearing capacity factor N_{ch} with embedment ratio (after Rowe & Davis, 1982a).

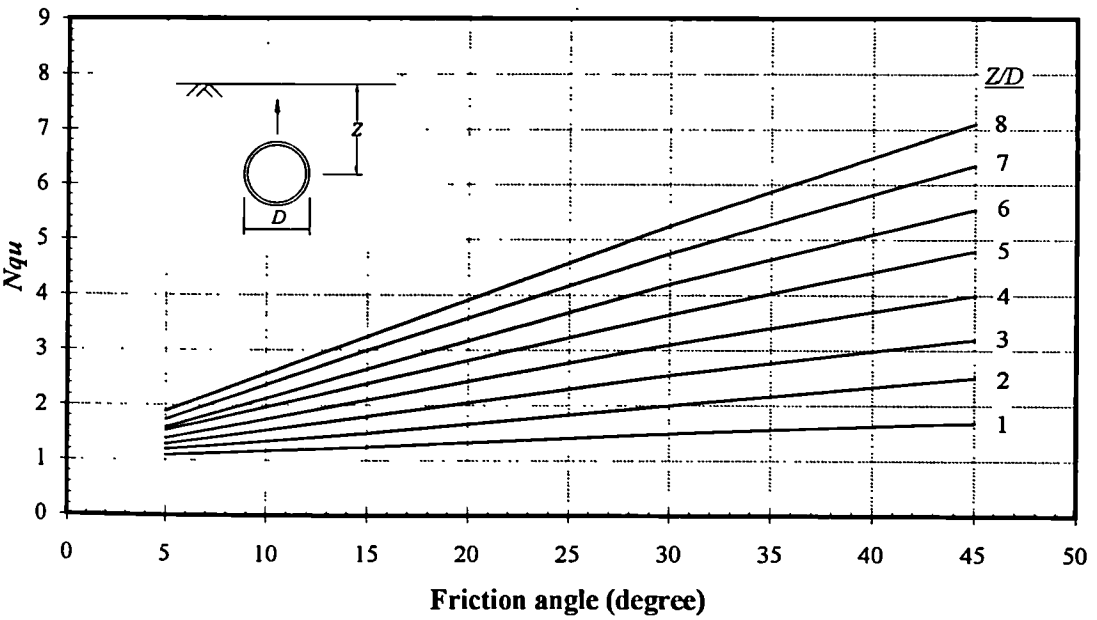

Fig. 2.31. Variation of bearing capacity factor N_{qu} with ϕ (after Rowe & Davis, 1982b).

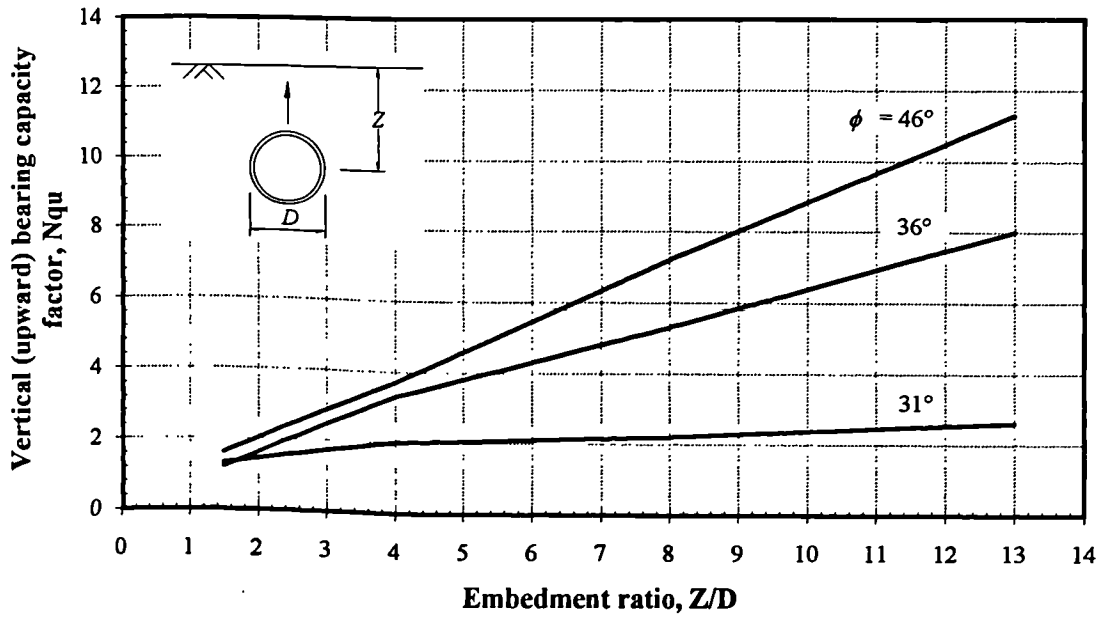

Fig. 2.32. Variation of vertical (upward) bearing capacity factor N_{qu} with embedment ratio for gas filled pipe (after Trautmann, O'Rourke & Kulhawy, 1985).

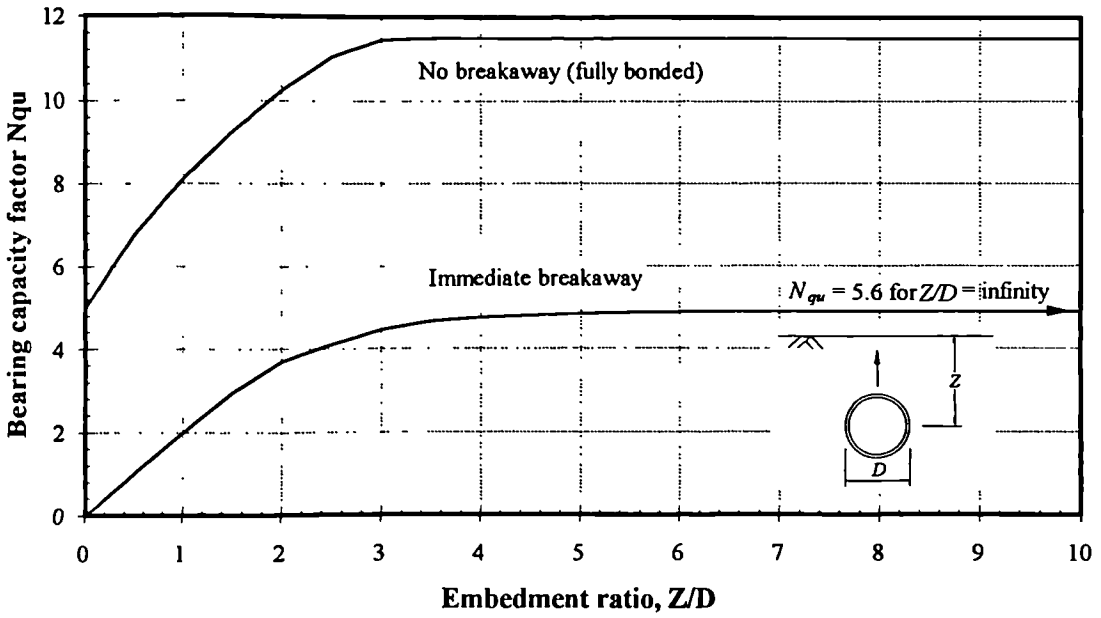

Fig. 2.33. Variation of the bearing capacity factor N_{qu} with embedment ratio (after Rowe & Davis, 1982a).

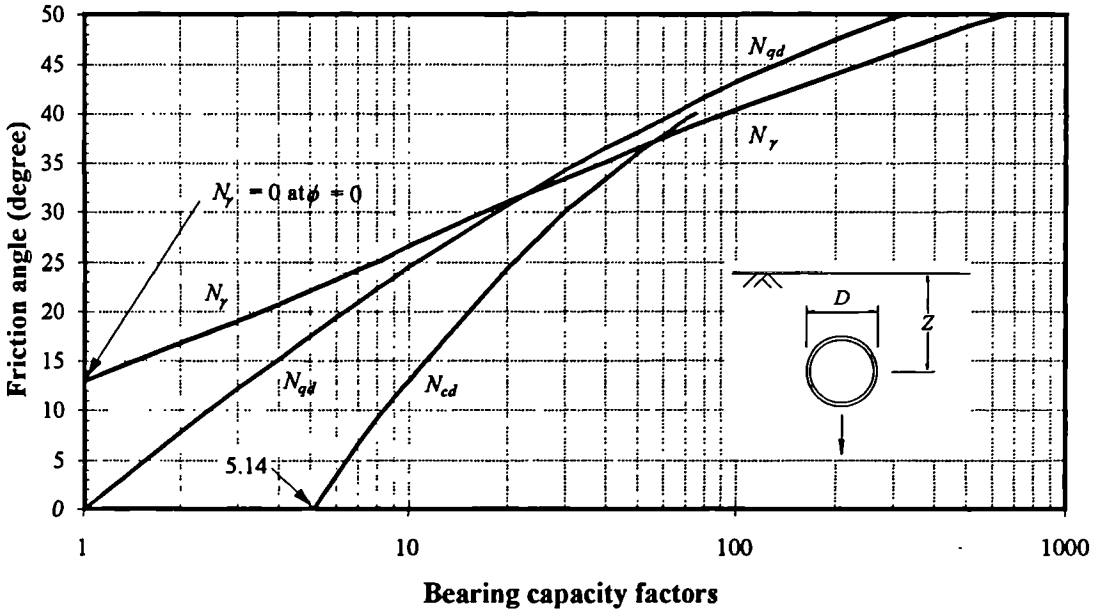

Fig. 2.34. Variation of vertical (downward) bearing capacity factors with ϕ (after Craig, 1992).

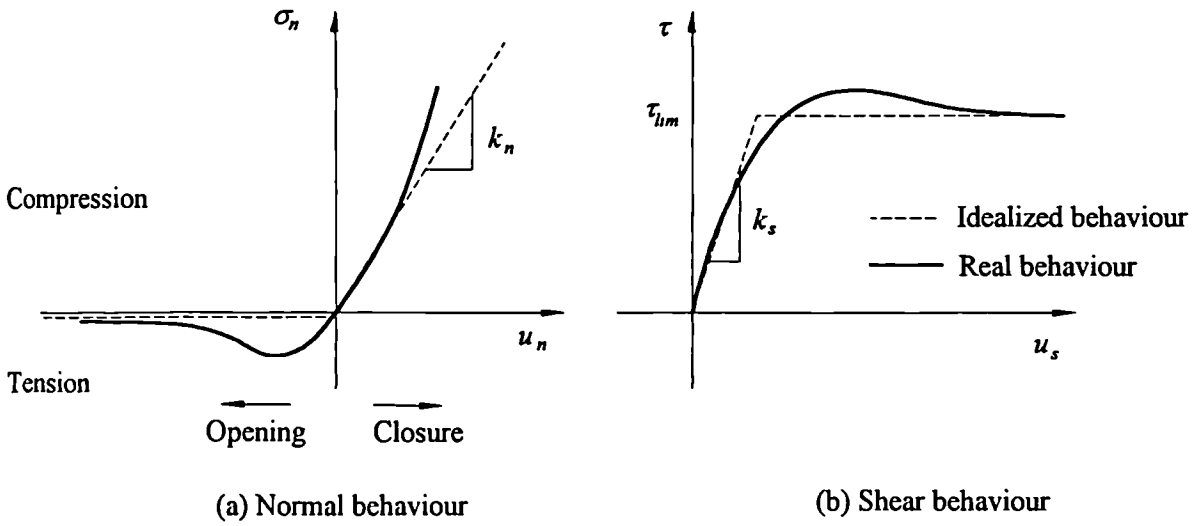

(a) Normal behaviour

(b) Shear behaviour

Fig. 2.35. Stress-strain relationships at soil/structure interface (after Desai & Nagaraj, 1988).

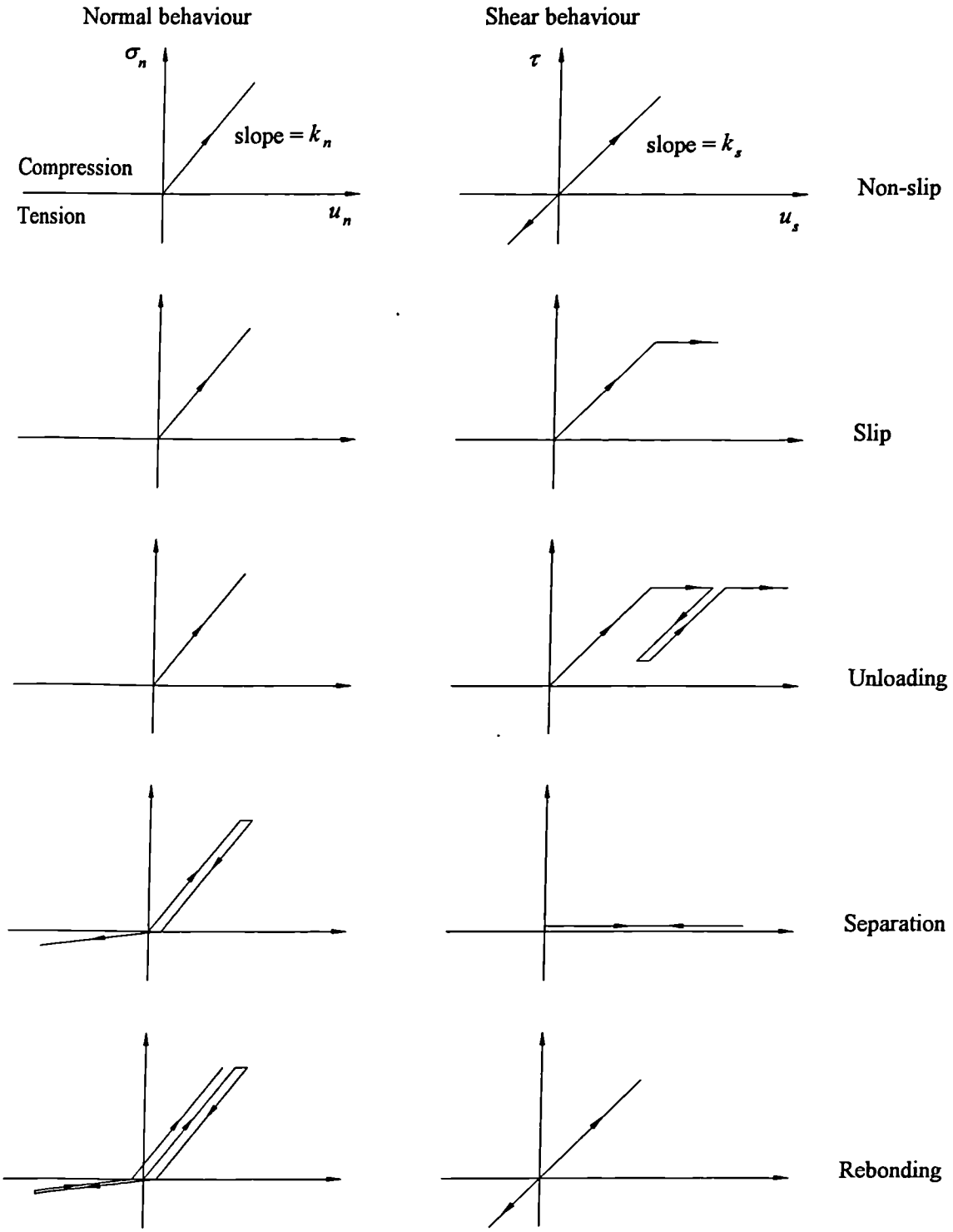

Fig. 2.36. Modes of behaviour at soil/structure interface.

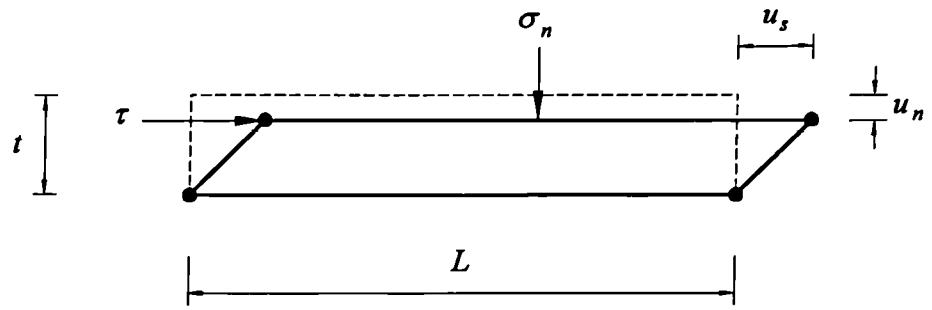

Fig. 2.37. Deformations of interface element due to normal stress and shear stress.

CHAPTER 3

CASE HISTORY: HILDERSTONE PIPE LOADING TESTS

3.1. Introduction

In order to provide direct fundamental data on the soil/pipe interaction behaviour of a buried pipeline, British Gas has conducted field tests on its own pipeline system. A series of field load tests have been performed at a location north-west of Hilderstone, Staffordshire in 1988 on a 36" (0.9144m) diameter submerged-arc welded pipeline. The pipe was made from steel material grade X60 conforming to British Gas Engineering Standard BGC/PS/LX1. A section of this transmission pipeline was isolated by two test pits A and C which were 100m apart as shown in Fig. 3.1. The geometry of the cross-section at the site was established from vertical dynamic cone penetration test results obtained with a Mackintosh probe and site photographs (Leach & Row, 1991). It was found that the pipeline was buried in a V-shaped trench of backfill material at a cover depth of 0.9m and surrounded by natural ground and a stronger clay material at a depth of 2.6m as shown in Fig. 3.2.

The results of two load tests (axial and lateral push tests) and laboratory tests to determine the soil properties are reported in this chapter and the results used for the numerical simulation in Chapters 6 and 7 to validate the predictive techniques described in Sections 2.6.2.3 and 2.6.3.1 for axial and lateral soil/pipe interactions respectively.

The pipe loading tests described in Section 3.2 and the laboratory testing for soil in Section 3.3.1 were conducted by British Gas. The data processing from the loading tests and the stress path tests described in Section 3.3.2 were carried out by the Author for this research.

3.2. Pipe Loading Tests

3.2.1. Axial Push Test

The objective of the test is to provide a shear stress/displacement relationship between the soil and the pipe. A total of twenty-four strain gauges were installed on the inner pipe wall of the test section for the measurement of longitudinal strain variations. The gauges were divided into eight groups (A to H), each group having three gauges arranged as shown in Fig. 3.3. Three LVDTs (Linear Voltage Displacement Transducer) were fitted at the two cut ends of the pipe with one at the loading end (pit A) and two at the free end (pit C) to measure the axial pipe displacement. Axial load was applied incrementally, in three stages (0 - 1000kN, 1000 – 2000kN and 2000kN to failure), by a loading system consisting of four hydraulic rams fitted in pit A.

The results of the tests, after making all the necessary corrections to the raw data to allow for initial readings and voltage variation, are presented in Figs 3.4 to 3.7. It should be noted that the results presented only consist of results from stage 3 (2000kN to failure) because the results of stages 1 and 2 were not available. Figure 3.4 shows the relationship between axial pipe displacement at the two ends and the applied loading. A maximum load of approximately 3800kN was reached before slippage occurred between the pipe section and the soil.

Figure 3.5 shows the variation of average axial strain (average of the three strain gauge readings at the particular section) along the length of the pipe at selected loads. The variation of axial strain at different locations is shown in Fig. 3.6. The negative strain readings (representing extension of the pipe section) at location H, which was at the edge of the test pit, may be caused by soil movement adjacent to the unsupported pit during the test.

By considering the axial strain distribution along the pipe and assuming linear variation between the strain gauges (Fig. 3.5), the shear stress mobilized between the strain gauge sections and the corresponding displacement of the section can be found. Figure 3.7 shows the relationship between the calculated shear stress and the pipe displacement at different loadings for all the sections (A to H). From Fig. 3.7, it can be seen that the shear stress distribution was quite scattered near failure, the data falling into two distinct bands. The upper band contains results from pipe sections A-B and C-D whilst the lower band consists of results from other sections. It can be seen, in Fig. 3.5 that the slope of the strain distribution at sections A-B and C-D is steeper than elsewhere, indicating that more load is carried between these sections. This may be due to variation of soil properties along the pipe, where the soil at Sections A-B and C-D are much stronger (shear stress = 23kN/m^2) and the rest are much weaker (shear stress = 13kN/m^2), as shown in Fig. 3.7. The geotechnical site investigation (Leach & Row, 1991) shows that the materials near the two pipe ends were different from each other, indicating that the shear strength of the soil may also be different. Another reason for the scattered shear stress distribution is the possible longitudinal bending of the pipe (a sine curve like bending profile may occur when pushing a long slender pipe) and induced additional strain in the pipe.

3.2.2. Lateral Push Test

The objective of the test is to provide a lateral load/displacement relationship (p-y curve) for the buried pipe. The test was carried out using the same pipe section as the axial push

test (the axial push test was carried out first). In addition to the twenty-four strain gauges fixed on the inner pipe wall, a rigid beam carrying ten LVDTs was mounted along the centre line of the pipe. The LVDTs were placed horizontally to the front and back of the pipe wall to measure the lateral displacement of the pipe, as shown in Fig. 3.8.

A rigid cross-brace was placed inside the pipe at the point where the loading was applied to avoid buckling of the pipe near the edge (see Fig. 3.8). Horizontal loading was applied incrementally by a single hydraulic ram fitted in pit A with a special semi-circular loading saddle which fitted the pipe's diameter. Details of the testing apparatus and the set-up have been reported by Booth (1991).

When the applied loading reached approximately 630kN, the loading ram reached its travel distance limit. The system was totally unloaded to reset the loading ram and then reloaded again. The test was terminated at a loading of approximately 735kN to avoid damage to the pipe. From photographs taken on site, a gap formed between the soil and the back of the pipe near the loading end at higher load.

Figure 3.9 shows the displacement profile along the length of the pipe at selected loadings. Figure 3.10 shows the load/displacement relationship positions at LT1 to LT6. From the displacement profiles at the front and back of the pipe (Fig. 3.9), it can be seen that the circular cross-section of the pipe turned to oval under the applied loading with a maximum ovality of about 1%. The variation of bending strain along the length of the pipe at selected loadings is shown in Fig. 3.11 and the variation of bending strain at location B is shown in Fig. 3.12.

From the bending strain distribution (Fig. 3.11), the variation of bending moment along the pipe can be obtained by:

$$M = \frac{2E_p I_p \times (\varepsilon \times D/d)}{D} \tag{3.1}$$

where d is the inner diameter of the pipe and the term D/d is a correction factor for the strain because the strain readings were at the inner wall of the pipe but the bending strain at the extreme fibres is required. Figure 3.13 shows the variation of the calculated bending moment along the pipe at selected loadings.

It should be noted that the straight lines joining the data points for the strain and bending moment distributions in Figs 3.11 and 3.13 are not representing the real shape of the strain and bending moment distributions. It is appreciated that the distributions between the data points are not linear and should be a smooth curve passing through the data points. There is no intention to assume the shape of the distribution of results and the straight lines are used so that the results stand out more clearly.

From sets of bending moment curves at different loadings, values of soil resistance p and pipe deflection y at points along the pile can be obtained by solving:

$$p = \frac{d^2 M(x)}{dx^2} \tag{3.2a}$$

$$y = \iint \frac{M(x)}{EI} \tag{3.2b}$$

where x is the horizontal distance from the loading end.

The first six values of the bending moment data, along with the known moment of zero at the loading end, have been fitted with a fifth degree polynomial. The polynomial expressions were twice differentiated (Eq. 3.2a) to obtain soil resistance p and then divided by the pipe diameter D to obtain the soil pressure P. Pipe deflection was obtained directly from the field test (Table 3.1) rather than solving Eq. (3.2b). A similar method was used by Brown & Shie (1990) to obtain p-y curves for a laterally loaded pile. Plotted on Fig. 3.14 are the calculated P-y curves at various locations along the pipe. The diversity of the curves at small displacement may be due to the deficiency of the number of strain gauges fixed near the loading end such that the polynomial fitted to the bending moment data was not very accurate. It seems more appropriate to use the results from the small displacement part of

the pipe (say at $x = 4.5$m) for the initial part of the *P-y* curve and for the final parts of the curve to use the results from that part of the pipe undergoing large displacement (at $x = 0.5$m) as shown in Fig. 3.14. The back-calculated *P-y* curve does not reach an ultimate pressure near the end but shows a gradual increase in soil pressure. There are two explanations for this:

i. This portion of the curve was calculated using the data from the reloading curves which may influence the soil behaviour due to the soil hysteresis (Fig. 3.10) and cause the discontinuity of the *P-y* curve.

ii. The pipeline was transited from the backfill to the stronger natural ground which thus gave a much higher reaction onto the pipe.

One of the centrifuge model test results on a laterally loaded pipe by Rizkalla, Poorooshasb & Clark (1992) also showed an increase in reaction on the pipe at the end of the *P-y* curve, and they suggested a similar reason to the latter explanation stated above.

Three of the non-linear *P-y* curve formulations summarized in Table 2.4 have been used to fit a hyperbolic curve to represent the *P-y* curve from the field test (the average curve in Fig. 3.14). The end portion of the *P-y* curve derived from the field test has been ignored in the curve fitting process due to the uncertainty mentioned. The P_u was taken as 190kN/m^2, y_u as 0.15m and k_i as 13823kN/m^3. The fitted curves are shown in Fig. 3.15. The formulation suggested by Georgiadis *et al* (1992) gives the worst fit to the field data. On the other hand, the formulations by Audibert & Nyman (1997) and Trautmann & O'Rourke (1985) both give good fit to the field data but the latter is slightly better.

3.3. Laboratory Testing for Soil

3.3.1. Previous Laboratory Tests

A geotechnical site investigation was carried out by Leach & Row (1991) to supplement the full scale loading tests. The purpose of the investigation was to quantify the nature and mechanical properties of the soils in the immediate vicinity of the pipeline. Sampling of the backfill material around the pipeline and the soil of the original ground took place at two open excavations placed 100m apart; these are marked SA and SB on the location plan (Fig. 3.1). Large diameter (106, 200 and 250mm) vertical "undisturbed" and bulk samples were obtained.

Dynamic cone penetration tests were performed using a Mackintosh probe to identify different soil strata. As discussed earlier it was found that the pipeline was buried in a V-shaped trench of backfill material at a cover depth of 0.9m and surrounded by natural ground and a stronger clay material at a depth of 2.6m as shown in Fig. 3.2.

Laboratory work included one-dimensional consolidation tests, direct shear box tests and triaxial compression tests (both drained and undrained). Other standard laboratory work included material description, particle size distribution, determination of moisture content, soil density, plasticity and specific gravity. The materials of the backfill were brown/grey brown mixed clayey to very clayey rounded sand and gravel containing coal fragments and some cobbles. The materials of the natural ground were greyish brown very clayey rounded gravelly sand containing coal fragments. The particle size distribution curves of the two soils are presented in Fig. 3.16. Table 3.1 summarizes some of the measured properties of the backfill and the natural ground. More detailed properties of the soils were reported by Leach & Row (1991).

Results of direct shear box tests on the backfill material indicated a material friction angle of 31° and a cohesion intercept of approximately 20kN/m^2. A series of shear box tests were also performed for soil sheared over a coal tar enamel coated surface representing the pipe surface. The arrangement of the modified direct shear box apparatus was described in a British Gas report (British Gas, 1994). The results give a friction angle of 23° and a cohesion intercept of 10kN/m^2.

3.3.2. Stress Path Tests

In order to measure the soil behaviour more realistically, it is preferable to perform tests in which the stress path followed in the laboratory is similar to that followed by the soil *in situ*. The triaxial tests conducted by Leach & Row (1991) were "standard triaxial compression tests" and thus the stress paths followed in the tests did not reflect a real *in situ* stress path (see Fig. 3.18). For the case of the lateral load test, three critical soil elements have been considered (two for the backfill and one for the natural ground) as shown in Fig. 3.17. Elements A and C were in front of the pipe (heavily stressed zone) and element B was just beneath the pipe.

During the load test, the estimated condition for element A and C is increasing horizontal stress but approximately constant vertical stress. For element B, both horizontal and vertical stresses were constant, *i.e.* pure shear. To approximate these *in situ* conditions in the stress path cell, triaxial extension tests (increasing radial stress, constant axial stress) were performed on samples of backfill and natural ground to simulate the behaviour of elements A and C respectively. For element B, a constant mean pressure test (increasing axial stress, decreasing radial stress) was performed on a backfill soil sample. The stress paths for the stress path tests are shown in Fig. 3.18.

Three specimens were formed from bulk soil samples recovered from pit SA because this was closer to the point of the load test (pit A). The specimens were recompacted to the

original *in situ* density and moisture content. Information of the soil specimens is summarized in Table 3.2.

The stress path tests were performed using the computer controlled stress path cell developed at ERS. The specimens were first recompressed to their *in situ* conditions (K_0 was estimated to be 0.5); each sample was then allowed to reach equilibrium under the action of the *in situ* pressure prior to testing. Drainage was not allowed at any stage of the test. The test results are summarized in Table 3.3, and typical plots of the results are presented in Figs 3.19 to 3.21.

From the test results it was noted that strength of the backfill material in the two different stress path tests was quite similar (tests Hil01, Hil02 and test by Leach & Row, 1991). The results for the natural ground (Fig. 3.21) show that the soil sample was very stiff such that the stress-strain behaviour was virtually linear up to the limit of the apparatus for that particular stress path. At the end of the test, it was decided to load the sample in standard triaxial compression up to the limit of the test apparatus, and the results are shown in Fig. 3.22. The stress-strain behaviour was still virtually linear up to a deviator stress of 160kN/m^2. Triaxial tests conducted by Leach & Row (1991) indicated a very high deviator stress at failure of over 400kN/m^2 for a remoulded sample taken at the same location and with a similar moisture content.

3.4. Single Element Test

From the results of the stress path test carried out in the previous section, the input parameters for each soil model described in Section 2.4 (the Elastic-perfectly plastic model, Modified Cam clay model, Non-linear elastic model and Elasto-plastic model) can be obtained. Single element tests have been performed to check whether the input parameters behave reasonably. A single 8-noded quadrilateral element was used to represent one

quarter of the soil specimen and axisymmetric analyses were carried out. The results for element A (Fig. 3.17) are shown in Fig. 3.23. The results of single element tests show that both the Elasto-plastic and the Non-linear elastic models could simulate the triaxial test quite well. For Modified Cam clay, the failure stresses of the analysis are similar to those in the triaxial test, but the strains were much smaller. This is because the soil sample was unsaturated, and during the triaxial test, small volume changes occurred due to compression of the air voids. However, the Modified Cam clay analysis assumed the soil to be fully saturated, and in the undrained analyses, the strains were under-estimated. For Elastic-perfectly plastic model, the relationship between mean stress and volumetric strain agreed quite well, but the agreement for the relationship between deviator stress and shear strain is not so good. This is because the initial slope of the non-linear stress strain curve has been used for the Young's modulus. Using a secant modulus could result in a better relationship for deviator stress and shear strain.

3.5. Previous Work and Proposed Methodology for Modelling the Lateral Push Test

Work has been done previously to numerically simulate the lateral push test, Booth (1991) and Ng (1993). A two stage analysis method involving the use of two analytical programs was adopted. Stage 1 is to predict the soil restraint around the pipe as it is displaced laterally through the soil. This information, expressed as a relationship between soil pressure and pipe displacement (*P-y* curve), is then used in stage 2 of the analysis to represent the spring stiffness in a Winkler's beam on elastic foundation model to predict the behaviour of the buried pipe.

Booth (1991) created a 2-D plane strain finite element mesh to simulate the test. The soil models adopted were Modified Cam clay and elastic-perfectly plastic for the backfill

material and the natural ground respectively. Both drained and undrained analyses were performed to simulate two extreme conditions for the rate of pore water pressure dissipation. The pipe was modelled as a rigid cavity and displaced in the horizontal direction by 25mm. The displacement of the pipe in the vertical direction was determined by a trial and error process until the total Y-reaction (vertical) around the pipe was equal to zero. The analyses performed by Booth were using a modified version of the finite element program CRISP84 developed in ERS.

The pressure-displacement relationship of the pipe was obtained by summing up the total X-reactions (horizontal) around the pipe and dividing by the pipe diameter plotted against the lateral pipe displacement. The *P-y* curve was then used in an in-house finite difference program developed in ERS called WOMOD, which is based on the Winkler's elastic beam on elastic foundation model, to represent the non-linear spring stiffness; the pipe was modelled as an elastic beam (for details of the model see Section 2.6.3.1). The lateral push test has been simulated using the program and the results compared with data from the field tests. Booth (1991) found that the tensile zone at the back of the pipe contributed significantly to the total reaction. This made the predicted *P-y* curve much stiffer than expected. In reality, the soil could not carry any tension (or could only carry a very small tensile stress). The way Booth overcame this problem was to consider only the reaction at the front of the pipe so that the soil at the back of the pipe has no effect on the *P-y* curve. This simple assumption together with an undrained analysis gave a reasonably good prediction of the pipe displacements during the load test. However, this assumption implies that the behaviour of the soil at the front is independent of the soil at the back of the pipe, which is not true when comparing the results of Ng (1993). The straining of soil and tensile stress that built up at the back in a soil model that allows tension to build up could influence the soil at the front. Moreover, this assumption cannot model the interaction between the soil/pipe contact surface.

Ng (1993) studied the problem in more detail. He compared the use of different soil models to represent the backfill material including Modified Cam clay, the Non-linear elastic model and the Elasto-plastic model (see Section 2.4 for more details of the soil models). The results indicated that the *P-y* curve predicted using Modified Cam clay was much stiffer at the initial stage than the other soil models. This is because the Modified Cam clay theory assumes the soil is incompressible for the undrained case whilst the other two models used results directly from the stress path test; the soil samples from Hilderstone had a few percent of air voids and this made it slightly compressible (see Table 3.3). However, all the soil models under-predict the pipe displacement (over-predicted the *P-y* curve) because they all assume full tension of the soil at the back of the pipe. To overcome this problem, Ng used the "no tension" option developed in ERS in the Elasto-plastic soil model; with this option if any soil element is in tension, the program reduces its strength and stiffness to very low values. In other words, the soil elements in the tensile zone (at the back of the pipe) become very weak thus very little tensile stresses can be built up. However, this approach still ignored the possible slip and separation at the soil/pipe interface which may significantly influence the predicted *P-y* curve.

Ng (1993) also found that the prescribed horizontal displacement of 25mm was not sufficient for the *P-y* curve to flatten out. To obtain a more representative *P-y* curve, the prescribed displacement in the analysis should cover the full displacement likely to be experienced by the pipe in the field. Good agreement with the field data was obtained by using the Elasto-plastic soil model with the no tension procedure and a larger prescribed displacement.

Thus Ng (1993) concluded that the two stage analysis method can be used successfully for predicting the behaviour of buried pipes subjected to ground movement, provided that the tension at the back of the pipe is taken into account and the prescribed movement of the pipe in stage one of the analysis covers the range of pipe displacements occurring in the field. He recommended that special interface elements may be used to model the separation

and slip between the soil and the pipe, and that the effects of ovality of the pipe under load should be considered. The work by Ng (1993) has been summarized and published as a technical paper (Ng, Pyrah & Anderson, 1994).

3.6. Summary

The results of a full scale *in situ* axial push test and a lateral push test on an existing transmission pipeline have been presented. Results of laboratory tests carried out previously by other researchers and additional stress path tests carried out for this research, to determine the properties of soils around the pipeline, have also been presented. Single element finite element analyses have been used to examine the accuracy of the derived input parameters for different soil models to represent the backfill soil, based on the stress path tests. Previous work to model the lateral push test has been critically evaluated. It was found that the previous methodology cannot accurately model the soil/pipe interaction and a more appropriate method is needed (see Chapter 7).

Material	Moisture Content (%)	Density (kg/m³)		G_s	e	S_r (%)	C_c	C_s	c_u (kN/m²)	ϕ'
		Bulk	Dry							
Backfill	14.2	2143	1877	2.64	0.41	91	0.068	0.015	29	39° (M=1.5)
Natural ground	12.5	2178	1936	2.62	0.35	94	0.041	0.013	108* at 10.4% ε	—

Table 3.1. Properties of backfill and natural ground from Leach & Row (1991).

Test Number	Sample Reference	Depth (m)	Material	Soil element	Diameter (mm)	Moisture Content (%)	Density (kg/m³)	
							Bulk	Dry
Hil01	SA9	0.9~1.5	Backfill	A	200	14.06	2070	1815
Hil02	SA9	0.9~1.5	Backfill	B	200	15.42	2070	1793
Hil03	SA8	0.9~1.5	Natural ground	C	200	11.30	2131	1915

Table 3.2. Information of the soil specimens used in the stress path tests.

Test Number	Specific Gravity	Void Ratio	S_r (%)	Air Voids (%)	c_u (kN/m²)	Elastic Properties (undrained)		
						E (kN/m²)	ν	G (kN/m²)
Hil01	2.59	0.43	85	4	20.6	8400	0.07	3925
Hil02	2.59	0.44	91	3	28.6	10617	0.14	4658
Hil03	2.60	0.36	82	5	> 80.0#	56000	0.17	23932

Table 3.3. Results of the stress path tests.

* Limit of the test apparatus, available shear strength exceeds this value.

\# Limit of the stress path cell reached, available shear strength exceeds this value.

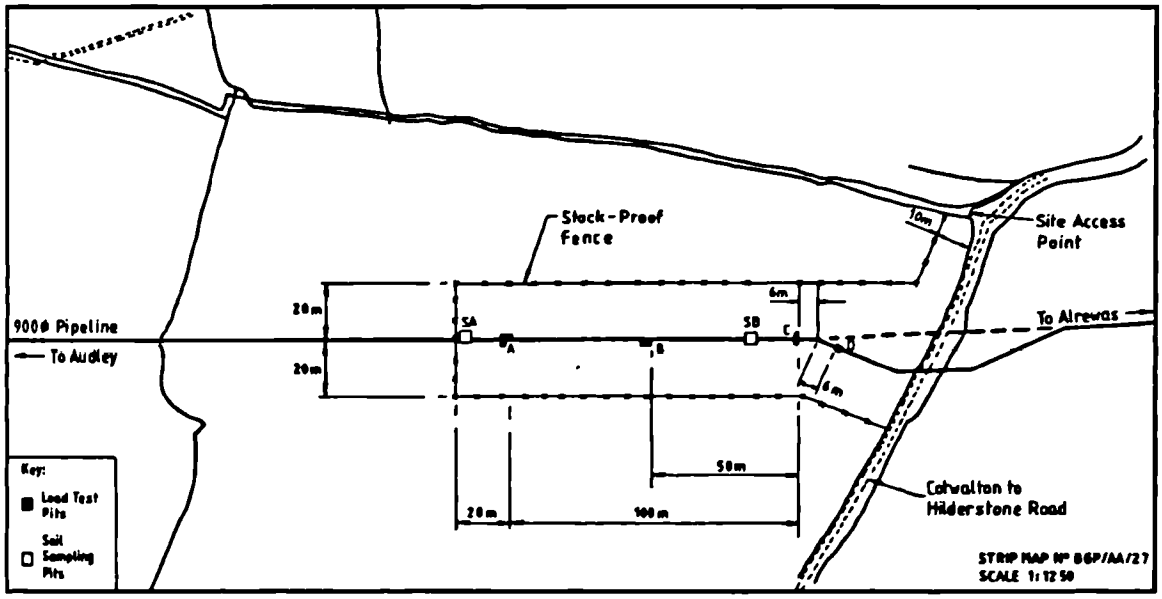

Fig. 3.1. Approximate location of excavations for soil sampling and the load tests (from Leach & Row, 1991).

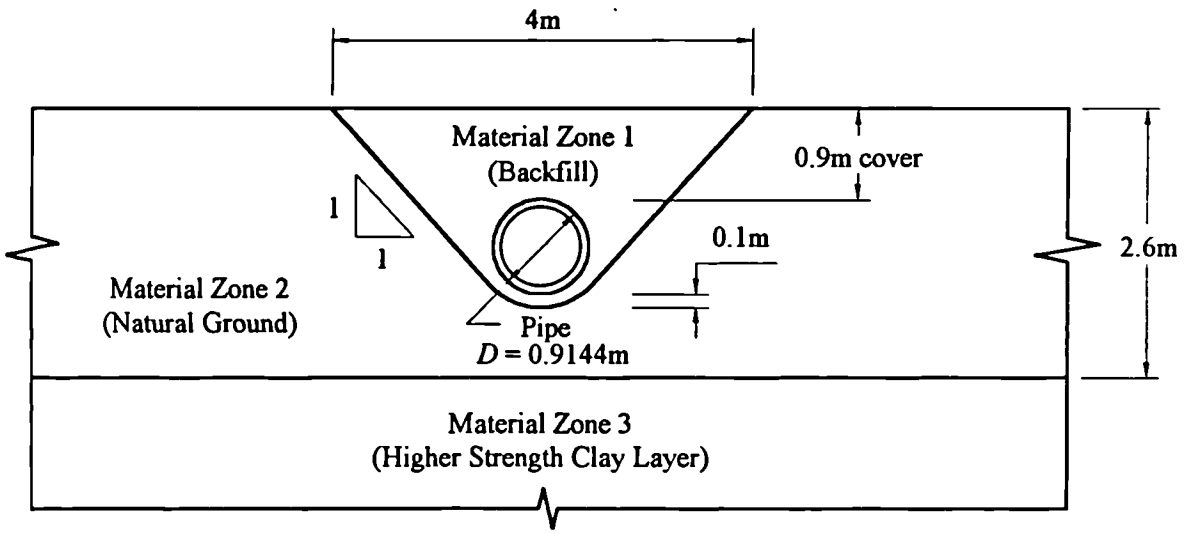

Fig. 3.2. Cross-section of the trench.

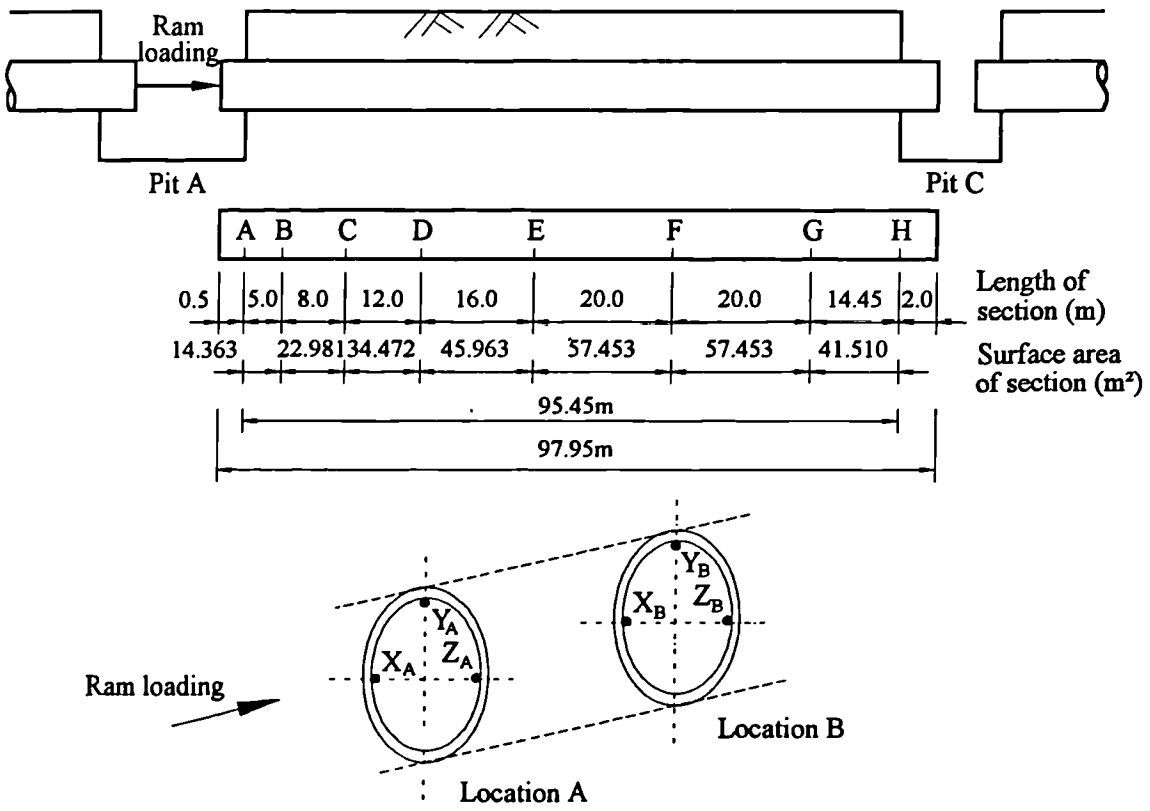

Fig. 3.3. Location of strain gauges along the test pipe section.

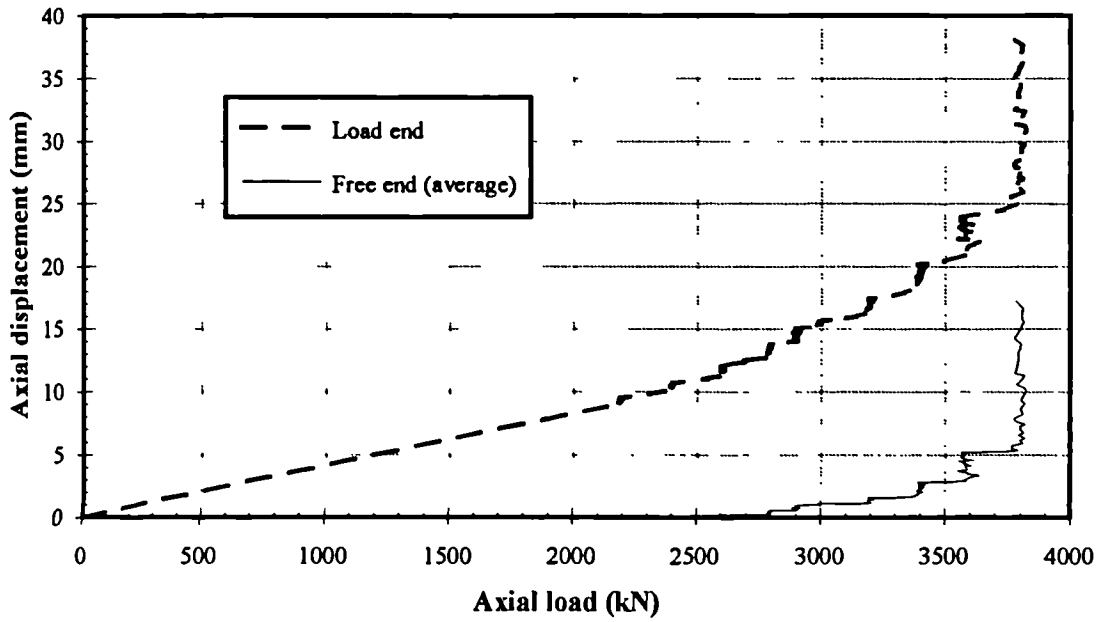

Fig. 3.4. Plot of axial load against axial pipe displacement at the two ends (axial push test).

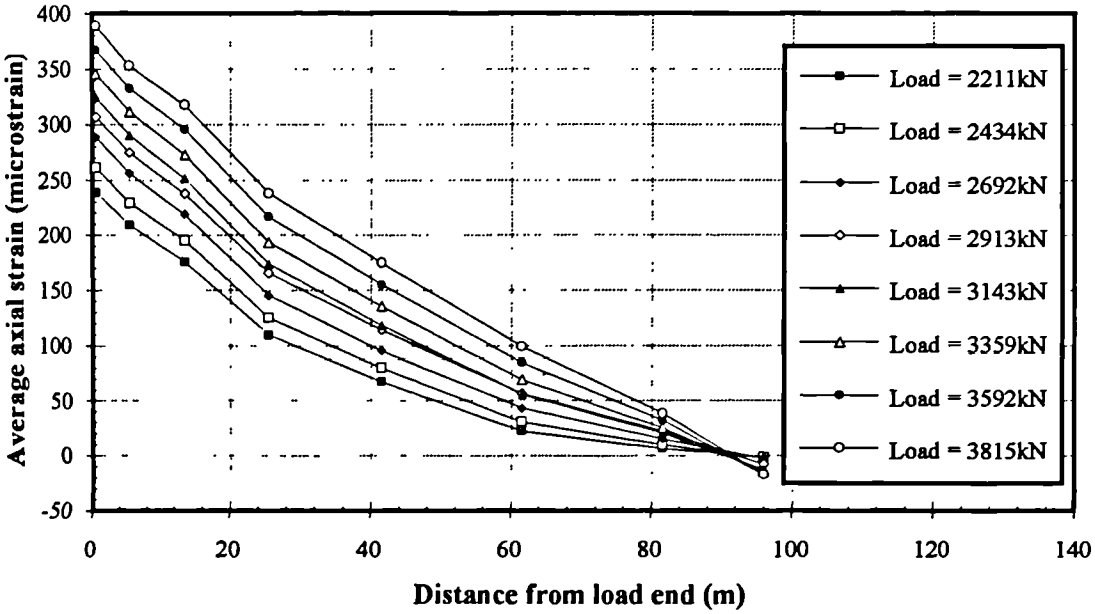

Fig. 3.5. Variation of strain along the length of the pipe at selected loadings (axial push test).

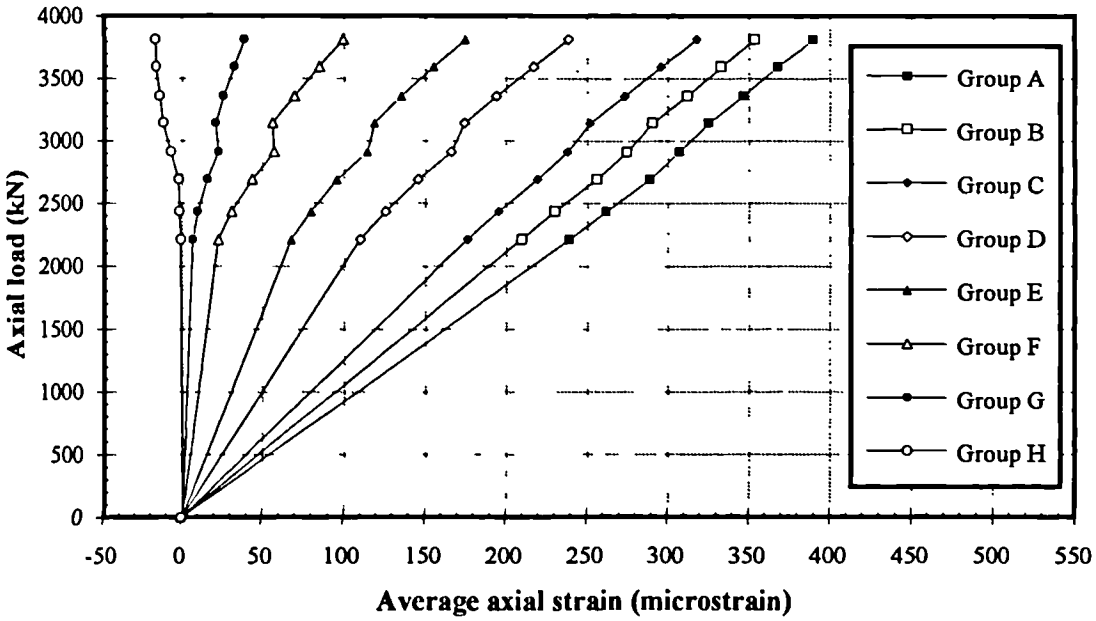

Fig. 3.6. Variation of strain at different location of the pipe (axial push test).

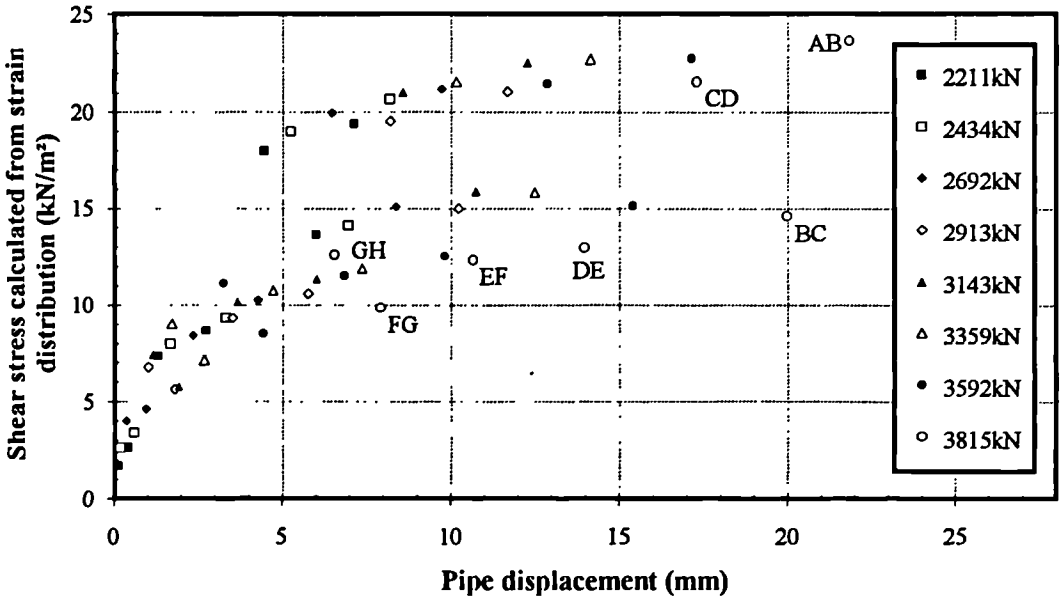

Fig. 3.7. Plot of calculated shear stress against pipe displacement (axial push test). The legends represent applied loadings. The labels AB, BC *etc.* indicate the pipe section for which the plotted shear stress has been calculated at a ram loading at 3815kN.

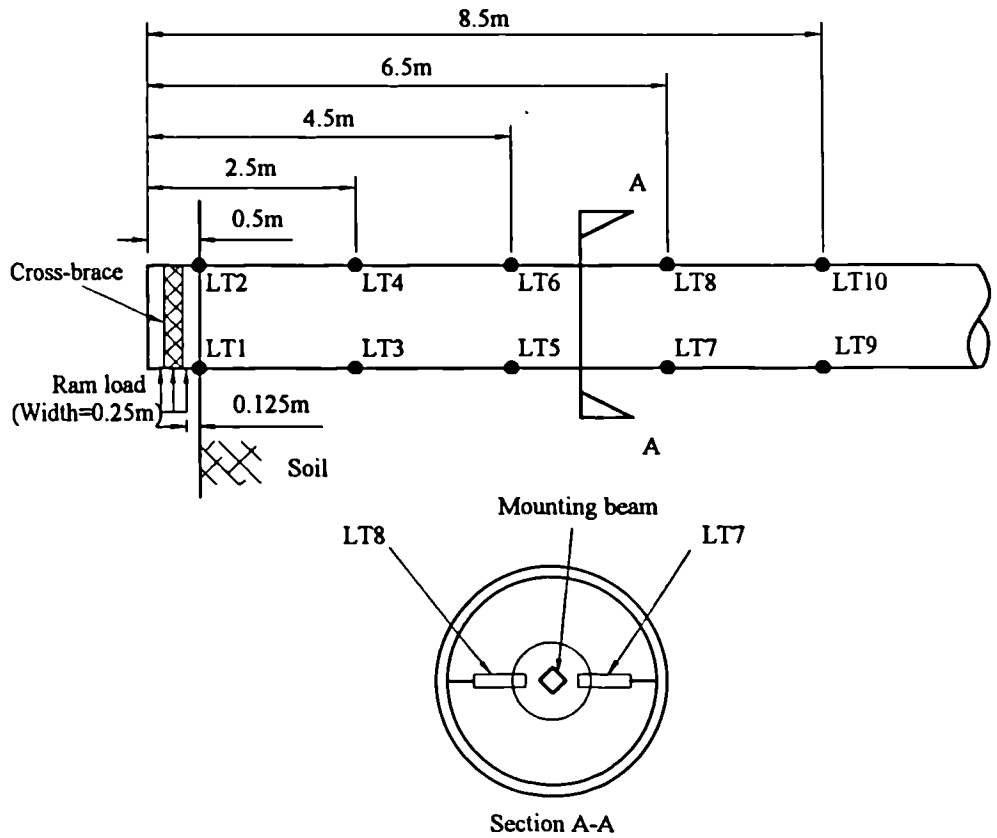

Fig. 3.8. Plan view and section showing position of displacement transducers (lateral push test).

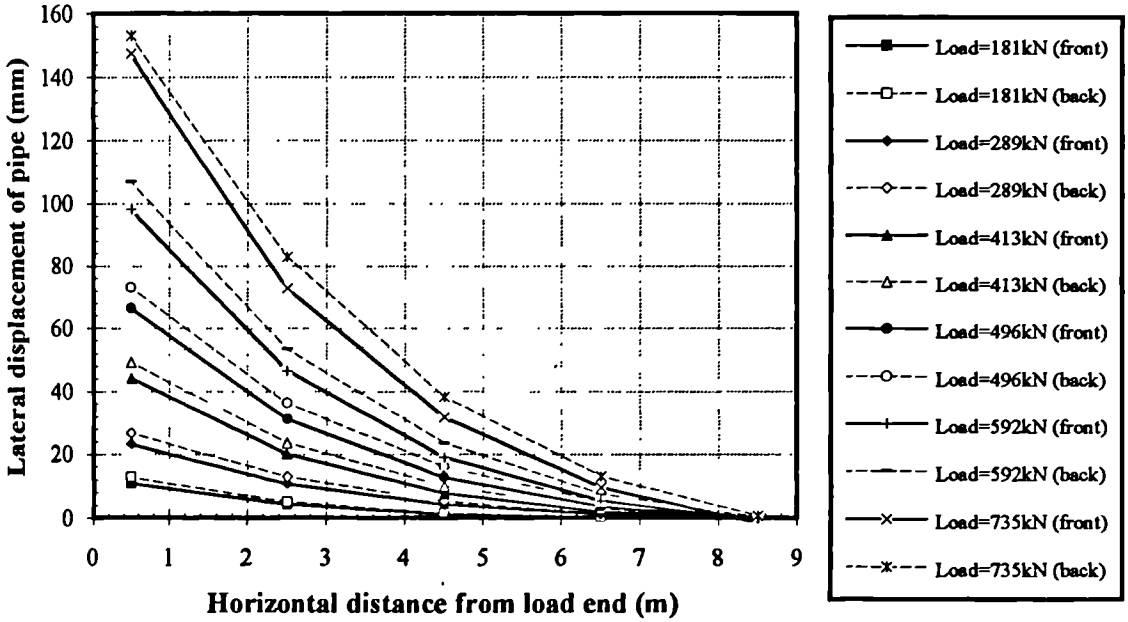

Fig. 3.9. Displacement profile along the length of the back of the pipe at selected loadings (lateral push test).

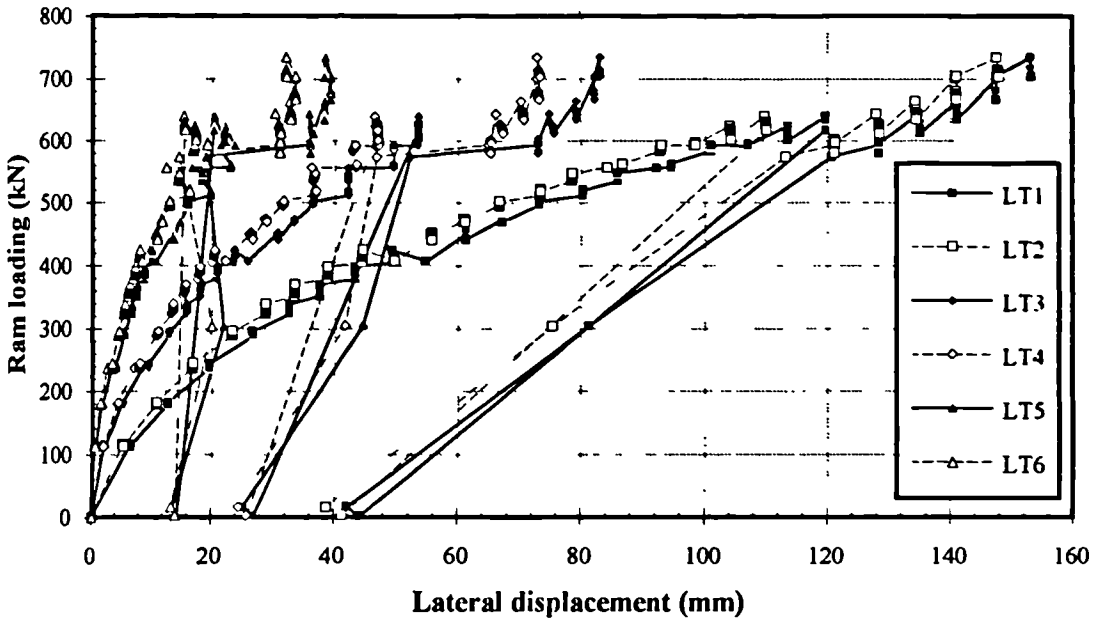

Fig. 3.10. Load/displacement relationship at displacement transducers LT1 to LT6 (lateral push test).

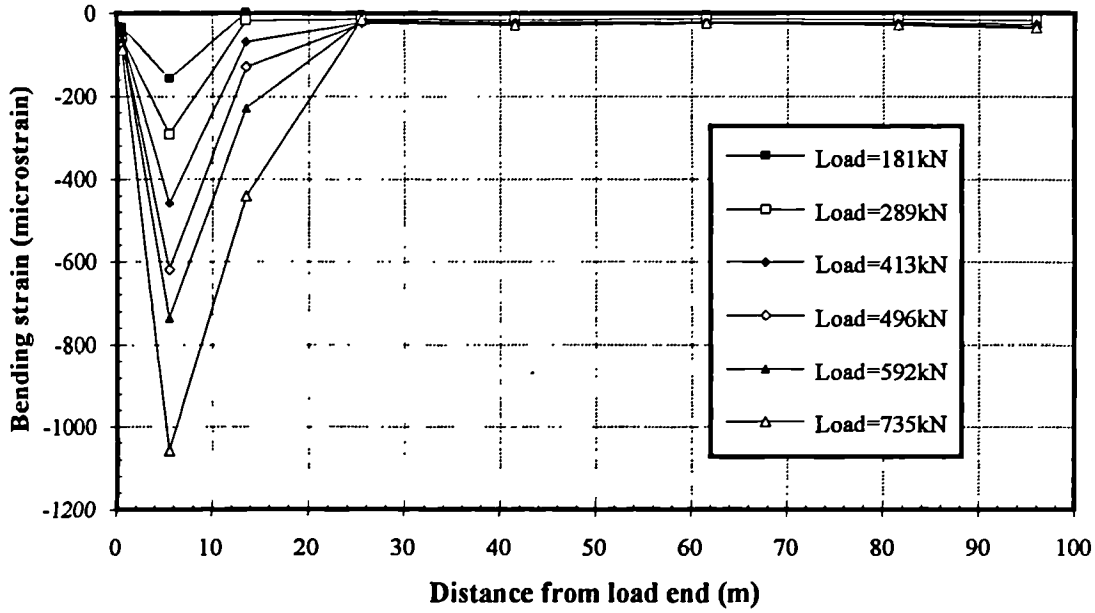

Fig. 3.11. Variation of strain along the length of the pipe at selected loadings (lateral push test).

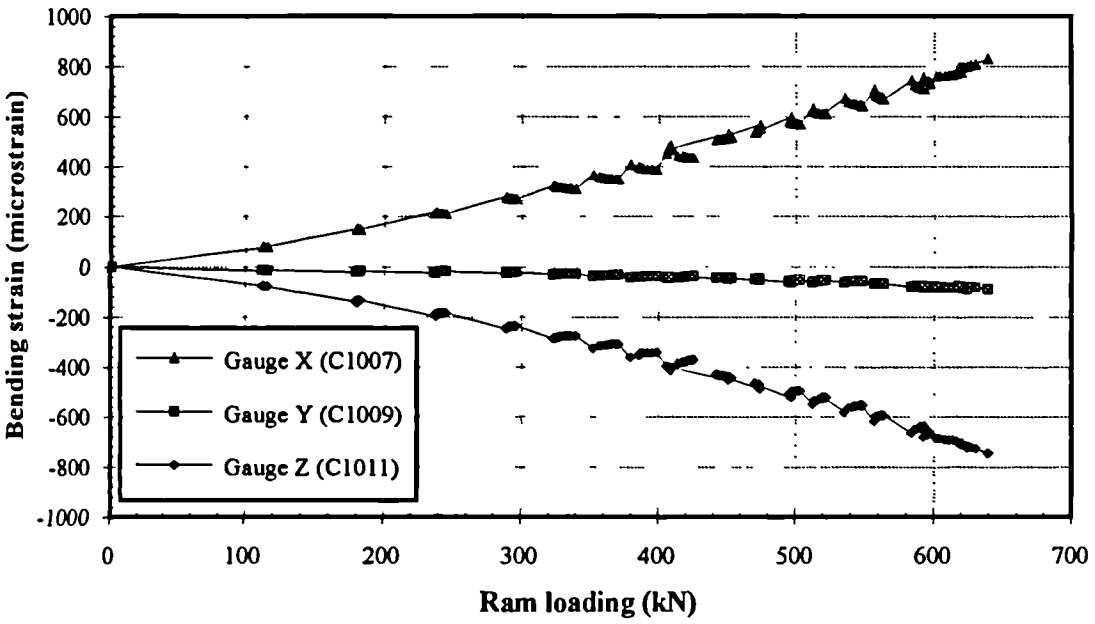

Fig. 3.12. Variation of strain at location B (lateral push test).

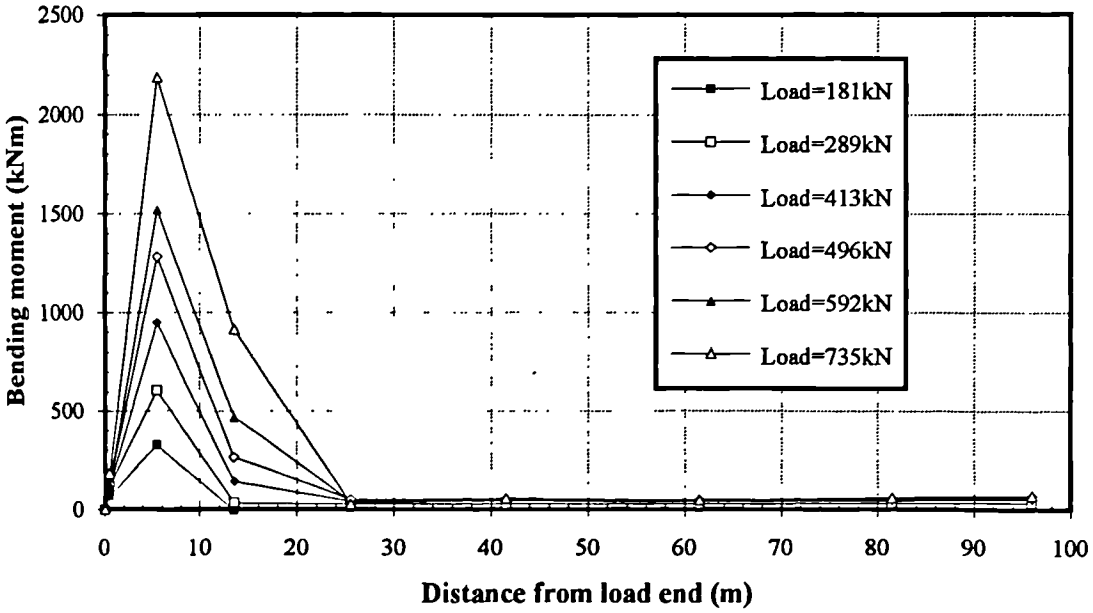

Fig. 3.13. Variation of bending moment along the pipe at selected loadings (lateral push test).

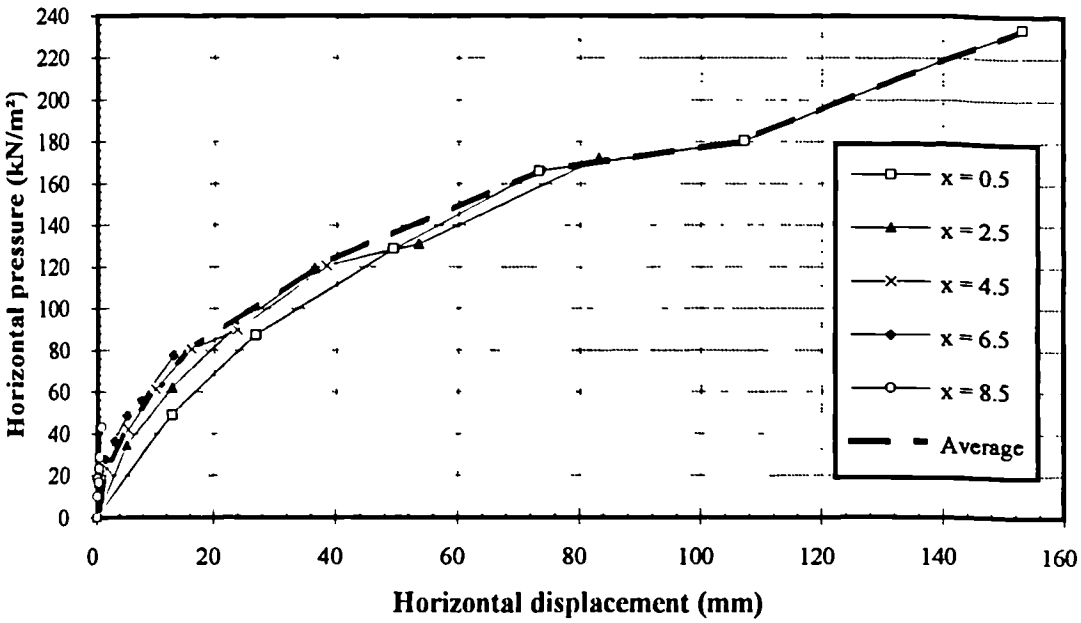

Fig. 3.14. Back-calculated *P-y* curves at various locations along the pipe (lateral push test).

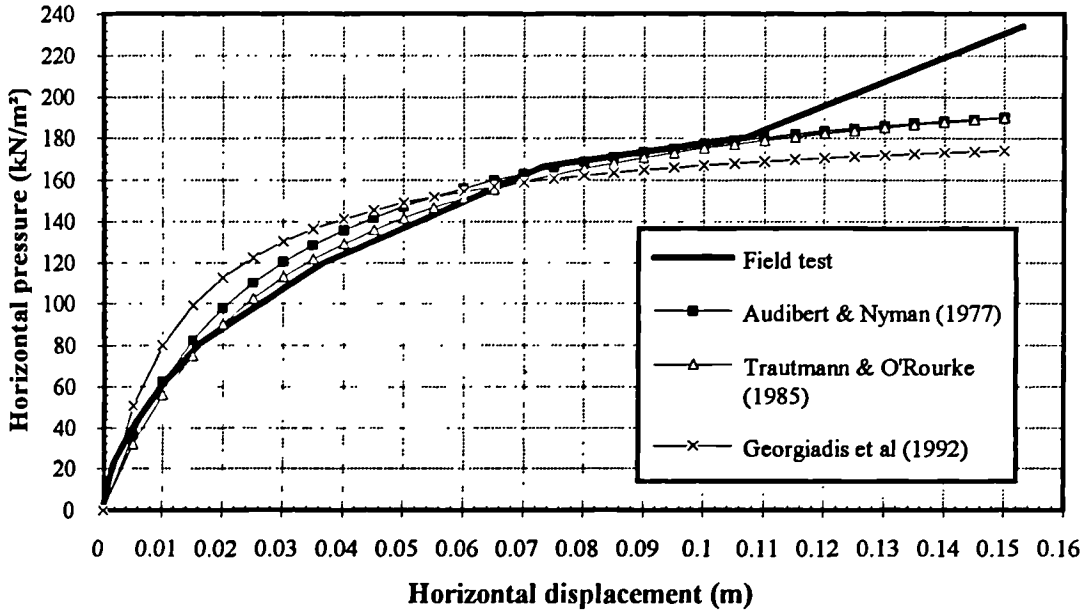

Fig. 3.15. Comparison of the *P-y* curve from field test with three suggested hyperbolic pressure-displacement curves.

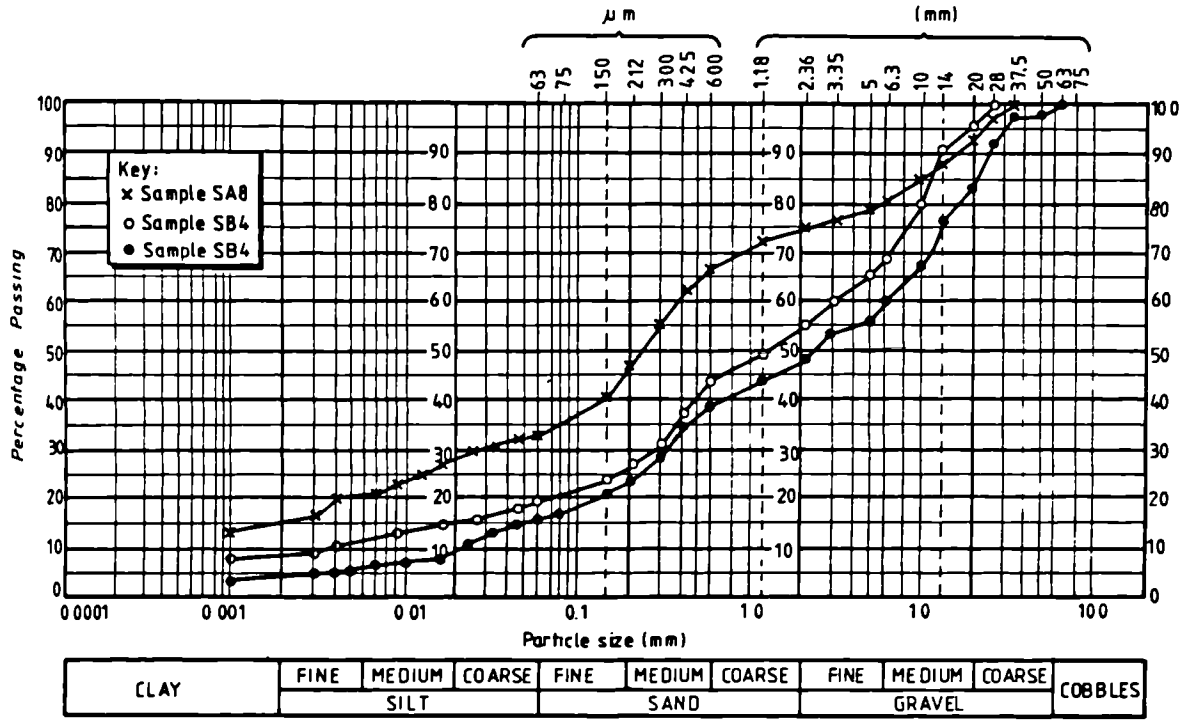

(a) Natural ground

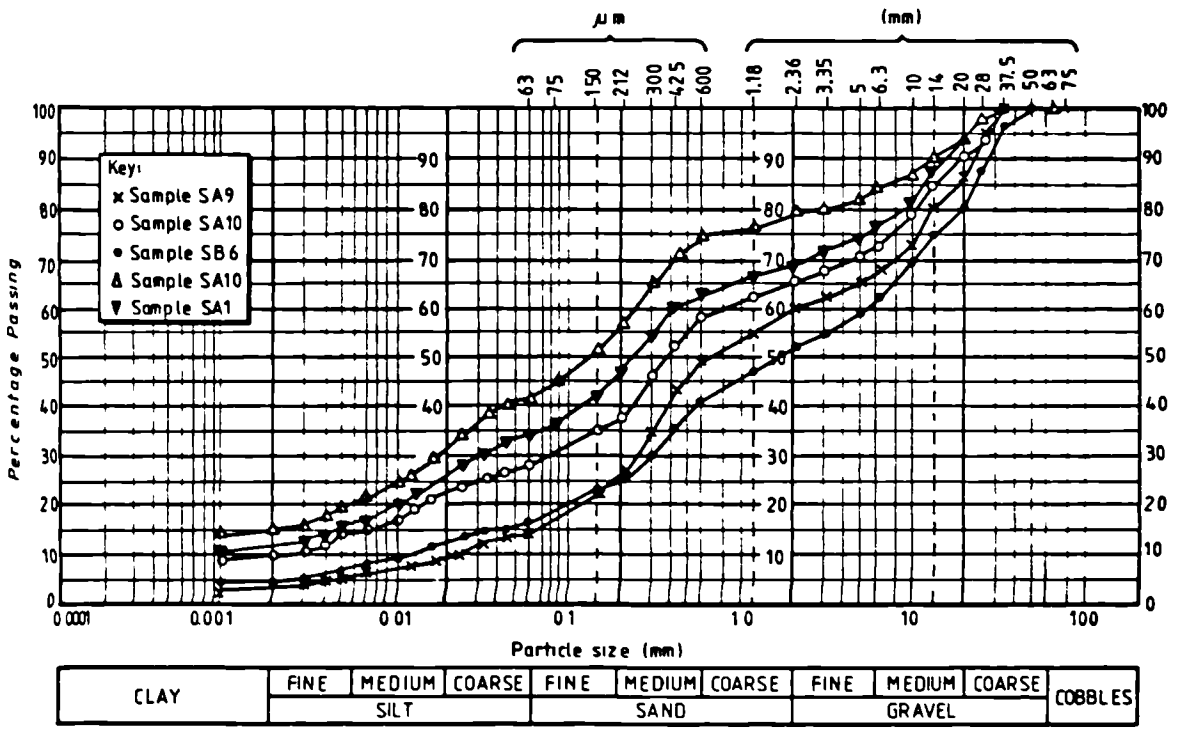

(b) Pipe backfill

Fig. 3.16. Partical size distribution curves for the soils (from Leach & Row, 1991). For the details of the legends refer to Leach & Row (1991).

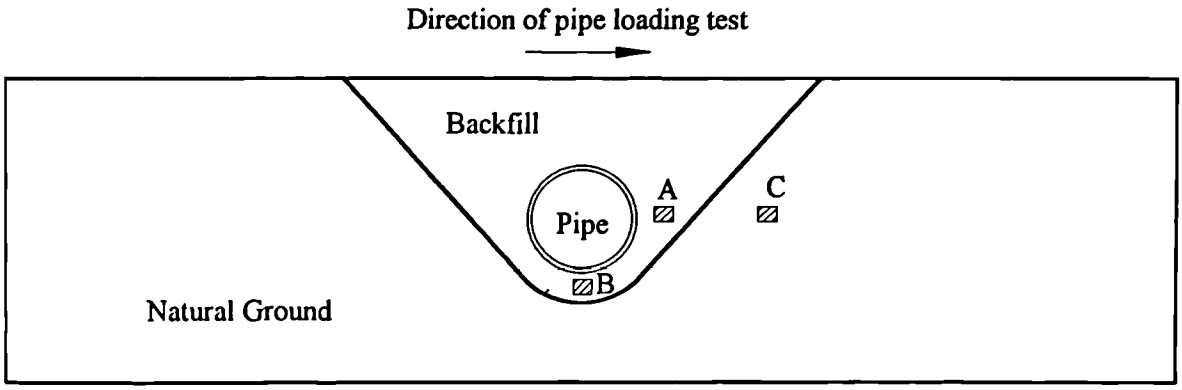

Fig. 3.17. Soil elements considered for stress path test.

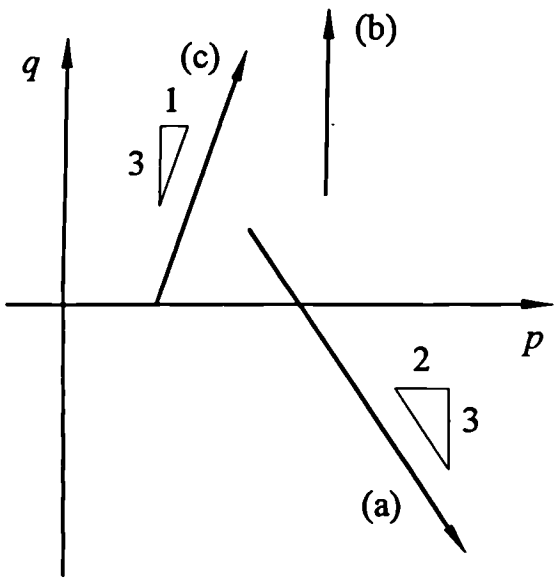

Fig. 3.18. Stress path for triaxial tests; path (a) for element A and C, path (b) for element B and path (c) for standard triaxial compression test.

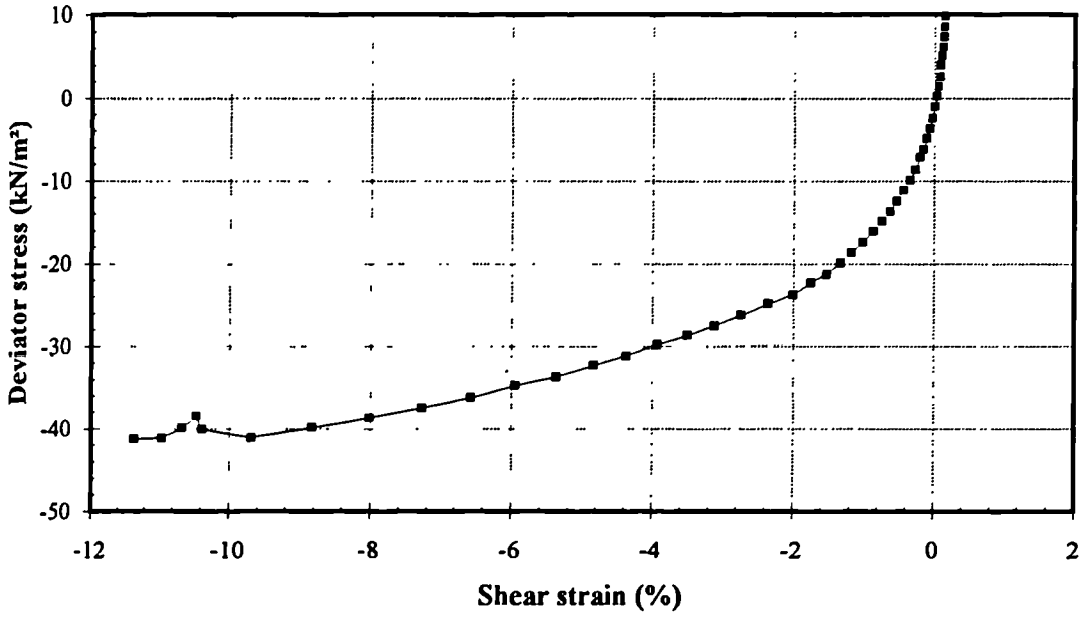

(a) Deviator stress against shear strain

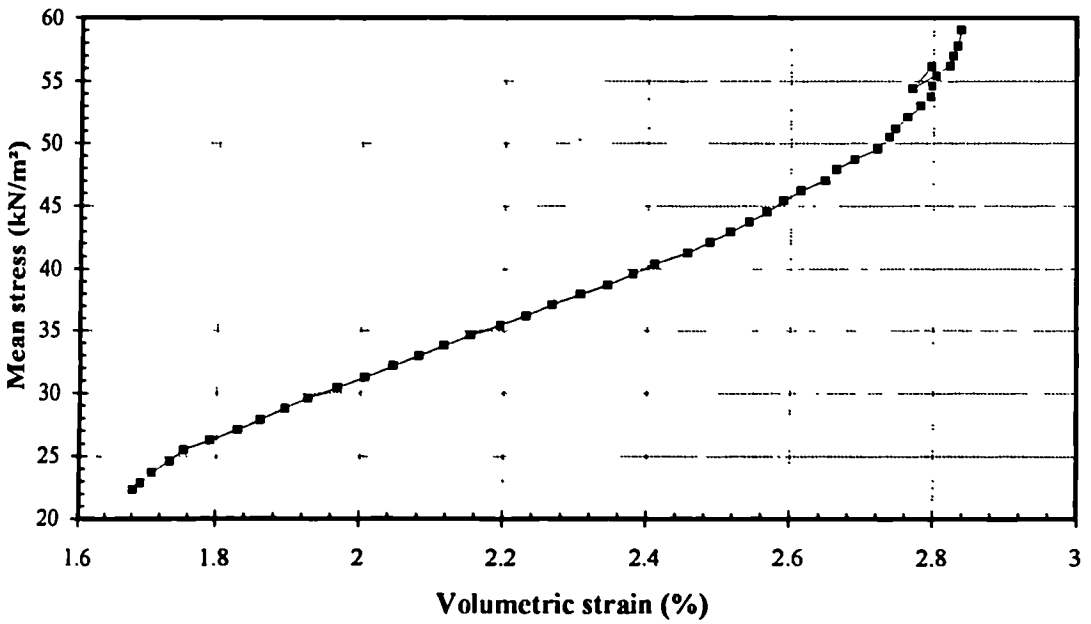

(b) Mean total stress against volumetric strain

Fig. 3.19. Typical results of stress path test Hil01.

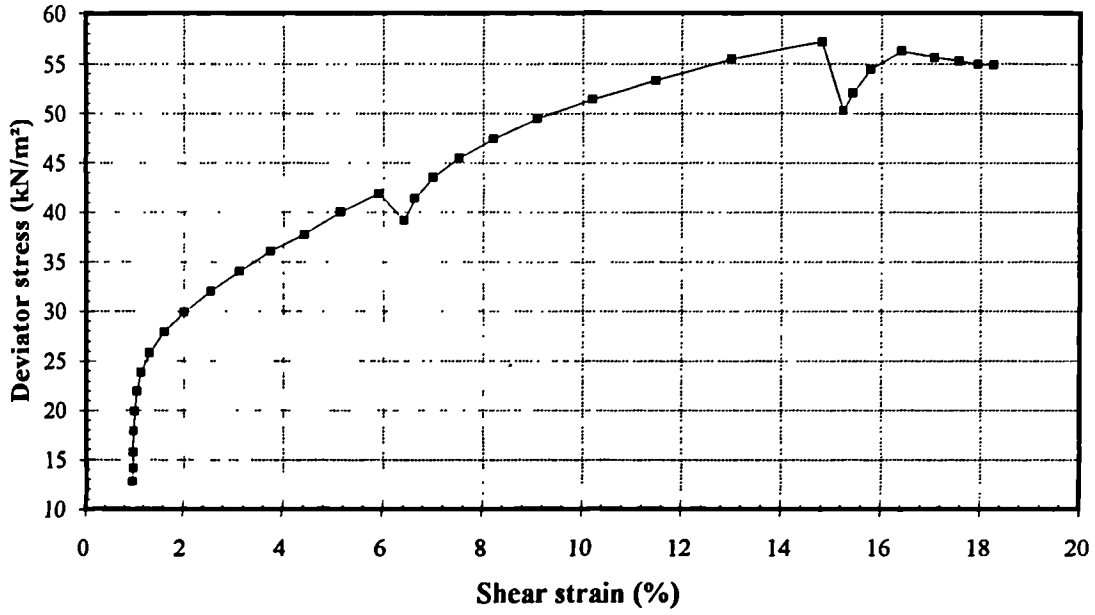

(a) Deviator stress against shear strain

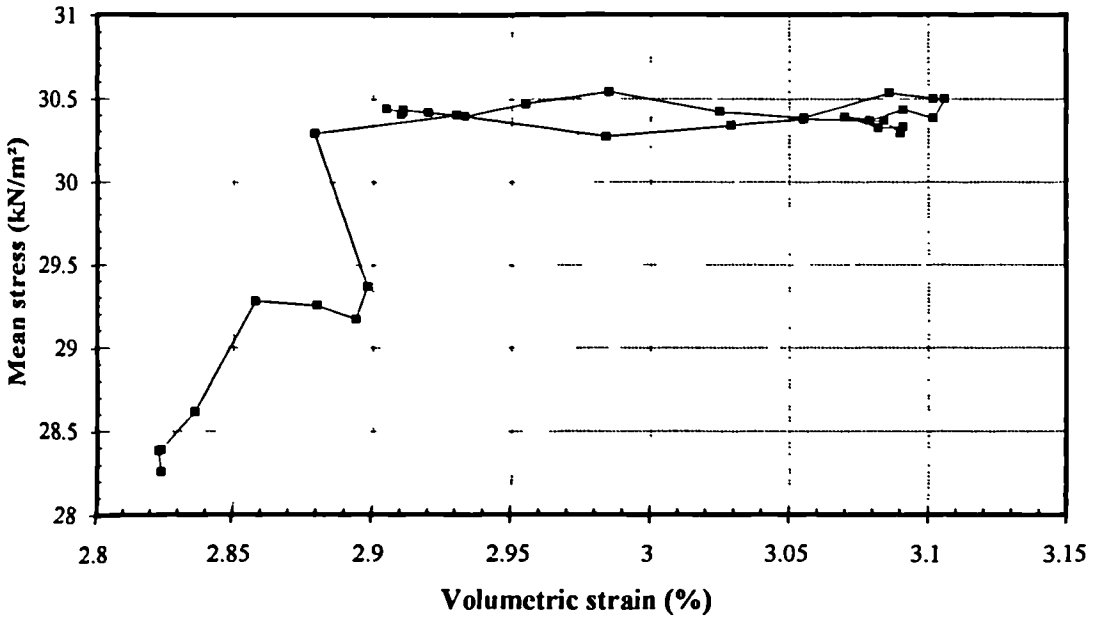

(b) Mean total stress against volumetric strain

Fig. 3.20. Typical results of stress path test Hil02.

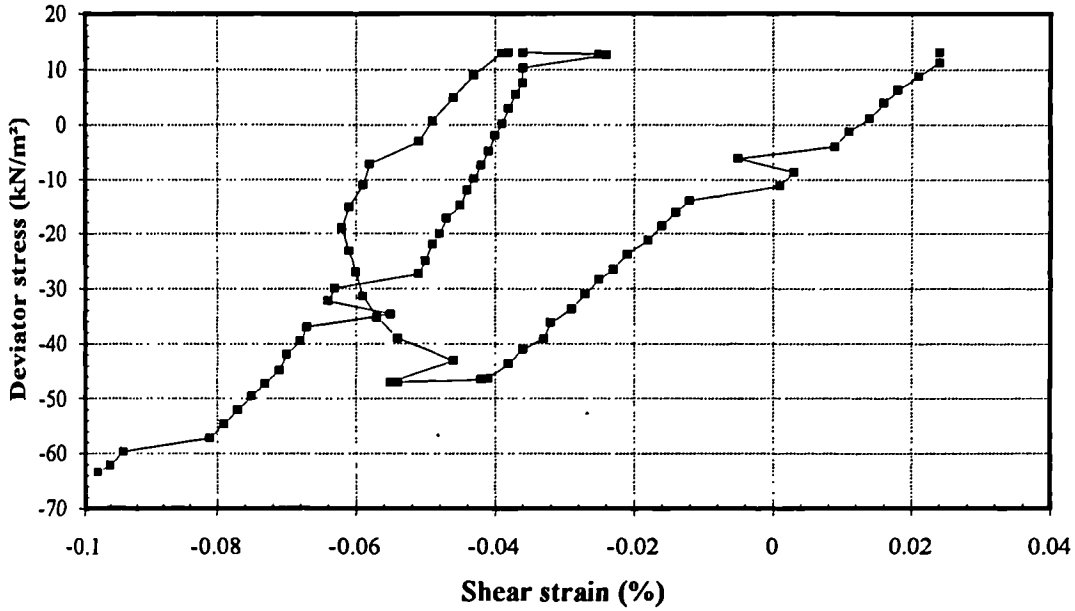

(a) Deviator stress against shear strain

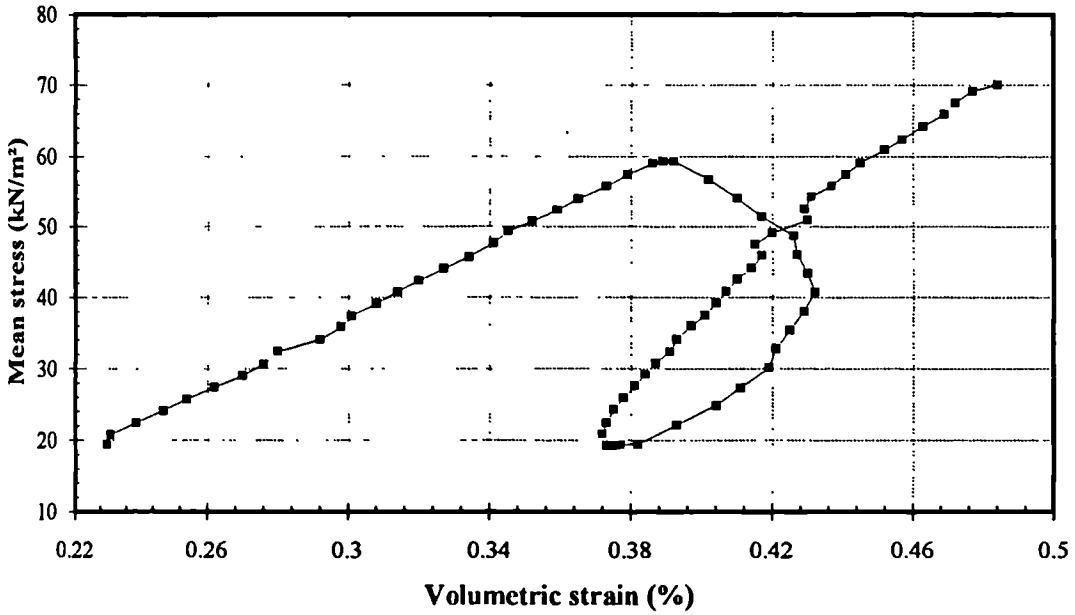

(b) Mean total stress against volumetric strain

Fig. 3.21. Typical results of stress path test Hil03 (stress path (a) in Fig. 3.18).

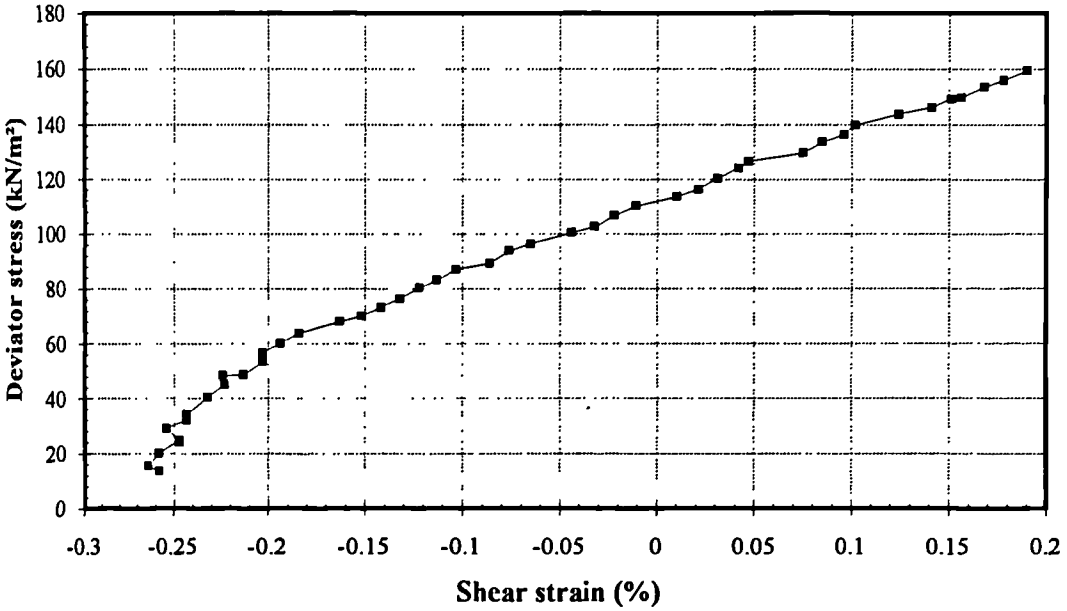

(a) Deviator stress against shear strain

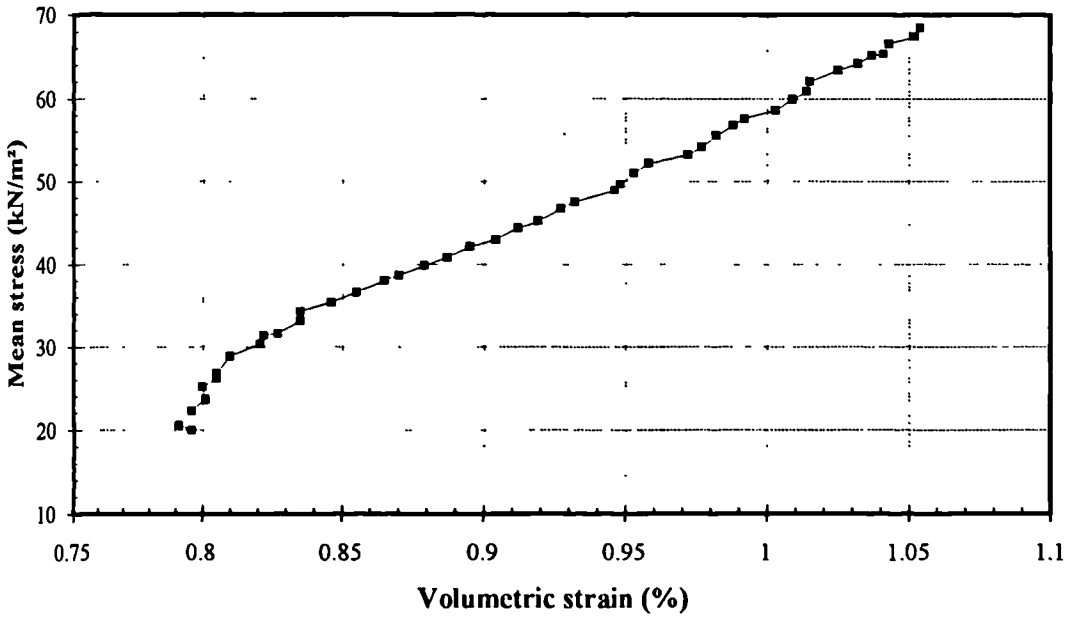

(b) Mean total stress against volumetric strain

Fig. 3.22. Typical results of stress path test Hil03 (stress path (c) in Fig. 3.18).

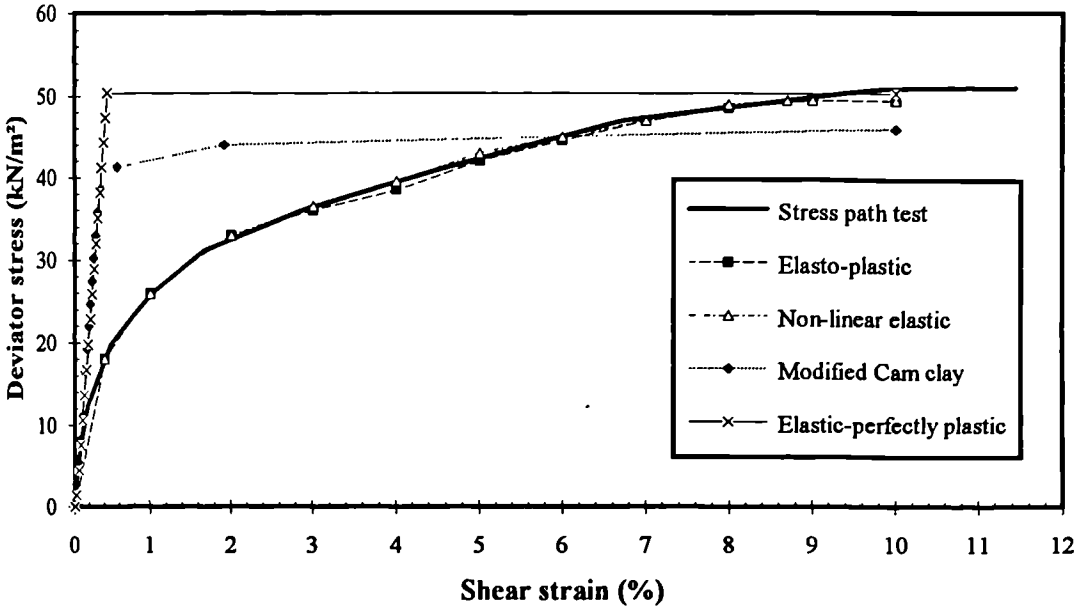

(a) Deviator stress against shear strain

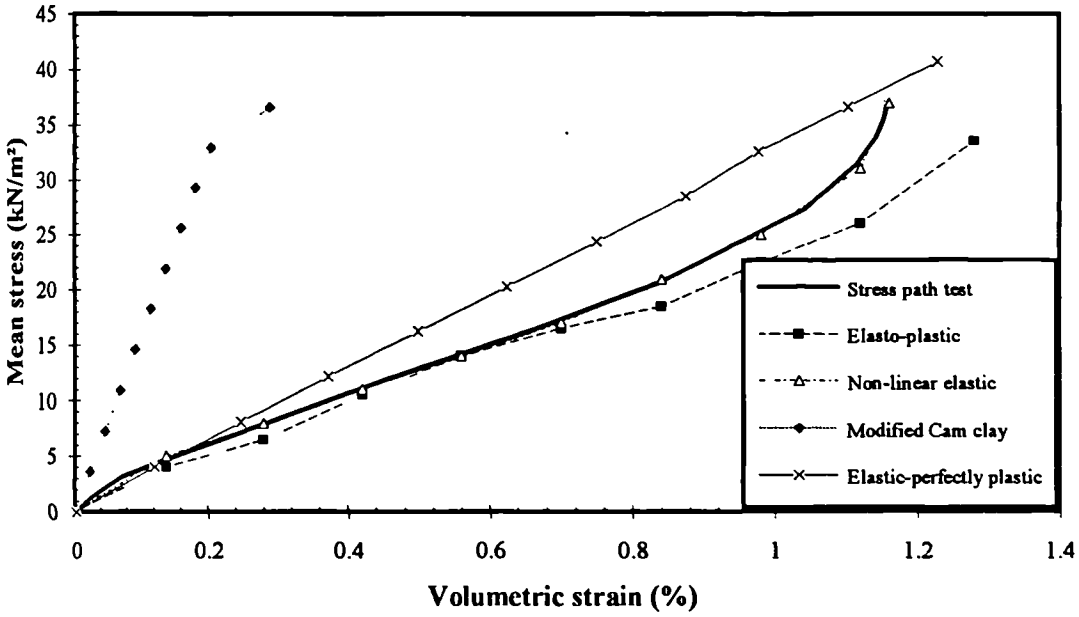

(b) Mean total stress against volumetric strain

Fig. 3.23. Typical results of single element test (element A in Fig. 3.17).

CHAPTER 4

MODELLING OF SOIL / PIPE INTERFACE USING INTERFACE ELEMENTS

4.1. Introduction

Interface elements have been used successfully to model soil/structure interface behaviour by many researchers (see Section 2.8). In this chapter three different kinds of interface element have been examined and their behaviour compared. The three interface elements are:

i. CRISP90 interface element — this is an 8-noded interface element with linear strain variation along the longer sides and constant strain along the narrow sides. It is available in the original CRISP90 FE program.

ii. DRCRISP interface element — this is a Goodman type of interface element. It has six nodes and no thickness. It is available in the FE program DRCRISP (Russell, 1992b), which is a modified version of CRISP84.

iii. Conventional quadrilateral element — this is the normal 8-noded quadrilateral finite element available in CRISP90 without any modification.

During this work some problems were experienced with all three of the interface elements. Due to the reasons explained in the subsequent sections, the CRISP90 interface element is the most appropriate element in modelling soil/pipe interface, and modifications have been

made to the element to overcome the problems and to improve its ability in modelling the normal behaviour.

4.2. Introduction to the Finite Element Program Suite Used in the Research

A suite of programs has been developed at the British Gas Engineering Research Station (ERS) to simplify, speed up and minimize errors in the preparation of data for an analysis and the subsequent examination of the results.

The finite element analysis process begins with the creation of a geometry and analysis model using a commercial software package PATRAN (PDA Engineering, 1989). A forward translator from PATRAN to CRISP90, named PATCSP90, uses the PATRAN output file to produce input files for the CRISP90 geometry and main programs. The problem is then solved using a modified version of CRISP90 which has two additional soil models developed by British Gas (Elasto-plastic model and Non-linear elastic model), modified interface element (see Section 4.4), and other modifications to produce results in a particular format for easy examination. A reverse translator from CRISP90 to PATRAN, named CSPPAT90, uses the output files from CRISP90 to produce results files containing displacements, nodal values and element values of stresses and strains which are then accessible by PATRAN for visual examination of selected results for selected stages of an analysis.

A "parameters file" translator, CSPPAR90, produces 29 unformatted direct access files, one file corresponding to each parameter (stresses and strains) from the CRISP90 output file. These files can be accessed by an X-Y plotting routine, CSPXY90, which uses the general graphical package GINO-F/GRAF. This provides a graphical display of one selected parameter against another for any selected element integration point for the complete

analysis (stress and strain paths). The parameter files can also be produced in a formatted form for input into spreadsheet programs.

For the elastic beam on elastic foundation program WOMOD, there is a simple post-processing X-Y plotting program using the package GINO-F/GRAF for visual examination of the displacements of the pipe and the soil, the bending strain and the shear force distributions along the length of the pipe.

4.3. Single Element Test

4.3.1. Introduction

In order to model the interaction between a buried pipeline and the surrounding soil, special interface elements may be used. As outlined in the introduction three kinds of interface element are examined; they are the CRISP90 interface element, the DRCRISP interface element and a conventional 8-noded quadrilateral element with elastic-perfectly plastic material properties. Because there is very little previous experience using these interface elements, single element tests have been performed to examine the behaviour of each element in different modes of deformation.

Figure 4.1 shows a single interface element set up in a 2-D plane strain FE mesh with the nodes at the base fixed in both horizontal and vertical directions. The length of the element was equal to 1.0 and the thickness (not applicable to DRCRISP interface element) was varied between 1.0 to 0.00001 which made the aspect ratio (length/thickness) of the interface element vary from 1 to 100,000. Displacement controlled tests were performed where horizontal and vertical displacements were applied to the top nodes.

4.3.2. Original CRISP90 Interface Element

This interface element has six material properties:

- c cohesion intercept (force/unit area)
- δ angle of friction of the interface (degree)
- K_n modulus in normal direction (force/unit area)
- K_s shear modulus (force/unit area)
- K_{sres} residual shear modulus (force/unit area)
- t thickness of interface element (unit length)

It should be noted that the program uses the normal stiffness k_n ($=K_n/t$) and the shear stiffness k_s ($=K_s/t$) to compute the behaviour of the element instead of using the shear and normal modulus. The stiffness values obtained from the direct shear box test are the **actual** stiffness values, and the **input** moduli should be equal to these **actual** stiffness values multiplied by a chosen value of t:

$$K_n = k_n \times t \tag{4.1}$$

$$K_s = k_s \times t \tag{4.2}$$

In specifying the nodal co-ordinates in the geometry input file, the manual (Britto & Gunn, 1990) stated that users can specify the same co-ordinates for the two rows of nodes along the length dimension of the element. The reason for this is because the actual thickness of the element is only used when computing the element properties. The potential shortcoming of this is the overlapping (cross-over) of the element nodes when compressive normal stress acts across the interface, as shown in Fig. 4.2. Users should be aware of this problem and may prefer to give the interface element a finite thickness in the mesh by specifying the actual co-ordinates of the nodes.

The shear behaviour in the elastic region is controlled by K_s/t as shown in Fig. 4.3. After reaching the limiting shear stress (defined as $\tau_{lim} = c + \sigma_n \tan\delta$), the shear stress is

maintained at τ_{lim} by making corrections within the loading increment (in subroutine OUTSLP). When unloading occurs, the original shear modulus will be reinstated. Figure 4.3 shows the result of a single element test with c = 30, δ = 30° and an applied normal stress = 100, the corresponding τ_{lim} = 66. The K_n/t ratio was kept constant (=1×10^7) for analyses with different thickness and they all showed exactly the same result, indicating that the performance of the element is not sensitive to the thickness.

The material property K_{sres} defines the shear modulus after reaching τ_{lim} and has very little effect on the shear behaviour once τ_{lim} is reached because of the stress correction mentioned previously. However, in subroutine DSLIP, the shear modulus K_s is changed to K_{sres} when the shear stress reaches $0.99\tau_{lim}$. This has two consequences:

i. If in a load increment the shear stress is beyond $0.99\tau_{lim}$ but has not yet reached τ_{lim} ($0.99\tau_{lim} < \tau < \tau_{lim}$), the shear modulus will be changed from K_s to K_{sres} and the shear stress-displacement relationship is as shown in Fig. 4.4. This is likely to happen when very small load steps are used in the analysis.

ii. During unloading, the beginning of the shear stress-strain relationship will be assigned a shear modulus equal to K_{sres} until the shear stress decreases to below $0.99\tau_{lim}$, after this the shear modulus returns to K_s as shown in Fig. 4.4.

These effects may not have too much influence on the shear behaviour in loading, unless K_{sres} is set to a very small value compared with K_s (as recommended in the user manual); in this case the behaviour in unloading could become very different from that expected. This unexpected behaviour may be unreasonable.

Analyses have shown that the value of K_{sres} does not have any effect on the element stresses in the slip mode, so the problem with unloading can be avoided by setting $K_{sres} = K_s$.

When the normal stress is in tension, representing the case in which the interface has separated, a correction is made in subroutine OUTSLP to correct the shear stress to zero or

a very small negative value according to the direction of normal strain increment. This makes the effect of the reduction of shear modulus by a large factor (100 in the program code in subroutine DSLIP, not 1×10^{-5} as stated in the manual) meaningless.

In subroutine OUTSLP, a further correction is made in the program to set the shear stress to zero when the normal stress is less than a very small positive value. This may cause problems for analyses with zero *in situ* stresses which give zero normal stress for the interface element to start off with, and lead to zero shear stiffness in the first increment of the analysis until the normal stress increases to a very small positive value (1×10^{-10}).

The expected normal behaviour of the original CRISP90 interface element is elastic, as stated in the user's manual, and controlled by K_n/t when the normal stress is compressive. The normal modulus is reduced by a factor of 100 when the normal stress is tensile, as shown in Fig. 4.5. Because CRISP uses a tangent stiffness approach to solve non-linear problems, the normal stiffness in any increment where the normal stress changes from compression to tension will be K_n/t. This may lead to a significant tensile stress in the element when either K_n or the increment steps are very large. In subroutine OUTSLP of the original program, a correction is made to overcome this problem such that the normal stress will correct back to a small negative value, as shown in Fig. 4.5.

It is reasonable to keep the tensile stress to a very low value if separation across the interface occurs. However, if in any subsequent increment the gap reduces (the direction of displacement reverses), the program restores the normal modulus to K_n immediately after the start of the increment of reverse displacement, as shown in the single element test result in Fig. 4.6. Physically a gap may still exist although the program assumes the interface has closed.

4.3.3. DRCRISP Interface Element

The interface element has five material properties:

- k_s shear stiffness (force/unit area/unit length)
- k_n normal stiffness (force/unit area/unit length)
- c cohesion intercept (force/unit area)
- δ angle of friction of the interface (degrees)
- k_{nt} normal stiffness at separation of interface (force/unit area/unit length)

Due to the formulation of the element, however, the element sides must be straight (*i.e.* cannot be specified as curved sides) even though it has mid-side nodes. The element was originally intended to model the interface between soil and reinforcement in reinforced embankment problems and only for monotonic loading.

The shear behaviour of the DRCRISP interface element is similar to the one in CRISP90. The elastic region is controlled by k_s, and after reaching the yield stress ($= c + \sigma_n \tan\delta$), the shear stiffness is set to zero. A correction is made to the element stress if any equilibrium error occurs after yielding. When unloading occurs, the elastic shear stiffness is restored When normal stress is tensile, the program will set $k_s = 1\times10^{-5}$ to avoid excessive equilibrium error and the shear stress to zero. When the normal stress is equal to or less than zero, the program will assume the element is in separation mode and zero shear stiffness is assigned to the element. This means the analysis should start off with some appropriate *in situ* stresses to keep the normal stress compressive if the interface is in contact at the beginning of the analysis.

Figure 4.7 shows the result of a single element test with the same material properties as the CRISP90 interface element in Section 4.3.2. Fluctuation of stress occurred when the element unloaded to negative stress.

The normal behaviour of the element is linear elastic and controlled by the normal stiffnesses k_n and k_{nt} in compressive normal stress and tensile normal stress respectively. A stress correction is made to the normal stress to maintain it at zero when separation occurs. From the results of a single element test (Fig. 4.8), it was found that the program crashed (zero pivot error) when the normal stress changed from compression to tension.

Clearly the formulation for the DRCRISP interface element has problems both in shear and normal behaviour once the stress goes negative. In the DRCRISP user's manual (Russell, 1992b) it is pointed out that the stress averaging method used in the element may cause a problem when tensile normal stress occurs. However, at the moment, it is recommended that the element should only be used in monotonic load, *i.e.* no unloading occurs in the analysis, and should not be used to model gap formation at an interface where the normal stress becomes tensile. It should be reiterated that the interface formulation was originally developed specifically for monotonic loading.

4.3.4. Conventional Quadrilateral Element

A conventional 8-noded quadrilateral element with elastic-perfectly plastic material properties was used to model interface behaviour. There are five material properties:

- E Young's modulus (force/unit area)
- ν Poisson's ratio
- c cohesion intercept (force/unit area)
- ϕ angle of friction (degree)
- J yield criterion

The values of E and ν were determined using Eq. (2.35) such that the behaviour of the element was the same as the previous two interface elements.

The shear behaviour of the element is similar to the previous two interface elements and is controlled by k_s (see Eq. 2.34) and τ_{lim} ($= c + \sigma_n \tan\phi$ for Mohr-Coulomb yield criterion).

Due to the formulation of the element, the shear and normal behaviour are coupled and, therefore, the element behaviour is sensitive to its thickness. Figure 4.9 shows the single element test results of the shear behaviour for different thicknesses (element width was 1.0). The E and ν values of each analysis were adjusted with the thickness of the element to give constant k_s and k_n values, using Eq. (2.35), for direct comparison of results. When the element was thick, coupling has a large influence on the behaviour. When the element was thin enough, the effect became negligible. No numerical problems were observed for an aspect ratio up to 100,000. Figure 4.10 shows the results of two analyses with different values of Poisson's ratio ν for $t = 0.01$. The shear behaviour is very similar; this is the case for any thickness, provided the aspect ratio of the element is large (over 100).

The normal stiffness of the element is identical in tension and compression, so the element cannot be used to model the separation at the interface. From the results plotted in Fig. 4.11, it can be seen that the normal behaviour is also sensitive to the element thickness. It should be noted that the element can yield in the normal direction as well as the shear direction. The element is weaker in tension than in compression when using the Mohr-Coulomb yield criterion because the tensile (negative) normal stress reduces the yield stress ($\tau = c + \sigma_n \tan\phi$). From the single element test results, it is recommended that an L/t ratio of at least 100 should be adopted if the conventional element is used to model interface behaviour.

4.4. Modifications to the CRISP90 Interface Element

4.4.1. Normal Behaviour

Based on the single element test results presented in the last section, it was decided that the CRISP90 interface element was the most appropriate, in terms of both shear and normal

behaviour, for modelling soil/pipe interaction in this research. However, modifications to the element's behaviour would have to be made in order to overcome some of the problems mentioned earlier and to improve its ability in modelling normal behaviour.

For the "gap" problem during closure of the interface (see Fig. 4.6), an attempt was made to prohibit the stress correction but this left significant tensile stress in the soil. Also, a problem of "overshoot" occurred where the gap was physically closed but the program still assumed it was open and assigned a normal modulus of $K_n/100$, as shown in Fig. 4.12.

A more reasonable approach for the modification is to retain the stress correction at the first increment into tension, but then by-pass the correction in any subsequent increments during tension. In programming terms, a flag system has been set up to control the normal behaviour. When $\sigma_n \geq 0$, flag = 0; after the first increment in tension, the flag is changed to 1. If flag = 0, a correction for tensile stress will be made; if flag = 1, the program will skip the correction. When in any subsequent increment the gap is closed and the interface returns to a state where $\sigma_n \geq 0$, the flag will be restored to zero. As a further modification, an extra soil parameter K_{nsep}, representing the normal modulus during separation, has been introduced into the input data. This is an alternative to internally setting the modulus to $K_n/100$ and results in improved flexibility in the control of material properties. A single element test on the modified element (Fig. 4.13) shows a much better response compared with Figs 4.6 and 4.12. However, a tiny gap remains after rebonding, in which the gap size is equal to the size of one increment. This is due to the fact that CRISP uses a tangent stiffness approach for non-linear solutions, so there is a one-increment lag for the correction of stress. If sufficiently small increment steps are used, the error will be negligible. By specifying a very small K_{nsep}, the tensile stress during separation can be kept to a minimum. No numerical problems have been observed by using a K_n/K_{nsep} ratio of up to 1×10^9.

For a cohesive soil, a small tensile stress can usually be sustained before separation occurs (see the experimental result in Fig. 2.35). In order to model this behaviour, and later to

study the effect of this tensile adhesion stress, a further modification was made to the normal behaviour. An extra soil parameter σ_{ntlim} was introduced to represent the limiting normal stress for adhesion. Figure 4.14 shows the idealized normal behaviour of an interface element which can sustain a limiting adhesion.

A revised flag system has been introduced such that when flag = 0, the interface is in contact; when flag = 1, the interface is in tension but within the limiting adhesion; when flag = 2, the interface is separated, as shown in Fig. 4.15. The normal stress correction is made after the first increment if the normal stress exceeds σ_{ntlim} and to a value equal to $K_{nsep}/K_n \times \sigma_{ntlim}$ rather than zero. This minimizes the gap problem when rebonding occurs.

Figures 4.16 and 4.17 show strain controlled and stress controlled single element test results, with different σ_{ntlim}, respectively. When σ_{ntlim} is specified as zero, the behaviour recaptures the same behaviour as the first modification (Fig. 4.13). It can be seen that the results of strain controlled test is slightly better than the stress controlled one during the transition between compression and tension. This is because non-uniform stress has developed across the integration points of the element in stress controlled test during the transition from tension to compression, *i.e.* some integration points having very small positive stress and some having very small negative stress, leading to inconsistency of normal stiffness across the element.

The value of the cohesion intercept determined from a direct shear box test with the soil sheared over the pipe surface material may be used for σ_{ntlim} and it may range from zero (dry sand) to the soil's cohesion intercept, depending on the bonding condition between the pipe and the soil. In very fine grain soil, however, the effect of suction between the pipe wall and the soil may lead to a much higher value of σ_{ntlim} than from the shear box test. To include any possible suction effect on σ_{ntlim}, it is better to determine it using special laboratory or *in situ* tests by pulling a plate made of the pipe wall material away from the soil.

4.4.2. Shear Behaviour

The shear behaviour has been modified such that it will follow the Mohr-Coulomb criterion when flag = 0 and 1, but the shear stress will be corrected to zero when flag = 2. Table 4.1 summarizes the modified behaviour of the CRISP90 interface element in different modes. The details of the modification including a tree diagram of the subroutines that have been modified and the listing of the modified FORTRAN code were documented in a report by Ng (1994).

4.5. Benchmark Tests to the Interface Elements

4.5.1. Long Elastic Block

In additional to the single element tests performed in Sections 4.3 and 4.4, it is also desirable to benchmark the interface elements with available analytical/closed-form solutions. The first benchmark considered was an analytical solution for soil/structure interface elements presented by Hird & Russell (1990). A long elastic block is bonded along one side to a rigid material with interface elements and the other side is free to slide. The block is loaded in compression at one end and restrained at the other. Figure 4.18 shows the geometry and the FE mesh of the analysis.

The three different interface elements have been tested. Table 4.2 summarizes the material properties of the elastic block and the interface elements.

At the beginning of the analysis, small vertical compressive stresses have to be applied to the interface elements (CRISP90 and DRCRISP interface elements) in order to keep the normal stress greater than zero such that the shear stiffness would not be set to zero at the onset of the analysis. The vertical stress does not influence the behaviour of the interface

elements because they are defined as purely cohesive ($\delta = 0$). Tensile normal stress has developed in the interface elements close to the loaded end of the block, as reported by Hird & Russell (1990).

The finite element results, as shown in Figs 4.19 to 4.21 for the CRISP90 interface element, the DRCRISP interface element and the conventional element respectively, indicate that all three kinds of interface element give very good agreement with the analytical solutions which are marked (T) in the figures.

4.5.2. Laterally Loaded Circular Pile in Cohesive Soil

The second benchmark considered was a circular pile loaded laterally in a cohesive soil presented by Randolph & Houlsby (1984). They assumed that the behaviour of the pile at great depth (> $3D$) could be approximated as a thin slice of pile and soil under plane strain conditions. Based on plasticity theory, they found that the exact solutions for the limiting lateral pressure on the pile disc to be $11.94c_u$ and $9.14c_u$ for a perfectly rough and a perfectly smooth soil/pile interface respectively. However, no allowance was made for possible breakaway of soil at the back of the pile.

Some previous researchers have tried to model this problem numerically. Kooijman & Vermeer (1988) used the finite element method with interface elements to model the slip between the soil and the pile, so that a rough pile, a smooth pile or any skin friction value between the two extreme conditions could be modelled. The numerical results agreed well with the theoretical solutions. However, the interface elements could not model separation between the pile and the soil and full tensile stress was carried at the back of the pile.

Lane & Griffiths (1988) also studied the problem using the finite element method. They used modified quadrilateral finite elements in which the degrees of freedom at a node were decoupled. This enables the element to model perfectly rough and smooth interfaces. They

first solved the problem for a purely cohesive soil permitting tension and good agreement with the theoretical solutions was obtained. They then introduced a criterion for permissible tension in the soil such that the tensile stress that could be carried varying from zero (no tension) to some permitted limit. The results, as shown in Fig. 4.22, indicate that as the permissible tension decreases, the stiffness and ultimate pressure of the *P-y* curves also decreases, although the maximum was not always well defined. They stated that in practice if the permissible tension $< 0.5c_u$ this can be approximated as no tension and if the permissible tension $> 10c_u$ this may be represented by full tension. From their plastic displacement vector plots, they observed that significant soil movement still occurred behind the pile for the no tension case in order to maintain mesh continuity, although the movement was reduced compared with the full tension case. The extent of the soil disturbance was also smaller for a smooth pile than for a rough pile.

In the present research, the problem has been studied again to test the ability of the interface element to model gap formation between the soil and the pile. Only the modified CRISP90 interface element has been tested. Figure 4.23 shows the FE mesh for the analysis which consists of 120 8-noded quadrilateral elements. The pile has a diameter of 2 units and a rigid boundary was placed at five pile diameters away from the edge of the pile.

The problem was first solved for a purely cohesive soil with elastic-perfectly plastic material properties and a Mohr-Coulomb yield criterion (c_u = 100, ϕ = 0, $E = 3\times10^5$, ν = 0.49) which permits tension. Excellent agreement was obtained to the analytical solution with an overestimate of approximately 3% as shown in Fig. 4.24.

A thin layer of interface elements was then introduced into the FE mesh to model the soil/pile surface. Using different values of c for the interface element, different τ_{lim} values of the soil/pile interface (*i.e.* roughness) have been modelled. In this case, a rough pile with $c = 5c_u$, smooth pile with $c = 0.001c_u$ and a realistic pile with $c = 0.5c_u$ of the soil. Also by changing the material parameter σ_{ntlim} of the interface element, full tension and no tension

have been modelled by setting a very high value ($100c_u$) and zero respectively. Figures 4.25 and 4.26 show the *P-y* curves predicted using interface element with full tension and no tension respectively, and each with three different skin friction assumptions of the pile. Excellent agreement was obtained with the closed-form solution for the full tension case. This demonstrates that the interface element handling full tension correctly. Some fluctuation of the *P-y* curve was found (Fig. 4.25) due to the correcting stress made for the equilibrium error after yielding of the soil in the finite element code. Reduced stiffness and ultimate pressure of the *P-y* curves was obtained for the no tension case (Fig. 4.26), although the maximum was not well defined.

The displacement vector plots and the contour plots of horizontal stress are shown in Figs 4.27 to 4.28 for a rough pile with full tension and no tension respectively. These demonstrate the effect of tensile stress at the back of the pile on the movement and stress distribution in the soil. The interface elements have effectively modelled the gap formation between soil and the back of the pile and have minimized the soil displacement at the back of the pile (compare Figs 4.27a with 4.28a). The tensile stresses developed in the soil at the back of the pile have also been minimized (compare Figs 4.27b with 4.28b). More detailed results of the stress and strain distributions in soil for the full tension and no tension analyses were reported by Ng (1994).

The effect of the limiting tension has been studied and the results are demonstrated in Fig. 4.29. The initial stiffness of the *P-y* curves with a non-zero tension limit were significantly higher than the no tension case. After the tension limit is reached the *P-y* relationships join the curve for no tension. This is due to the opening of the interface and the resulting lack of tensile stress transfer across it and is consistent with the real behaviour of soil/pile interface (Fig. 2.35). This is in contrast to the analysis by Lane & Griffiths (1988), who assumed that constant tensile stresses can be maintained in the soil at the back of the pile after reaching the permissible tension (Fig. 4.22). It is suggested that the present analyses, using the modified CRISP90 interface element, have modelled the tensile

behaviour at the soil/pile interface more realistically referring to the actual behaviour of the soil/pile interface.

4.6. Summary

Three different kinds of interface element have been examined and their behaviour compared. The DRCRISP interface element, originally developed for modelling the interface between soil and reinforcement in reinforced embankment problems and only for monotonic loading, is not suitable to model problems with unloading and/or interface separation. The conventional 8-noded quadrilateral element is excellent in modelling shear behaviour but failed to model separation at interface. The CRISP90 interface element, though having unsatisfactory performance in some cases, was the most appropriate element to model soil/pipe interface, and modifications have been made to overcome the problems and to improve its ability in modelling the normal behaviour. The result of single element tests and benchmark tests have shown that the modified CRISP90 interface element can satisfactorily model all modes of deformation of soil/structure interface.

In the following chapter, the modified CRISP90 interface element will be used in the modelling of the axial push test (Section 3.2.1) using a simplified 2-D FE analysis. The model can substantially save computational effort and still provide reasonably good results. In Chapter 7, the modified CRISP90 interface element will also be used in 2-D plane strain FE analyses to obtain the pressure-displacement relationship of the soil spring in the elastic beam on elastic foundation model (Chapter 6) for the modelling of the lateral push test described in Section 3.2.2.

Flag	0	1	2
Status of interface element at normal direction	Contact	Adhesion	Separation
Normal stress	$\sigma_n \geq 0$ (compression)	$0 \geq \sigma_n \geq \sigma_{ntlim}$ (only changing from contact to adhesion and before reaching σ_{ntlim})	$0 > \sigma_n$ (after σ_{nt} reached σ_{ntlim})
Normal modulus	K_n	K_n	K_{nsep}
Limiting shear stress	$\tau_{lim} = c + \sigma_n \tan\delta$	$\tau_{lim} = c + \sigma_n \tan\delta$ (but greater than zero)	$\tau_{lim} = 0$
Shear modulus	K_s	K_s	$K_s/1\times10^5$

Table 4.1. Modified behaviour of the interface element at different modes of deformation.

	Material properties
Elastic block	$E = 1\times10^5$, $\nu = 0$, $G = 5\times10^4$
CRISP90 interface element	$c = 30$, $\delta = 0$, $K_s = 1\times10^2$, $K_n = 1\times10^4$, $t = 0.01$
DRCRISP interface element	$c = 30$, $\delta = 0$, $k_s = 1\times10^4$, $k_n = 1\times10^6$
Conventional element	$c = 30$, $\phi = 0$, $E = 299$, $\nu = 0.495$, thickness = 0 01

Table 4.2. Material properties of the elastic block and interface elements

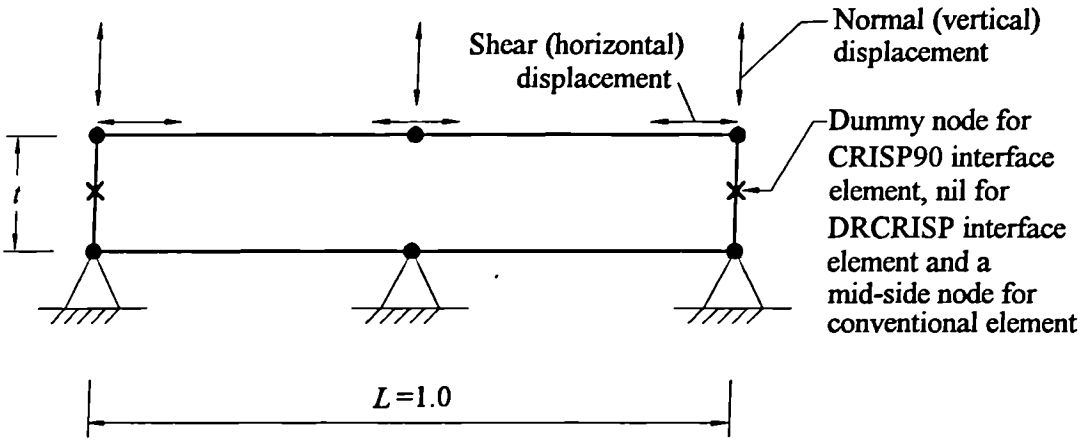

Fig. 4.1. General geometry of single interface element test.

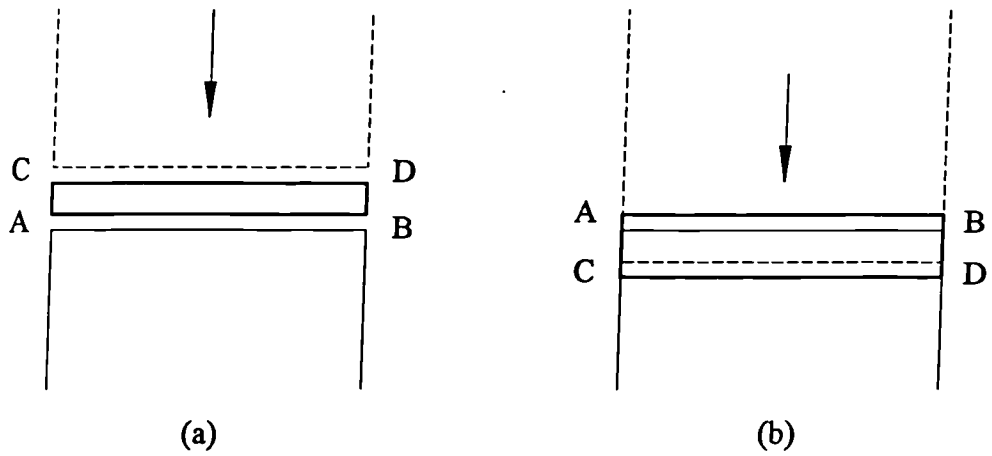

Fig. 4.2. Overlapping of the CRISP90 interface element in the normal direction when coinciding double-nodes used under compressive normal stress.

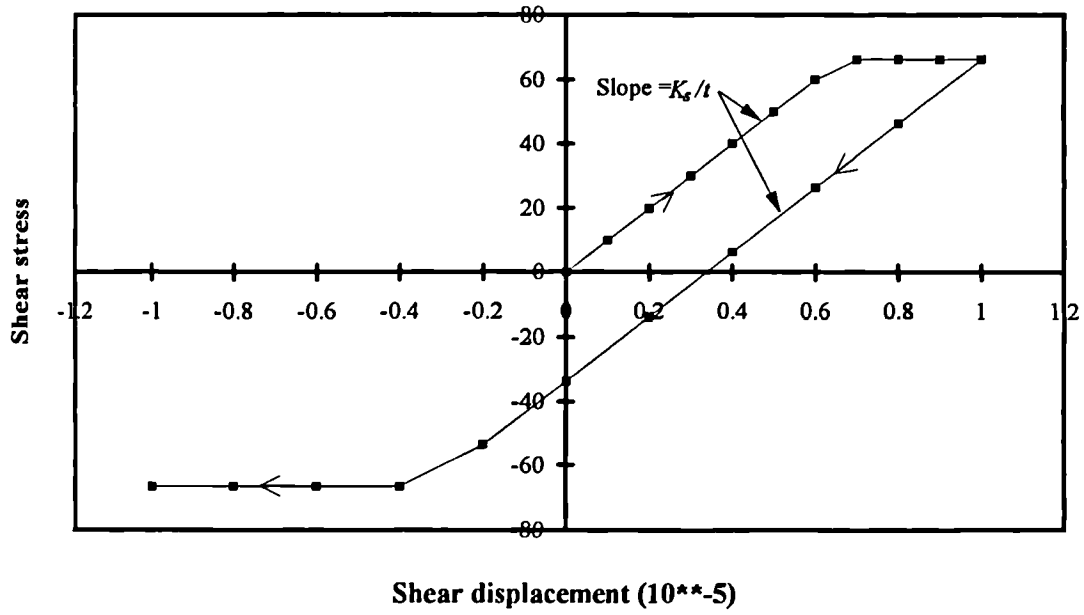

Fig. 4.3. Single element test result for shear behaviour of the CRISP90 interface element.

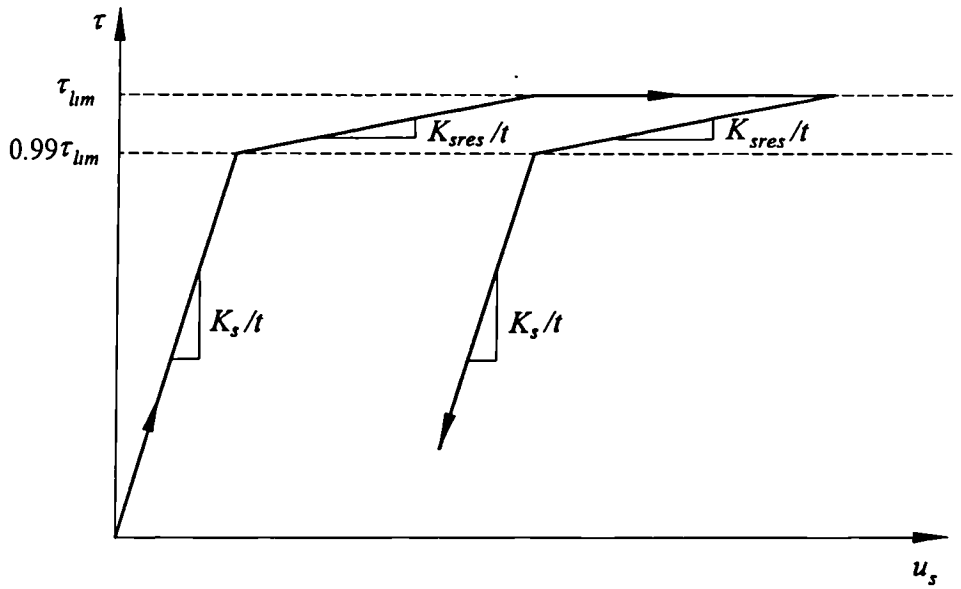

Fig. 4.4. Shear stress-strain relationship of the CRISP90 interface element when very small load steps are being used.

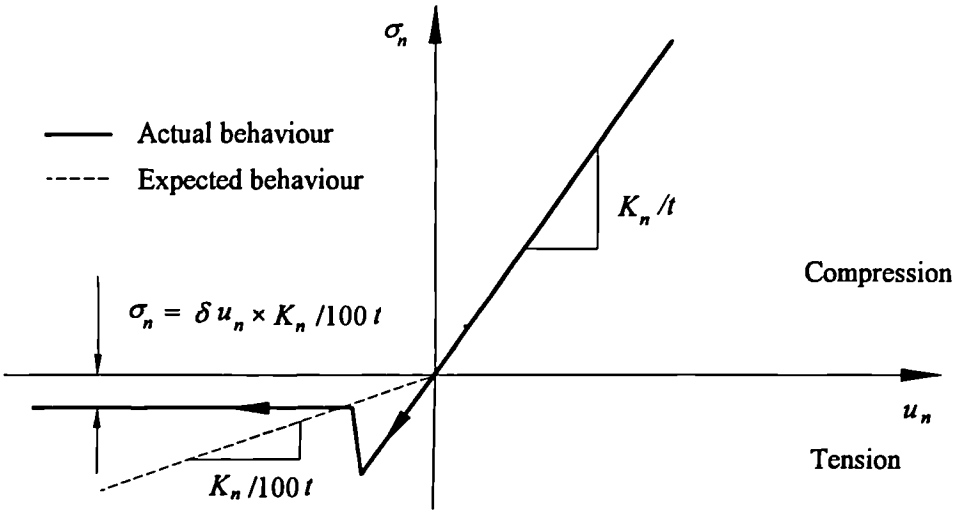

Fig. 4.5. Expected and actual normal behaviour of the original CRISP90 interface element.

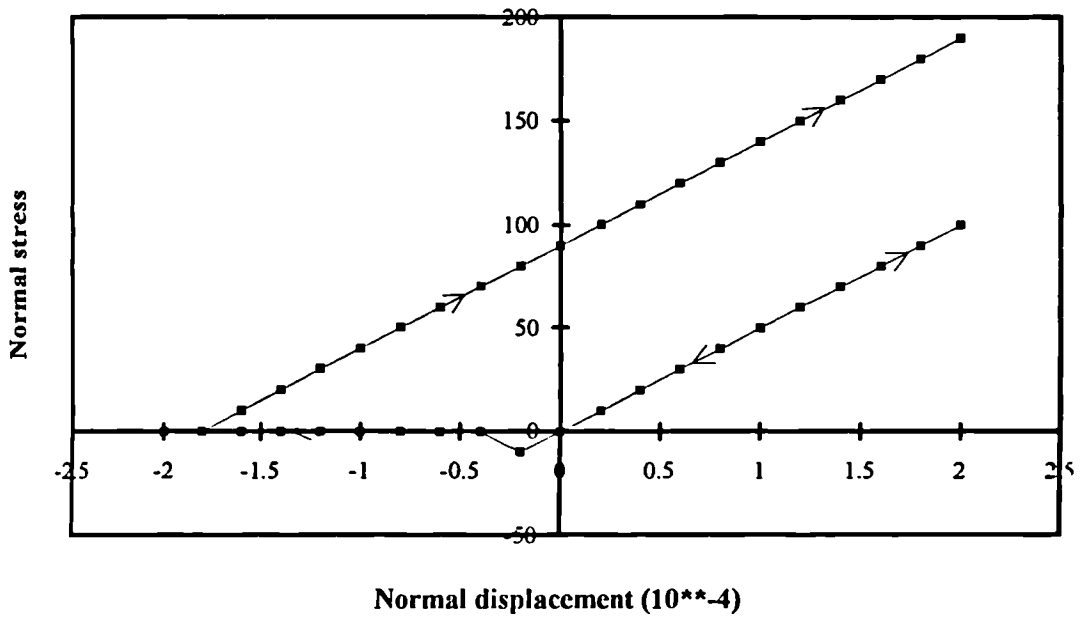

Fig. 4.6. Single element test result for normal behaviour of the original CRISP90 interface element when reversal of displacement occurs.

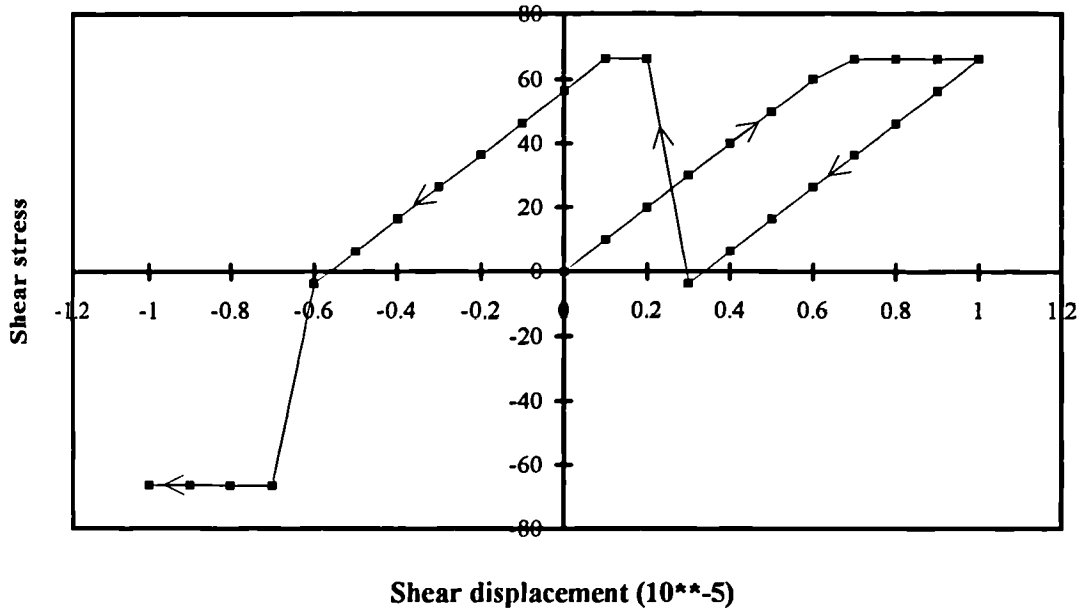

Fig. 4.7. Single element test result for shear behaviour of the DRCRISP interface element under compressive normal stress.

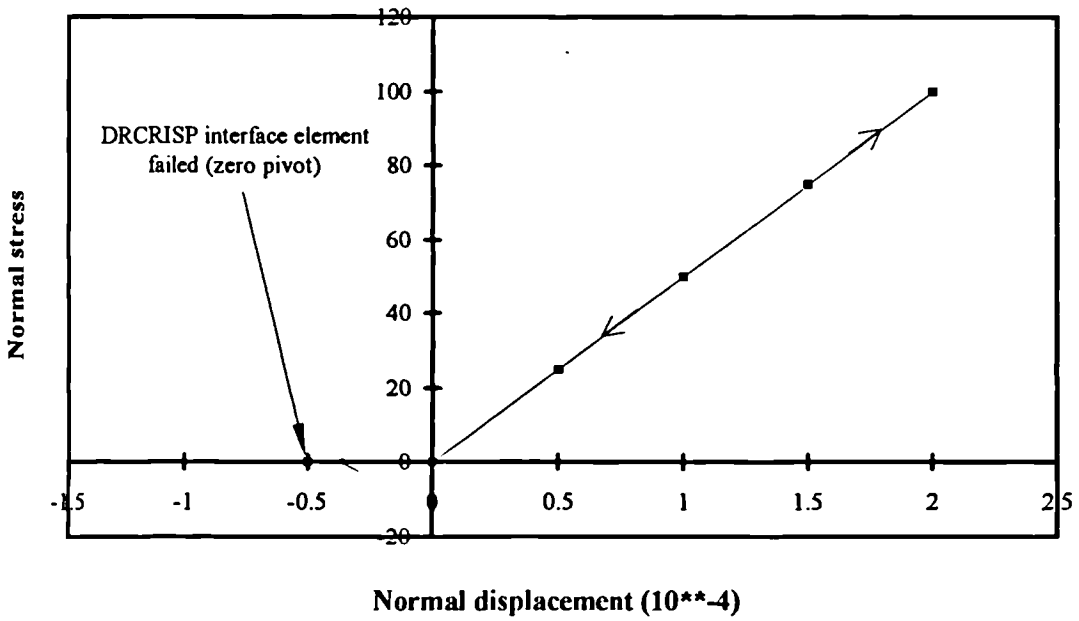

Fig. 4.8. Single element test result for normal behaviour of the DRCRISP interface element.

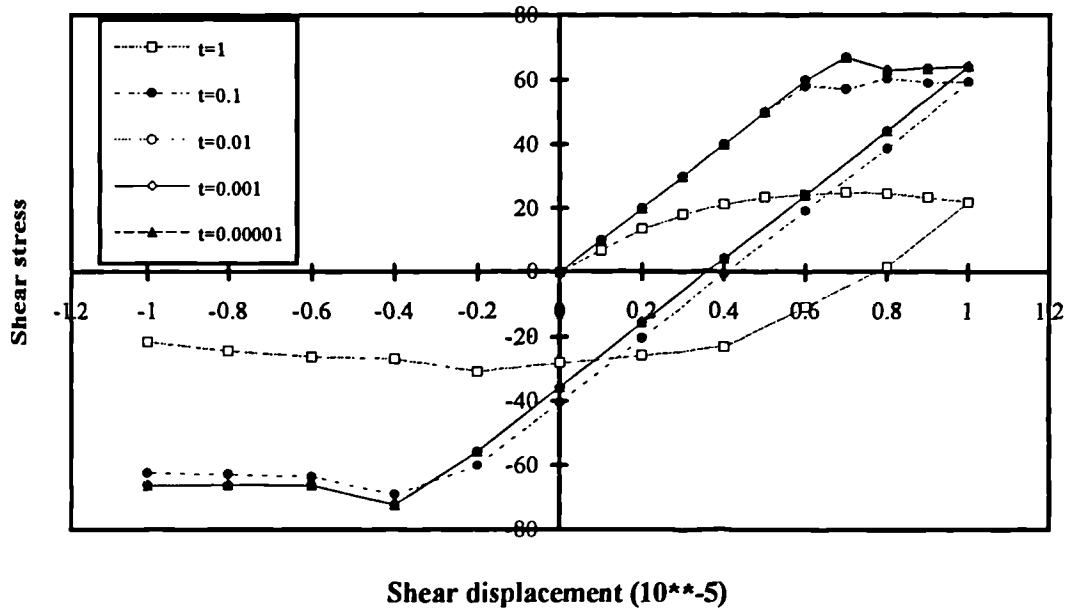

Fig. 4.9. Single element test results for shear behaviour of conventional quadrilateral element with different thickness.

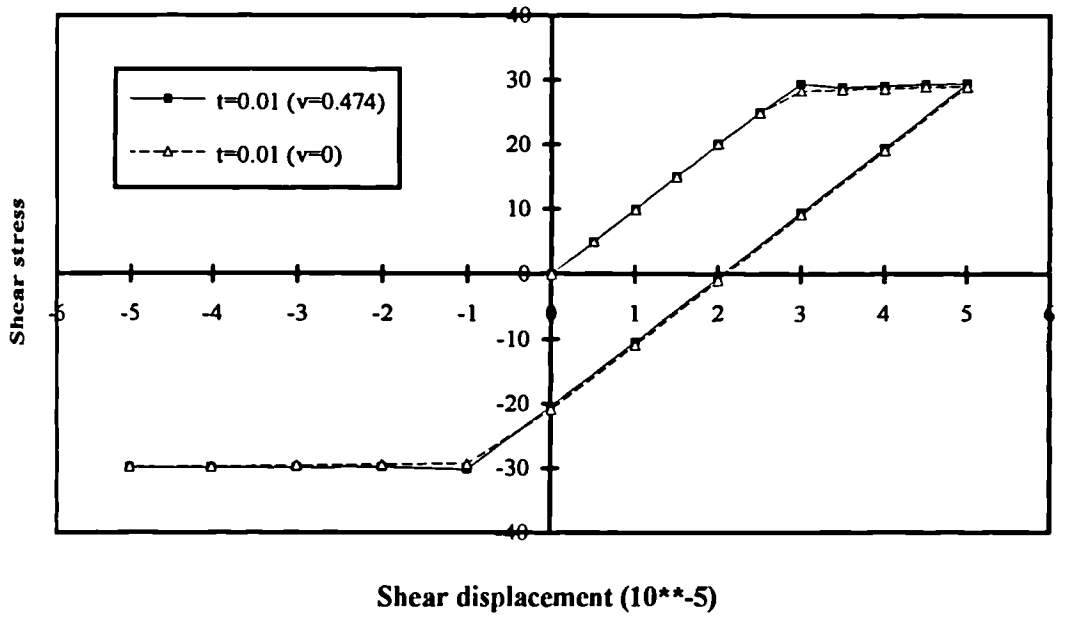

Fig. 4.10. Single element test results for shear behaviour of conventional quadrilateral element having different Poisson's ratio.

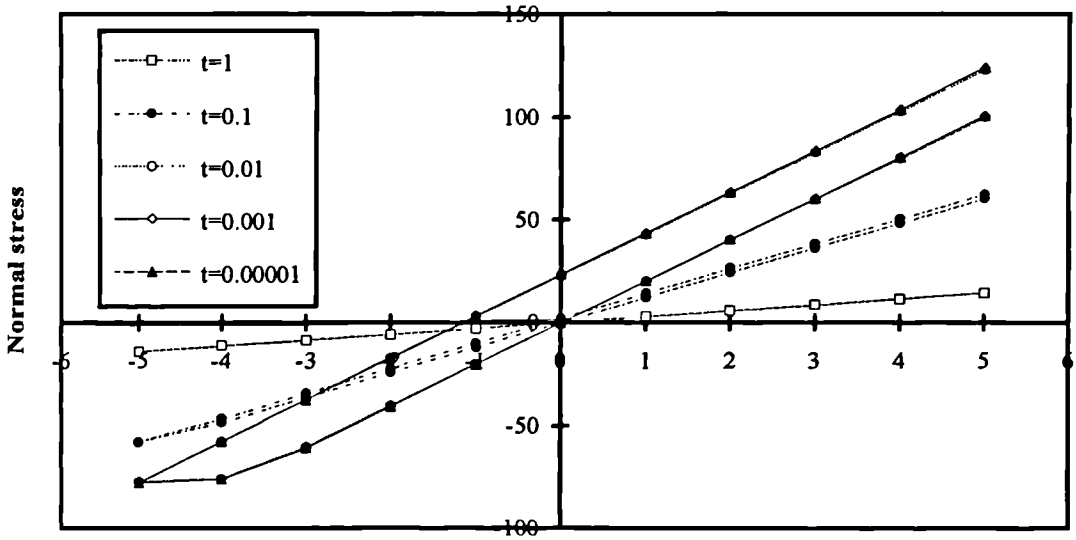

Fig. 4.11. Single element test results for normal behaviour of conventional quadrilateral element with different thickness.

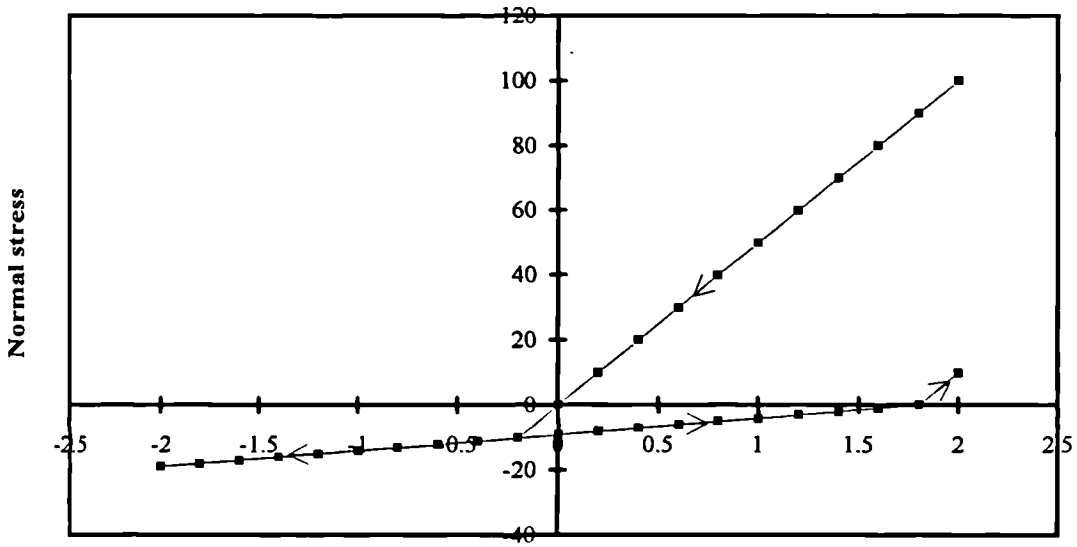

Fig. 4.12. Single element test results for normal behaviour of the CRISP90 interface element with no correction of stress during separation.

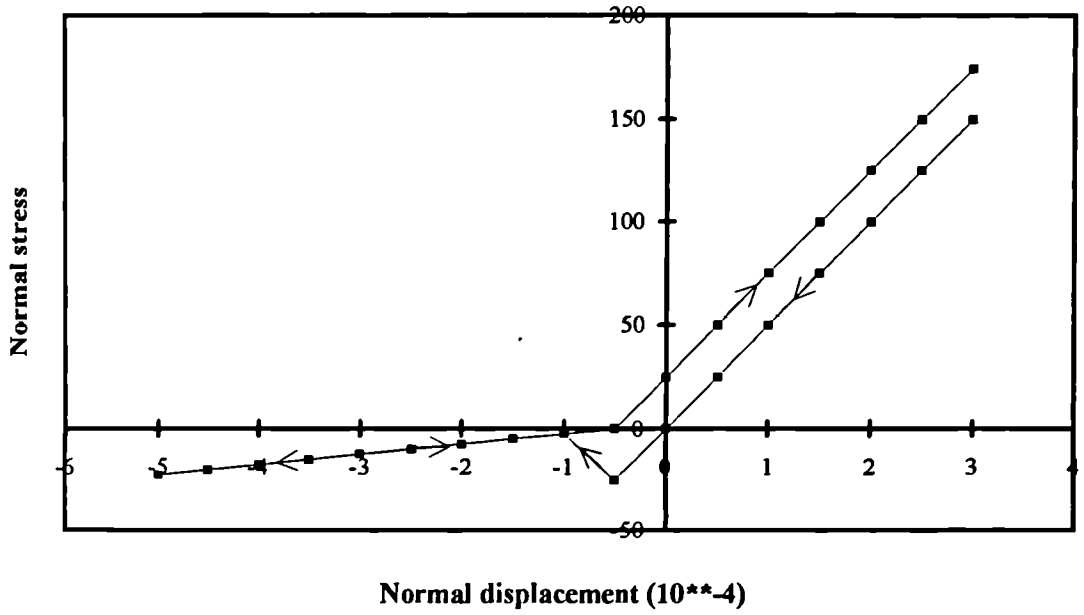

Fig. 4.13. Single element test result for normal behaviour of the CRISP90 interface element after modification.

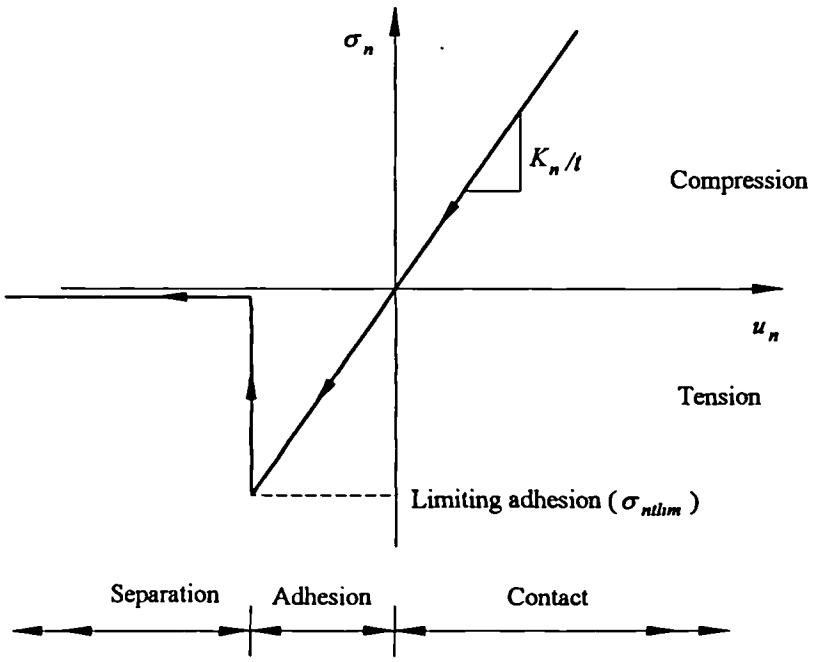

Fig. 4.14. Idealized normal behaviour of an interface element which can sustain a limiting adhesion.

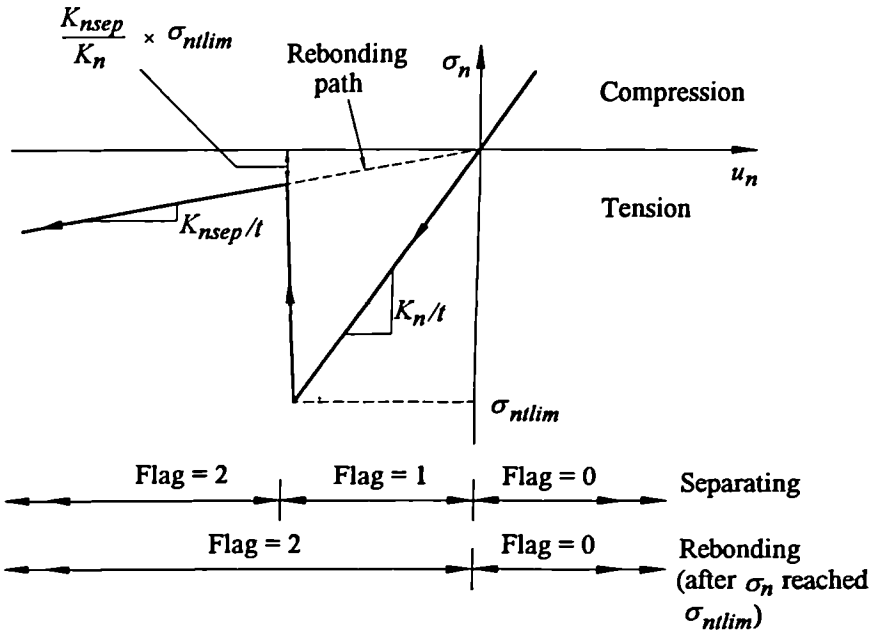

Fig. 4.15. The normal behaviour of the modified CRISP90 interface element to sustain a limiting adhesion.

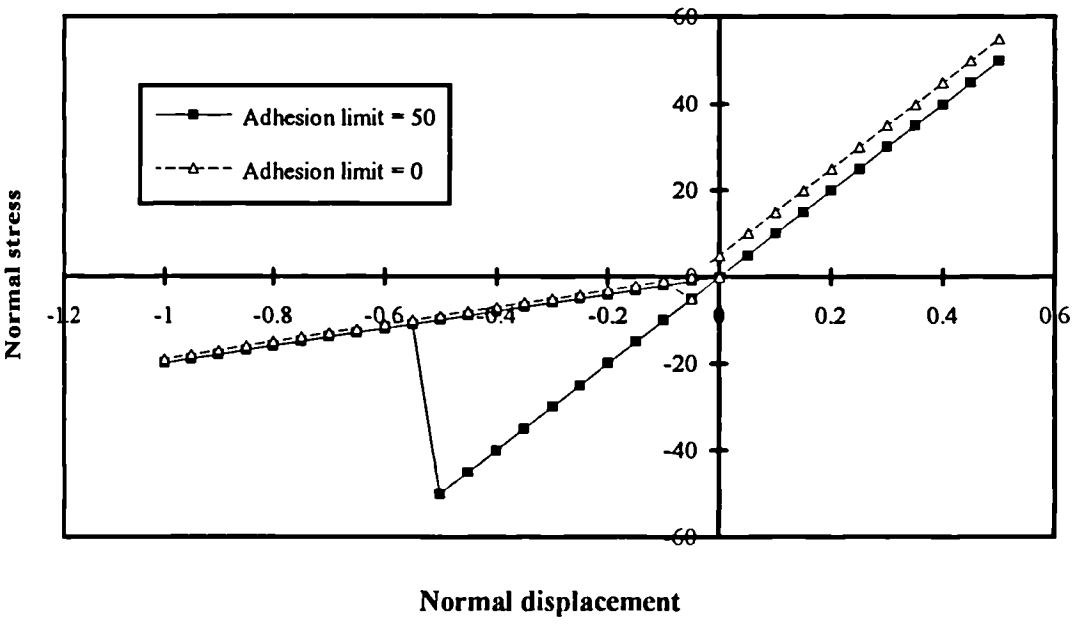

Fig. 4.16. Strain controlled single element test results for normal behaviour of the CRISP90 interface element after the modification for limiting adhesion.

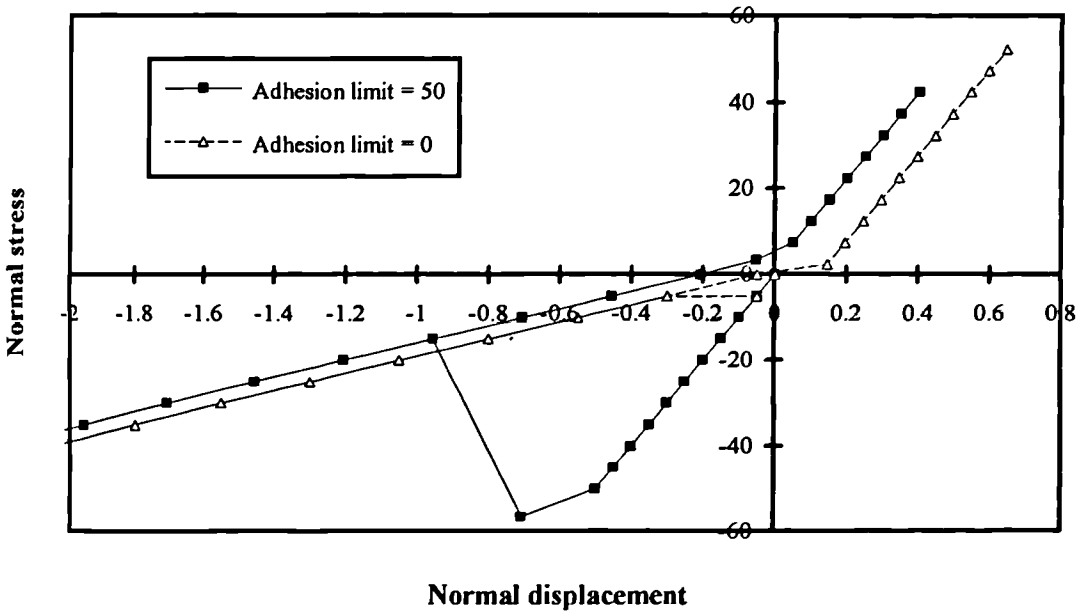

Fig. 4.17. Stress controlled single element test results for normal behaviour of the CRISP90 interface element after the modification for limiting adhesion.

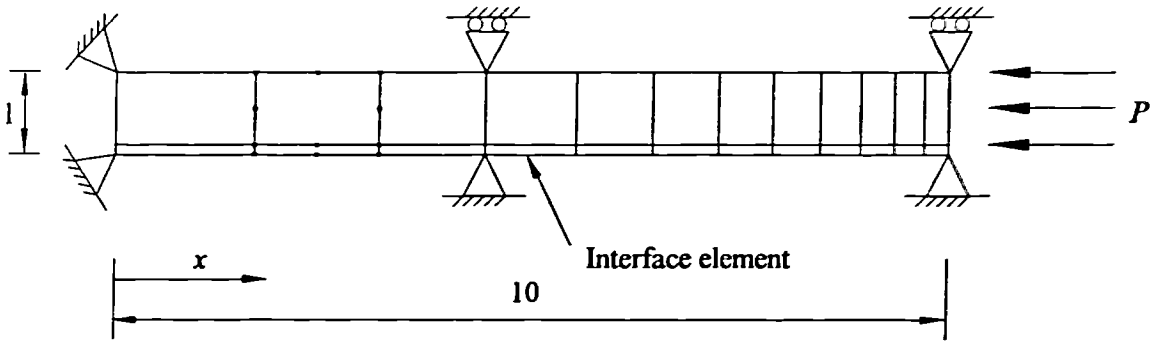

Fig. 4.18. The geometry and FE mesh for the long elastic block benchmark.

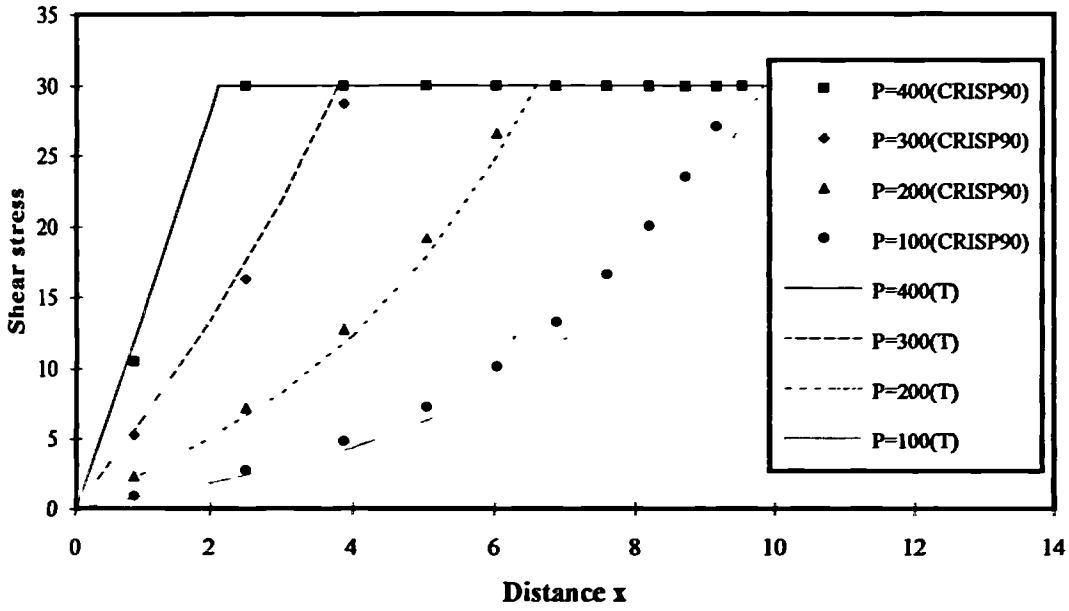

Fig. 4.19. Distribution of shear stress along the interface using the CRISP90 interface elements.

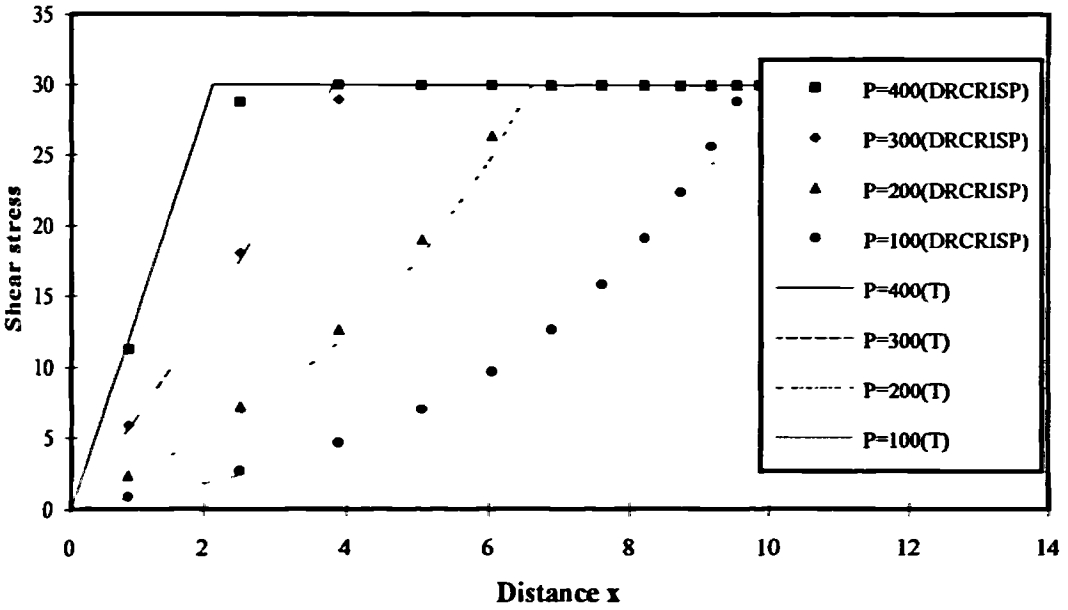

Fig. 4.20. Distribution of shear stress along the interface using the DRCRISP interface elements.

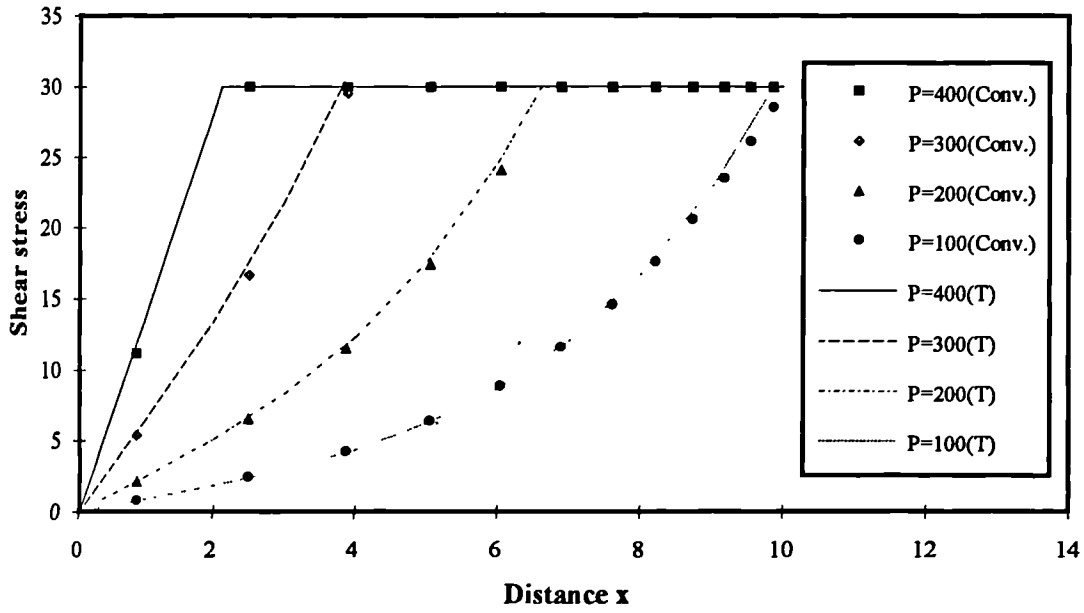

Fig. 4.21. Distribution of shear stress along the interface using the conventional elements.

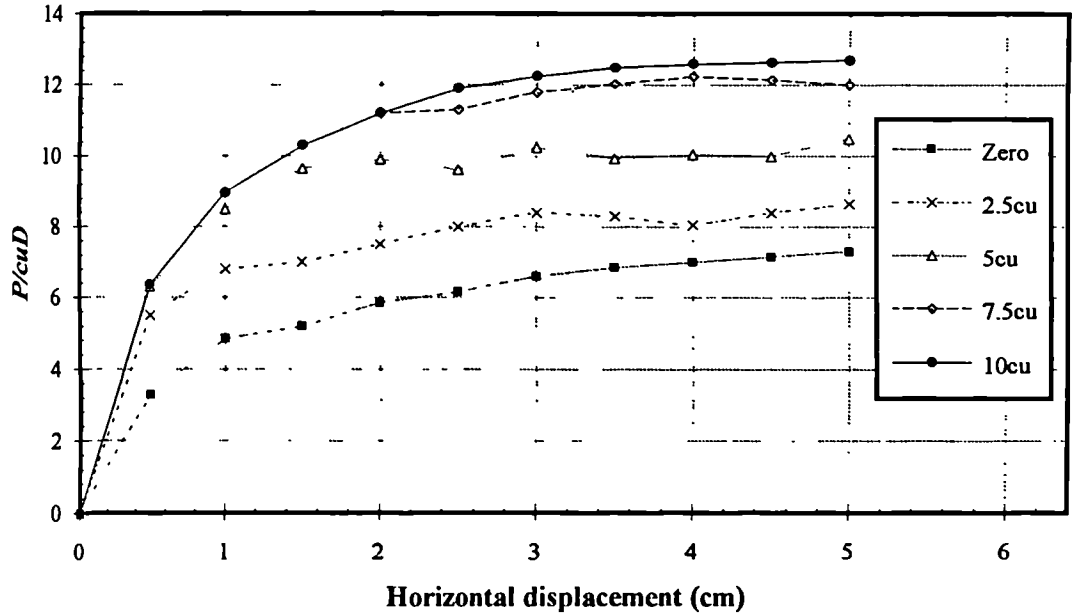

Fig. 4.22. Effect of permissible tension on load-displacement response of a rough pile in cohesive soil with $\nu = 0.3$ (after Lane & Griffiths, 1988).

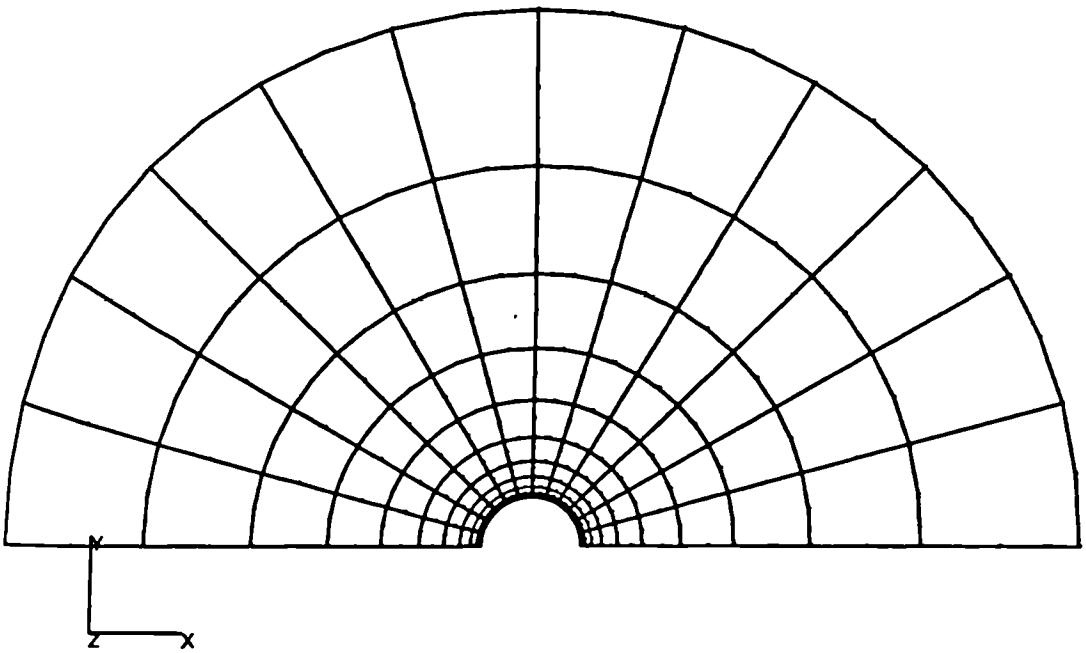

Fig. 4.23. The FE mesh for the benchmark of laterally loaded circular pile.

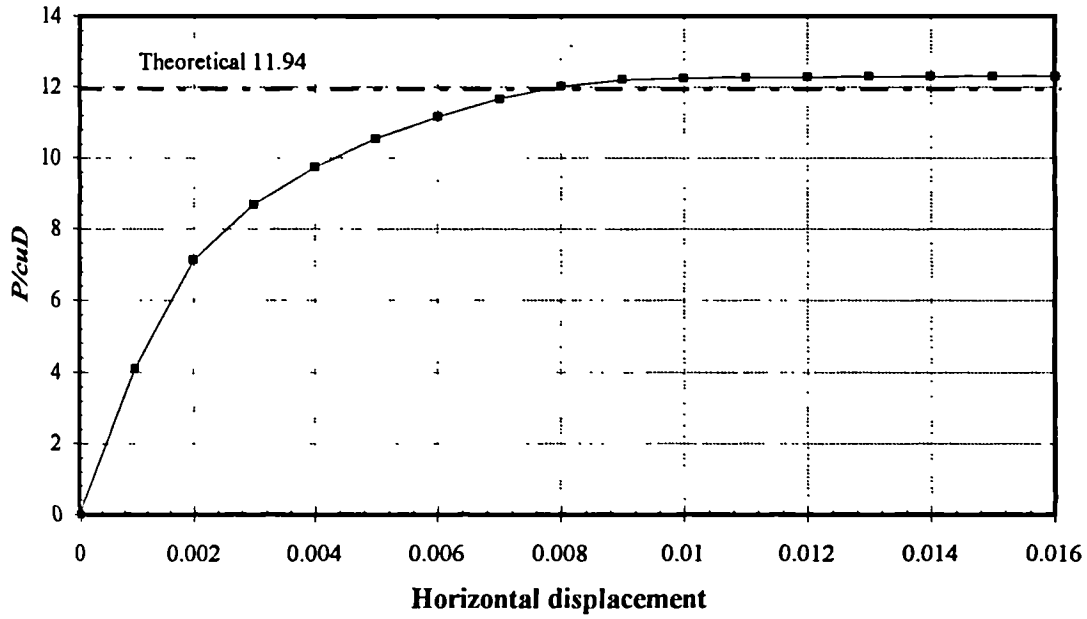

Fig. 4.24. Load-displacement response of a rough pile in cohesive soil (full tension).

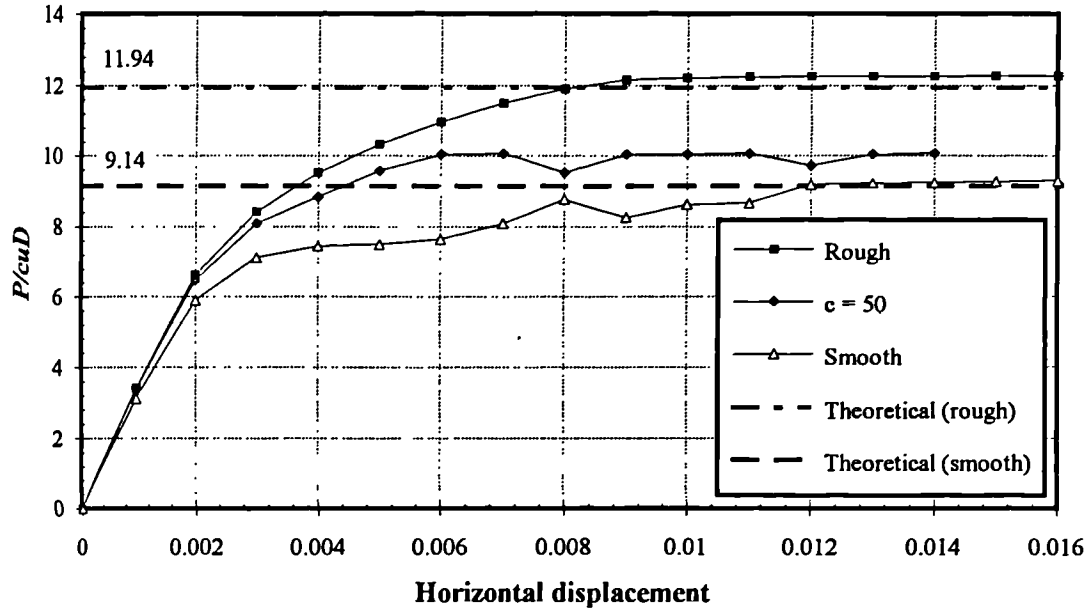

Fig. 4.25. Load-displacement responses of a pile carrying full tension in cohesive soil with different roughness (using interface elements).

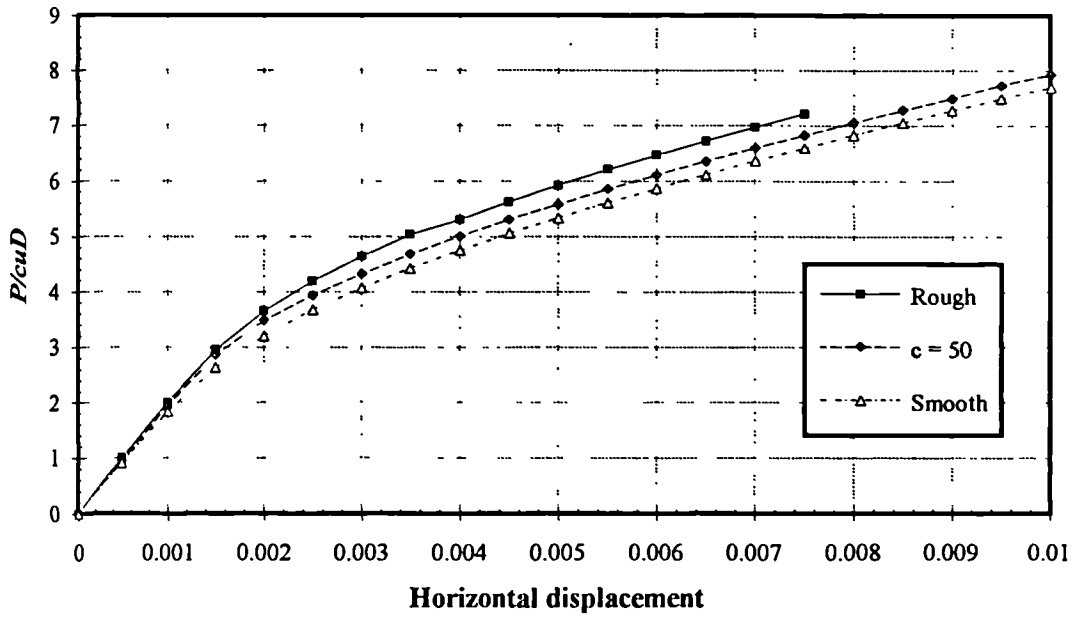

Fig. 4.26. Load-displacement responses of a pile carrying no tension in cohesive soil with different roughness (using interface elements).

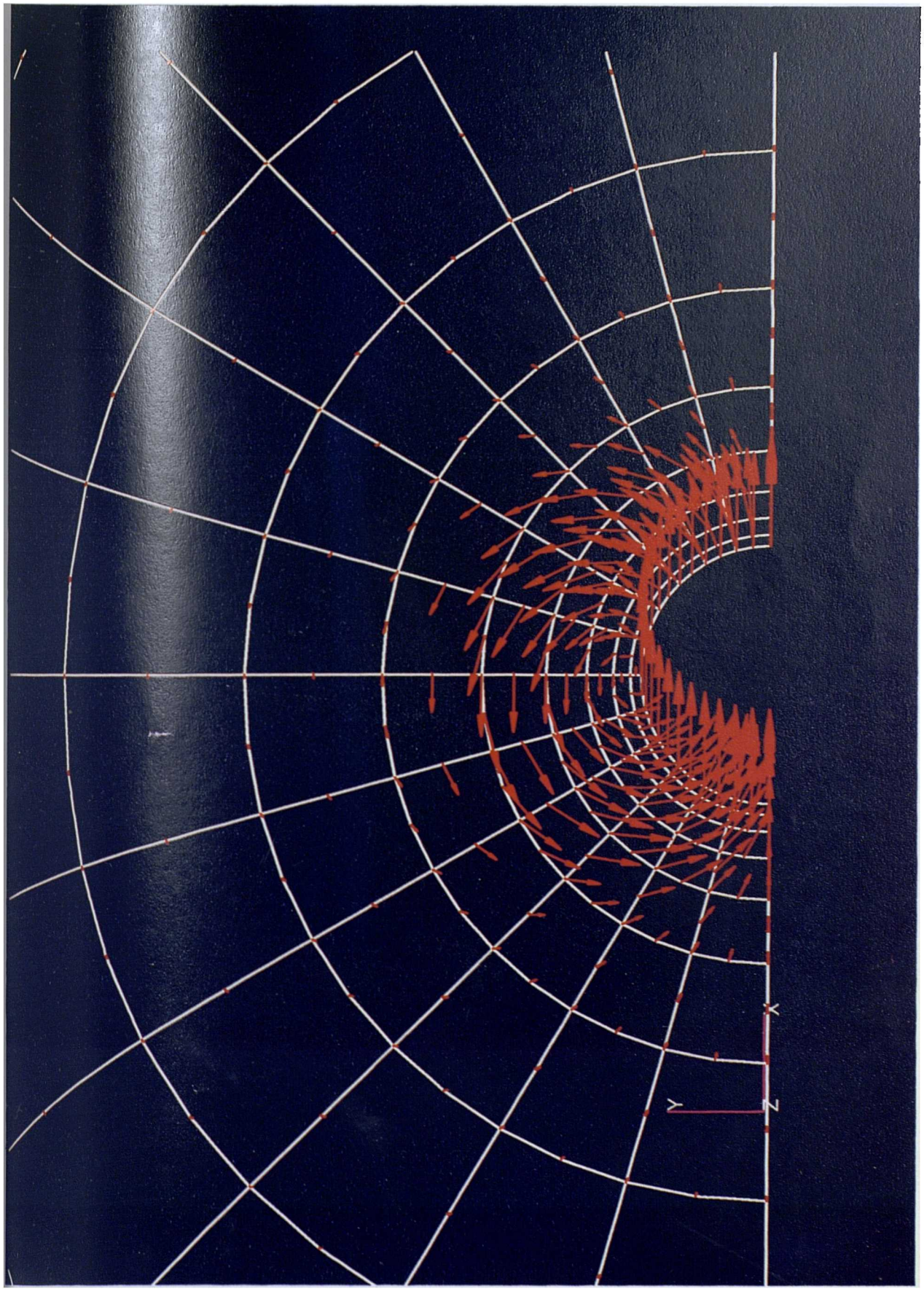

Fig. 4.27 (a). Displacement vectors of a laterally loaded rough pile with full tension.

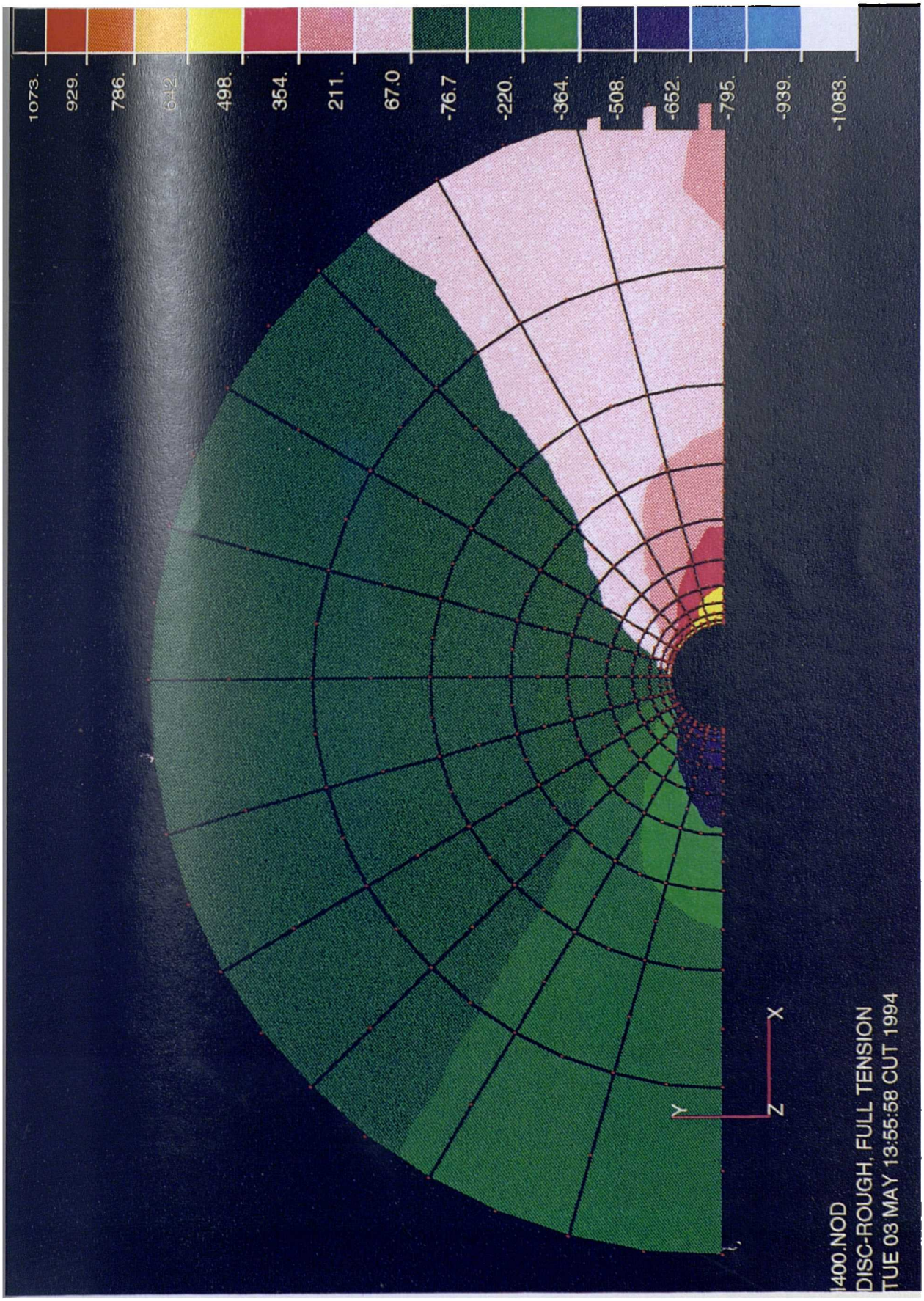

Fig. 4.27 (b). Horizontal stress contour of a laterally loaded rough pile with full tension.

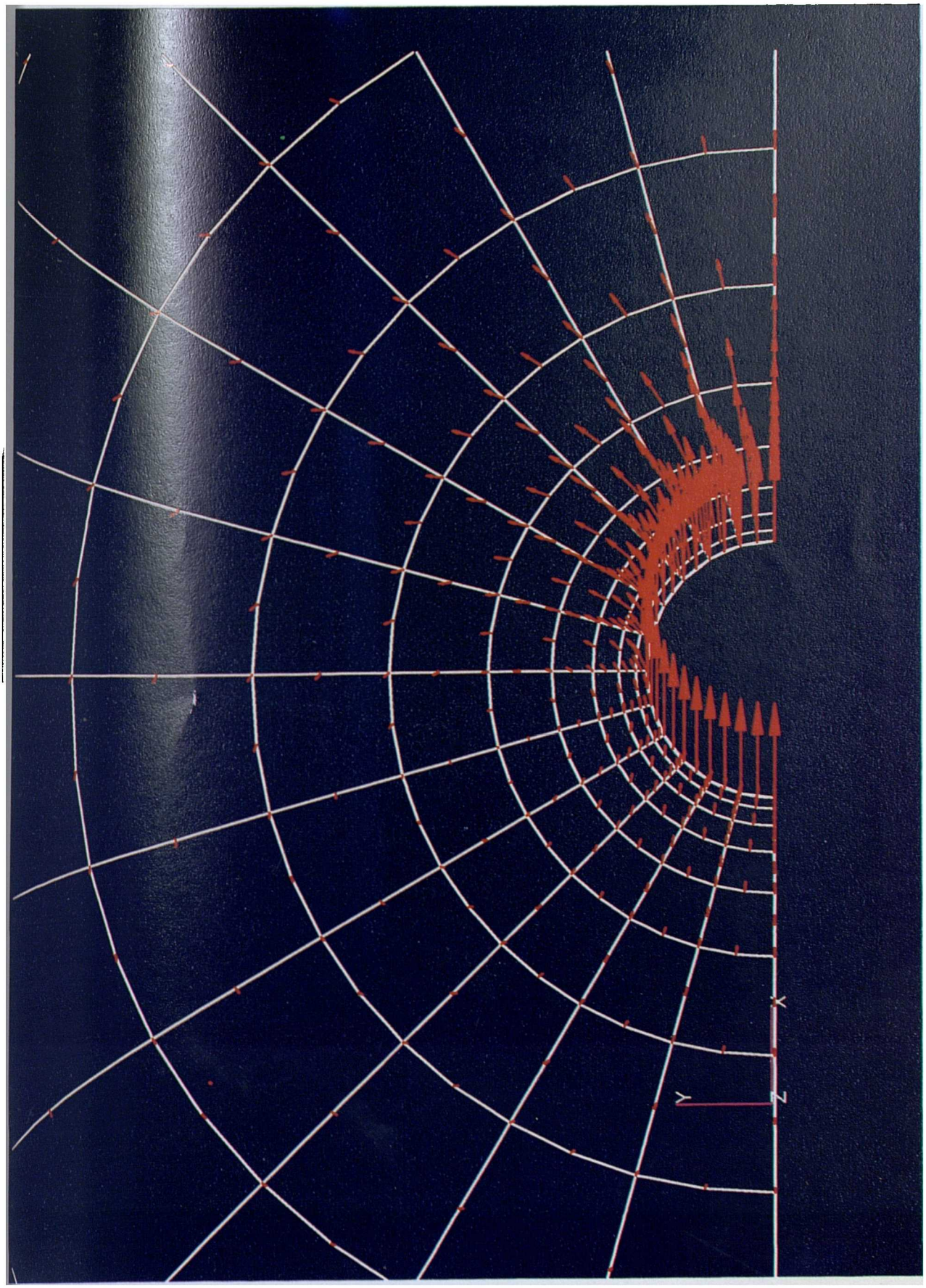

Fig. 4.28 (a). Displacement vectors of a laterally loaded rough pile with no tension.

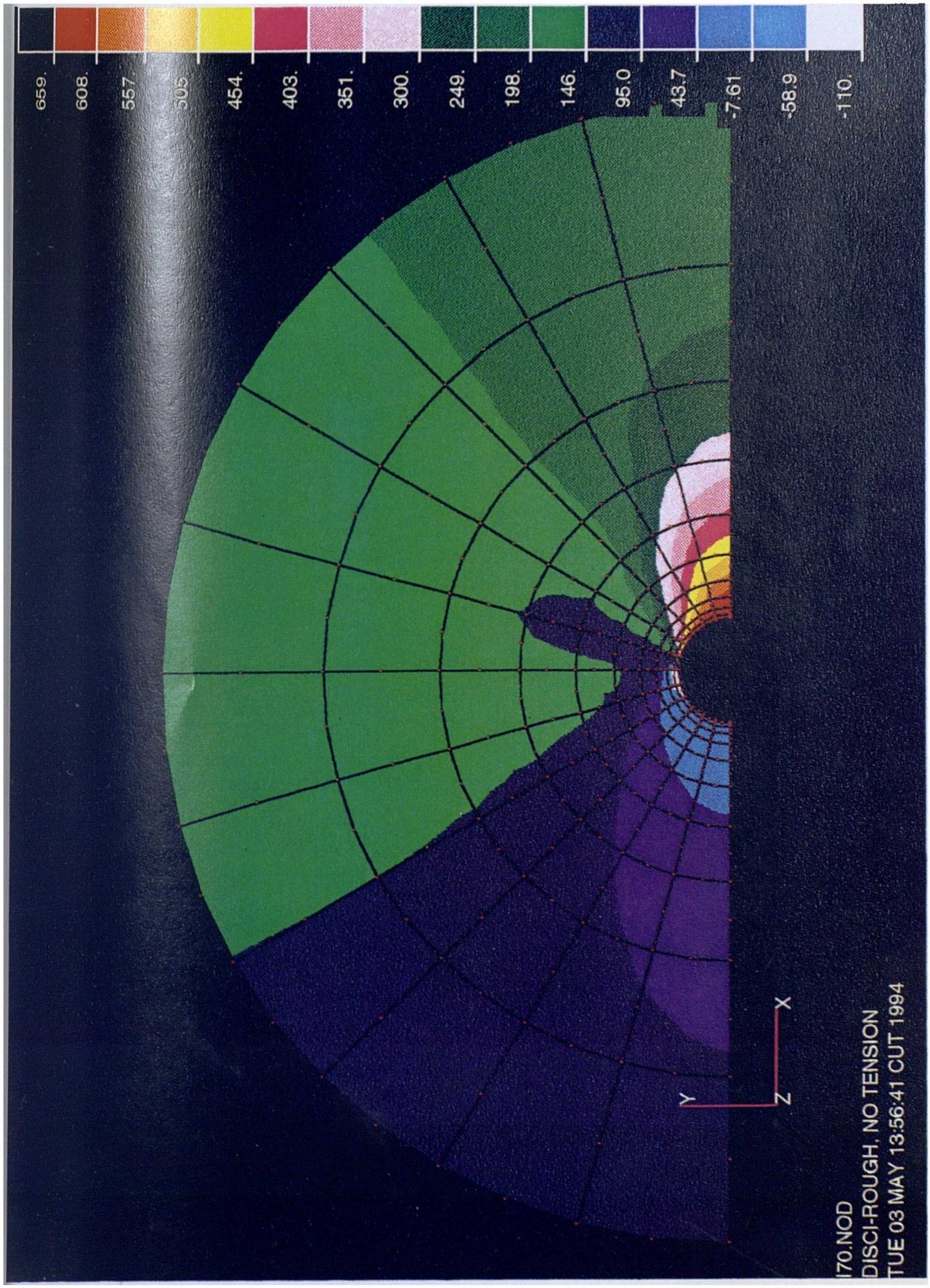

Fig. 4.28 (b). Horizontal stress contour of a laterally loaded rough pile with no tension.

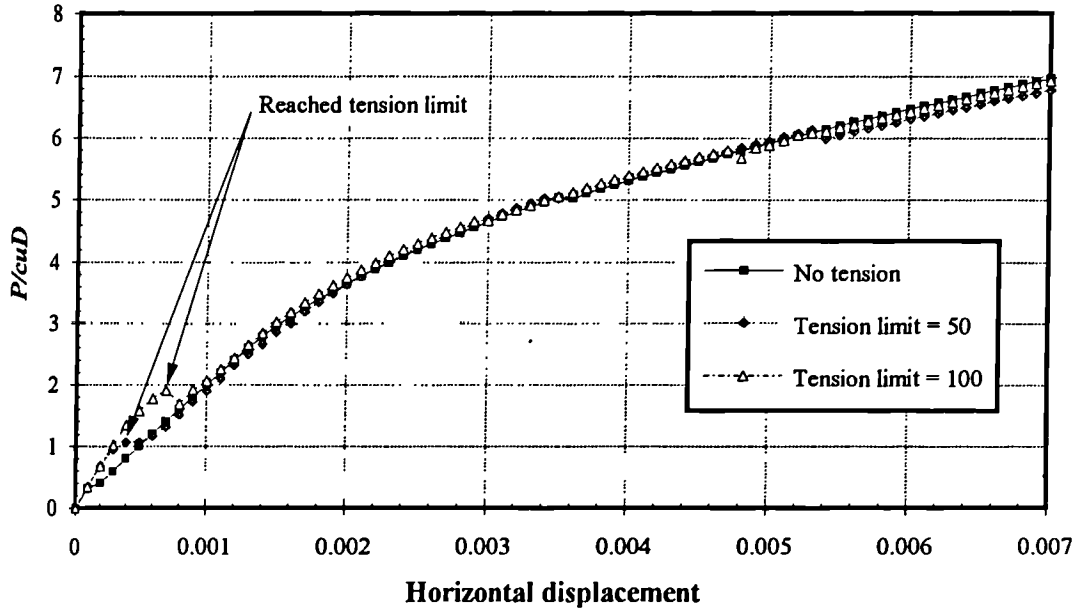

Fig. 4.29. Load-displacement responses of a rough pile with different tension limit in cohesive soil (using interface elements).

CHAPTER 5

NUMERICAL MODELLING OF THE AXIAL PUSH TEST

5.1. Introduction

The 1-D models described in Sections 2.6.2.1 and 2.6.2.2 may be used to numerically simulate the axial push test and has the advantage of being simple to formulate and to use. However, the 1-D approach ignores the existence of the surrounding soil and fails to predict the total displacement of the pipe. Whilst a three-dimensional finite element method is more appropriate, due to the 3-D nature of the geometry this would be very expensive. Also as a 3-D interface element is not available in the FE program, 3-D analysis is not possible at the moment and a 2-D finite element model is proposed. It is a simplified version of the full 3-D model in that it retains the essential influence of the surrounding soil and is more sophisticated than the 1-D approach. The results of the axial push test (Section 3.2.1) will be used to validate the simplified 2-D model in the following section.

5.2. The Simplified 2-D Finite Element Model

The proposed 2-D model consists of a flat steel plate buried in the soil and subject to plane strain conditions, as shown in Fig. 5.1. The non-uniform radial pressure acting around the pipe is first replaced with an equivalent uniform normal pressure. The pipe is then idealized as a flat plate having plane strain conditions. The thickness of the plate is equal to the

thickness of the pipe wall. A layer of soil equal to the thickness of the cover depth of the pipe is placed on top of the plate for applying the *in situ* stresses (the normal pressure). It has to be noted that a 2-D axisymmetric model can also be used, but the absence of an axisymmetric interface element in CRISP90 means only the plane strain model is feasible.

The ultimate axial resistance per unit length of the pipe can be expressed as:

$$r_u = (c_i + \sigma_{nav} \tan\delta)\pi D \tag{5.1}$$

where c_i is the cohesion intercept at the soil/pipe contact surface and σ_{nav} is the average normal stress acting around the pipe section.

Assuming a normal stress distribution as shown in Fig. 5.2, the average normal stress acting on the pipe can be estimated:

$$\begin{aligned}\sigma_{nav} &= \frac{\gamma}{4}(2C+D)(1+K_0) \\ &= \frac{\gamma Z}{2}(1+K_0)\end{aligned} \tag{5.2}$$

Substituting Eq. (5.2) into Eq. (5.1):

$$r_u = \pi D c_i + \frac{\gamma Z}{2}(1+K_0)\pi D \tan\delta \tag{5.3}$$

From the results of direct shear box tests by Leach & Row (1991), the shear properties of the soil/pipe interface are: c_i = 10kN/m² and $\delta = 23°$. The average normal stress acting on the Hilderstone test pipe is estimated, by Eq. (5.2) and using K_0 = 0.37 (from Ng, 1993), to be 19.4kN/m². However, the pipe is empty, so the weight of the soil occupied by the pipe is deducted (the weight of the pipe was ignored, *i.e.* the stress at the bottom of the pipe is changed from $\gamma(C+D)$ to γC, Fig. 5.2). Thus the average normal stress acting on the Hilderstone pipe is re-estimated to be 14.7kN/m² and the ultimate axial resistance 16.2kN/m² or 46.6kN per metre run of the pipe.

It can be shown, however, that the average shear stress mobilised at the soil/pipe interface when failure occurred during the axial load test was lower than this value. The average shear stress mobilised was equal to:

$$r_u = \frac{\text{Total axial load at failure}}{\text{Total contact surface area between soil / pipe}} = \frac{3800\text{kN}}{274.2\text{m}^2} = 13.9\text{kN/m}^2$$

which does not agree with the estimated ultimate axial resistance of 16.2kN/m² (overestimated by 17%). It should be noted that the average value of the back-calculated shear stress in Fig. 3.7 for all the sections at loading = 3815kN (just before failure), with weighting to the length of the section, is equal to 14.0kN/m², which agrees well with the above calculated r_u value of 13.9kN/m².

Thus two sets of analysis were performed: one with the estimated r_u = 16.2kN/m² and the other with the back-calculated r_u = 13.9kN/m² which act as a comparison for checking the accuracy of the results using the estimated r_u.

A finite element mesh consisting of 203 elements was constructed as shown in Fig. 5.3. The pipe was modelled using elastic material properties of E = 209×10⁶kN/m² and ν = 0.3 An elastic-perfectly plastic model was used for the soil, in which E = 8400kN/m², ν = 0 07 and c = 20.6kN/m² (results from stress path test Hil01, Table 3.1). The soil/pipe interface was modelled using both modified CRISP90 interface elements and conventional 8-noded quadrilateral elements with elastic-perfectly plastic material properties (see also Chapter 4) However, preliminary analysis showed that the soil yielded at very early stage thus giving a very large and unreasonable soil displacement. It was found that an average c value of 25kN/m² (average of the backfill c_u in Table 3.1 and c_u of Hil01 and Hil02 in Table 3.3) gave much better results and for this reason the c value of 25kN/m² was used for the soil in later analyses.

The average normal stress was applied at the soil/pipe interface by setting up appropriate *in situ* stresses. Preliminary analysis showed, however, that the normal stress was substantially

reduced due to the yielding of the overlying soil, and tensile normal stress developed close to the loaded end. This reduction of normal stress, which was assumed to remain approximately constant, significantly influenced the behaviour of the interface elements. To overcome this problem, an equivalent cohesion of 16.2kN/m^2 and zero friction angle have been used for the first set of analyses. Thus the changes of normal stress has no influence to the analyses.

Two analyses were performed using conventional and CRISP90 interface elements. The predicted failure loads, as shown in Fig. 5.4, were approximately 4400kN and 4600kN for conventional quadrilateral elements and CRISP90 interface elements, which over-predict the result of the field test (3800kN) by 15 and 20% respectively. Figure 5.5 shows the displacement distribution of the overlying soil at different sections of the pipe. The soil displacement is much greater near the loaded end where large relative displacement between the soil and the pipe occurred, representing slip at the soil/pipe interface.

The predicted strain distributions, as shown in Figs 5.6 and 5.7, agreed well with the field test results (Group A strain gauges are 0.5m from the loaded end and Group E gauges 41.5m from the loaded end, see Fig. 3.3). Figures 5.8 and 5.9 show the relationship between shear stress and total pipe displacement predicted by the FE analysis using the conventional and the CRISP90 interface elements respectively. The shear stress values have been obtained using two different methods: the first method is by taking the results directly from the integration points of the interface elements, and the second method is by back calculation from the strain distribution along the pipe (*i.e.* the same method used in Section 3.2.1 to obtain the shear stress along the pipe for the field test). Both methods give similar results, suggesting that the method using the strain results of the pipe to calculate the shear stress is reliable.

One important relationship that has not been measured (and very difficult to measure) in the field test is the relationship between shear stress and relative soil/pipe displacement. This

relationship is required by the numerical model for analysis of the axial behaviour of the pipe and was obtained by means of direct shear box tests (Section 3.3.1). To investigate whether the relationship between shear stress and relative soil/pipe displacement measured in the direct shear box test is the same as in the field test, the results from the FE analyses have been examined. Figures 5.10 and 5.11 show the relationships between shear stress obtained by the two methods mentioned earlier and the relative displacement between the soil and the pipe for the analysis using CRISP90 interface elements. The relative displacement was taken as the difference between the displacement of the top and bottom nodes of the interface element. The relationships yielded a shear stiffness of 88000kN/m^3 and 80000kN/m^3 for the first and second methods to obtain the shear stress (taken directly at the interface and back-calculated from strain results) respectively. The results agree well with the input shear stiffness of 88000kN/m^3 for the interface element which was obtained by the direct shear box tests.

The second set of analyses was performed using an ultimate axial resistance of 13.9kN/m^2. The predicted failure loads agreed well with the field test (Fig. 5.12), but the predicted strain (Figs 5.13 and 5.14) and the shear stress-pipe displacement relationships (Figs 5.15 and 5.16) are not as good as the prediction using r_u = 16.2kN/m^2. These may be due to the previous suggestion made in Section 3.2.1 that the soil properties varied over the length of the tested pipe section thus the distribution of strain and shear stress also varied along the pipe.

It can be concluded that the proposed 2-D FE model is capable of modelling the axial push test if the *in situ* stress acting on the pipe is accurately estimated. More comparisons with field tests and a full 3-D FE analysis are needed to further validate the proposed 2-D model.

5.3. Summary

A new two-dimensional finite element model has been proposed to model the behaviour of a buried pipe subjected to an axial load. It is a simplified version of a 3-D FE model which is more realistic than a 1-D model. The 2-D model is able to model the essential influence of the surrounding soil (shear dilation and contraction), in a simplified manner, that the 1-D model cannot do. The limitations of the 2-D model are the idealization of the uniform loading and surrounding soil, also the boundary constraint (see also Section 8.6). The results of the Hilderstone axial push test have been used to validate the proposed model and the agreement was satisfactory. It is concluded that the proposed model is capable of modelling the axial load behaviour provided that the following facts can be estimated accurately: the *in situ* stresses acting on the pipe, the properties of the interface between the soil and the pipe, the material properties of the surrounding soil and the geometry of the site.

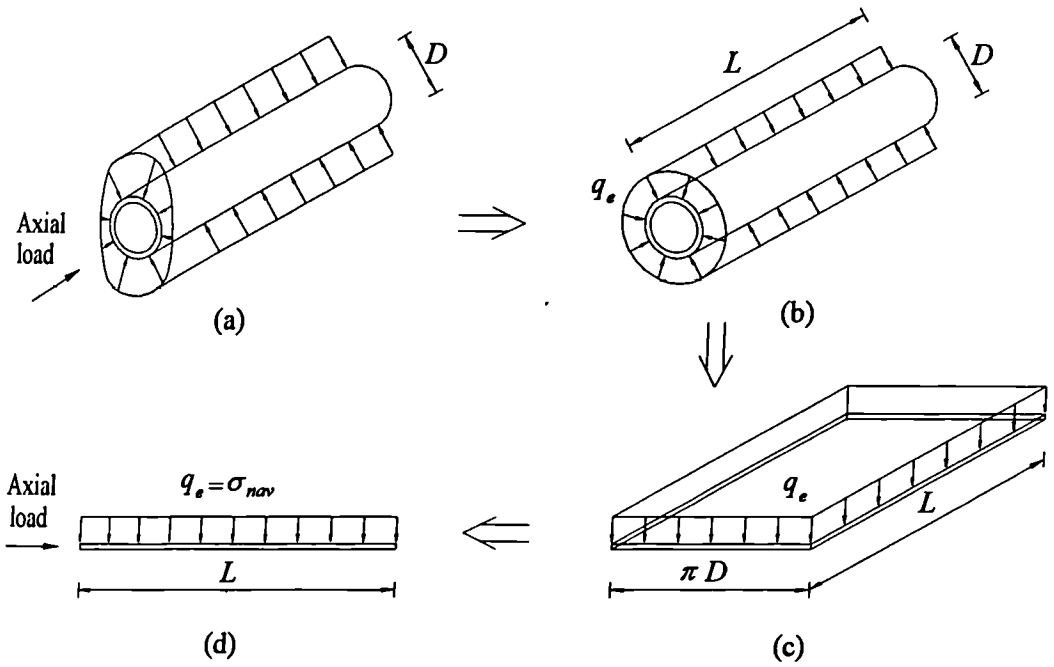

Fig. 5.1. Concept of the simplified 2-D model for axial push test: (a) actual radial (non-uniform) pressure distribution; (b) equivalent uniform radial pressure distribution; (c) idealize the pipe to a flat plate; (d) idealize the plate having plane strain condition.

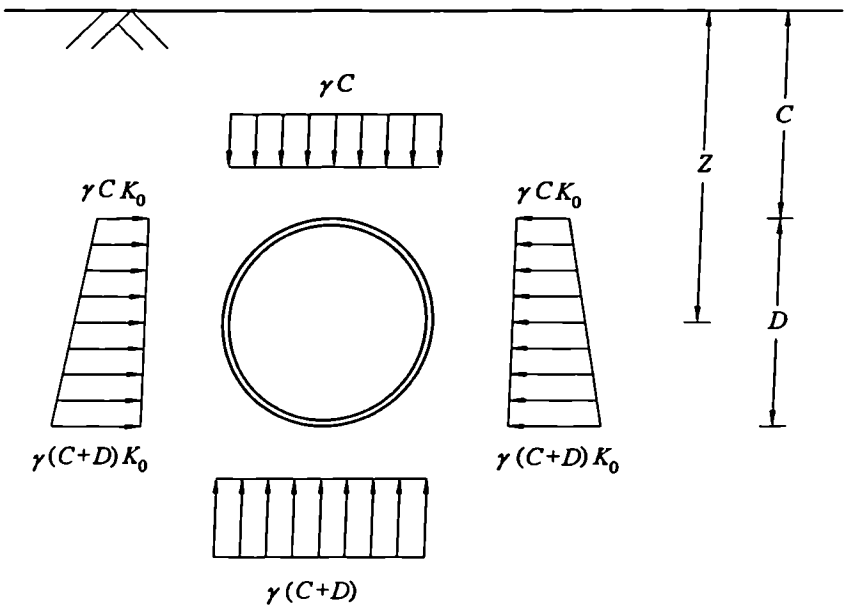

Fig. 5.2. Idealized stress distribution around a buried pipe (assuming weight of pipe + weight of fluid inside ≈ weight of soil).

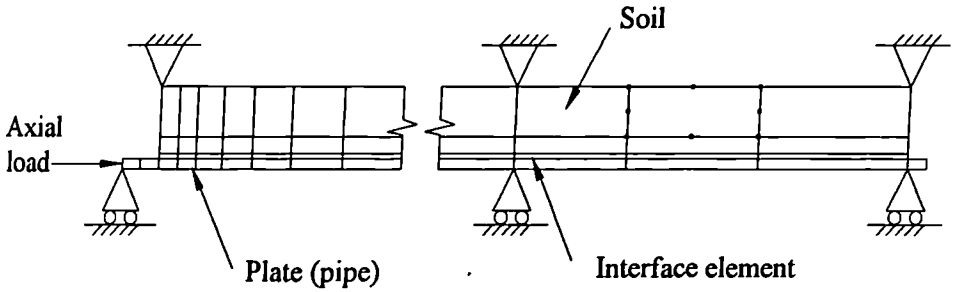

Fig. 5.3. Two-dimensional finite element mesh used to model the axial push test.

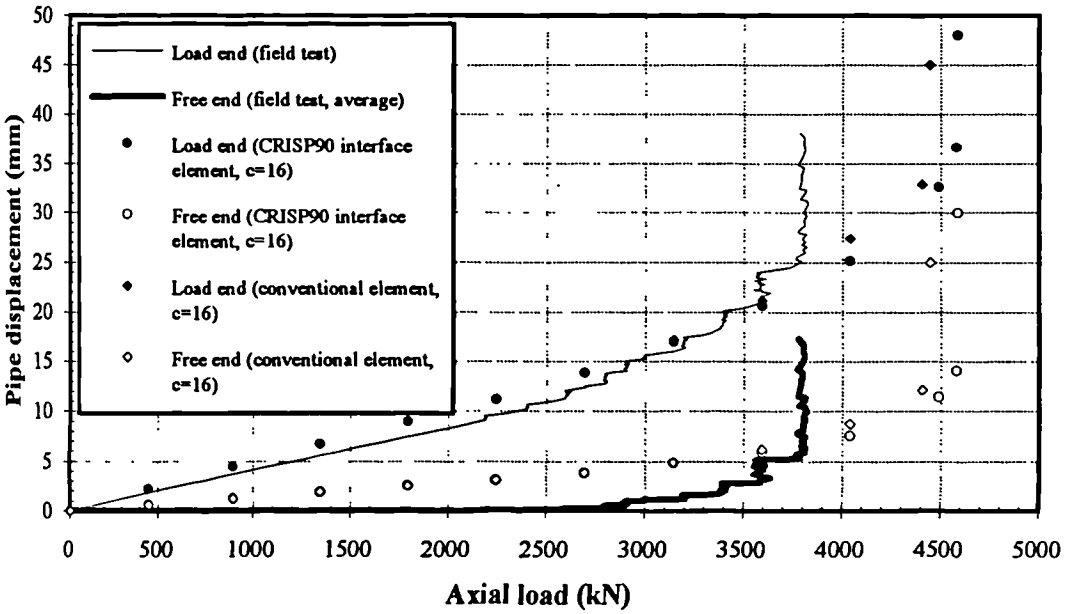

Fig. 5.4. Predicted relationship of pipe displacement-axial load at the two pipe ends for the axial push test.

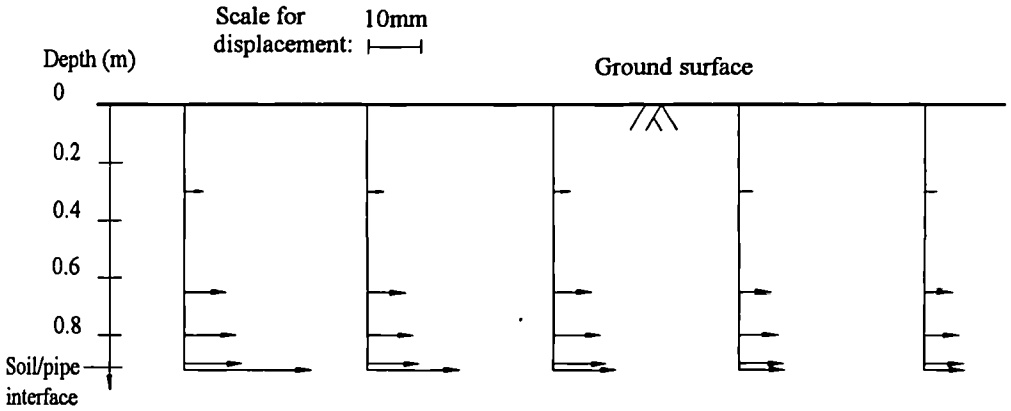

Distance from load end (m)	1.02	22.47	46.16	70.76	91.27
Relative displacement at interface (mm)	13.44	6.96	1.35	0.15	0.13

Fig. 5.5. Displacement readings at the soil and the interface for the analysis using the CRISP90 interface element at load = 4039kN.

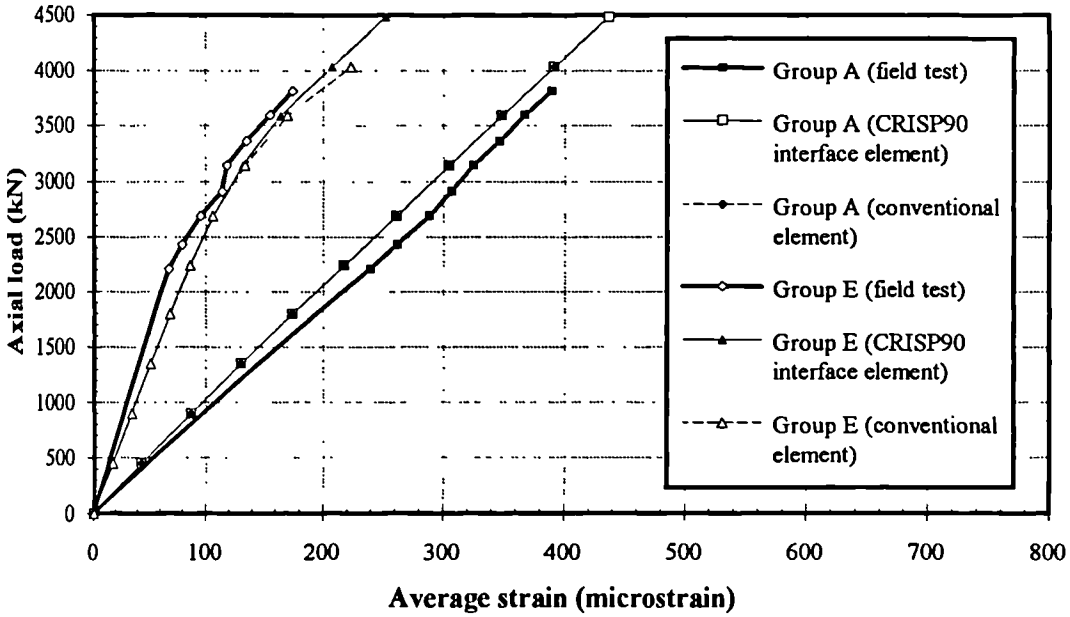

Fig. 5.6. Variation of strain at selected pipe sections for the axial push test.

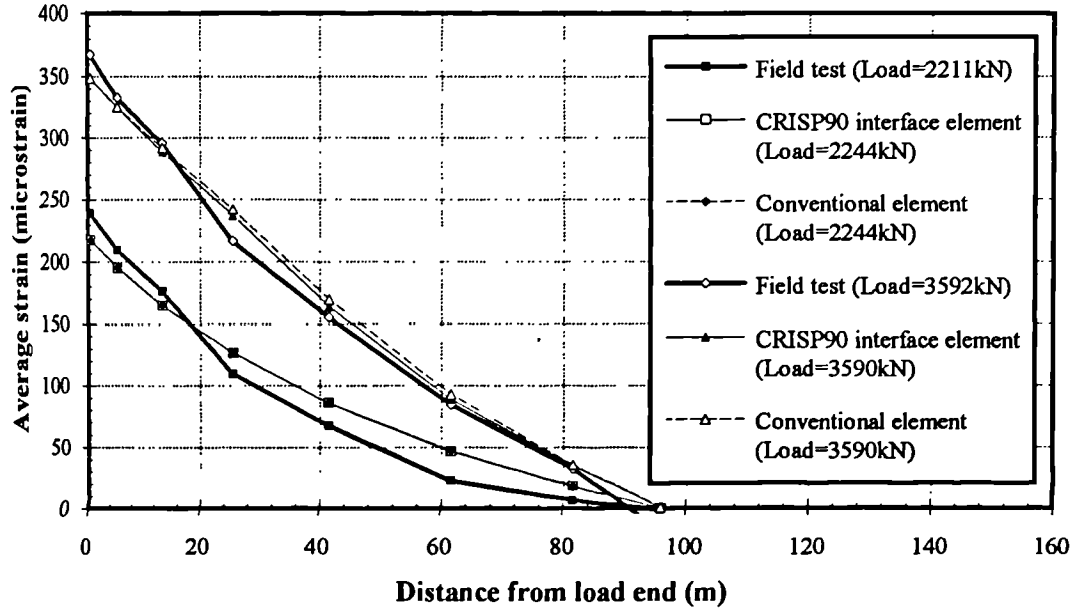

Fig. 5.7. Variation of strain along the pipe at selected loadings for the axial push test.

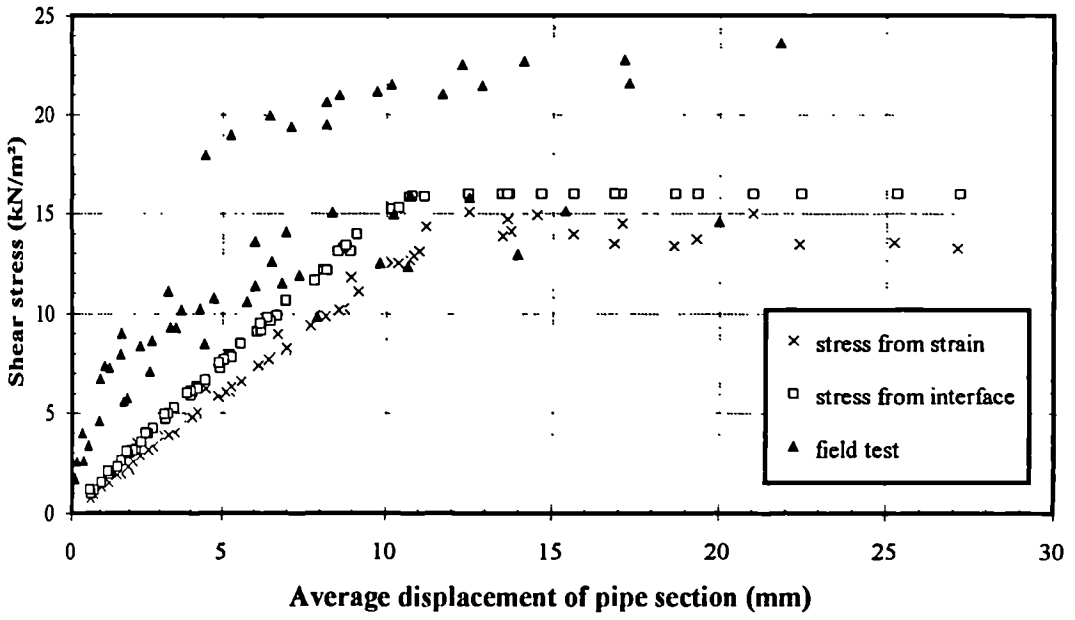

Fig. 5.8. Shear stress against pipe displacement for the analysis using conventional element as interface element.

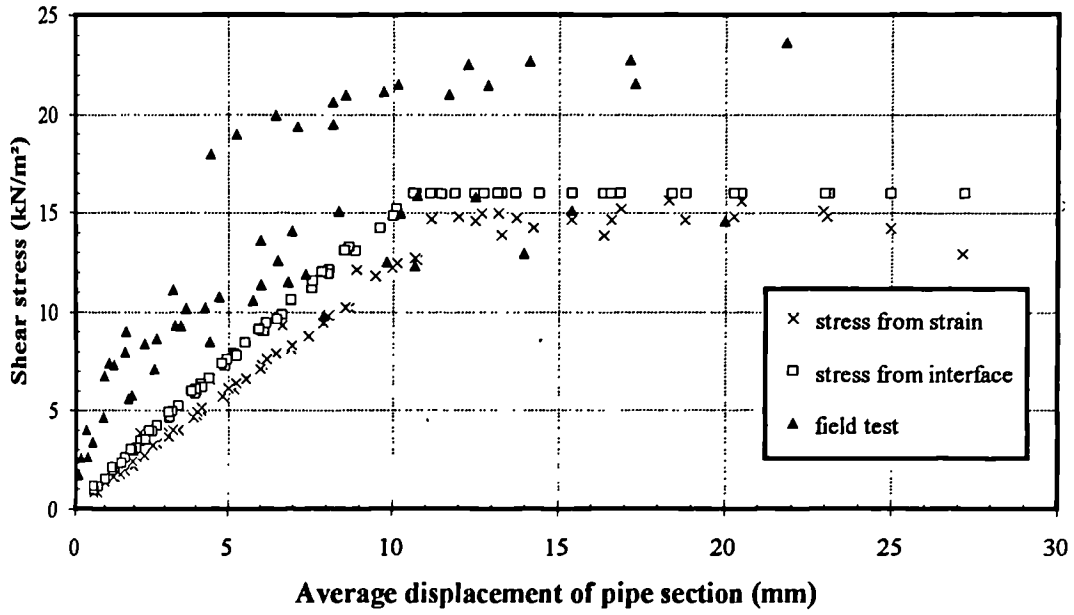

Fig. 5.9. Shear stress against pipe displacement for the analysis using the CRISP90 interface element.

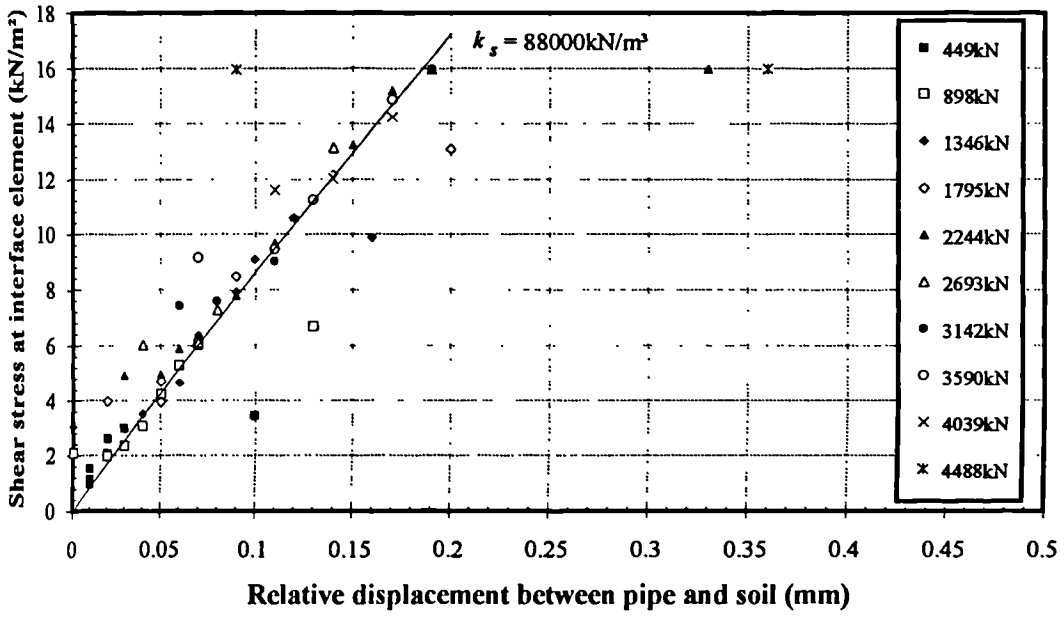

Fig. 5.10. Shear stress taken directly from the interface elements against relative soil/pipe displacement for the analysis using the CRISP90 interface element (Legends represent applied loading).

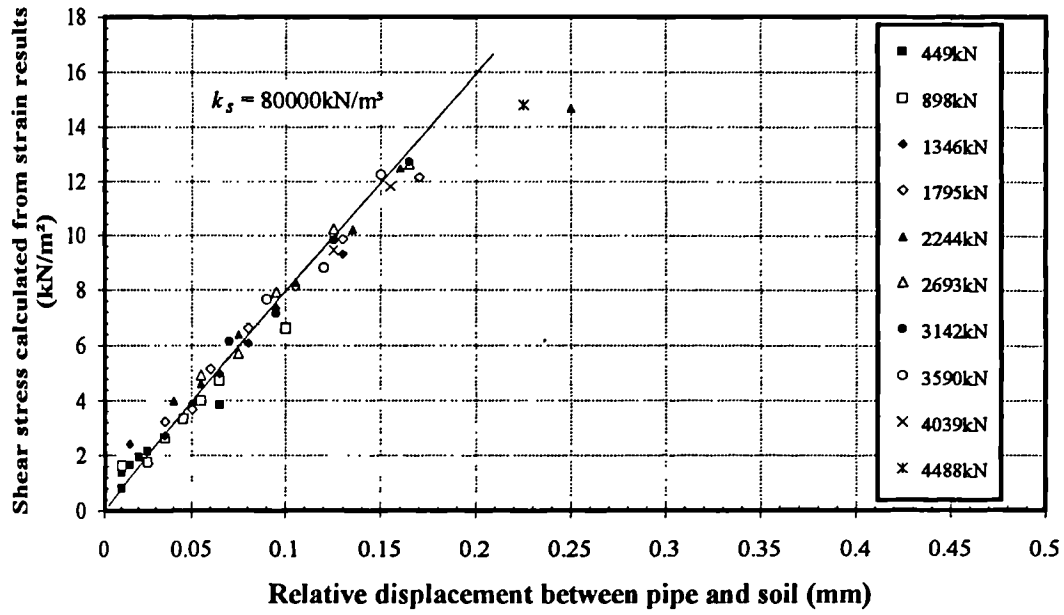

Fig. 5.11. Shear stress calculated from strain results against relative soil/pipe displacement for the analysis using the CRISP90 interface element (Legends represent applied loading).

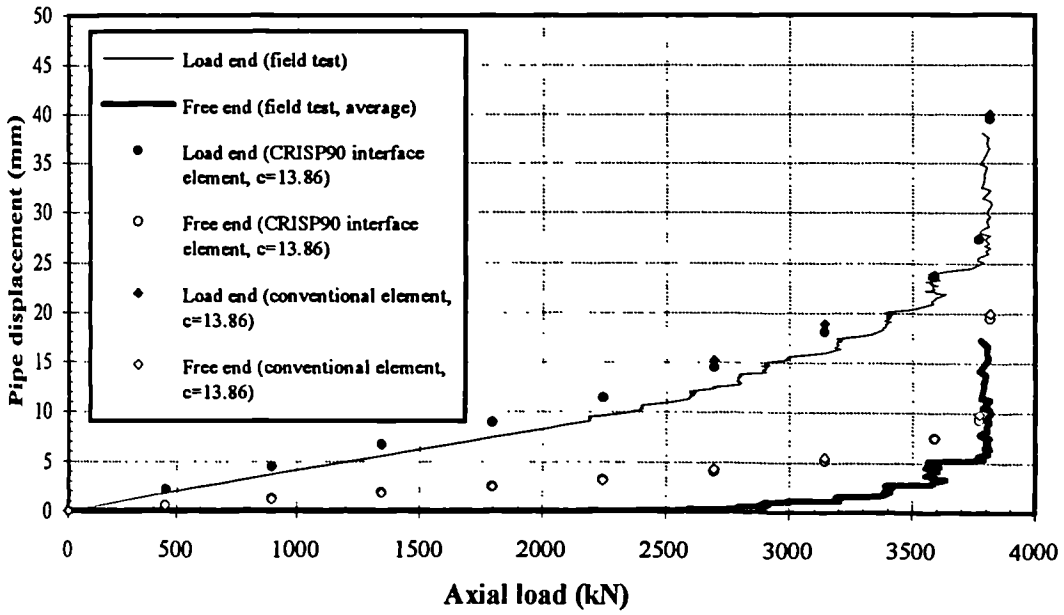

Fig. 5.12. Predicted relationship of pipe displacement-axial load at the two pipe ends for the axial push test with ultimate axial resistance = 13.86kN/m².

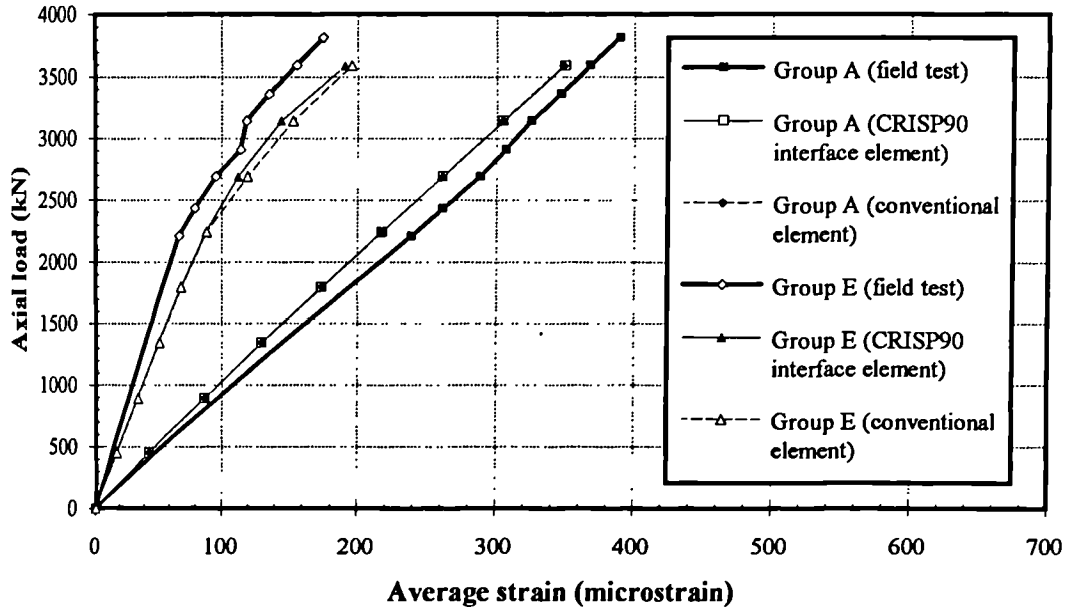

Fig. 5.13. Variation of strain at selected pipe sections for the axial push test with ultimate axial resistance = 13.86kN/m².

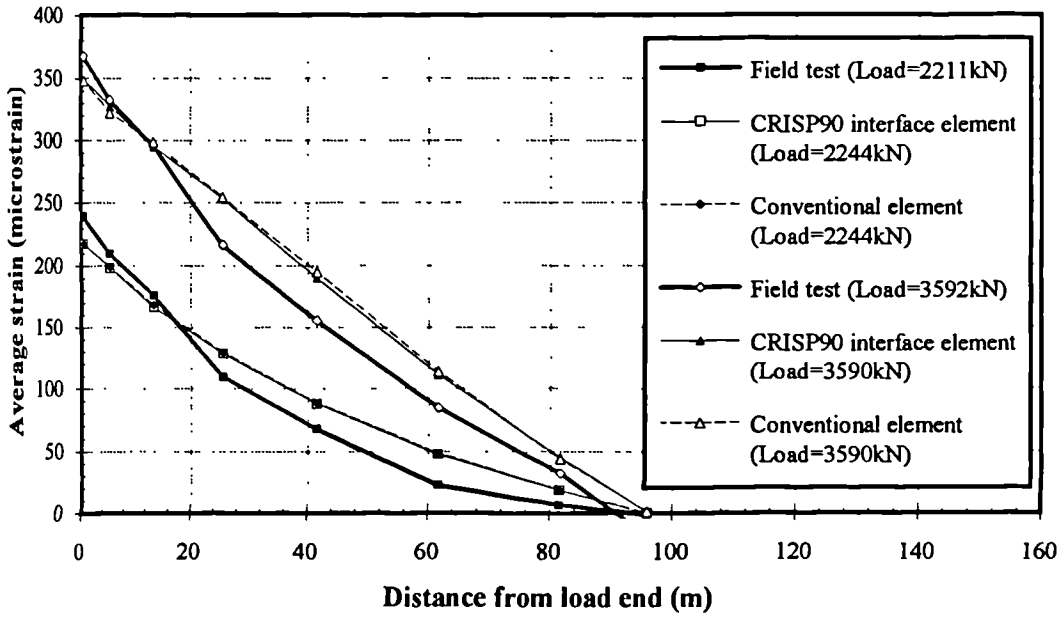

Fig. 5.14. Variation of strain along the pipe at selected loadings for the axial push test with ultimate axial resistance = 13.86kN/m².

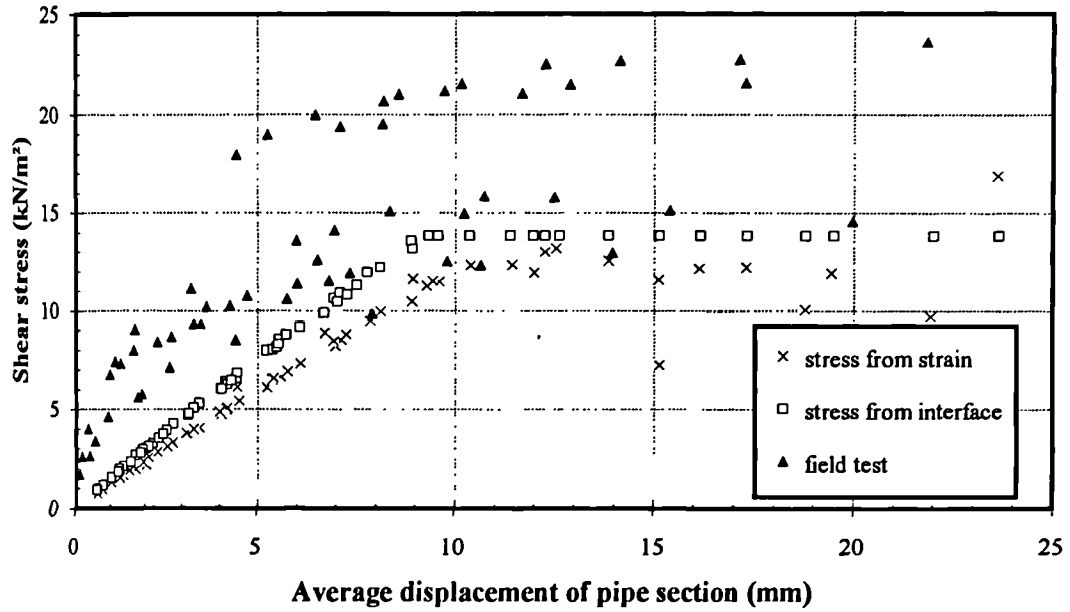

Fig. 5.15. Shear stress against pipe displacement for the analysis using conventional element with ultimate axial resistance = 13.86kN/m².

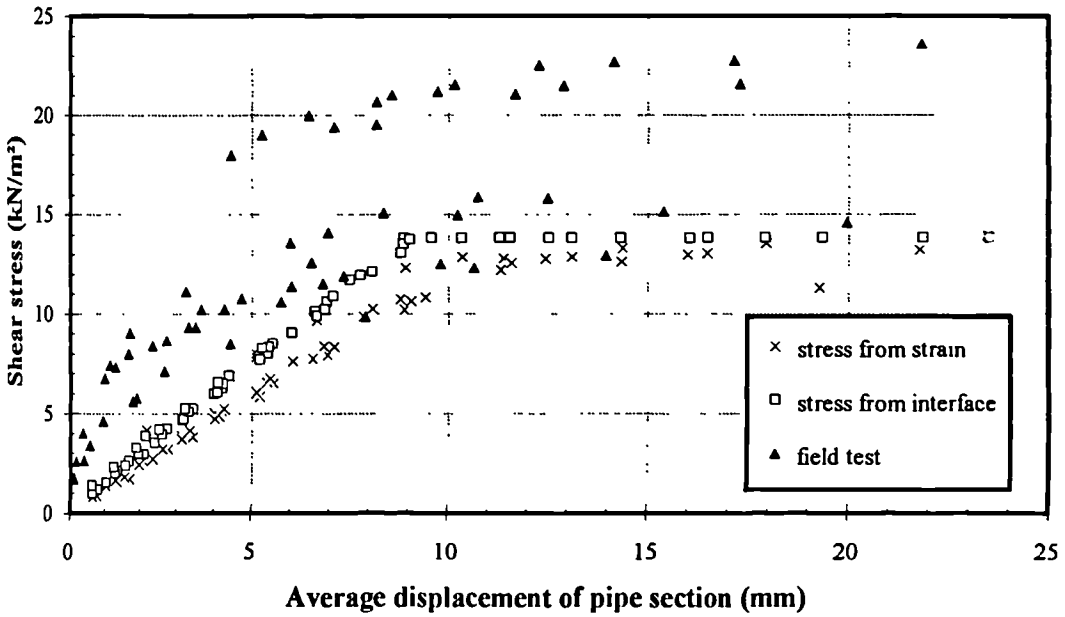

Fig. 5.16. Shear stress against pipe displacement for the analysis using the CRISP90 interface element with ultimate axial resistance = 13.86kN/m².

CHAPTER 6

MODIFICATIONS TO THE ELASTIC BEAM ON ELASTIC FOUNDATION PROGRAM

6.1. Introduction

The classical elastic beam on elastic foundation approach has been used for modelling laterally loaded piles for over half a century. In the last two decades, researchers have used extensively the experience gained in understanding the behaviour of laterally loaded piles in the modelling of laterally loaded buried pipelines. The classical approach assumes the pipe behaves as an elastic beam whose behaviour is governed by the simple theory of bending of a straight beam (Eq. 2.8) and the soil foundation is approximated by a series of discrete elastic "Winkler" type springs. The research related to this approach has been concentrated on the behaviour of the soil springs. From the earliest model, assuming linear elastic behaviour of the soil springs and then later the bilinear elastic model, to the non-linear *P-y* curve approach, the accuracy of describing the soil spring behaviour has been greatly improved. The shear coupling of neighbouring springs introduced by Georgiadis & Butterfield (1982) and the spring-dashpot system introduced by Puswewala *et al* (1993) to model creep behaviour are also attempts to improve the modelling of the soil (see Section 2.9.2). However, little attention has been directed to the behaviour of the elastic beam (pipe). It is true to say that the greatest uncertainty about the beam on elastic foundation approach is on the determination of the soil spring behaviour, but the modelling of the elastic beam (the pipe) should not be overlooked. It is known that in some situations the simple elastic beam theory is not adequate. The following sections review some of these

"secondary effects", including the plastic behaviour of the pipe, ovality of the pipe section and the shear deformation, and indicate how they were implemented into the existing elastic beam on elastic foundation program "WOMOD". The limitations of WOMOD and the effects of other factors are also discussed in this chapter.

6.2. Introduction to WOMOD

The computer program WOMOD, written in FORTRAN 77, is based on the classical elastic beam on elastic foundation approach for modelling the behaviour of a linear buried pipeline of uniform geometry and material, subjected to a ground displacement field and/or external applied loading acting in a direction perpendicular to the longitudinal axis of the pipe. The soil spring stiffness can be characterized as linear or non-linear. The pipe end conditions can be specified as completely free, free to displace but fixed in rotation and change of slope or completely fixed. Joints of specified rotational stiffness, and local pipeline displacement and/or rotational constraints can also be defined. The pipeline is assumed to be linear elastic and only the bending behaviour is considered. The fourth order differential equation is approximated numerically using finite difference terms (see Section 2.6.3.1). Figure 6.1 shows the flowchart of the program.

6.3. Plastic Behaviour of Pipe

In the original WOMOD, the pipeline is modelled as an elastic beam. However, when loading is large enough, the material of the pipeline may reach the plastic stage and have a very different behaviour. To model the plastic behaviour, a bilinear relationship similar to the relationship adopted by Trigg & Rizkalla (1994), is used for the stress-strain curve for the pipe material as shown in Fig. 6.2. The stress-strain curve of the pipe is linear up to the

yield point (defined by the yield stress σ_{yi} or yield strain ε_{yi}), and is controlled by Young's modulus E_p. At the end of each increment, a check is made to detect whether or not the pipe material has yielded. After yielding, the Young's modulus is reduced to a much lower value, E_2. At present, E_2 has been defined as a very small value to represent a perfectly plastic behaviour.

To demonstrate the effect of the plastic behaviour, an arbitrary example problem has been solved. A 25m long pipeline having D = 0.334m, d = 0.312m, $E_p = 119\times10^6$kN/m^2 and σ_{yi} = 5×10^4kN/m^2, is fixed at both ends and subjected to a soil displacement field. The non-linear soil springs were defined using the hyperbolic curve suggested by Georgiadis *et al* (1992) where k_i = 33911kN/m^3 and P_u = 136kN/m^2 (Table 2.4). Figures 6.3a to 6.3c show the predicted pipe displacement, bending strain and bending moment distributions along the pipe respectively, for both elastic and plastic pipes. They clearly shown that the behaviour of elastic and plastic pipe materials are very different when the pipe is loaded into the plastic range. The pipe displacement and bending strain were under-predicted and the bending moment was over-predicted using elastic material property.

6.4. Ovality of Pipe Cross-Section

The circular pipe cross-section can deform into an oval shape due to soil displacement and/or external loading (see also Section 2.2.3). The degree of ovality depends on the E_pI_p value of the pipe cross-section, loading magnitude and the support condition. Assuming a uniform lateral pressure is acting on the pipe, and ignoring the restraint by the overburden soil (such a pipeline is usually buried at relatively shallow depth, so the effect of overburden soil is usually very small), the change in diameter of the pipe, δD, perpendicular to the direction of pressure loading, is given by Young (1989):

$$\delta D = 0.1667 PR^4 \times \frac{12\left(1-\nu_p{}^2\right)}{E_p t^3} \qquad (6.1)$$

where P is the uniform pressure loading (see Fig. 6.4).

The ovality of the pipe cross-section has three effects. First, the second moment of area of the cross-section is reduced which makes the pipe more flexible and results in greater pipe movement due to the loading. On the other hand, the increased diameter mobilizes more restraint from the soil and causes less pipe displacement. Finally, the bending strain at the extreme fibre is reduced due to the decreased distance to the neutral axis. The three effects are illustrated in Fig. 6.4. At the end of each increment, the current pressure on the soil spring is used to calculate the ovality of the pipe and the pipe diameters (defining the elliptical shape of the cross-section of the deformed pipe) are updated.

The net result of the three effects depends on the soil restraint and the stiffness of the pipe. A parameteric study has been performed on a 25m long pipeline having D = 0.9144m, d = 0.8826m, $E_p = 209\times10^6$kN/m² and $\nu = 0.3$. It is fixed at both ends and subjected to a 1m long UDL of 2000kN/m at the centre. The surrounding soil is represented by the hyperbolic non-linear spring model suggested by Georgiadis *et al* (1992). A k_i value of 15000kN/m³ was used and five different values of P_u were tested: 50, 100, 150, 200 and 250kN/m². The P_u values are equivalent to c_u values of 8 – 40kN/m² and this range is the typical strength of "very soft" to "soft" backfill material.

Figure 6.5 shows the variation of the factors R_{disp} and R_{strain} with P_u, where R_{disp} is the ratio between the maximum pipe displacement with ovality corrections and the maximum pipe displacement without ovality correction, and R_{strain} is a similar ratio for the maximum strain on the pipe. For the lower values of the soil restraint, the net effect was greater displacement and greater strain, but for higher values, the net effect was less displacement and less strain. The P_u values where zero net effect occurred were approximately 139kN/m² for R_{disp} and 62kN/m² for R_{strain} in this particular example. The maximum net effect was on the bending strain which reduced by 1.2% for P_u = 250kN m² (the highest value of soil restraint considered). The results indicated that unless the soil is very soft, the

effects of ovality on the pipe are usually reduction of displacement and bending strain. A more detailed study is needed to investigate the effect of different pipe geometries, pipe strengths and soil restraints on ovality of the pipe.

6.5. Shear Deformation of Pipe

6.5.1. Uncoupled Solution

The simple beam theory adopted in the original WOMOD program assumes that the pipe deflection is only due to bending. However, the coexisting shear force can provide additional deflection due to distortion of the section as shown in Fig. 6.6. The effect of shear deformation on the deflection of beams is usually relatively small when compared with the effect of bending and is commonly ignored. However, if the span/depth ratio of the beam is very small, or the beam is made of material with a small value of G_p compared with E_p, the resulting shear deformation may not be negligible (Marshall & Nelson, 1990).

The additional deflection due to shear u_v is given by Marshall & Nelson (1990):

$$u_v = \int \frac{V dx}{G_p A_s} \tag{6.2}$$

where V is the shear force, G_p is the shear modulus of pipe and A_s is the area of cross-section to resist shear. The value of A_s is dependent on the shape of the cross-section, and account has also been taken for the non-uniform distribution of shear stress across the cross-section. For a thin-walled hollow circular section, A_s = 0.5 × cross-sectional area of the pipe (Young, 1989).

To investigate the significance of the shear deformation in buried pipeline problems, Eq. (6.2) has been implemented into WOMOD. At the end of each increment, the shear force

distribution is calculated and the shear force integrated over the whole length of the pipe to obtain the additional displacement due to shear deformation (Eq. 6.2). The total pipe displacement can be obtained by adding the displacement due to bending and shear together.

An example problem has been solved which involved a cantilever beam 10m long and subjected to a 100kN/m UDL acting on the entire length. The same pipe geometry and material for the example problem in Section 6.4 have been used. Excellent agreement was obtained between the analytical solution and the numerical solution by WOMOD, as shown in Table 6.1. The end displacement of the pipe due to shear deformation is approximately 2% of the displacement due to bending alone.

6.5.2. Coupled Solution

The solution presented in the previous section is relatively easy to implement into WOMOD. However, it can only be applied to problems involving direct external loading. For loading due to soil displacement, the magnitude of the load is $p = k_h D(u_s - u_p)$ (Eq. 2.9). If an additional shear displacement is added to the total pipe displacement at the end of the analysis similar to the uncoupled solution, incompatibility will occur between the final total pipe displacement and the pipe displacement used for the calculation of the load. Thus a coupled solution has to be used for soil displacement loading cases. Timoshenko (1955) presented an equation for bending of a straight beam including shear deformation:

$$\frac{d^2y}{dx^2} = -\frac{1}{E_pI_p}\left(M + \frac{E_pI_p}{G_pA_s}p\right) \tag{6.3}$$

Rewriting Eq. (6.3) in terms of displacement gives:

$$\frac{d^4u_p}{dx^4} + \frac{d^2p}{dx^2} \times \frac{1}{G_pA_s} = \frac{p}{E_pI_p} \tag{6.4}$$

By substituting Eq. (2.9) for the loading p into Eq. (6.4), and then using finite difference terms to approximate the fourth order differential quantity (use Eq. 2.10) and the second

order differential quantity (similar to Eq. 2.7), a coupled solution can be obtained. Appendix B shows the derivation of Eq. (6.4) using finite difference approximation for a complete pipeline.

An attempt was made to implement Eq. (6.4) into WOMOD. However, problems arose during the implementation and these have not been resolved within the time available for this research. Further investigations are needed for the implementation of Eq. (6.4).

6.6. Limitations of the Modified WOMOD

There are several limitations of the modified WOMOD:

i. WOMOD does not perform iterations within each increment, therefore even linear analysis has to be performed using a number of increments in order to utilize the modifications.

ii. The post-yield behaviour of the cross-section has not been considered. In practice after the extreme fibre reaches the yield stress, the bending moment can still increase above the yield moment M_y because the plastic region extends inwards towards the neutral axis until the full plastic moment M_p is reached. The ratio of the plastic moment to yield moment is solely a function of the shape of the cross-section and is called the shape factor f. For a circular pipe, the shape factor is given by Gere & Timoshenko (1990):

$$f = \frac{M_p}{M_y} = \frac{16D\left(D^3 - d^3\right)}{3\pi\left(D^4 - d^4\right)} \tag{6.5}$$

and for a very thin walled pipe, $f \approx 1.27$.

Further modification has to be made to the 1-D formulation used in WOMOD for modelling this post-yield behaviour. One possible way is to divide the cross-

section of the pipe into a number of elements. According to the distance of each element from the neutral axis, the strain at each element can be calculated. Thus yielding can take place at an individual element rather than the whole cross-section in the present approach. An average Young's modulus for the whole pipe cross-section can then be obtained by integrating the Young's modulus of each element.

iii. The stress-strain relationship of the pipe material is, at present, modelled as bilinear elastic with E_2 defined as zero. Nevertheless, the relationship can easily be modified to a bilinear elastic hardening relationship in WOMOD by changing the value of E_2.

iv. The determination of the section ovality using Eq. (6.1) is rather crude. The restraint offered from the overburden soil has been ignored and the external load causing the ovality has been idealized as uniformly distributed. In addition, Eq. (6.1) is only applicable when the pipe is elastic, thus when the pipe has yielded, the oval shape is under-predicted.

v. The uncoupled solution for shear deformation that has been implemented into WOMOD is only applicable to direct external loading (for example, the lateral load tests performed near Hilderstone, Section 3.2.2). For soil displacement loading, the coupled solution outlined in Section 6.5.2 must be used; this may be implemented into WOMOD in the future.

vi. Because the modifications for section ovality and shear deformation are based on elastic theory, they should not be used when plastic deformation of the pipe is going to occur.

Figure 6.7 shows the flowchart of the modified WOMOD including plastic behaviour, ovality and uncoupled shear deformation of the pipe.

6.7. Other Possible Improvements

6.7.1. Large Displacement Effect

The pipe deflection calculated by WOMOD is obtained by solving the differential equations for a beam based on the assumption of small displacement. When the slope and deflection of the pipe become large, the exact differential equation of the deflected pipe must be used. Also, the tensile stress caused by the elongation of pipeline length due to large transverse deflection must be considered.

The exact differential equation of the pipe deflection, assuming that the material of the pipe remains linearly elastic, is given by Gere & Timoshenko (1990):

$$\frac{\frac{d^2y}{dx^2}}{\left[1+\left(\frac{dy}{dx}\right)^2\right]^{3/2}} = -\frac{M}{E_p I_p} \tag{6.6}$$

Expressing Eq. (6.6) in terms of the applied loading p instead of moment M, and after considerable manipulation, the equation becomes:

$$\frac{d^4y}{dx^4}+2\frac{d^3y}{dx^3}+\frac{3\frac{dy}{dx}\left(\frac{d^2y}{dx^2}\right)^2\left\{\left[1+\left(\frac{dy}{dx}\right)^2\right]\left(1-\frac{d^2y}{dx^2}\frac{d^3y}{dx^3}\right)-\left(\frac{dy}{dx}\frac{d^3y}{dx^3}\right)\right\}}{\left[1+\left(\frac{dy}{dx}\right)^2\right]^{5/2}} = -\frac{p}{E_p I_p}\left[1+\left(\frac{dy}{dx}\right)^2\right]^{3/2} \tag{6.7}$$

Whilst Eq. (6.7) could be implemented into WOMOD, Gere & Timoshenko (1990) illustrated that unless very large displacement is encountered, the solutions given by small deflection theory are sufficiently accurate. For a cantilever beam of length L and subjected to a vertical load p at the end, the solutions by small and large deflection theories are virtually the same up to a u_p/L ratio of 0.2, as shown in Fig. 6.8. This compares to 2m deflection of a 10m long pipe, and is unlikely to occur except in exceptional cases such as landslides, fault movements and earthquakes. Therefore the modified version of WOMOD,

based on the small deflection theory, is still valid for most practical cases, but Eq. (6.7) would have to be implemented into WOMOD to model very large displacement problems.

6.7.2. Simultaneous Axial and Lateral Loading

In traditional practice, pipelines are independently analysed with regard to the effect of axial and lateral loads. The two effects are then combined using Eq. (2.1) to give a net effect. This approach is relatively simple but it ignores the interaction between the axial and the lateral pipe response and is only applicable for elastic pipe behaviour.

A 2-D model is needed to properly analyse the combined effect of axial and lateral loading. For example, a lateral load could induce bending of the pipe but also axial tensile stress due to elongation of the pipe. In addition, axial compression tends to increase the bending effect due to the additional bending moment caused by the eccentricity of the axial load. These interactions cannot be modelled by WOMOD and modifications are needed to include these axial effects.

6.8. Summary

The computer program WOMOD which is based on the classical elastic beam on elastic foundation approach for modelling the behaviour of linear buried pipeline has been modified to improve the modelling of the pipe. Plastic behaviour of the pipe, ovality of the cross-section of the pipe and shear deformation effects have been implemented into the original WOMOD. The modifications have been tested and the modified behaviours are satisfactory. Limitations of the modified WOMOD have been outlined and other possible modifications to improve WOMOD briefly mentioned. The modified version of WOMOD will be used in the following chapter to model the lateral push test (Section 3.2.2).

	Analytical solution (Marshall & Nelson, 1990)	WOMOD solution	Error (%)
End displacement due to bending only (m)	$\frac{PL^2}{8E_pI_p} = 0.13201$	0.13198	0.023
End displacement due to shear deformation only (m)	$\frac{PL^2}{2G_pA_s} = 0.00277$	0.00277	0.000
Total displacement (m)	0.13478	0.13475	0.022

Table 6.1. Comparison of the analytical and WOMOD solutions for the example problem.

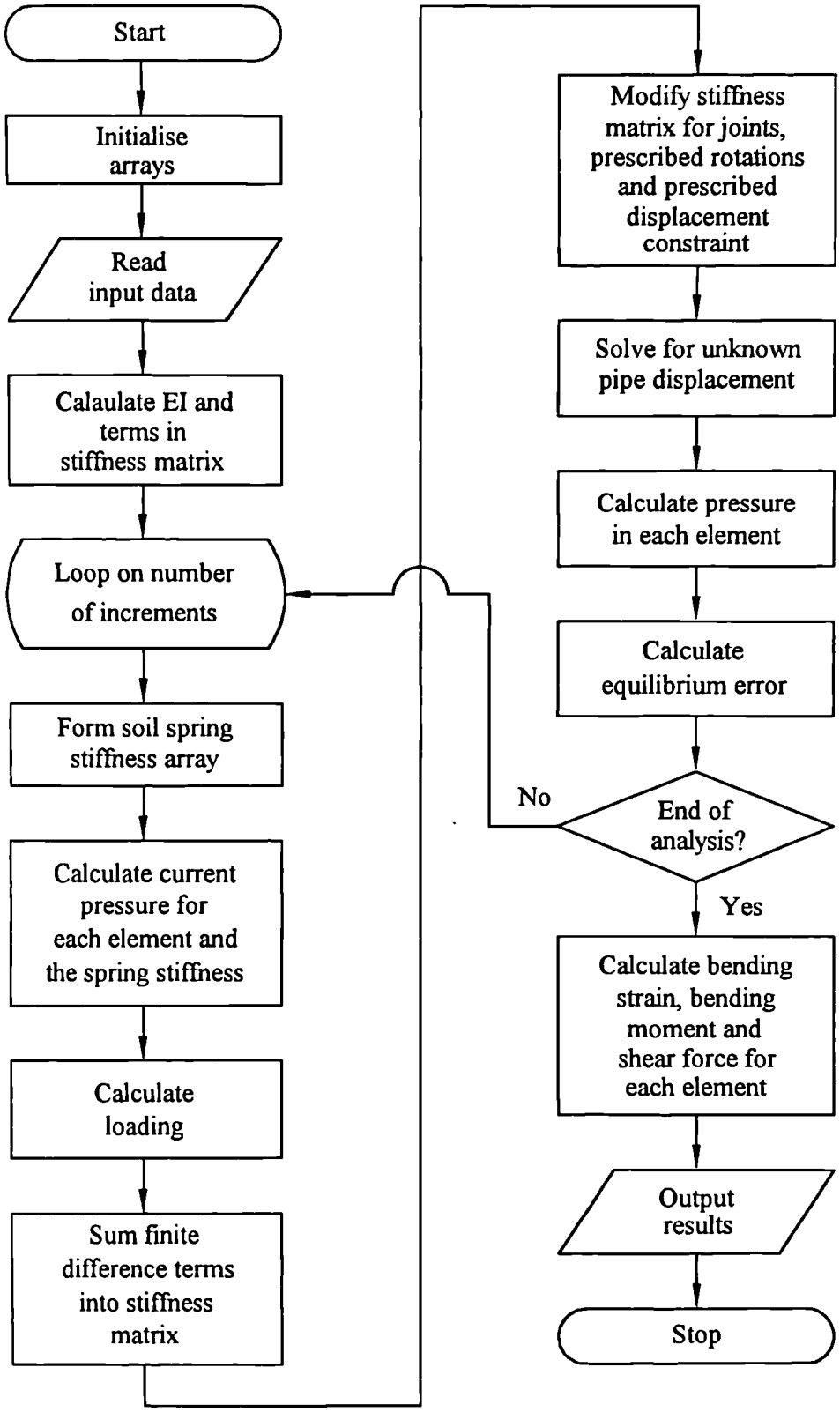

Fig. 6.1. Flowchart of the program WOMOD.

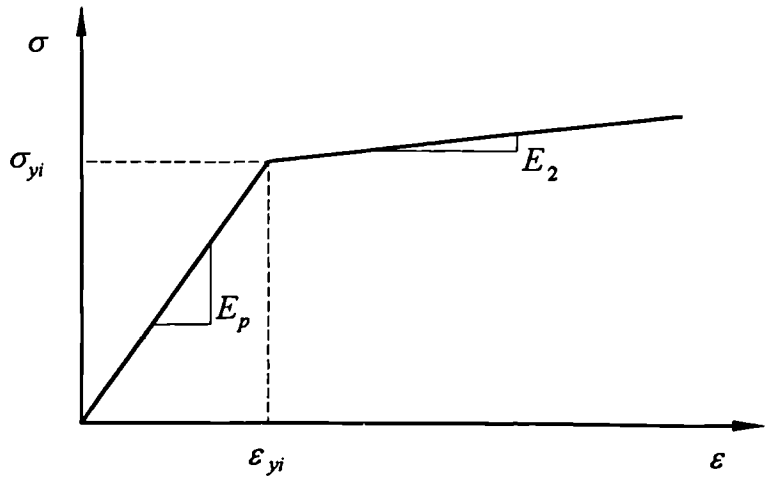

Fig. 6.2. Bilinear stress-strain relationship for plastic pipe material.

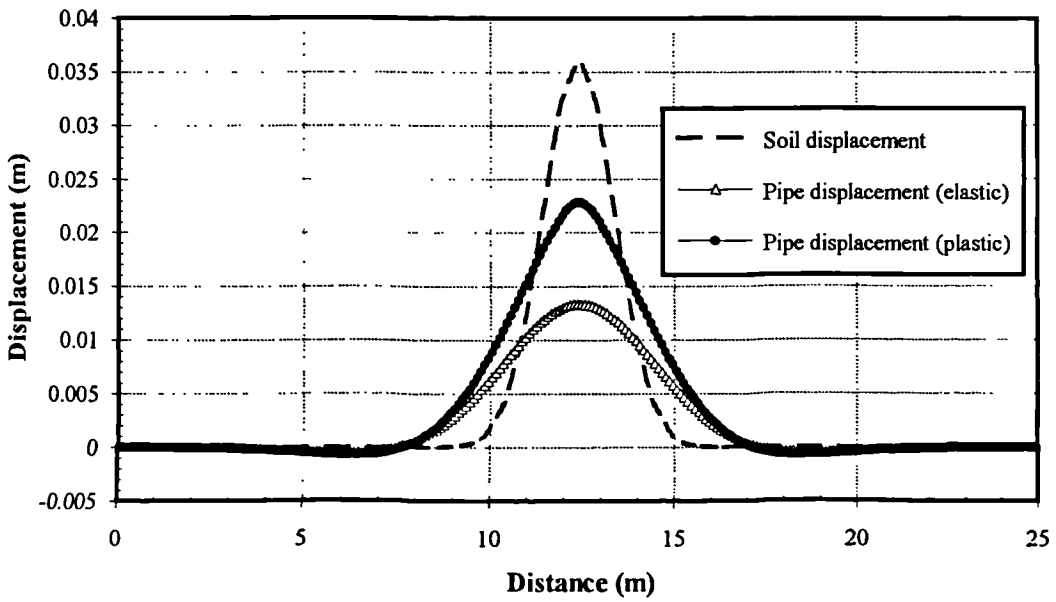

(a)

Fig. 6.3. Distribution of results along the pipe for the example problem (a) displacement profile.

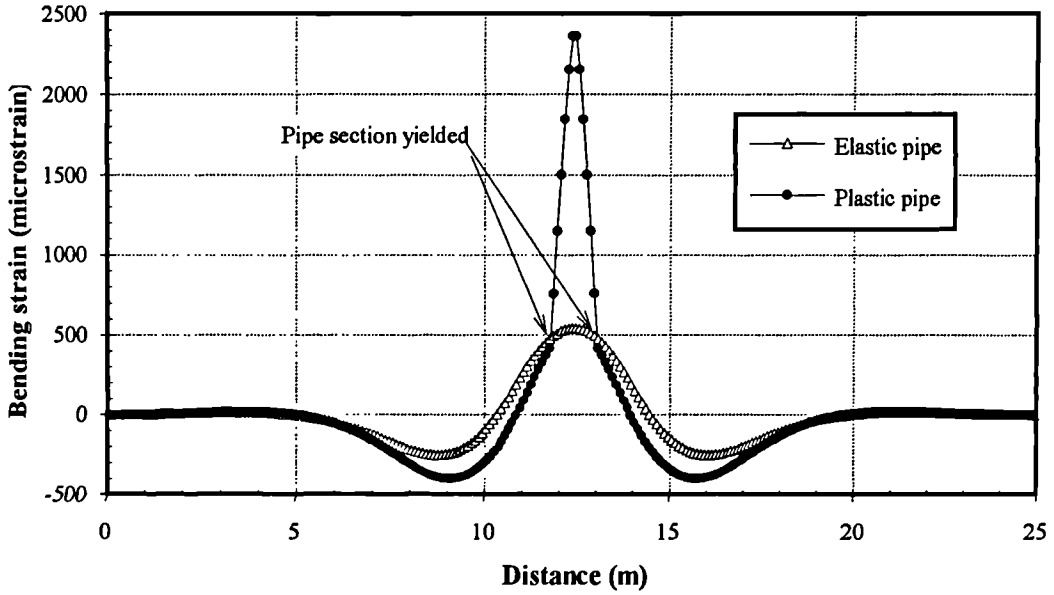

(b)

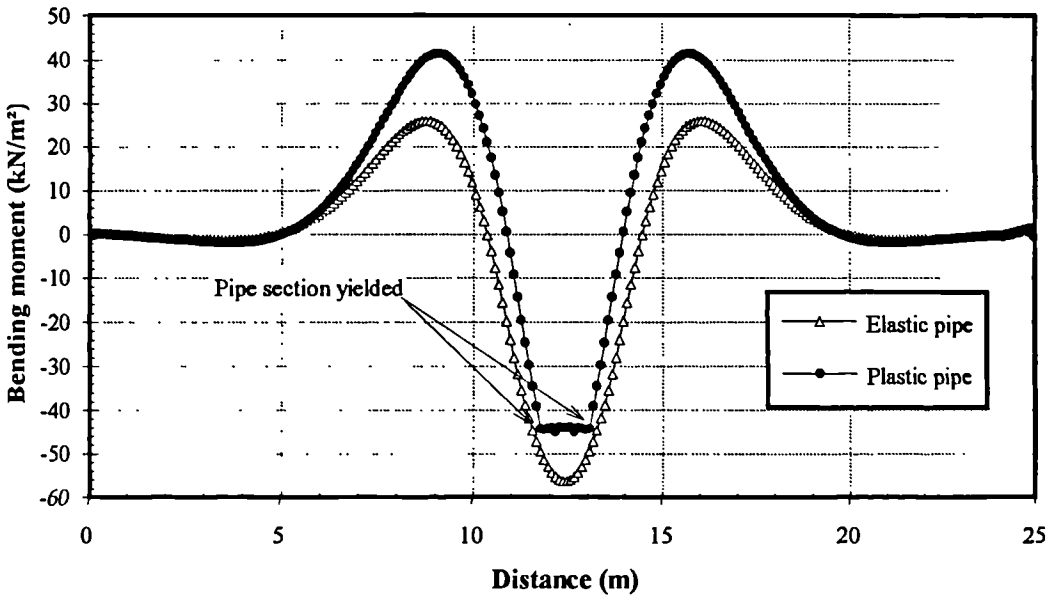

(c)

Fig. 6.3. Distribution of results along the pipe for the example problem (b) bending strain, (c) bending moment.

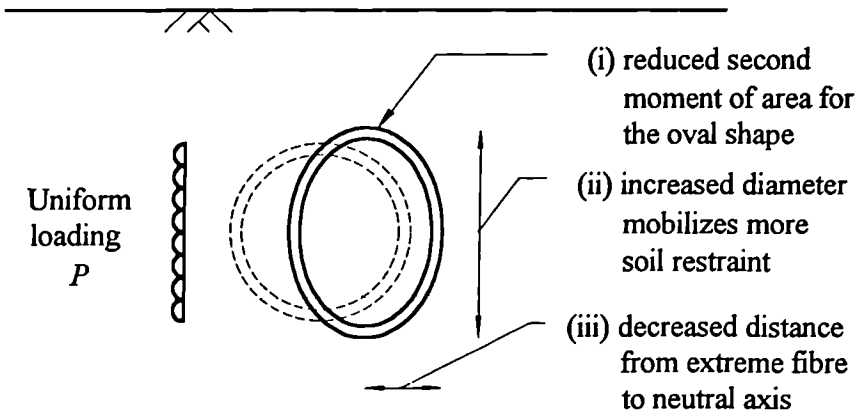

Fig. 6.4. The three effects of ovality of the pipe cross-section in WOMOD.

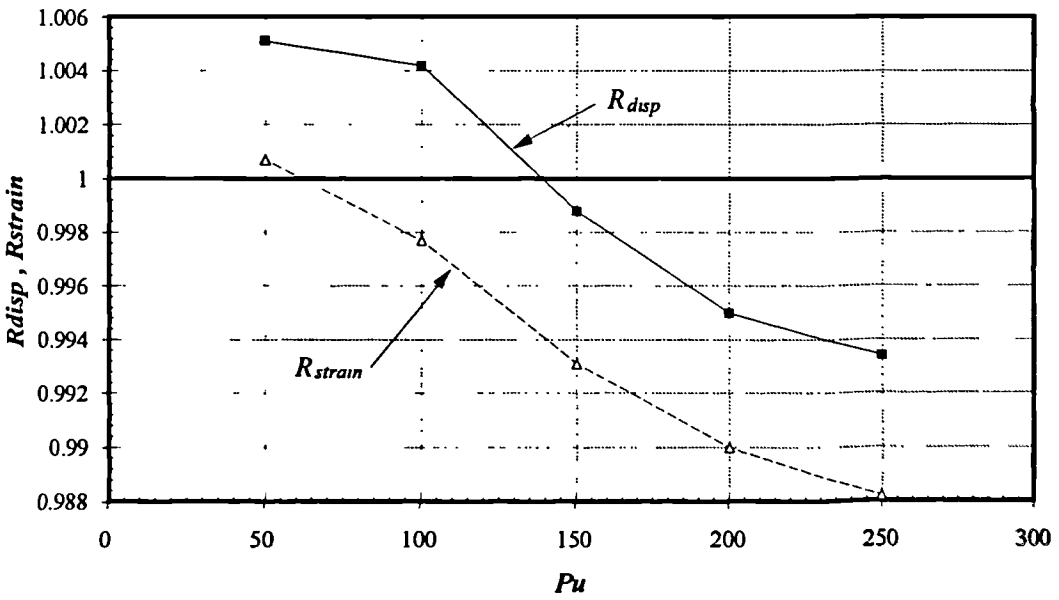

Fig. 6.5. Variation of the factors R_{disp} and R_{strain} with P_u.

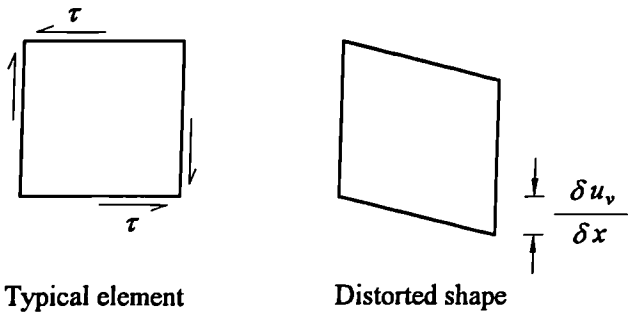

Fig. 6.6. Deflection due to distortion of the section by shear force.

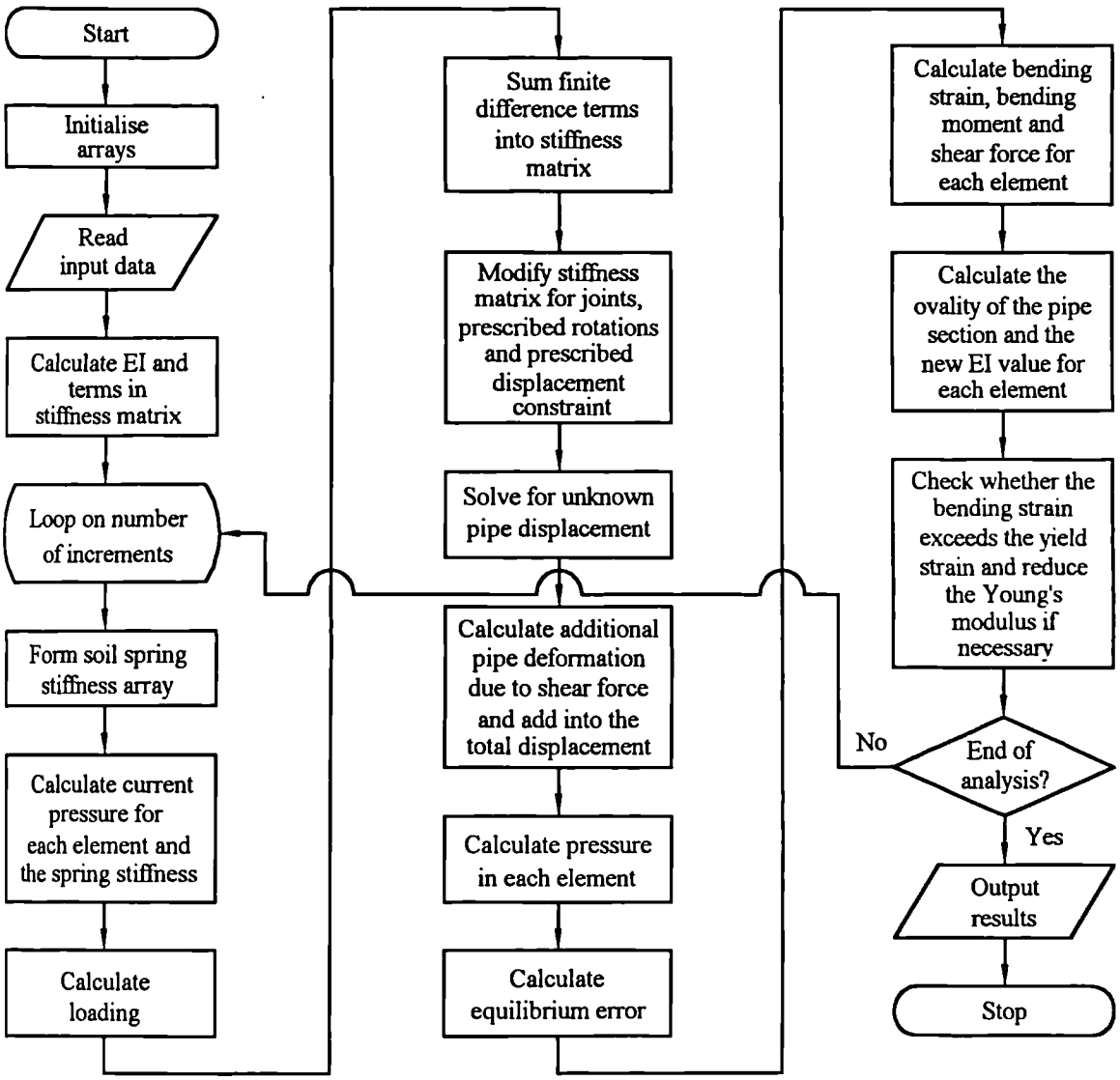

Fig. 6.7. Flowchart of the modified WOMOD.

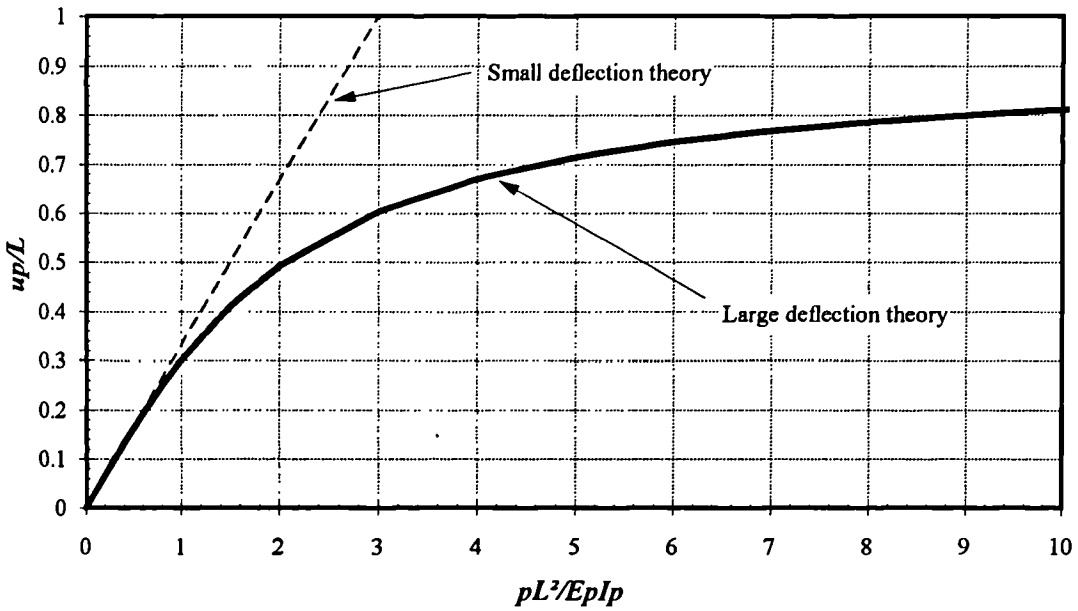

Fig. 6.8. Effect of large deflection on the vertical deflection u_p of a cantilever beam with a concentrated load p at the free end (after Gere & Timoshenko, 1990).

CHAPTER 7

NUMERICAL MODELLING OF THE LATERAL PUSH TEST

7.1. Introduction

Numerical models have been used by many researchers in an attempt to better understand pipeline response to lateral ground loading for use in design and risk analysis. Although the 3-D FE method is the most direct and comprehensive way to analyse the behaviour of laterally loaded pipelines, it is too expensive to be used as a day-to-day analytical tool. On the other hand, the elastic beam on elastic foundation approach is the most economic and widely used method, despite it being developed over a century ago. The approach is relatively simple when compared with the 3-D FE method, but still captures the essential features of the problem.

British Gas has developed a two stage analysis technique for the modelling of laterally loaded pipelines. The first stage uses a finite element program to predict the restraining effect of the soil as a function of pipe displacement. This is accomplished by performing a 2-D plane strain FE analysis. These predictions are then used in stage 2 which models the behaviour of pipelines, employing an elastic beam on elastic foundation program. Booth (1991) and Ng, Pyrah & Anderson (1994) have used the above methodology to numerically simulate the lateral push test (see Section 3.5). It was found that, in stage 1, the assumed tensile behaviour of the soil at the back of the pipe plays a significant part in the determination of the *P-y* curve. Booth (1991) tackled this problem by using a highly

simplified method which considered only the reaction at the front of the pipe and ignored the reaction at the back. This assumption implies that the behaviour of the soil at the front (in compression) is independent of the soil at the back (in tension) of the pipe, which is not true when compared to the results of Ng *et al* (1994). The straining of soil and tensile stress generated at the back of the pipe in a soil model that allows tension to build up could influence the behaviour of the soil at the front. Also when the pipe is moving obliquely upward, which is likely to happen in the Hilderstone case as shown by Ng *et al* (1994), the distribution of reaction force is not symmetrical about the vertical centre line of the pipe and this leads to error when using the method propounded by Booth (1991). A better approach used by Ng *et al* (1994) is to use a "no tension" soil model, such that virtually no tensile stress can occur. However, this approach still ignores the possible slip and separation at the soil/pipe interface which may significantly influence the predicted *P-y* curve.

In Section 7.2, the stage 1 analysis using the 2-D finite element method is extended to use interface elements to model slip and separation at the soil/pipe interface and at the interface between the backfill and the natural ground. A number of different soil models will be used to represent the backfill material including the Elastic-perfectly plastic model, Modified Cam clay, the Non-linear elastic model and the Elasto-plastic model and their behaviour compared (see Section 2.4 for more details of the soil models). The modified beam on elastic foundation program WOMOD (Chapter 6) is used in Section 7.3 to perform the stage 2 analysis to model the Hilderstone lateral push test. A parametric study is discussed in Section 7.4; this was carried out to study the influence of the relative strength between the natural ground and the backfill, the width of the trench and the angle of the trench sides. The empirical relationships presented in Section 2.7.3.2 to predict the *P-y* curve will be compared with the predictions made for the stage 1 analysis in Section 7.5. This comparison allows an assessment of the empirical methods which may be used to estimate a non-linear *P-y* curve quickly.

7.2. The 2-D Plane Strain Finite Element Analysis to Predict the *P-y* Curve

7.2.1. Rigid Cavity Model

This is the same model used by Ng *et al* (1994). The geometry of the FE mesh is based on the *in situ* measurements made at the site (Fig. 3.2). The pipe is not included in the FE mesh but is modelled as a rigid cavity. From previous analyses by Booth (1991) and Ng *et al* (1994), the soil movement was found to be localized in the region of the trench and it is appropriate to fix the lower boundary of the model at the surface of the stiff clay stratum and to assume that the displacement is constrained in both directions along this boundary. The left and right hand boundaries were both positioned at a distance of 5m from the centre line of the pipe and constrained in the horizontal direction, but free to move in the vertical direction. Five metres was considered to be sufficient for the boundary not to significantly influence the soil/pipe behaviour. The 2-D plane strain finite element mesh, as shown in Fig 7.1, consists of 184 8-noded quadrilateral elements. The elements coloured in red represent the backfill and the elements in green represent the natural ground.

In order to simulate the lateral movement of a rigid pipe, all the cavity nodes were subjected to the same amount of prescribed displacement. A prescribed horizontal pipe displacement of 0.2m was chosen, which is based on the recommendation made by Ng (1993) to cover the full range of displacement likely to be experienced by the pipe. In this case the maximum horizontal pipe displacement experienced in the Hilderstone pipe loading test was approximately 0.16m (see Fig. 3.10), thus 0.2m is considered to be enough to cover the range of the likely pipe displacement, while not leading to excessive computing time.

The analyses were performed using a modified version of the finite element program CRISP90, which has two additional soil models developed by British Gas (The Elasto-plastic model and the Non-linear elastic model), the modified interface element presented in

Section 4.4 and other modifications for the post-processing of the results. Because CRISP90 uses a tangent stiffness approach for non-linear solutions, the accuracy depends on the chosen size of increment. If too few increments are used, the method produces a solution which tends to drift away from the correct solution. For this reason, preliminary analyses were carried out to test the sensitivity of the results to different numbers of increments. It was found that 500 increments should be used for the Elastic-perfectly plastic model and 4000 increments for the other models to give accurate results for a prescribed horizontal pipe displacement of 0.2m.

In order to give a true representation of the pipe movement, possible vertical movement (upward or downward) needs to be assessed. The method that Booth (1991) and Ng *et al* (1994) used to determine the possible vertical movement is to carry out a number of analyses each having a displacement of 25mm in the *X*-direction (horizontal) but different displacements in the *Y*-direction (vertical). By plotting the total *Y*-reaction of the pipe against *Y*-displacement for each analysis, the actual vertical pipe movement for zero vertical reaction could be estimated. This method was used for the work described in Section 3.5. The current version of CRISP90 has a new "auto-float" option, developed by Cambridge University, so that the vertical movement can be determined in one analysis. By assuming an initial vertical movement of the pipe, the program calculates the total vertical reaction of the pipe at the end of each increment. Adjustment to the vertical movement is then made within the program in the next increment according to the sign of the reaction force. The vertical reaction will slowly converge to zero with an automatically calculated vertical movement of the pipe. Thus the rigid pipe will 'float" up or down during the analysis to maintain a zero vertical reaction for a prescribed horizontal movement. This new version of CRISP90 was used for all the analyses carried out in this chapter.

The backfill material has been modelled using four different soil models, including the Elastic-perfectly plastic model, Modified Cam clay, the Non-linear elastic model and the Elasto-plastic model. The natural ground could also be modelled using these different soil

models, thus different combinations of model to represent the backfill and the natural ground can be used. However, this would require a large amount of analyses. In addition, the behaviour of the pipe is dominated by the backfill material (Ng *et al*, 1994), so the Elasto-plastic model was used throughout for the natural ground to reduce the number of analyses.

All the soil models described above are capable of resisting tension and compression equally. The tensile strength of real soils, however, is only a small fraction of the compressive strength. In conventional soil mechanics it is convenient to assume that soil cannot take any tension. In the Non-linear elastic model and the Elasto-plastic model, there is an option for using a "no tension" criterion. If any soil element is in tension, the program reduces its strength and stiffness to a very low value such that only a small amount of tensile stress can be developed.

The *in situ* stresses for the Elasto-plastic model are usually set to zero because the way that the material parameters were evaluated from the stress path tests has already taken into account the state of *in situ* stress. When using the no tension criterion, an assumed zero *in situ* stress could lead to fatal errors in the results because the program would interpret all the soil elements as initially in tension and give them a very low stiffness at the beginning of analysis. To eliminate this problem, **isotropic** *in situ* stresses equal to the average *in situ* stress have been applied when using the no tension criterion to simulate the soil as initially in compression. The reason for using isotropic *in situ* stresses rather than K_0 stresses is because K_0 stresses would induce additional deviator stress in the soil, which has already been taken into account in the material parameters, thus the starting q value will be incorrect when interpreting the material parameters from the curves shown in Fig. 2.15, and lead to error in the analysis. The results of preliminary analyses show that the presence of isotropic *in situ* stresses did not influence the behaviour of the soil models.

Isotropic *in situ* stresses also have to be applied when using the Non-linear elastic model since zero *in situ* stress would lead to zero p value and cause numerical problems when calculating q/p (see Fig. 2.14 for the stress-strain relationship of the model). Since the starting value of q/p of the model must equal to zero, isotropic *in situ* stresses rather than K_0 stresses have to be used to give an initial q value of zero.

Six analyses were performed using the four 'full tension" soil models and the two 'no tension" soil models mentioned above. The upper part of Table 7.1 summaries the information of all the analyses and the results of the analyses are summarized in the upper part of Table 7.2, including the final vertical movement of the pipe, the ultimate pipe displacement y_u, the ultimate pressure P_u, the maximum pressure, the normalised ultimate pipe displacement with Z, the normalised ultimate pressure with average c_u and the normalised maximum pressure with average c_u. It should be noted that the ultimate pressures are not well defined in most analyses since the P-y curves have not flattened out within the prescribed displacement. However all the P-y curves have a reasonably well defined straight portion at the end, thus the ultimate pressure and the ultimate displacement are defined as the values at the point just entering the straight portion, *i.e.* at the break in slope of the curves, as defined in Fig. 7.2.

Figures 7.3 and 7.4 show the displacement vectors, distributions of the deviator stress q, the total mean stress p and the shear strain ($=\frac{1}{\sqrt{2}}\gamma_{oct}$, where γ_{oct} is the octahedral shear strain) for the analyses using the Elasto-plastic model with full tension and no tension respectively

It can be seen that a clear flow pattern has developed for the full tension model (Fig. 7.3a) In the no tension model (Fig. 7.4a), the soil movement for the backfill behind the pipe is reduced and the overall mechanism changed. It should also be noted that the soil movement in the natural ground behind the pipe has increased in the no tension model because the soil in this region is subject to tensile stresses and the no tension criterion reduces its strength and stiffness.

The plot of the mean total stress for the no tension model (Fig. 7.4c) clearly demonstrates that the tensile stresses developed in the soil behind the pipe are nearly eliminated when compared with the stress distributions for the full tension model (Fig. 7.3c), where the tensile stresses generated at the back of the pipe are nearly as high as the compressive stresses in front of the pipe.

The shear strain distribution is also changed when using the no tension model (compare Figs 7.3d and 7.4d). The shear strain is mainly concentrated around the soil/pipe interface and the trench interface between the backfill and the natural ground.

In order to verify the assumed stress paths used for the stress path tests in the determination of the material parameters of the soils, the stress paths predicted by the FE analyses were examined. Plotted in Figs 7.5a to 7.5c are the total stress paths for four soil elements (at the top, bottom, back and the front of the pipe) for the Elasto-plastic model with and without tension. For the element in front of the pipe, both full tension and no tension analyses show that the horizontal stress increases as expected (Fig. 7.5a), but the vertical stress also increases significantly during the analysis (Fig. 7.5b) although it was assumed to remain constant in the stress path test (Section 3.3.2). This is due to the vertical movement of the pipe which induces the vertical stress. The relationships between changes in q and p (Fig. 7.5c) show that the paths rise at an initial gradient of 1/3, which is flatter than the expected gradient of –3/2 (Fig. 3.18). It should be noted that the q values calculated from the FE analysis are always positive such that the stress paths shown in Fig. 7.5c do not have a negative gradient like the one shown in Fig. 3.18.

The stress paths for the full tension element at the back of the pipe show that both tensile horizontal stress and tensile vertical stress have developed (Figs 7.5a and 7.5b); these are nearly as high as the compressive stress for the element in front of the pipe. Although the horizontal and vertical stresses for the top element stay reasonably constant (Figs 7.5a and 7.5b) and the q-p path remains vertical (Fig. 7.5c), the bottom element shows tensile

stresses have built up quite significantly (Figs 7.5a and 7.5b) and the tensile p leads to a gradient of –3 for the q-p stress path (Fig. 7.5c).

The stress paths for the no tension model show that the tensile stresses developed in the soil (mainly at the back of the pipe) are greatly reduced when compared with the corresponding stress paths for the full tension model.

The pressure-displacement relationship, which is used to represent the behaviour of the equivalent soil spring in the stage 2 calculation, has been obtained by plotting the average soil pressure P for different X-displacement, where $P = \Sigma R/A$ (ΣR is the total reaction force at the nodes around the pipe and A is the projected area of the pipe = pipe diameter for a rigid pipe). The pressure-displacement relationships (P-y curve) from all the analyses are plotted in Fig. 7.6. The results suggest that soil models which cannot take into account the "no tension" behaviour may predict very high ultimate pressures and spring stiffnesses. It should be noted that the P-y curve for the Non-linear elastic full tension model is quite unstable. It is because when the pipe is displaced laterally, the soil at the back of the pipe is unloading. When it has unloaded to a stage where p is close to zero, numerical problems occur while the program calculates the q/p term to obtain the shear modulus of the soil (see Section 2.4.4 for the model's stress-strain relationships). The P-y curve from the analysis using the Elasto-plastic no tension model gives the closest match with the P-y curve from the field test.

The no tension model, however, still ignores the interaction between the soil/pipe contact surface, *i.e.* the separation and slippage. Also, the volumetric strain of the soil at the back of the pipe was greatly over-predicted since mesh continuity has to be maintained. These limitations of the model lead to the use of interface element to model the separation and slippage in the next section.

7.2.2. Model With Interface Elements Around the Pipe

7.2.2.1. Parametric Study of the Properties of the Interface Element

In order to model the separation at the soil/pipe interface due to the tensile stress developed at the back of the pipe, a second FE model with interface elements was used. The geometry of this model is similar to the previous rigid cavity model but the pipe ring has been included in the mesh. A layer of interface elements (the modified CRISP90 interface element, Section 4.4) was placed between the pipe ring and the soil. The interface elements can model the separation at the soil/pipe interface due to the tensile stress and any possible slip between the soil/pipe interface due to high shear strain (see Fig. 7.3d). The results of the direct shear box test (Leach & Row, 1991) listed in Section 3.3.1 were used for the material properties of the interface elements. Isotropic *in situ* stresses were used in all the analyses to ensure the interface elements are initially in compression and to avoid separation occurring at the onset of the analysis.

A parametric study has been carried out to examine the effect of roughness and limiting adhesion using the Elasto-plastic full tension model. The predicted *P-y* curves are shown in Fig. 7.7. The legends shown in Fig. 7.7 refers to the three roughness characteristics used in the analyses (smooth, rough and realistic, the latter being the properties measured in the direct shear box test) and the three values used for the limiting adhesion (σ_{ntlim} = 0 for no tension, *i.e.* immediate breakaway, σ_{ntlim} = 10kN/m^2 is the measured adhesion from the direct shear box test and σ_{ntlim} = 50kN/m^2 is an arbitrary figure to account for suction). Examination of the first three curves, with realistic roughness and different adhesion limits, shows a much higher initial stiffness for the *P-y* curves with a non-zero adhesion limit than the immediate breakaway case. After the adhesion limit is reached the *P-y* relationships are almost identical to the curve for immediate breakaway, similar to the behaviour of the benchmark test for a laterally loaded circular pile in cohesive soil described in Section 4.5.2. When comparing the curves having a σ_{ntlim} of 10kN/m^2 but different roughness values, they

show that the analyses using the rough interface and the smooth interface form the upper and lower bounds respectively. The *P-y* curve using the realistic roughness lies between the bounds but closer to the curve for the rough interface.

The study demonstrates that the limiting adhesion only affects the initial part of the *P-y* curve and once the limiting adhesion is reached, the *P-y* curves behave as the immediate breakaway condition ($\sigma_{ntlim} = 0$). This suggests that the limiting adhesion only affects the behaviour of the pipe at very small deflections, provided that σ_{ntlim} is small when compared with P_u. The roughness of the pipe is, however, more important when determining the ultimate pressure and should be measured accurately by laboratory tests. In all of the following analyses, the laboratory test results of Leach & Row (1991) are used for the properties of the interface element (realistic roughness, $\sigma_{ntlim} = 10kN/m^2$).

7.2.2.2. Displacement Controlled Analysis

Six displacement controlled analyses were performed and the details of each analysis is summarized in the middle part of Table 7.1. The results of the analyses are summarized in the middle part of Table 7.2.

The displacement vectors, distributions of the deviator stress, the mean stress and the shear strain are shown in Figs 7.8 and 7.9 for the analyses using the Elasto-plastic model with full tension and no tension respectively. In both analyses, the displacement patterns are very similar (Figs 7.8a and 7.9a). The soil in front of the pipe displaces laterally and upward, following the sloping side of the trench. Little movement of the soil occurs behind the pipe for the no tension model and virtually no movement for the full tension model. Separation at the interface elements behind the pipe indicates that a gap has formed. Slip also occurs between the soil and the pipe at the top and bottom of the pipe.

Since the interface elements behind the pipe have separated, very little tensile stress can be transferred to the soil. This is evident in the distribution of mean total stress in Fig. 7.8c for

the full tension analysis; only small amounts of tensile stresses have developed. The mean total stress distribution for the no tension analyses (Fig. 7.9c) shows that nearly all the tensile stresses are eliminated.

The shear strain distributions (Figs 7.8d and 7.9d) show that no shear strain was developed behind the pipe due to the formation of a gap. High shear strain is still developed at the trench interface in front of the pipe which justifies the use of interface elements along the trench wall as discussed in the next section.

The total stress paths for the four soil elements of the Elasto-plastic models with and without tension (Figs 7.10a to 7.10c) follow similar tracks as for the rigid cavity model. The differences are the smaller compressive stress in the front element and the greatly reduced tensile stresses for the top, bottom and back elements for the full tension model. The gradient of the *q-p* stress path for the front element is 3/4, which is steeper than the gradient of the rigid cavity model but still flatter than the expected gradient of –3/2.

Figure 7.11 shows the predicted *P-y* curves for all six analyses. Except the Elastic-perfectly plastic model which shows a clear peak and strain softening behaviour, the other models all exhibit a strain hardening behaviour and show no clear peak strength.

7.2.3. Model With Interface Elements Around the Pipe and Along the Trench Sides

7.2.3.1. Displacement Controlled Analysis

The previous two sets of analyses demonstrated the importance of the tensile stress developed in the soil at the back of the pipe, and the roughness of the soil/pipe interface. In this model, a layer of interface elements is placed along the trench between the backfill and the natural ground to model any possible slip due to high shear strain developed between the two materials (see Fig. 7.8d). Results of the direct shear box test on the backfill

material by Leach & Row (1991) listed in Section 3.3.1 are used for the properties of the interface element.

Similar to the previous two models, six analyses were performed. Their information is summarized in the lower part of Table 7.1 and the results of the analyses are summarized in the lower part of Table 7.2.

The results of the displacement vectors, distributions of the deviator stress, the mean stress and the shear strain are shown in Figs 7.12 and 7.13 for the analyses using the Elasto-plastic model with full tension and no tension respectively.

There is not much difference in the displacement patterns between the two analyses and the results are similar to the corresponding analyses presented in Section 7.2.2. A gap has formed behind the pipe and slip has occurred at the soil/pipe interface (Figs 7.12a and 7.13a). In addition, with this model slip has also occurred between the backfill and the natural ground in front of the pipe.

The distributions of stress are very similar to the corresponding analyses in Section 7.2.2. However, the stresses are discontinuous across the trench interface due to the slippage that has occurred (Figs 7.12b, 7.12c, 7.13b and 7.13c).

The shear strain distributions (Figs 7.12d and 7.13d) show that no shear strain has transferred across the trench to the natural ground. The shear strain has been accommodated by the slippage of the interface elements.

The total stress paths for the four soil elements of the Elasto-plastic models with and without tension (Figs 7.14a to 14c) show little difference in the overall behaviour with the previous model (Figs 7.10a to 7.10c). The tensile stresses developed are much smaller than the compressive stresses. The gradient of the *q-p* stress path for the front element is 3/5 compares with the previous prediction of 3/4 and the *q-p* stress paths for the top and bottom elements are reasonably vertical (Fig. 7.14c).

The predicted *P-y* curves for the analyses are shown in Fig. 7.15. No clear peaks are shown in the curves and they all indicate a strain hardening behaviour except the Elastic-perfectly plastic model, which shows a constant level once the maximum value is reached.

7.2.3.2. Stress Controlled Analysis

All of the above analyses were displacement controlled and it was assumed the pipe moves as a rigid circular shape. However, this assumption is not strictly correct since ovalization of the pipe cross-section has been measured during the Hilderstone pipe loading test (Section 3.2.2). This change in shape may influence the overall behaviour, including the predicted *P-y* curve since the increased diameter of the pipe leads to a larger projected area of the pipe (see Fig. 6.4). For this reason, a stress controlled analysis is performed using the same Elasto-plastic model as in Section 7.2.3.1 to examine the effect of the flexibility of the pipe cross-section.

A uniformly distributed pressure is applied horizontally at the back of the pipe over the entire diameter. The uniform pressure is converted into nodal forces and their magnitudes are proportional to the projected vertical length between two nodes.

The information of the analysis is shown in the bottom part of Table 7.1 and the results summarized in the bottom part of Table 7.2.

The overall displacement pattern for the stress controlled analysis (Fig. 7.16a), is essentially the same as for the displacement controlled analysis (Fig. 7.12a). However, the displacement vectors clearly show that, as well as moving obliquely upward, the pipe has also rotated as the bottom of the pipe has larger displacement than at the top. The back of the pipe has separated from the soil, and slip occurred along the trench and at the bottom part of the soil/pipe interface. Squashing of the pipe cross-section has also occurred but the magnitude is too small to be noticed in Fig. 7.16a. The vertical diameter of the pipe ring

has increased by 10mm (≈ 1.1%) which agrees well with the measured value of 1% in the Hilderstone pipe test (Section 3.2.2).

The distributions of the deviator stress, mean total stress and the shear strain of the stress controlled analysis (Figs 7.16b to 7.16d) are very similar to the displacement controlled analysis (Figs 7.12b to 7.12d), with discontinuity of stresses across the trench sides.

The total stress paths of the displacement controlled analysis and stress controlled analysis (ERSE-P.F.3.F) shown in Figs 7.14a to 7.14c are similar. The *q-p* stress paths in front of the pipe for the stress controlled analyses, however, are very curvy, with steep gradient near the beginning and the end, but flatter in the middle portion.

The predicted *P-y* curve is plotted in Fig. 7.15 (ERSE-P.F.3.F) together with the *P-y* curve predicted by the displacement controlled analyses. No clear peak is shown in the *P-y* curve. The maximum pressure of the stress controlled analysis is approximately 9% greater than the equivalent displacement controlled analysis.

7.3. Elastic Beam on Elastic Foundation Analysis

7.3.1. *P-y* Curves From the Field Test

The *P-y* curve back-calculated from the strain distribution measured in the field test (Section 3.2.2) is used in this section to simulate the lateral push test using the modified elastic beam on elastic foundation program WOMOD (Chapter 6). The purpose of this is to check whether the behaviour of the pipe can be reproduced by WOMOD, so as to examine the validity of the back-calculated *P-y* curve.

In order to assess the influence of each modification made in the modified WOMOD, a preliminary analysis was carried out using the "average" *P-y* curve shown in Fig. 3.14 for the behaviour of the soil springs, with an applied load of 592kN. Figures 7.17a and 7.17b show the predicted pipe displacement and bending strain distributions along the pipe, using the different version of WOMOD described in Chapter 6. The modification for plastic behaviour of the pipe material has no effect on the analysis since the pipe is in its elastic stage. The analysis with the shear deformation correction predicted a 1.7% decrease in the maximum pipe displacement due to distribution of the shear force on the pipe, but a 3.1% increase in the maximum bending strain when compared with the analysis without any correction. The analysis with ovality correction predicted a 2.6% decrease in the maximum pipe displacement and a 2.0% decrease in the maximum bending strain. The net results of the analysis with all the corrections are a 4.1% decrease in the maximum pipe displacement but a 1.2% increase in the maximum bending strain. From the above results, it can be concluded that the modifications to WOMOD influence the behaviour of the pipe but not in a substantial way. The following analyses have been carried out using the modified WOMOD with all the corrections applied.

The four *P-y* curves shown in Fig. 3.15, which represent the "average" *P-y* curve back-calculated from field data and the three hyperbolic pressure-displacement relationships to fit the curve, have been used to define the behaviour of the soil springs in the WOMOD analysis and hence, to assess the suitability of the three hyperbolic *P-y* formulations in describing the field *P-y* curve.

Figures 7.18 to 7.21 show the results of the distributions of the lateral displacement and bending strain of the pipe. The predicted distributions of pipe displacement (Fig. 7.18) and bending strain (Fig. 7.19) agree quite well with the field test. At low applied load (181kN), the initial stiffness of the *P-y* curve dominates the behaviour of the pipe, but at high applied load (592kN), the behaviour is controlled by the stiffness near the end of the *P-y* curve. The *P-y* curve by Georgiadis *et al* (1992) has a slightly better prediction at low load, but at

high load, the *P-y* curve by Trautmann & O'Rourke (1985) is much better. The predicted displacement profiles in Fig. 7.18, generally, have poor match near the loading end where a much sharper curvature was measured in the field test. This may be due to the soil near the opening (the test pit) providing less restraint to the pipe (see Section 7.3.5).

In practice, it is the maximum pipe displacement and bending strain that are of interest and comparisons of these are made in Figs 7.20 and 7.21. The maximum pipe displacement is defined as the displacement at 0.5m from the loaded end of the pipe, where displacement transducer readings are available. Unfortunately the maximum bending strain is not well defined from the results of the field test due to the deficiency of the number of strain gauges fitted in the pipe. The value at 5.5m is used to define the maximum bending strain as strain gauge results are available at this position. It can be seen that all analyses under-predict the maximum pipe displacement (Fig. 7.20) but the maximum bending strains agree very well (Fig. 7.21). For both results, the *P-y* curve by Trautmann & O'Rourke (1985) provided the best agreement.

It should be reiterated that the distributions of displacement and strain for the field test are not linear between the data points (*e.g.* Figs 7.18 and 7.19). The straight lines joining the data points are solely used to make the results distinct from the predicted curves.

7.3.2. *P-y* Curves From the Rigid Cavity Model

The six *P-y* curves predicted using the rigid cavity model (Fig. 7.6) in Section 7.2.1 were used to represent the behaviour of the soil springs in the WOMOD analysis. The results of the analyses are shown in Figs 7.22 to 7.25. The displacement and bending strain profiles plotted in Figs 7.22 and 7.23 show that the results using the *P-y* curves predicted by the 'full tension" models give poor agreement with the field test results. All these soil models

under-predict the pipe movement and bending strain, suggesting that the *P-y* curves are too stiff. At low load, the prediction by ERSE.N.1* is better, but the prediction by ERSE-P.N.1 is better at high load. The maximum displacement results (Fig. 7.24) show that analysis ERSE.N.1 gives a slightly better prediction than ERSE-P.N.1, but the maximum bending strain results (Fig. 7.25) show an excellent agreement for ERSE-P.N.1 with the field test.

7.3.3. *P-y* Curves From the Model With Interface Elements Around the Pipe

The six *P-y* curves predicted in Section 7.2.2 (Fig. 7.11) were used to represent the behaviour of the soil springs in the WOMOD analysis. The results of the analysis are shown in Figs 7.26 to 7.29. The displacement profiles (Fig. 7.26) indicate that the predictions by ERSE.F.2, ERSE.N.2 and ERSE-P.F.2 are very close and provide the best fit to the field test. In the bending strain profiles (Fig. 7.27), the above three soil models all give reasonably good prediction but ERSE-P.F.2 is slightly better. The results of maximum pipe displacement (Fig. 7.28) and maximum bending strain (Fig. 7.29) suggest that the best fitted curves are ERSE.F.2 and ERSE-P.F.2. The results by E-P.2 generally under-predict and MCC.2 over-predict the field test result, especially at high load.

7.3.4. *P-y* Curves From the Model With Interface Elements Around the Pipe and Along the Trench Sides

The seven *P-y* curves predicted in Section 7.2.3 (Fig. 7.15) were used to represent the behaviour of the soil springs in the WOMOD analysis. The results of the analysis are shown

* For ease of presentation, an analysis name is used rather than the full description of the analysis. For details of the analysis name see Table 7.1.

in Figs 7.30 to 7.33. The displacement profiles (Fig. 7.30) show that the predictions by the Non-linear elastic models and the Elasto-plastic models have the best agreement with the field test results. The bending strain profiles shown in Fig. 7.31 indicate that the analysis ERSE-P.F.3.F gives the best fit to the field test in a general sense. The results of maximum displacement (Fig. 7.32) show that the best agreement with the field test is ERSE.F.3, but ERSE-P.F.3.F have a better agreement for the maximum bending strain in Fig. 7.33.

7.3.5. Model With Reduced Spring Stiffness to Account for Soil Weakening Near the Opening

The lateral pipe loading test has been modelled successfully by WOMOD in the previous sections. However, in terms of the displacement profile, the agreement was not very good near the loading end. The measured displacement profile for the field test showed a much sharper curvature near the loading end, while the results from WOMOD predicted a more gentle curvature.

Studies of site photos show that, although there was some sheet piling installed to support the excavation (the test pit), the soil near the sheet piling was highly disturbed. Thus the strength of the soil near to the pit could be significantly weaker than the normal strength.

By assuming a weaker soil zone in the first 0.5m from the soil/pit interface, analyses were carried out using the six most promising *P-y* curves in the previous sections: Trautmann & O'Rourke, 1985 (Section 7.3.1), ERSE-P.N.1 (Section 7.3.2), ERSE.F.2 (Section 7.3.3), ERSE-P.F.2 (Section 7.3.3), ERSE.F.3 (Section 7.3.4) and ERSE-P.F.3.F (Section 7.3.4). The soil in the weakened zone was assumed to have a strength half that of the rest of the soil and the results of the analysis are shown in Figs 7.34 to 7.37.

The effects of the weakened zone are an increased displacement and increased bending strain (Figs 7.34 and 7.35) compared with the corresponding original results. However, the

predicted displacement profiles near the loading end still do not match with the measured one. For maximum pipe displacement (Fig. 7.36) all curves give good agreement with the field test except the curves of Trautmann & O'Rourke (1985) and ERSE-P.N.1, which under-predict the displacement. The results of maximum bending strain (Fig. 7.37), however, show that the curves by Trautmann & O'Rourke (1985) and ERSE-P.N.1 have the best agreement with the bending strain results, while others over-predict the strain. Generally, if the analysis has good agreement in displacement, it tends to over-predict the strain, and if the analysis has good agreement in strain, it tends to under-predict the displacement.

Additional analyses assuming a linear reduction of the strength (in three steps) in the weakened zone were carried out. However, the predicted results are very similar to the above analyses. No improvement was gained in the matching of the displacement profile near the loaded end of the pipe.

7.4. Parametric Study for the 2-D FE Analysis to Predict the *P-y* Curve

The purpose of the parametric study is to investigate the influence of several factors in the prediction of the *P-y* curve using 2-D finite element analysis, including the relative strength between the natural ground and the backfill, the width of the trench and the angle of the sides of the trench.

Ten FE meshes were created based on the mesh used for the Hilderstone pipe loading test described in Section 7.2.3, which has interface elements around the pipe and along the trench sides. The first six meshes all have vertical (90°) trench sides, but with a different trench width: 1.2m, 1.4m, 1.6m, 1.8m, 2.0m and 2.5m. The other four meshes have a different angle for the trench sides: 30°, 45°, 60° and 75°, where the mesh for 45° is exactly

the same as the mesh used in Section 7.2.3 for the Hilderstone case. The Elasto-plastic full tension model was used for both backfill and natural ground, similar to the analysis ERSE-P.F.3 (see Table 7.1). The parameters of the backfill are based on the stress path test results presented in Section 3.3.2. However, the material parameters for the natural ground were not based on the stress path test results, but were based on the parameters of the backfill, with factored results of shear strength (by scaling up or down the q-ε_s^p relationship of the backfill, Fig. 2.15). This enables a direct comparison of the strength between the natural ground and the backfill. Different ratios of strength between the natural ground and the backfill, R_c, have been used for each mesh, ranging from 0.8 to 10.0 (the material parameters for the backfill remained unchanged while the strength of the natural ground was increased, or decreased for R_c less than 1).

Thirty-six displacement controlled analyses were performed on meshes having trenches with vertical sides with trench width equal to 1.2m, 1.4m, 1.6m, 1.8m, 2.0m and 2.5m, each with a range of different values of R_c. After the analyses, the pressure-displacement relationships of the pipe can be obtained as described in Section 7.2.1. The P-y relationships were non-dimensionalized (P/c_u - y/D, where c_u is the undrained shear strength of the backfill) and plotted in Figs 7.38a to 7.38f for W = 1.2m, 1.4m, 1.6m, 1.8m, 2.0m and 2.5m respectively

In order to assess the effect of W/D and R_c in the prediction of the P_u value of the P-y curves (as defined in Fig. 7.2), the P_u value of each of the thirty-six P-y curves were normalized with the c_u of backfill ($P_u/c_u = N_{ch}$) and then plotted against R_c in Fig 7.39 The results show that as the trench width increases (the width of the trench W has been non-dimensionalized with the pipe diameter D) the value of N_{ch} decreases. In other words, the proximity of the pipe to the natural ground has a major influence on the ultimate pressure of the P-y curve. The N_{ch} - R_c relationships start to level off at $R_c \approx 5$ for W/D less than approximately 2 and at $R_c \approx 2$ for W/D larger than approximately 2. Figure 7.40 shows the relationships between N_{ch} and the W/D ratio. N_{ch} generally increases with decreasing W/D

and increasing R_c. After R_c reaches approximately 5, further increase of the R_c does not give a higher N_{ch} value.

The effect of R_c and *W/D* on the vertical displacement of the pipe was also studied. The results of the thirty-six analyses were used for the plot of vertical displacement/horizontal displacement (y/z) against R_c in Fig. 7.41, which shows a similar general trend as Fig. 7.39. The y/z ratios start to level off at $R_c \approx 5$ for *W/D* ratio up to 1.5, but the y/z - R_c relationship for *W/D* = 1.3 does not show a peak even at $R_c = 10$. For *W/D* less than approximately 2, the y/z - R_c relationships are very similar, but when *W/D* is greater than approximately 2, Fig. 7.41 indicates a much smaller vertical displacement of the pipe.

The effect of R_c and *W/D* on the ultimate horizontal displacement y_u (defined in Fig. 7.2) were studied in Fig. 7.42. It shows the relationships between normalized y_u with Z (y_u/Z) and R_c for different *W/D* ratios. The normalized horizontal displacements at ultimate pressure (y_u/Z) start to level off at $R_c \approx 5$. The y_u/Z - R_c relationships are similar for *W/D* less than 1.5. It can be seen that the y_u values decrease with decreasing *W/D* ratios. When *W/D* $\approx$ 1.5, further decrease of *W/D* ratio has little effect on y_u.

After the effects of R_c and *W/D* on trenches with vertical sides was studied, the influence of R_c was studied for trenches with sloping sides. Forty displacement controlled analyses were performed on meshes with a trench angle equal to 30°, 45°, 60° and 75°, each with ten different values of R_c. Figures 7.43a to 7.43d show the dimensionless pressure-displacement relationships for the analyses with a trench angle of 30°, 45°, 60° and 75° respectively.

The effect of R_c and angle of the sides of the trench in the prediction of P_u was studied in Fig. 7.44 which plotted N_{ch} against R_c for different angles of trench sides. It can be seen that the analyses with flatter angles of trench sides have lower N_{ch} values. This is because less restraint was mobilized in the natural ground. The N_{ch} value levels off at $R_c \approx 2$ for angles up to 60°, but the N_{ch} value does not level off until $R_c \approx 5$ for an angle = 75°. Figure

7.45 plots the relationships of N_{ch} against the angle of trench sides for the ten different R_c values. N_{ch} generally increases with increasing angle of trench sides and increasing R_c. After R_c reaches approximately 3, further increase of R_c does not give a significantly higher N_{ch} value.

The general nature of the relationships between y/z and R_c for different angles of trench sides plotted in Fig. 7.46 is very similar to Fig. 7.41. The y/z ratios start to level off at $R_c \approx$ 5 for angles up to 60°, but the y/z - R_c relationship for an angle of 75° does not reach an asymptote even at $R_c = 10$. The direction of the movement is slightly flatter than the angle of the trench sides when $R_c > 5$.

The effect of R_c and angle of the sides of the trench in the prediction of y_u was studied in Fig. 7.47, in which the general nature is very similar to Fig. 7.42. The y_u value start to level off at $R_c \approx 5$ for steeper angles of trench sides and level off at $R_c \approx 2$ for flatter angles of trench sides.

In order to study the general shape of the P-y curve, all seventy-six dimensionless pressure-displacement relationships shown in Figs 7.38 and 7.43 from the parametric study have been plotted in Fig. 7.48 in a normalized form as P/P_u against y/y_u. Three of the hyperbolic P-y curve formulations listed in Table 2.4 have been used to fit a curve to the data in Fig. 7.48. The formulation suggested by Georgiadis *et al* (1992) gives the worst fit to the data. On the other hand, the formulations by Audibert & Nyman (1977) and Trautmann & O'Rourke (1985) both agree well but the former is slightly better.

7.5. Comparison With Other Methods of Predicting the *P-y* Curve

It has been demonstrated in the previous sections that the finite element method is a suitable technique for the determination of the soil restraint to laterally loaded pipelines. However, when there is no access to a computer to carry out the FE analysis, or when a quick calculation is required in a design office, a simple but accurate method is required. In Section 2.7.3.2, some empirical relationships suggested by other researchers to determine the formulation of the non-linear *P-y* curve (Table 2.4), the ultimate pressure P_u (Table 2.6) and the ultimate pipe displacement y_u for cohesive soil were presented. In order to examine the validity of these empirical relationships, the results of the Hilderstone lateral pipe loading test have been used for comparison.

Firstly, the prediction of P_u is examined. Table 7.3 shows the predicted values of N_{ch} ($N_{ch} = P_u/c_u$) for the six formulations listed in Table 2.6, together with the N_{ch} value back-calculated from the Hilderstone test. The current state-of-practice formulations most often used in routine design are those of Rowe & Davis (1982a) and the ASCE (1984) recommendations based on Hansen's model (Hansen, 1961), as stated by Rizkalla *et al* (1992). Both under-predict the value of N_{ch}. The prediction by Reese (1958) is the closest to the field test and the other formulations all under-predict N_{ch}, except the prediction by Rowe & Davis (1982a) for the no breakaway condition. It is noted that the P_u/c_u values predicted by the FE models in Section 7.2 (Table 7.2) are generally lower than the N_{ch} value measured in the Hilderstone test but agreed quite well with the formulation by Rowe & Davis (1982a) for the immediate breakaway condition.

These empirical formulations, however, are all based on the assumption that the soil condition is homogeneous, *i.e.* only one material exists near to the pipe, which is often not the case. In practice, most pipelines are laid in an excavated trench and then backfilled with other material and the backfill is usually weaker than the natural ground, similar to the

situation at Hilderstone. As has been demonstrated in the parametric study in Section 7.4, the existence of two distinct materials can influence the overall behaviour of the pipeline under external loading.

By normalizing the values of N_{ch} with respect to the value of N_{ch} at R_c equals 1 (*i.e.* homogeneous soil condition) in Fig. 7.39, the relationships of a new factor F_{ch} to R_c is obtained (see Fig. 7.49). The curves plotted in Fig. 7.49 are based on the normalized data points of the parametric study results in Fig. 7.39, and by interpolation techniques to obtain values of F_{ch} at convenient *W/D* ratios, smooth curves are then drawn through the F_{ch} data points. The factor F_{ch} can be included in the general equation to determine P_u (Eq. 2.19) to correct N_{ch} for the influence of the backfill trench:

$$P_u = c_u N_{ch} F_{ch} \tag{7.1}$$

where c_u is the undrained shear strength of the backfill.

The factor F_{ch} shown in Fig. 7.49 is applicable only to vertical trench sides, and there should be a family of figures for different values of the angle of the trench sides. However, due to time limitations, a parametric study for the full range of angle of trench sides with different R_c and *W/D* ratio was not possible. Nevertheless, the results of the N_{ch} - R_c relationship for different angles of trench sides in Fig. 7.44 have been used to compare with the results in Fig. 7.39 and approximate relationships have been obtained to relate the angle of the sides of the trench with a factor F_{ac} for different R_c ratios, which can be used to correct the factor F_{ch} for different angles of trench sides, as shown in Fig. 7.50. The factor F_{ac} can then be combined into Eq. (7.1) to include the influence of the angle of the trench sides:

$$P_u = c_u N_{ch}\left[(F_{ch} - 1) \times F_{ac} + 1\right] \tag{7.2}$$

where F_{ch} is for vertical trench sides plotted in Fig. 7.49.

The last column of Table 7.3 shows the re-calculated P_u/c_u using Eq. (7.2), and the new prediction using the values of N_{ch} proposed by ASCE (1984) agrees quite well with the Hilderstone test result.

After the prediction of P_u was examined, the prediction of y_u by empirical methods is studied. The pipe displacement at ultimate load y_u suggested by ASCE (1984) is $0.05Z$, which under-predicts the actual value measured in the Hilderstone test, $0.111Z$. On the basis of the results of the parametric study shown in Fig. 7.42, relationships for the non-dimensional ultimate displacement y_u/Z with R_c under different W/D ratios are suggested for trenches with vertical sides as shown in Fig. 7.51. Similar to Fig. 7.49, the curves in Fig. 7.51 were obtained by interpolation techniques to obtain values of y_u/Z at convenient W/D ratios and smooth curves are then drawn through the data points. The predicted value of y_u by Fig. 7.51 is $0.044Z$ for Hilderstone, which is similar to the suggestion by ASCE (1984). In order to apply Fig. 7.51 to trenches with non-vertical sides, a correction factor F_{ay} is suggested in Fig. 7.52, which is based on a comparison between Figs 7.42 and 7.47. The factor F_{ay} can then be used to multiply the prediction of y_u using Fig. 7.51 to include the effect of the angle of the trench sides. The new y_u predicted using Figs 7.51 and 7.52 is $0.095Z$, which agrees well with the Hilderstone test.

Figure 7.53 shows the relationships that can be used to predict the vertical movement of the pipe as a ratio of the horizontal movement based on the results of the parametric study presented in Figs 7.41 and 7.46. The relationships are obtained from the parametric study of a trench with vertical sides, but can also be used for other angles in the absence of a more comprehensive parametric study.

After the estimation of P_u and y_u, a mathematical formulation can then be used to estimate the locus of the non-linear P-y curve. The first three hyperbolic P-y curve formulations listed in Table 2.4 were used in Chapter 3 to fit the P-y curve derived from the field test (Fig. 3.15). It was found that the formulation by Trautmann & O'Rourke (1985) provided

the best agreement. From Fig. 7.48, the best agreement for the normalized data from the parametric study is by Audibert & Nyman (1977). For the normalized data of all the *P-y* curves from the 2-D FE analysis in Section 7.2, the best fitted curve is the formulation by Audibert & Nyman (1977), as shown in Fig. 7.54. The results in Figs 3.15, 7.48 and 7.54 all suggest that the formulations by Audibert & Nyman (1977) and Trautmann & O'Rourke (1985) both give good predictions for the shape of the *P-y* curve, and the difference between them is small. One can use either of them in practice, or use the mean value of the two formulations:

$$P = \frac{y}{\frac{0.16y_u}{P_u} + \frac{0.84y}{P_u}} \tag{7.3}$$

Thus a non-linear *P-y* curve can be estimated using Eq. (7.3). The ultimate pressure P_u can be estimated by Eq. (7.2) where N_{ch} can be found using the Brinch-Hansen bearing capacity factor (ASCE, 1984) in Fig. 2.27, together with Figs 7.49 and 7.50 to correct the N_{ch} value for the existence of a backfill trench. The ultimate displacement y_u can be determined by Figs 7.51 and 7.52.

7.6. Summary

Two-dimensional plane strain finite element analyses have been carried out to predict the pressure-displacement relationship of the pipe in the Hilderstone lateral pipe loading test. Tensile stresses if allowed to develop in the soil at the back of the pipe significantly affect the predicted *P-y* curve. The shear stress around the pipe and along the trench also influences the behaviour of the *P-y* curve. It has been found that using the Non-linear elastic model and the Elasto-plastic model together with interface elements around the pipe and along the trench soil interface give satisfactory prediction of the *P-y* curve.

The predicted *P-y* curves were used in the modified elastic beam on elastic foundation program WOMOD to predict the behaviour of the pipeline in the Hilderstone pipe test. Satisfactory agreement was obtained using the *P-y* curves predicted by the Non-linear elastic model and the Elasto-plastic model both with interface elements.

A parametric study has been carried out using the 2-D FE model with interface elements around the pipe and along the trench sides. The influence of the relative strength between the natural ground and the backfill (R_c), width of the trench (*W/D*) and the angle of the trench sides has been studied. Results show that these factors significantly influence the behaviour, in terms of the pressure-displacement relationship of the pipe, unless the R_c ratio is small and *W/D* ratio is large.

Using the results from the parametric study, a new factor F_{ch} has been introduced to correct the N_{ch} value, used in the determination of P_u when a backfill trench exists; this factor includes the effect of R_c and the *W/D* ratio. A factor F_{ac} has also been derived to include the effect of the angle of the sides of the trench in the determination of P_u. New relationships have also been suggested to determine y_u for different conditions of R_c, *W/D* and angle of the trench sides. In addition, a relationship to estimate the vertical pipe movement has been suggested. These factors and relationships are all presented in easy to use graphical formats and can readily be used by practising engineer in routine design work.

Analysis group	Analysis name*	Soil model for backfill	Soil model for natural ground	Number of increments	Prescribed horizontal displacement
Rigid cavity model (Section 7.2.1)	E-P.1	Elastic-perfectly plastic	Elasto-plastic (full tension)	500	0.2 (m)
	ERSE.F.1	Non-linear elastic (full tension)	Elasto-plastic (full tension)	4000	0.2
	ERSE.N.1	Non-linear elastic (no tension)	Elasto-plastic (no tension)	4000	0.2
	MCC.1	Modified Cam clay	Elasto-plastic (full tension)	4000	0.2
	ERSE-P.F.1	Elasto-plastic (full tension)	Elasto-plastic (full tension)	4000	0.2
	ERSE-P.N.1	Elasto-plastic (no tension)	Elasto-plastic (no tension)	4000	0.2
Model with interface elements around the pipe (Section 7.2.2)	E-P.2	Elastic-perfectly plastic	Elasto-plastic (full tension)	500	0.2
	ERSE.F.2	Non-linear elastic (full tension)	Elasto-plastic (full tension)	4000	0.2
	ERSE.N.2	Non-linear elastic (no tension)	Elasto-plastic (no tension)	4000	0.2
	MCC.2	Modified Cam clay	Elasto-plastic (full tension)	4000	0.2
	ERSE-P.F.2	Elasto-plastic (full tension)	Elasto-plastic (full tension)	4000	0.2
	ERSE-P.N.2	Elasto-plastic (no tension)	Elasto-plastic (no tension)	4000	0.2
Model with interface elements around the pipe and along the trench (Section 7.2.3.1)	E-P.3	Elastic-perfectly plastic	Elasto-plastic (full tension)	500	0.2
	ERSE.F.3	Non-linear elastic (full tension)	Elasto-plastic (full tension)	4000	0.2
	ERSE.N.3	Non-linear elastic (no tension)	Elasto-plastic (no tension)	4000	0.2
	MCC.3	Modified Cam clay	Elasto-plastic (full tension)	4000	0.2
	ERSE-P.F.3	Elasto-plastic (full tension)	Elasto-plastic (full tension)	4000	0.2
	ERSE-P.N.3	Elasto-plastic (no tension)	Elasto-plastic (no tension)	4000	0.2
Ditto but stress controlled analysis (Section 7.2.3.2)	ERSE-P.F.3.F	Elasto-plastic (full tension)	Elasto-plastic (full tension)	3000	Prescribed horizontal load = 150kN

* The analysis name is generally formed by three parts, the first part, just before a full stop, is the name of the soil model. The second part, between the two full stops (only for Non-linear elastic and Elasto-plastic models), represents full tension (F) or no tension (N) used for the soil model. The final part, containing a number from 1 to 3, represents the mesh (analysis group) for the analysis.

Table 7.1. Combinations of soil model, number of increments and prescribed horizontal displacement for the 2-D FE analyses.

Analysis group	Analysis name	Vertical movement (mm)	Ultimate horizontal displacement y_u (m)	Ultimate pressure P_u (kN/m²)	Maximum pressure P_{max} (kN/m²)	Normalised y_u with Z	Normalised P_u with average c_u	Normalised P_{max} with average c_u
Rigid cavity model (Section 7.2.1)	E-P.1	7.6	0.060	333	336	0.044	12.8	12.9
	ERSE.F.1	80.1	0.070	321	538	0.052	12.4	20.7
	ERSE.N.1	185.8	0.050	94	149	0.037	3.6	5.7
	MCC.1	32.6	0.016	251	400	0.012	9.7	15.4
	ERSE-P.F.1	0.0	0.140	387	393	0.103	14.9	15.1
	ERSE-P.N.1	110.1	0.040	121	229	0.029	4.7	8.8
Model with interface elements around the pipe (Section 7.2.2)	E-P.2	75.4	0.050	159	140	0.037	6.1	6.2
	ERSE.F.2	169.1	0.020	87	188	0.015	3.3	7.2
	ERSE.N.2	195.2	0.024	90	216	0.018	3.5	8.3
	MCC.2	170.4	0.030	90	115	0.022	3.5	4.4
	ERSE-P.F.2	152.4	0.100	134	147	0.074	5.2	5.6
	ERSE-P.N.2	134.1	0.020	107	149	0.015	4.1	5.7
Model with interface elements around the pipe and along the trench (Section 7.2.3.1)	E-P.3	75.1	0.040	117	114	0.029	4.5	4.5
	ERSE.F.3	200.4	0.012	79	178	0.009	3.0	6.8
	ERSE.N.3	190.7	0.012	80	202	0.009	3.1	7.8
	MCC.3	166.8	0.012	88	108	0.009	3.4	4.2
	ERSE-P.F.3	152.6	0.100	130	142	0.074	5.0	5.5
	ERSE-P.N.3	130.8	0.024	106	146	0.018	4.1	5.6
Ditto but stress controlled analysis (Section 7.2.3.2)	ERSE-P.F.3.F	average movement vertical = 136.2 horizontal = 245.8	0.090	135	162	0.069	5.2	6.2
Hilderstone lateral pipe loading test		—	0.150	190	234	0.111	7.3	9.0

Table 7.2. Results of the 2-D FE analyses for different models.

Original results from	Proposed formulation	$N_{ch}\left(=\frac{P_u}{c_u}\right)$	$\frac{P_u}{c_u}$ using Eq. (7.2)
Reese (1958)	$N_{ch}=2+\frac{\gamma Z}{c_u}+2\sqrt{2}\frac{Z}{D}$	7.2	8.5
Matlock (1970)	$N_{ch}=3+\left(\frac{\sigma_n'}{c_u}\right)+J\left(\frac{Z}{D}\right)$ (Take $J=0.4$)	4.7	5.5
Poulos & Davis (1980)	$N_{ch}=3+\frac{\gamma Z}{c_u}+0.5\frac{Z}{D}$	4.8	5.7
Rowe & Davis (1982a)	$N_{ch}=2$ to 11.5 For the value of N_{ch}, see Fig. 2.30.	No breakaway: 9.4 Immediate breakaway: 4.2	No breakaway: 11.1 Immediate breakaway: 5.0
Randolph & Houlsby (1984)	$N_{ch}=2+\frac{\gamma Z}{c_u}+1.5\frac{Z}{D}$	5.2	6.1
ASCE (1984) based on Hansen (1961)	$N_{ch}=2.8$ to 7.8 For the value of N_{ch}, see Fig. 2.27.	5.5	6.5
Hilderstone lateral pipe loading test	—	7.3	—

Table 7.3. Predicted values of N_{ch} for the Hilderstone lateral pipe loading test by the proposed formulations in Table 2.6 and modified formulation to include the effects of existence of backfill trench (Eq. 7.2).

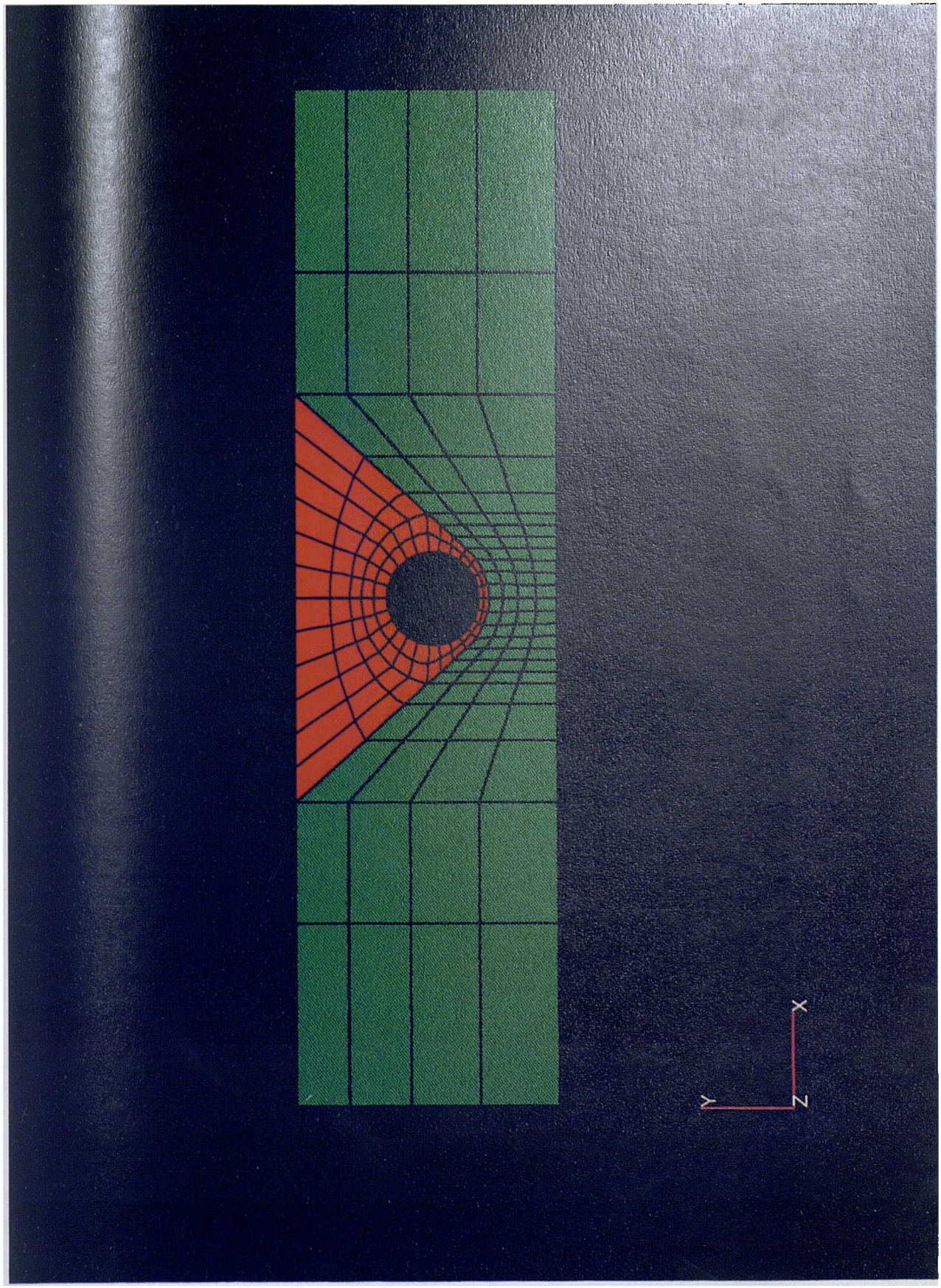

Fig. 7.1. Two-dimensional finite element mesh for the rigid cavity model.

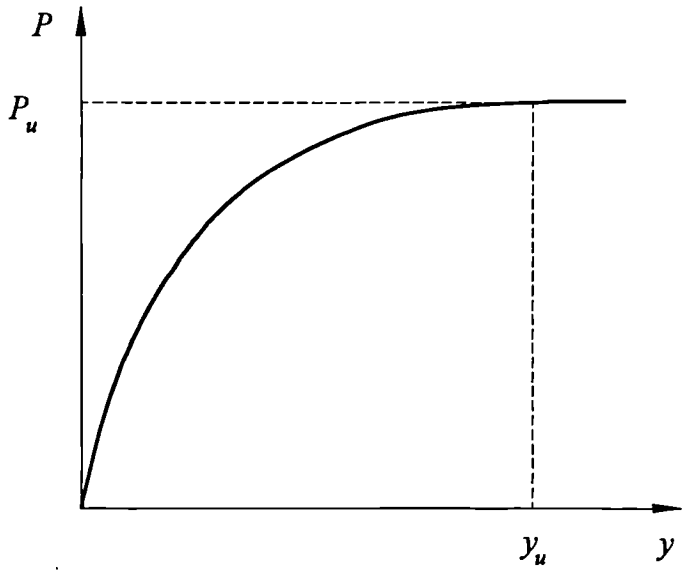

(a) *P-y* curve that flattened out

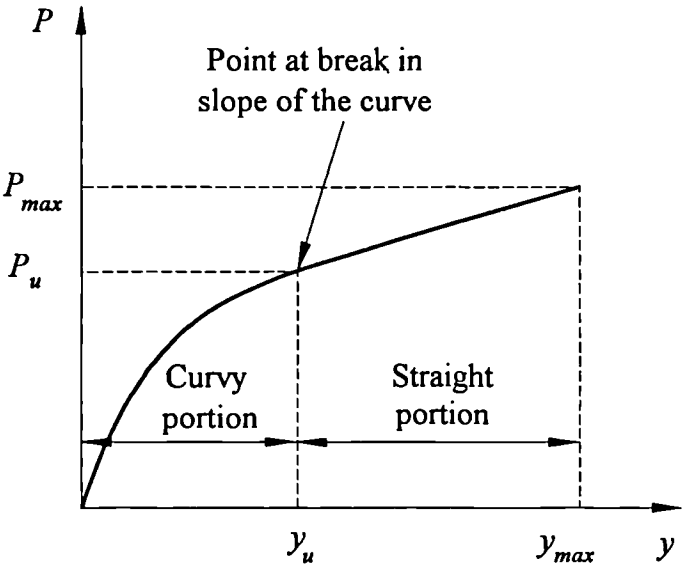

(b) *P-y* curve that does not flatten out

Fig. 7.2. Definitions of P_u and y_u of *P-y* curve.

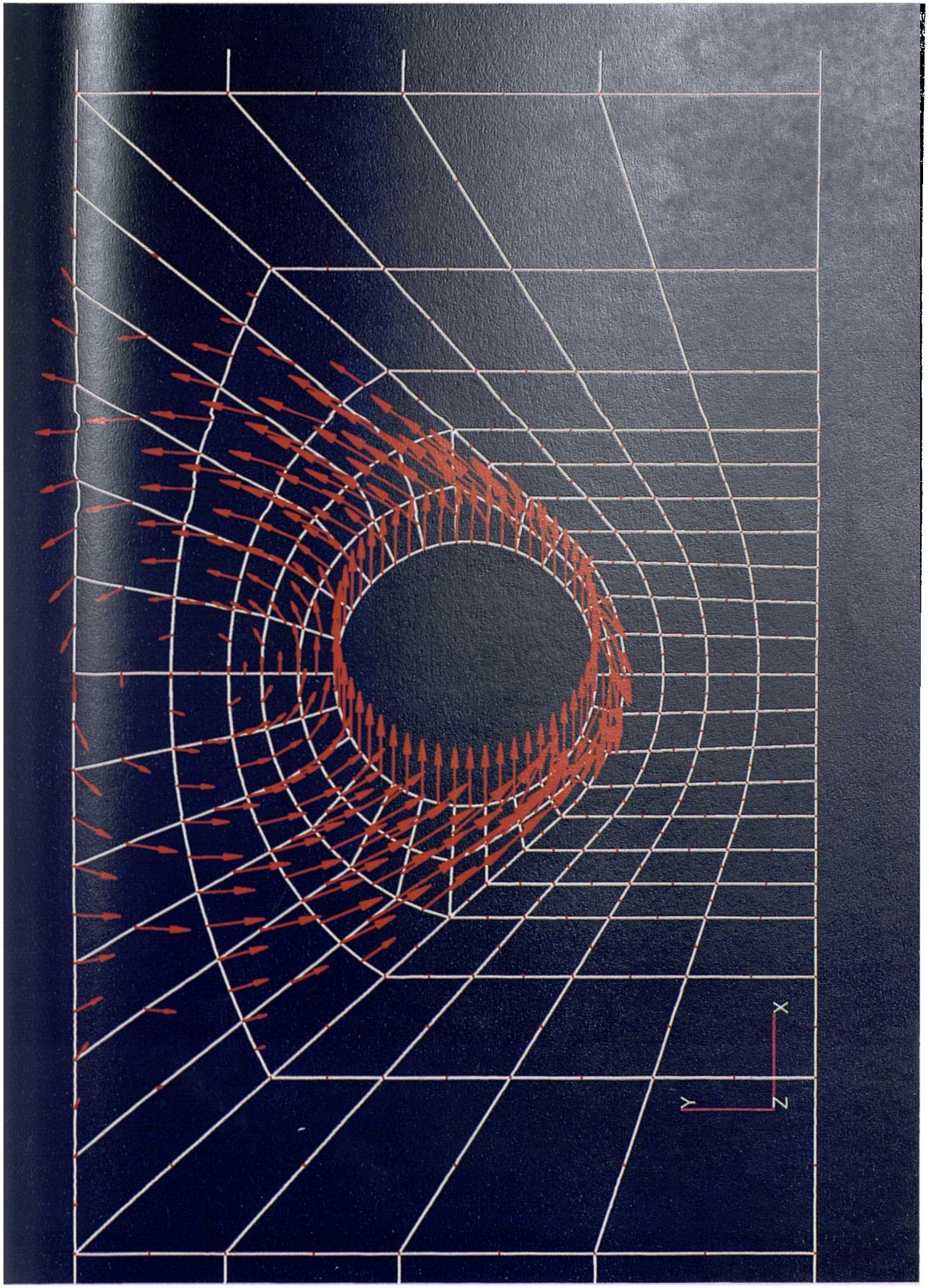

Fig. 7.3 (a). Displacement vectors of analysis ERSE-P.F.1 (full tension).

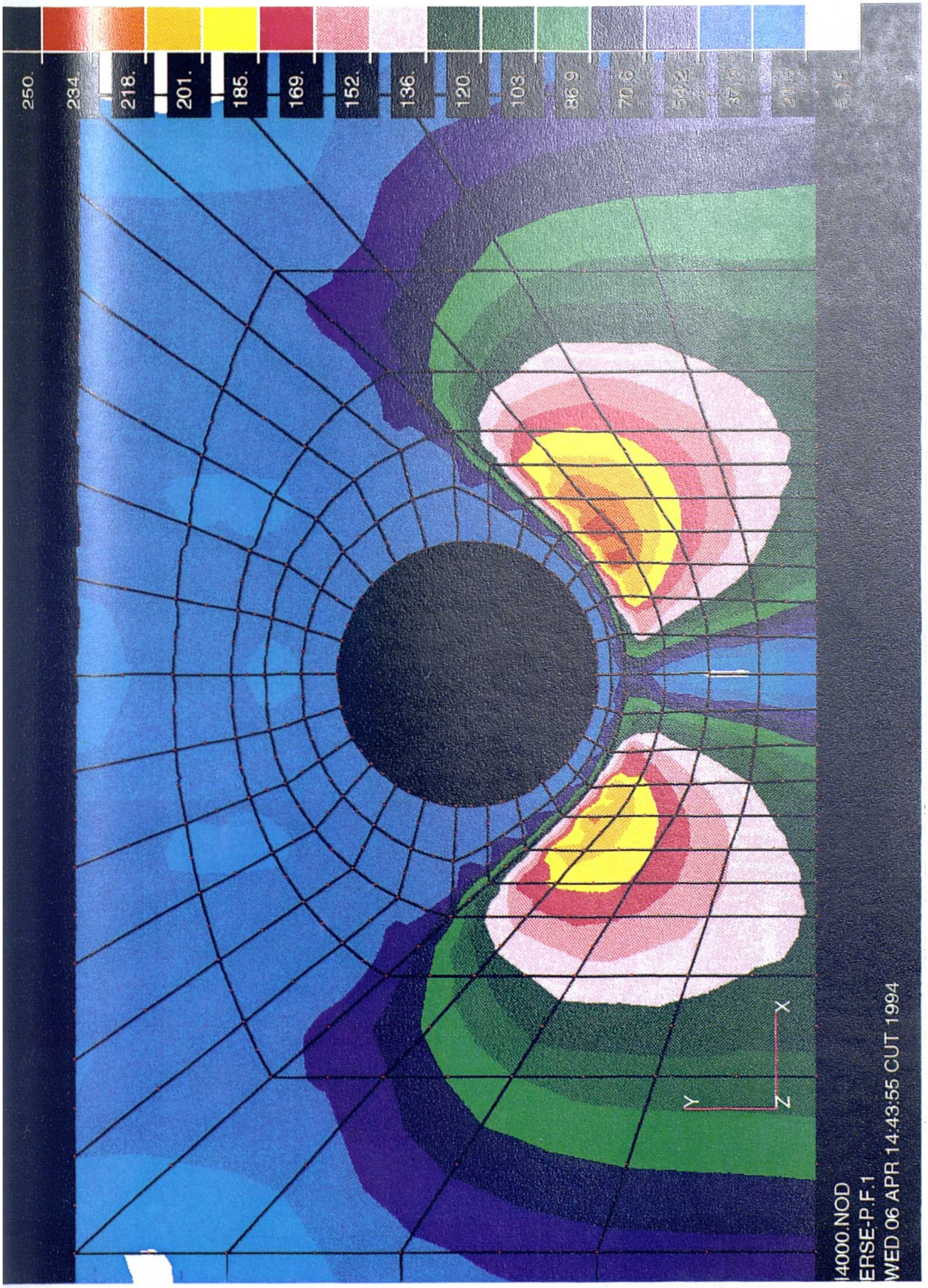

Fig. 7.3 (b). Deviator stress contour of analysis ERSE-P.F.1 (full tension).

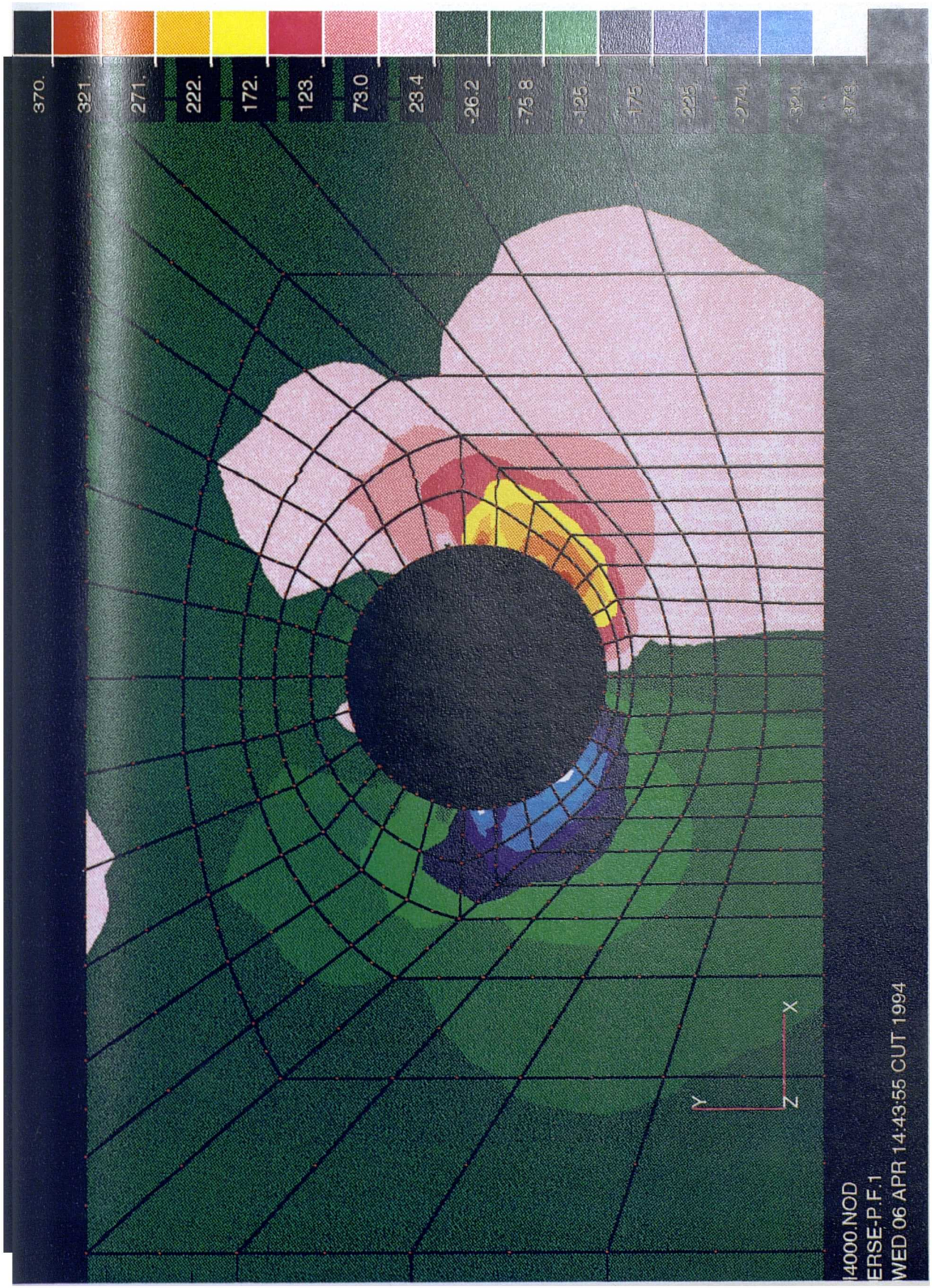

Fig. 7.3 (c). Mean total stress contour of analysis ERSE-P.F.1 (full tension).

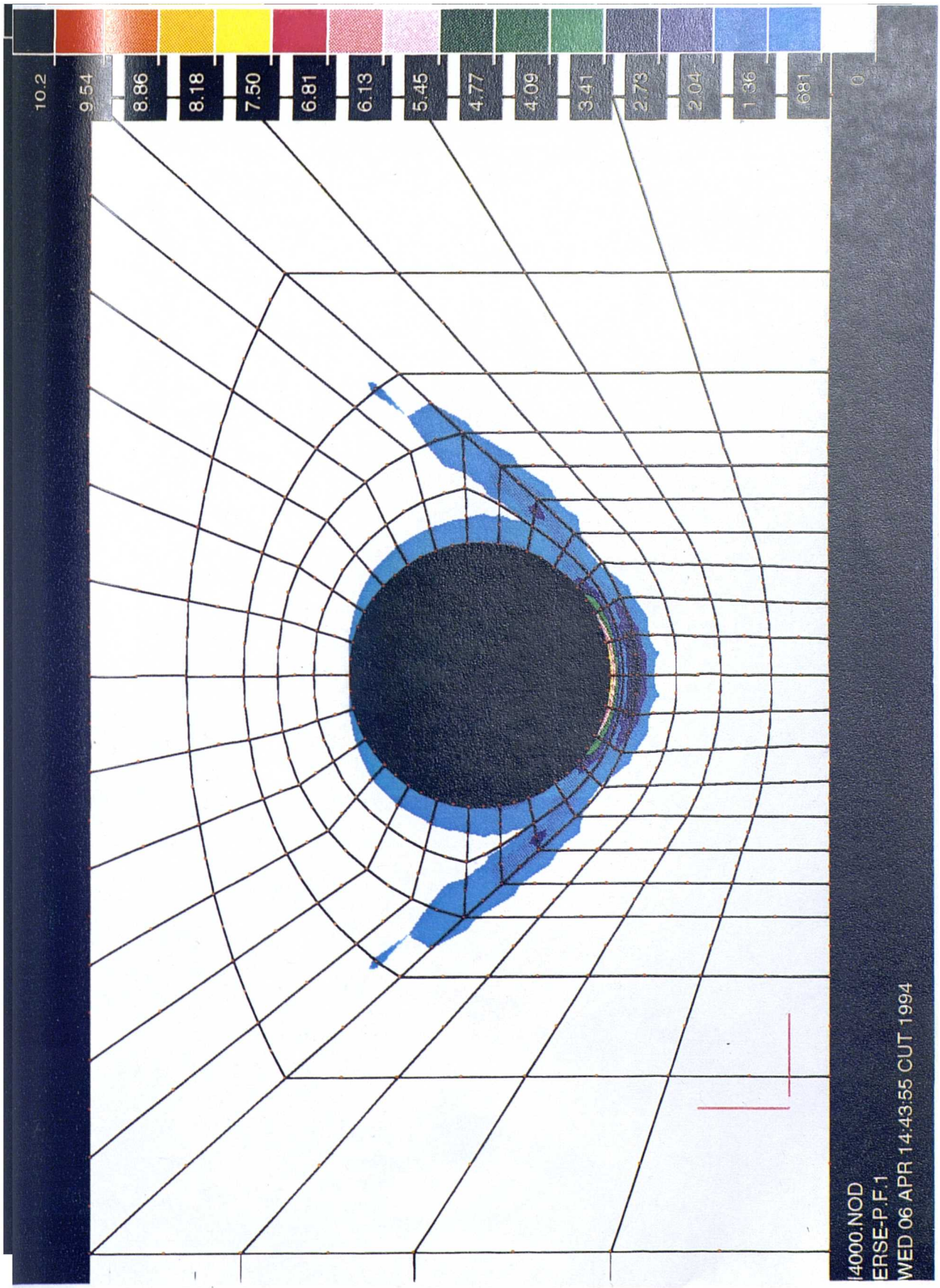

Fig. 7.3 (d). Shear strain contour of analysis ERSE-P.F.1 (full tension).

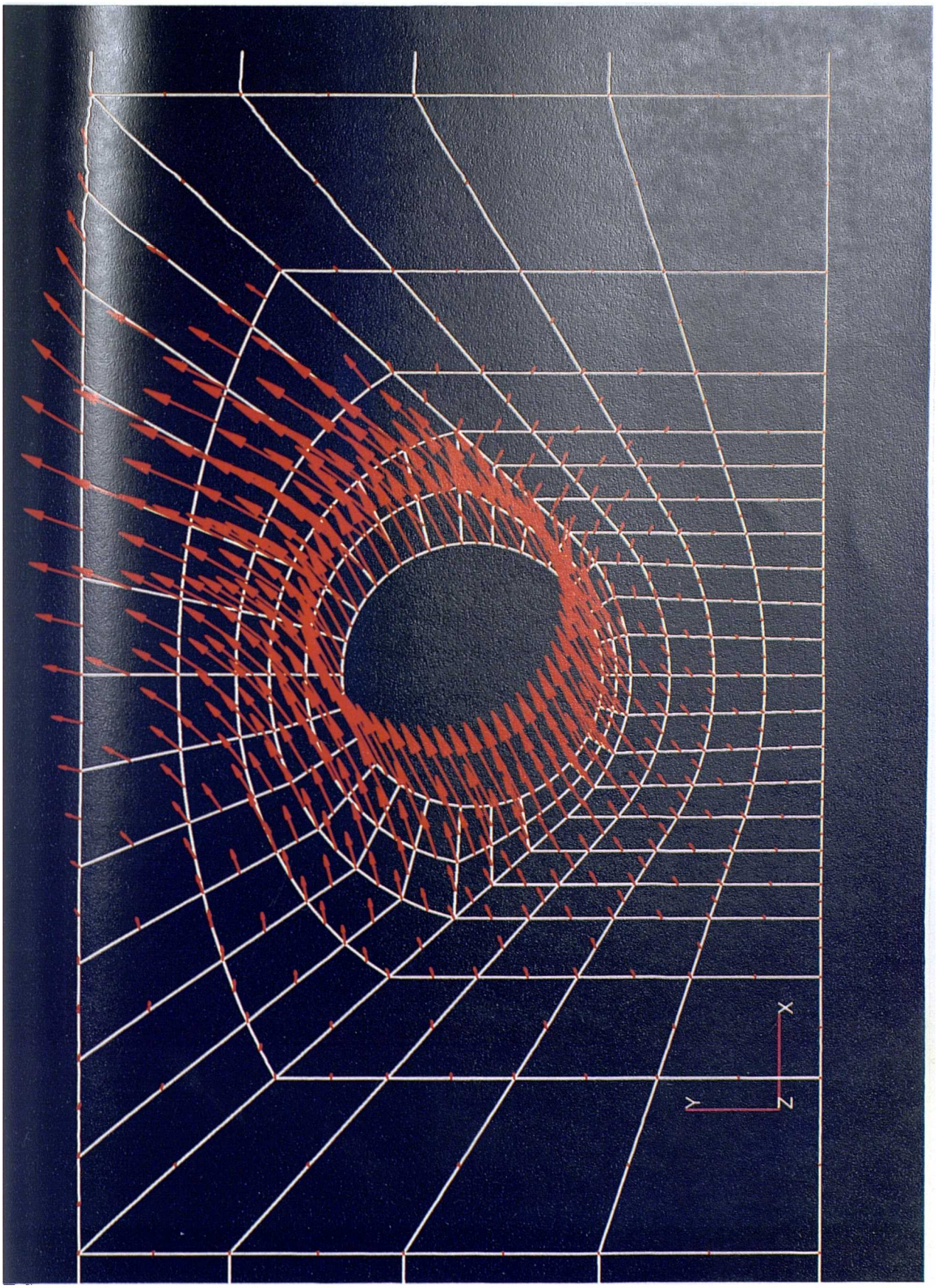

Fig. 7.4 (a). Displacement vectors of analysis ERSE-P.N.1 (no tension).

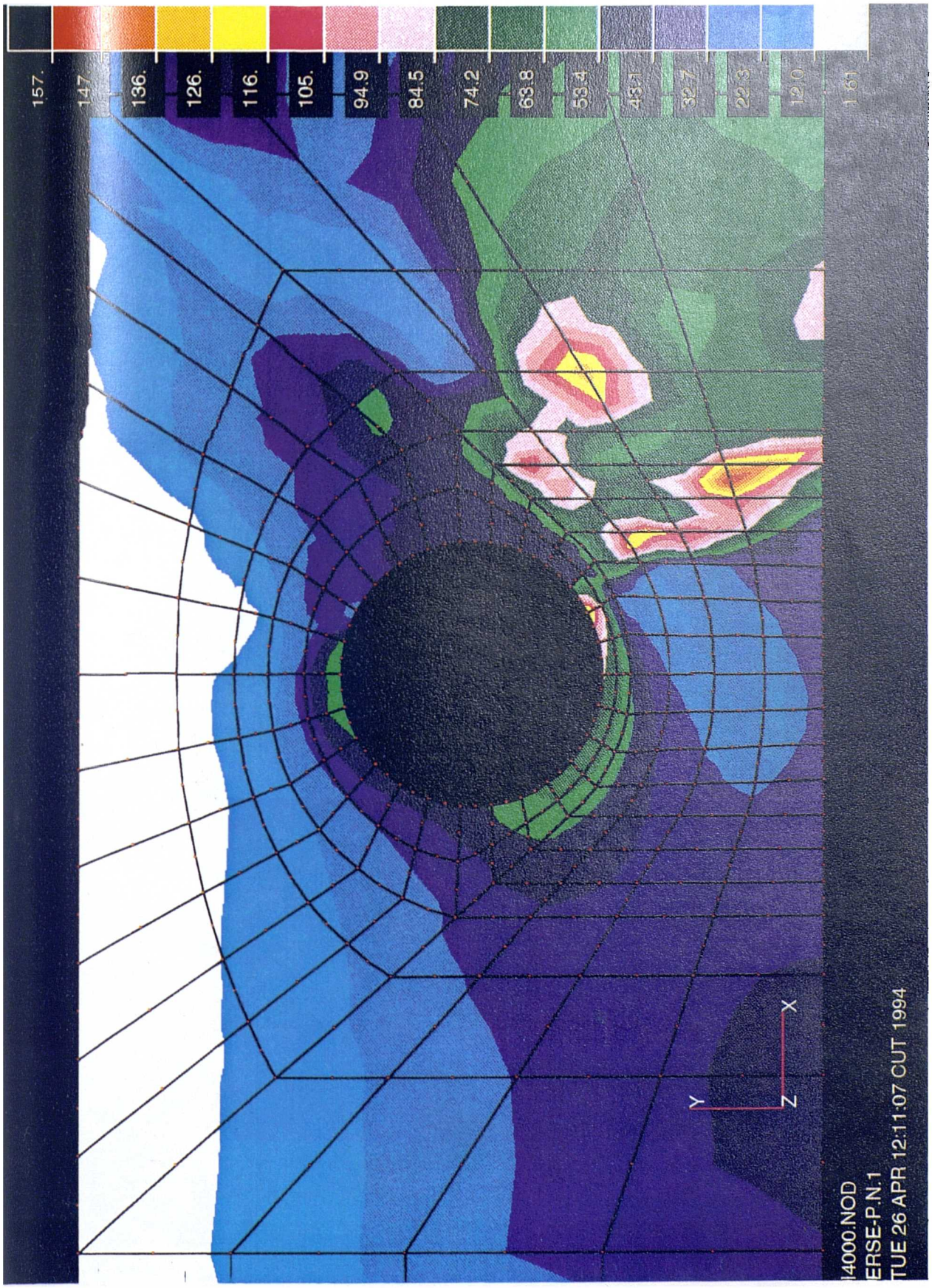

Fig. 7.4 (b). Deviator stress contour of analysis ERSE-P.N.1 (no tension).

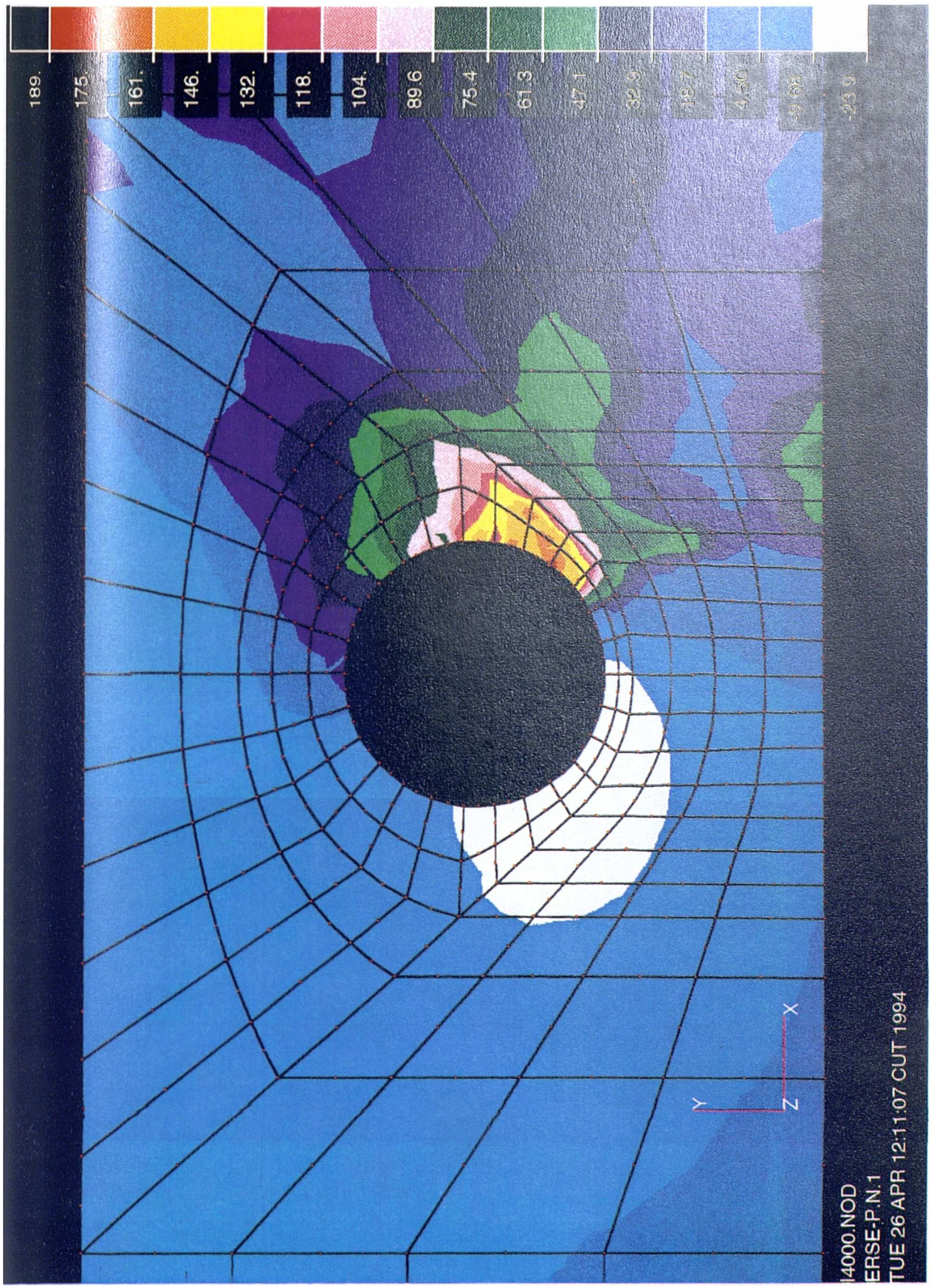

Fig. 7.4 (c). Mean total stress contour of analysis ERSE-P.N.1 (no tension).

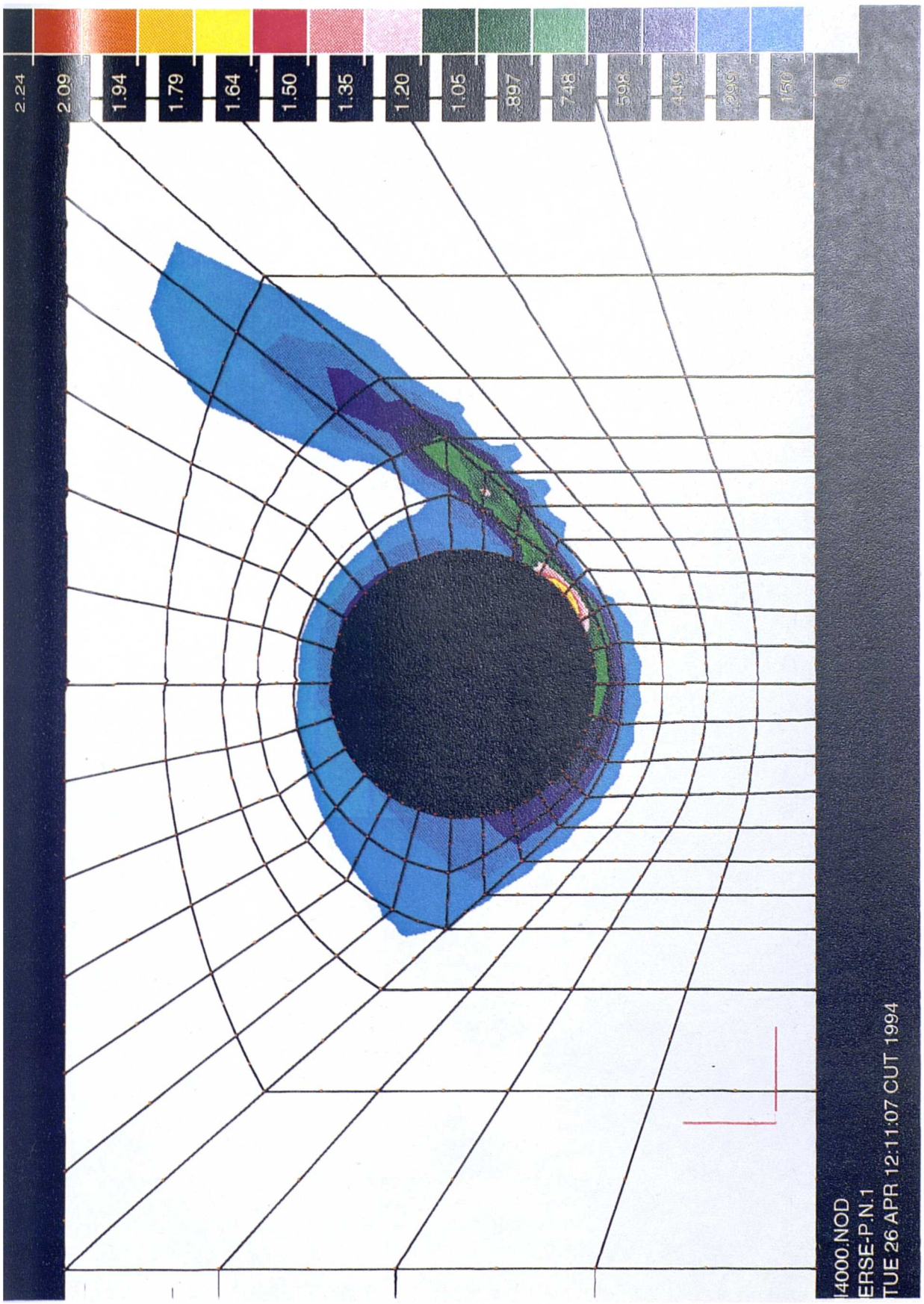

Fig. 7.4 (d). Shear strain contour of analysis ERSE-P.N.1 (no tension).

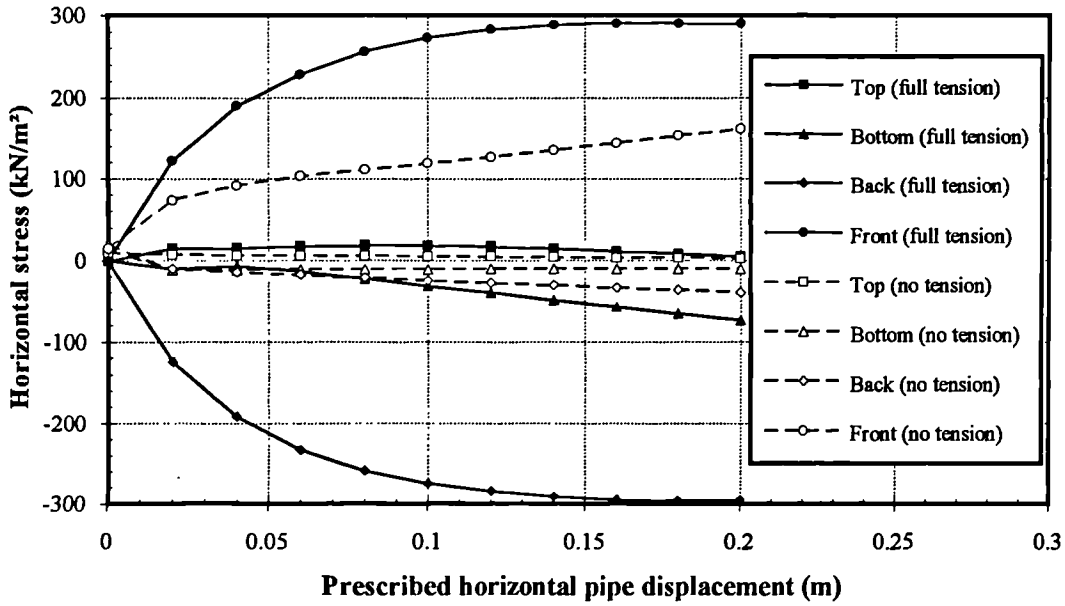

(a)

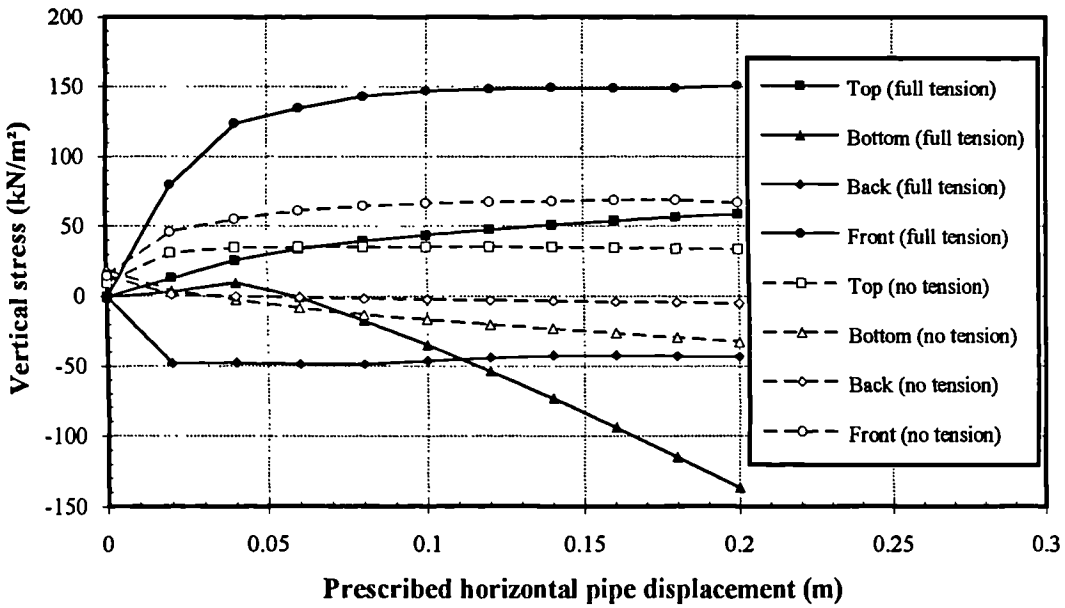

(b)

Fig. 7.5. Total stress paths at the top, bottom, back and the front of the pipe for the Elasto-plastic models with and without tension in the rigid cavity model (a) horizontal stress, (b) vertical stress.

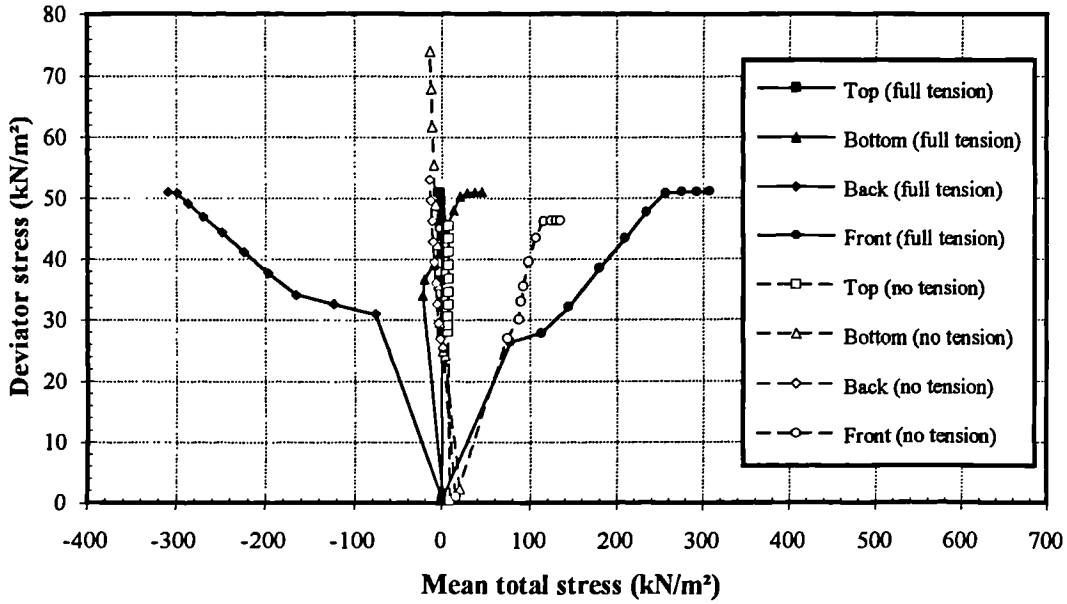

(c)

Fig. 7.5. Total stress paths at the top, bottom, back and the front of the pipe for the Elasto-plastic models with and without tension in the rigid cavity model (c) *q-p* path.

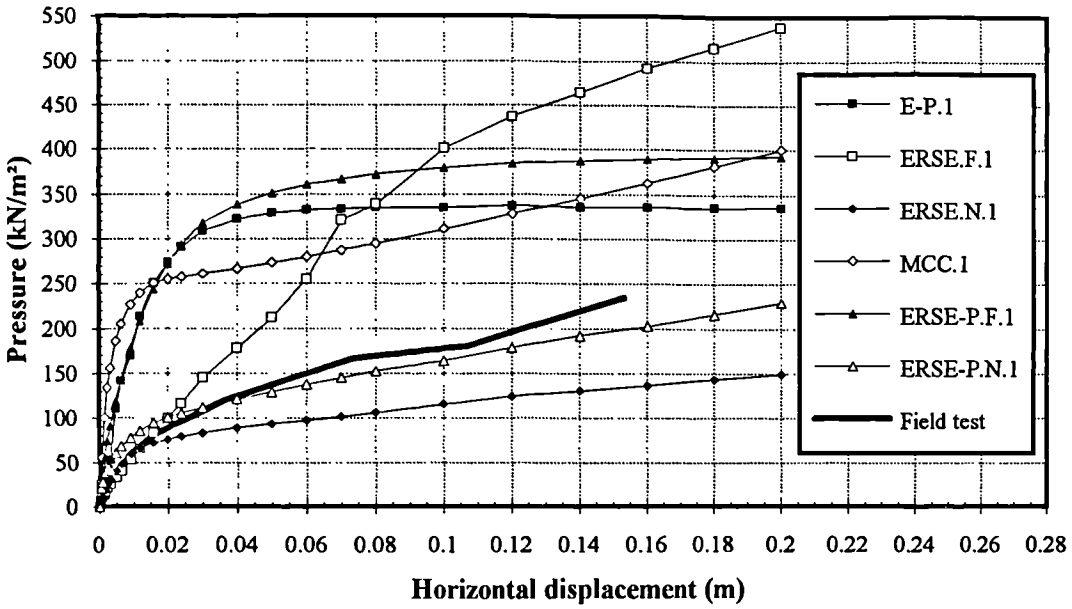

Fig. 7.6. The pressure-displacement relationships predicted by different analyses in the rigid cavity model (see Table 7.1 for the description of analysis names in the legend).

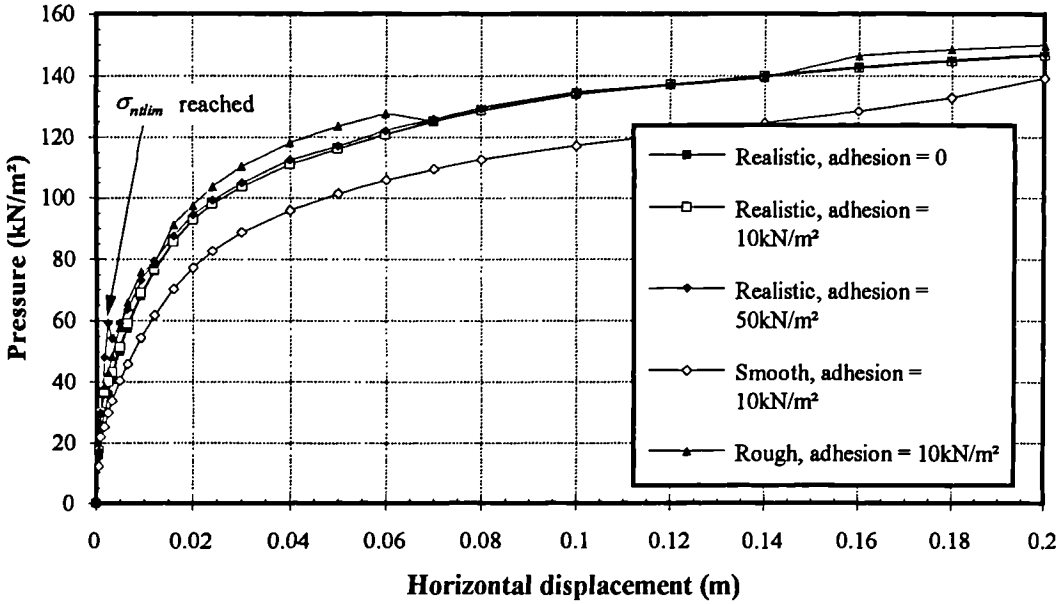

Fig. 7.7. The predicted pressure-displacement relationships using the Elastio-plastic full tension model with different roughness and limiting adhesion in the model with interface elements around the pipe.

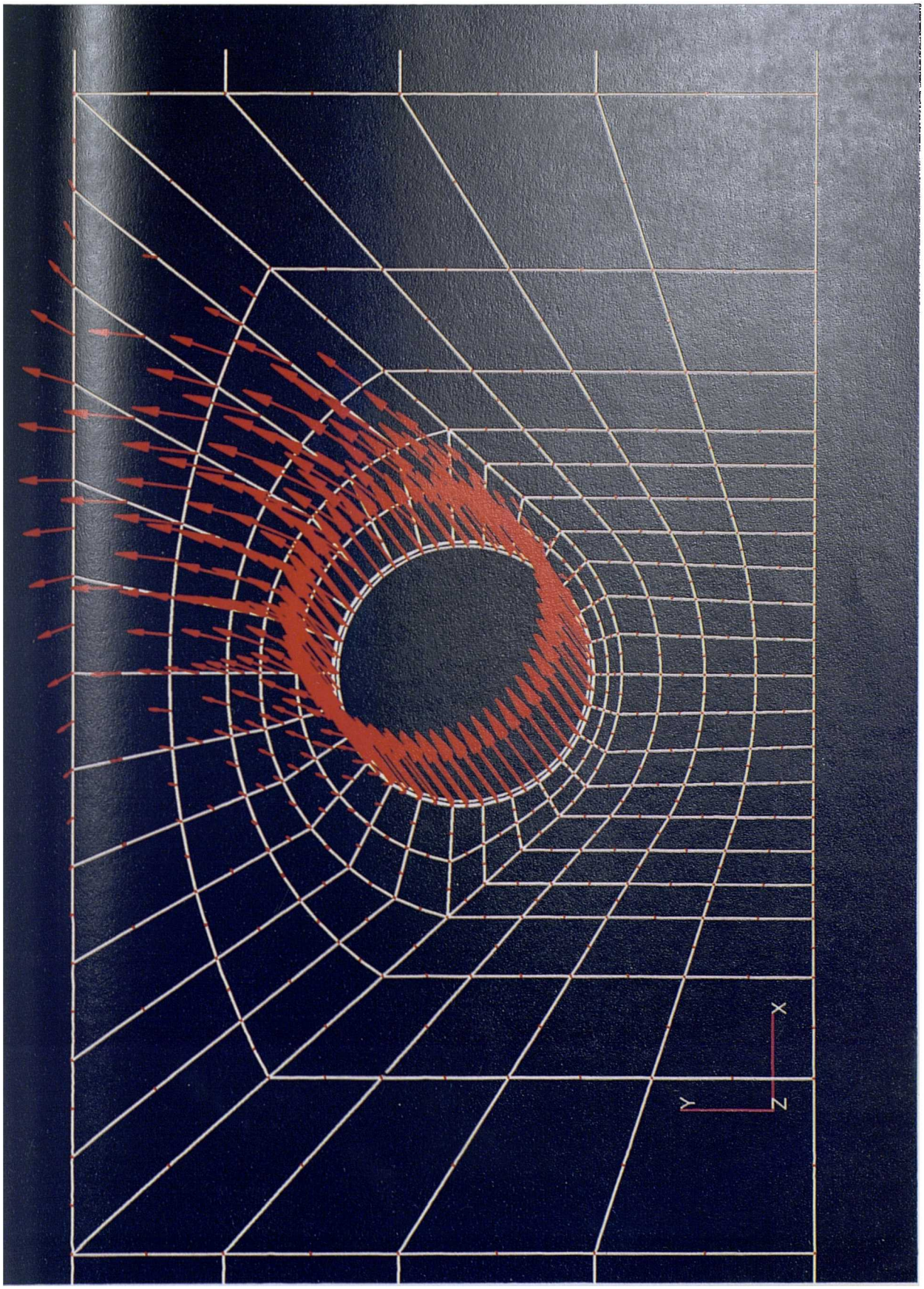

Fig. 7.8 (a). Displacement vectors of analysis ERSE-P.F.2 (full tension).

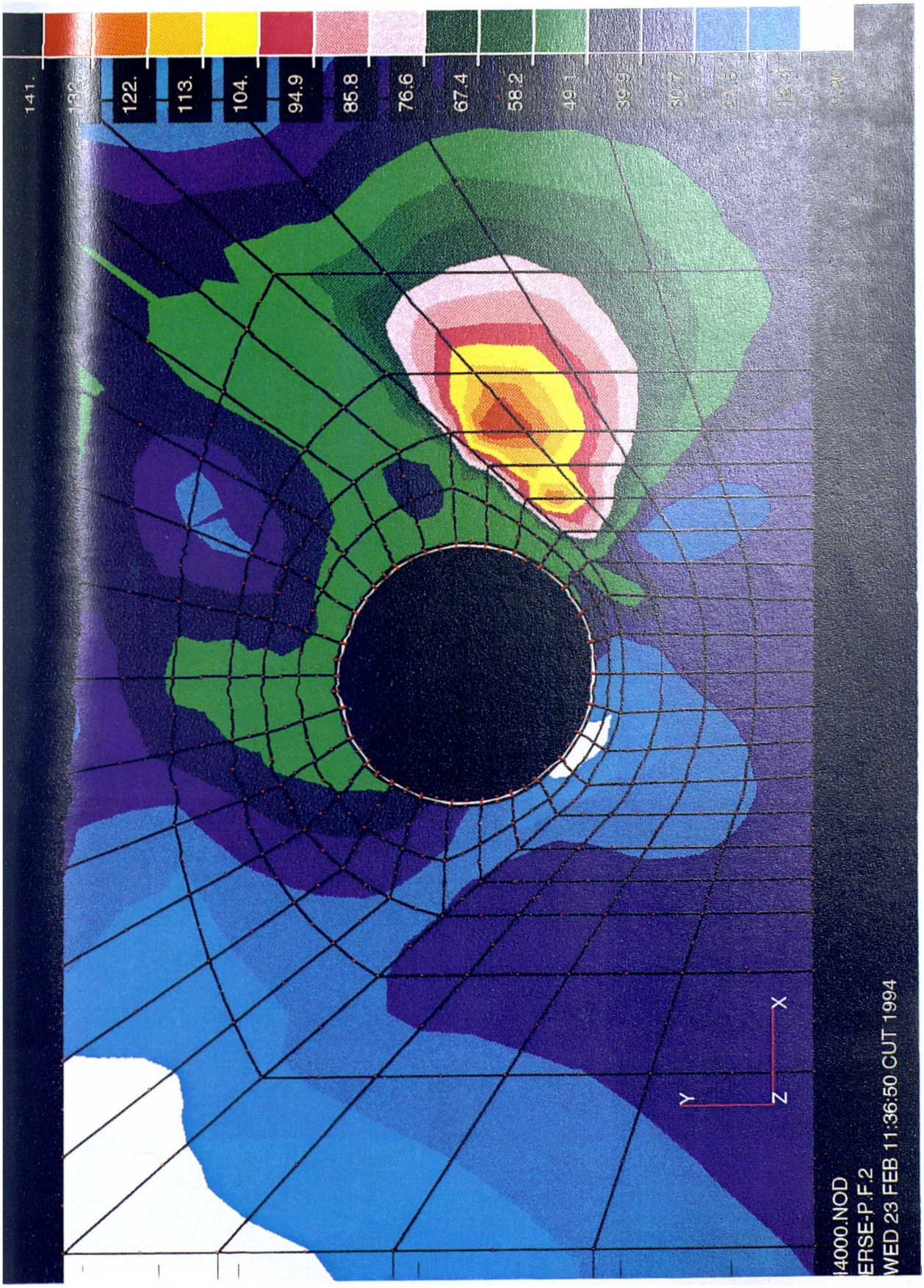

Fig. 7.8 (b). Deviator stress contour of analysis ERSE-P.F.2 (full tension).

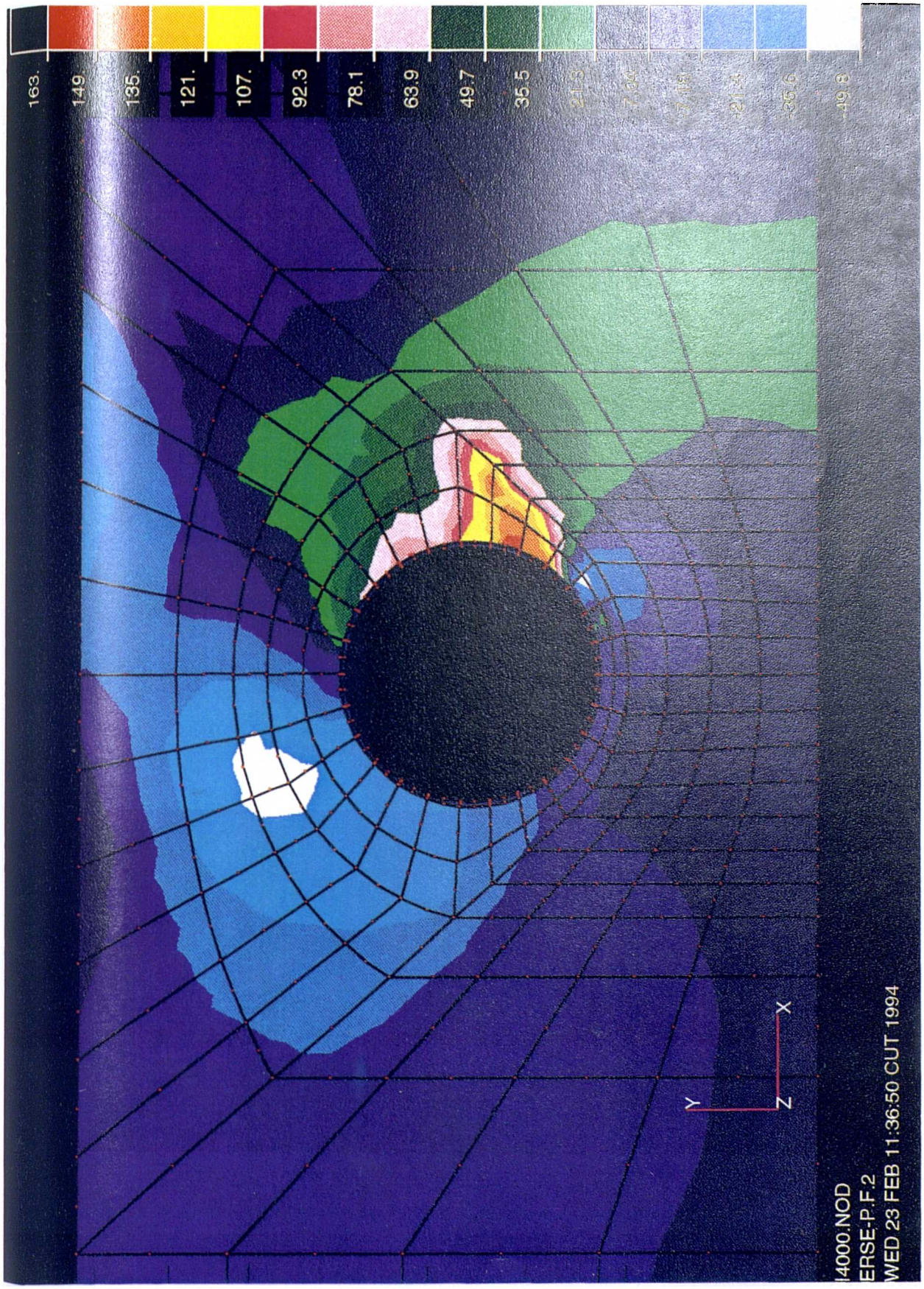

Fig. 7.8 (c). Mean total stress contour of analysis ERSE-P.F.2 (full tension).

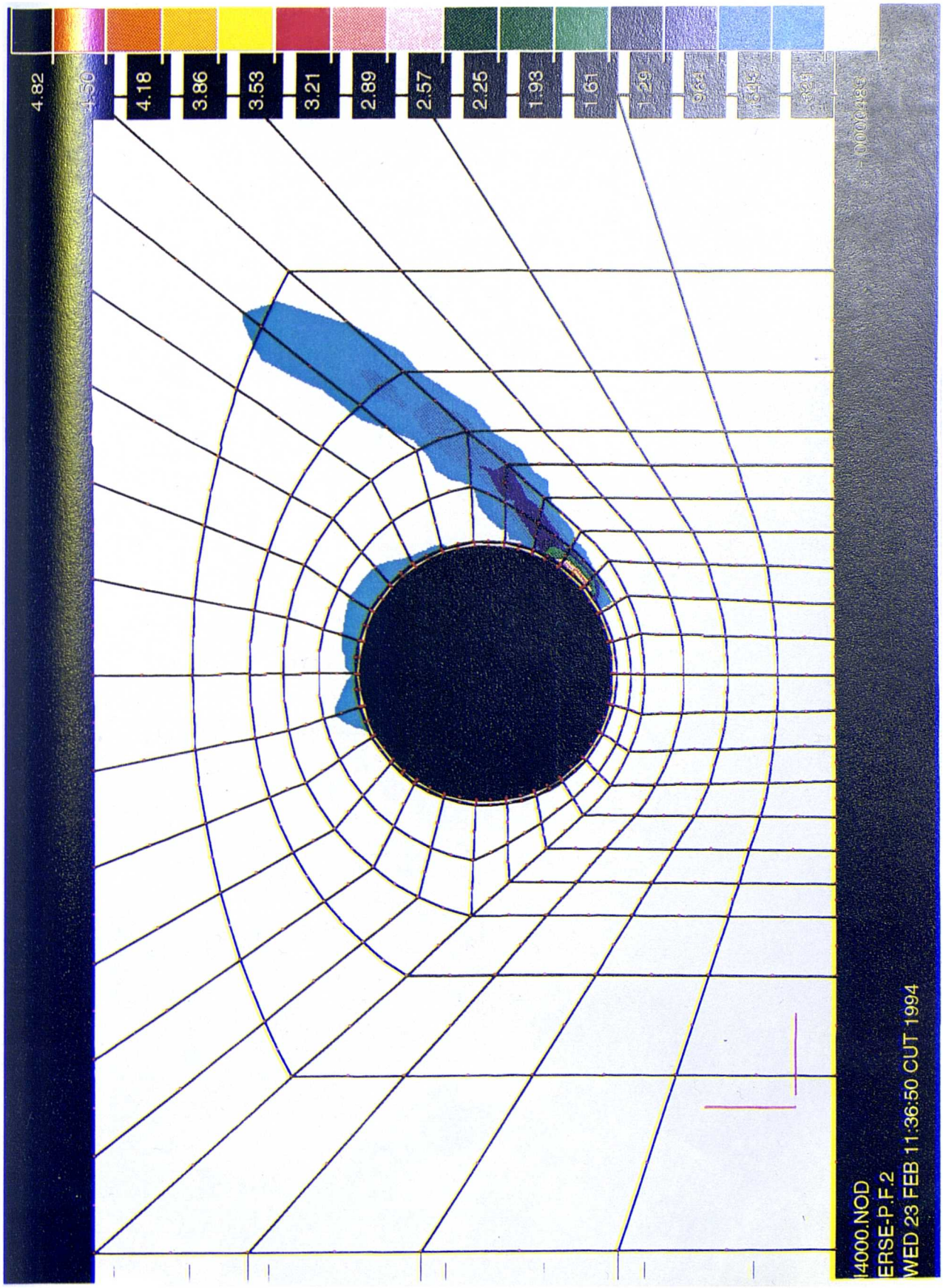

Fig. 7.8 (d). Shear strain contour of analysis ERSE-P.F.2 (full tension).

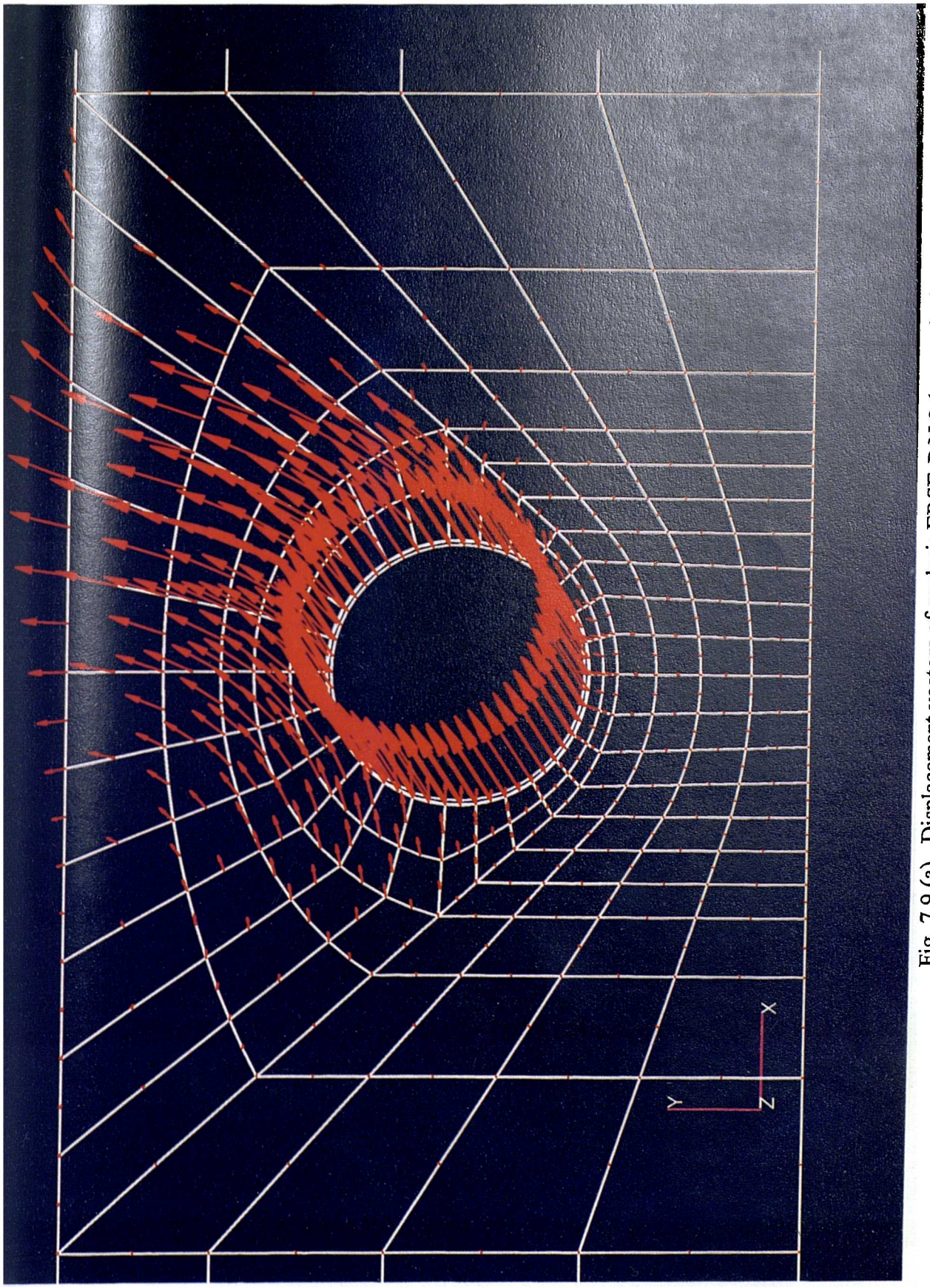

Fig. 7.9 (a). Displacement vectors of analysis ERSE-P.N.2 (no tension).

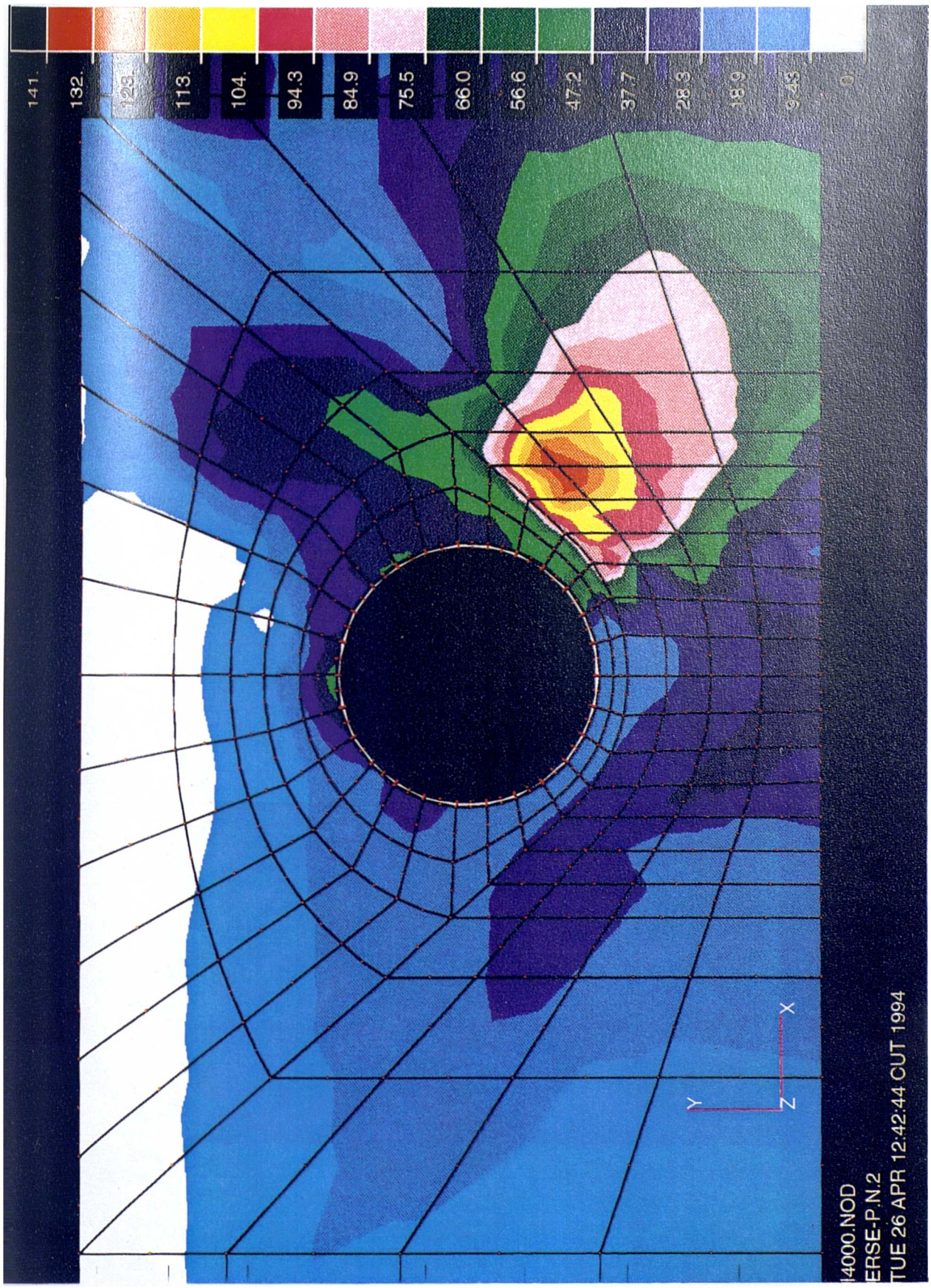

Fig. 7.9 (b). Deviator stress contour of analysis ERSE-P.N.2 (no tension).

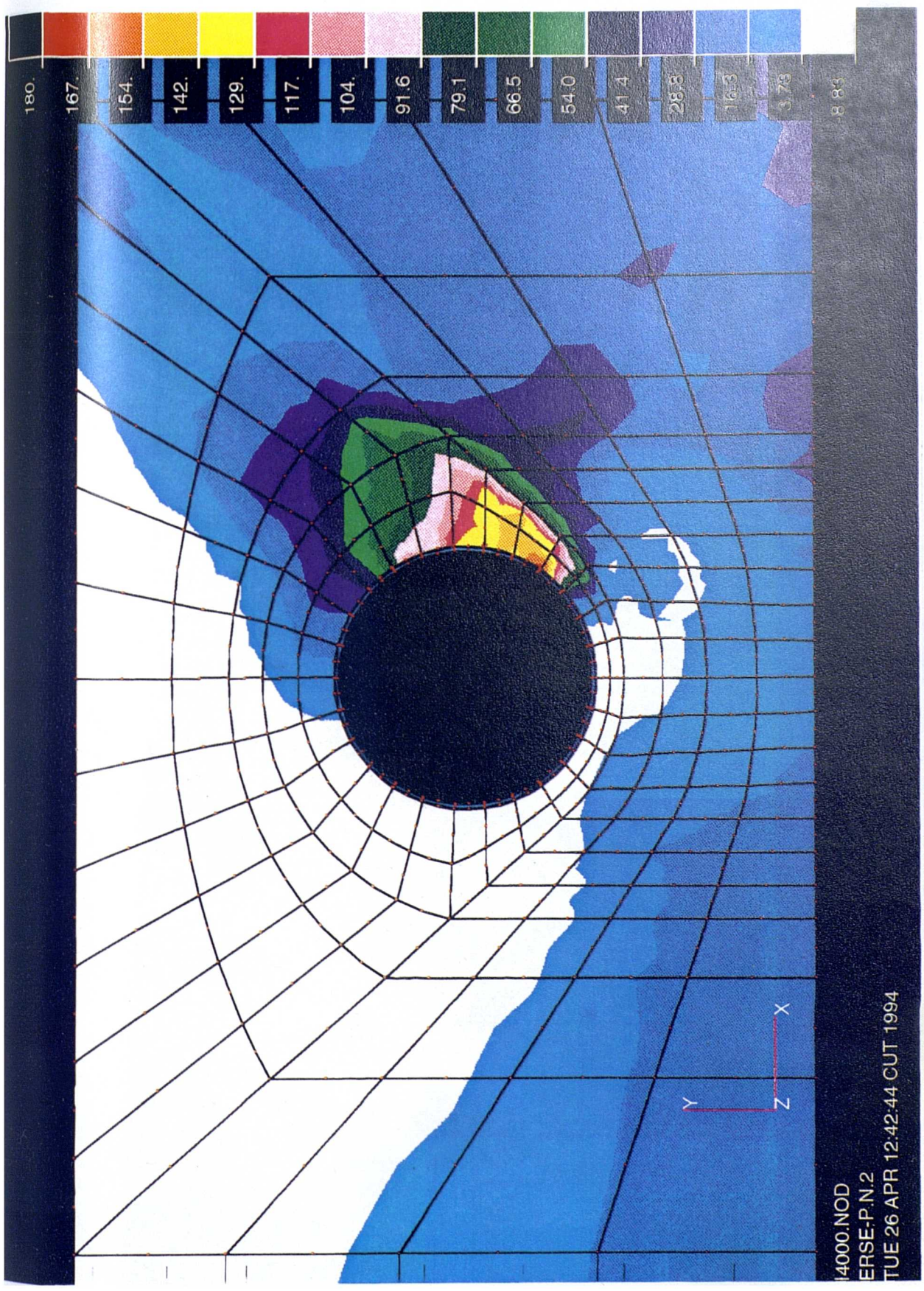

Fig. 7.9 (c). Mean total stress contour of analysis ERSE-P.N.2 (no tension).

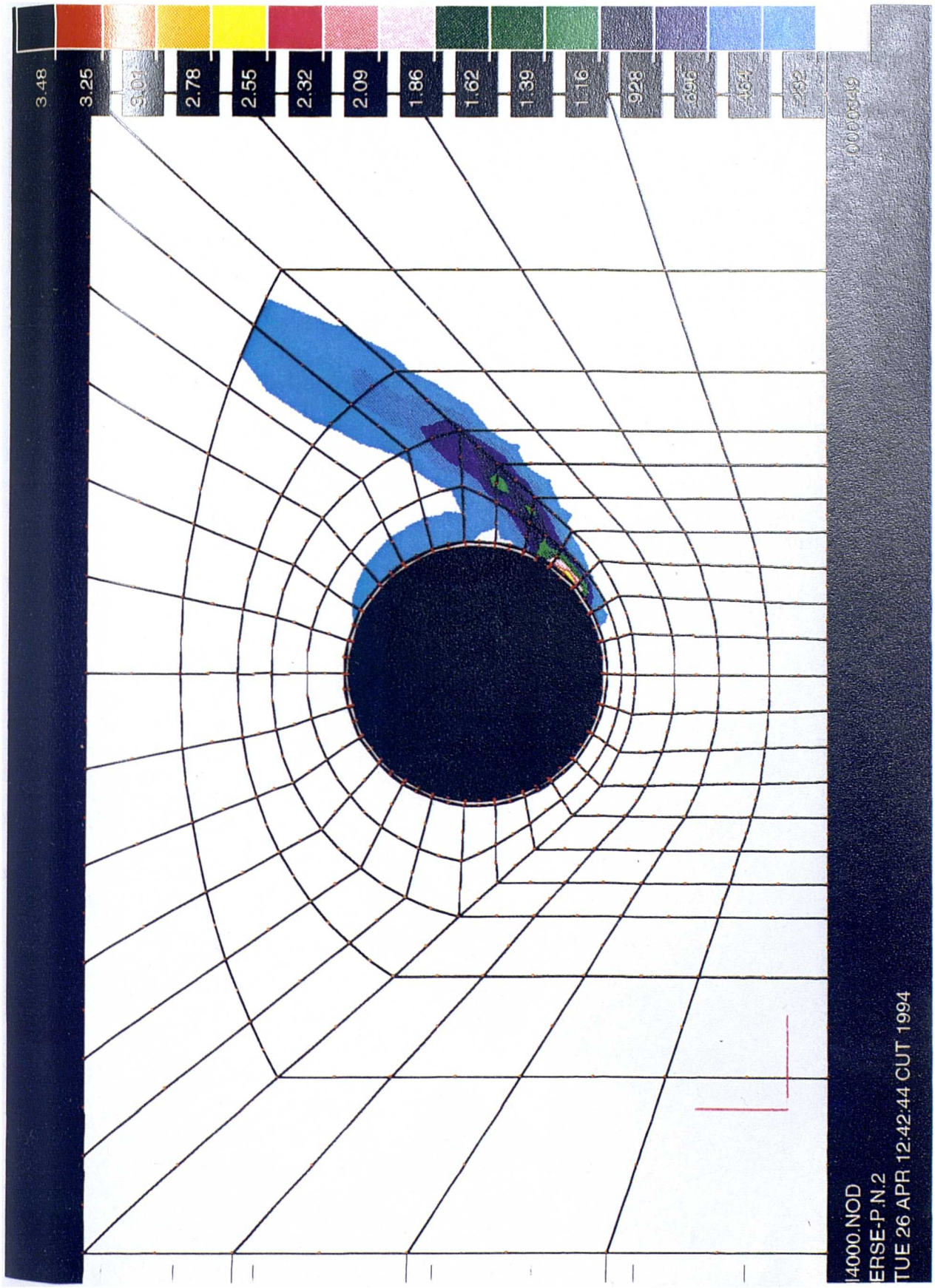

Fig. 7.9 (d). Shear strain contour of analysis ERSE-P.N.2 (no tension).

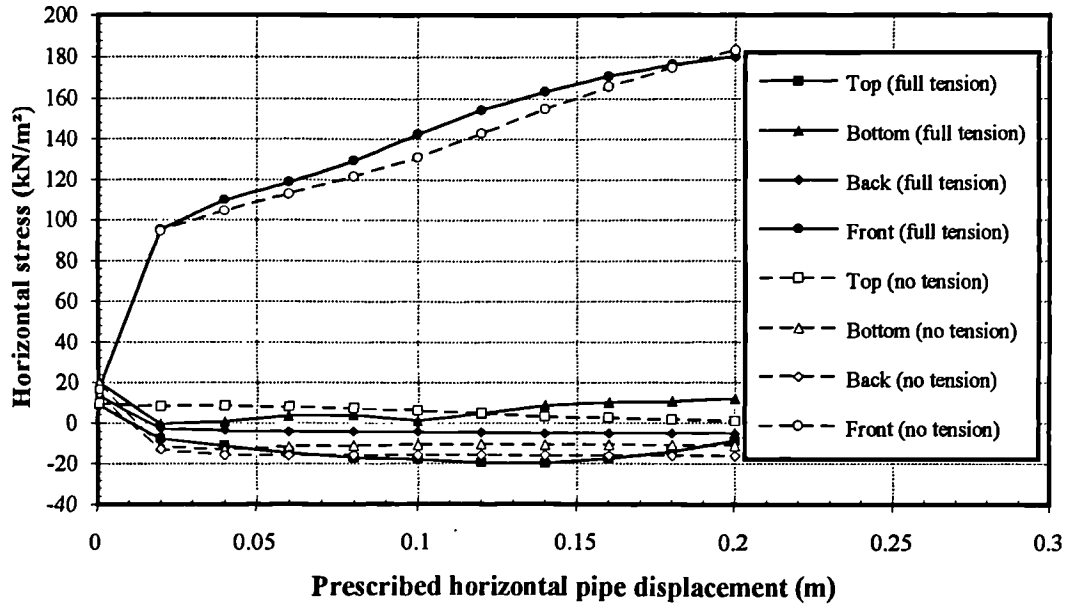

(a)

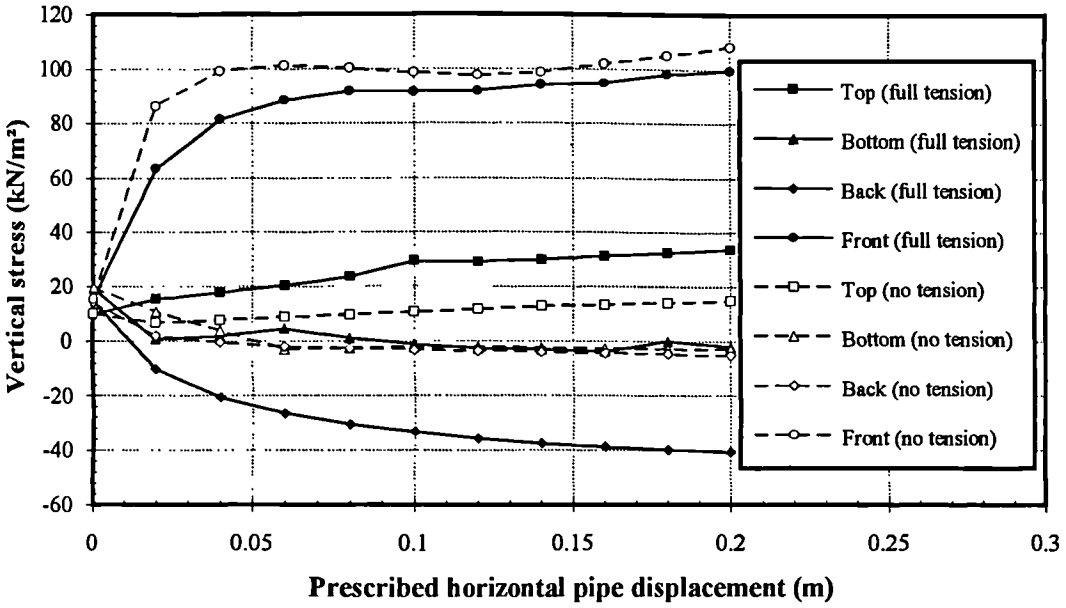

(b)

Fig. 7.10. Total stress paths at the top, bottom, back and the front of the pipe for the Elasto-plastic models with and without tension in the model with interface elements around the pipe (a) horizontal stress, (b) vertical stress.

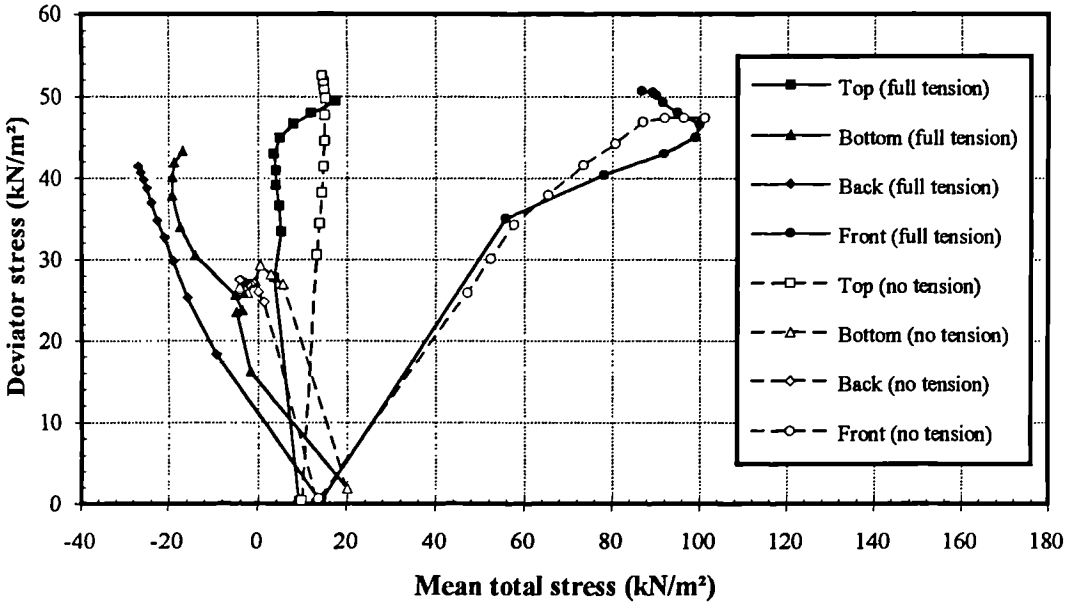

(c)

Fig. 7.10. Total stress paths at the top, bottom, back and the front of the pipe for the Elasto-plastic models with and without tension in the model with interface elements around the pipe (c) *q-p* path.

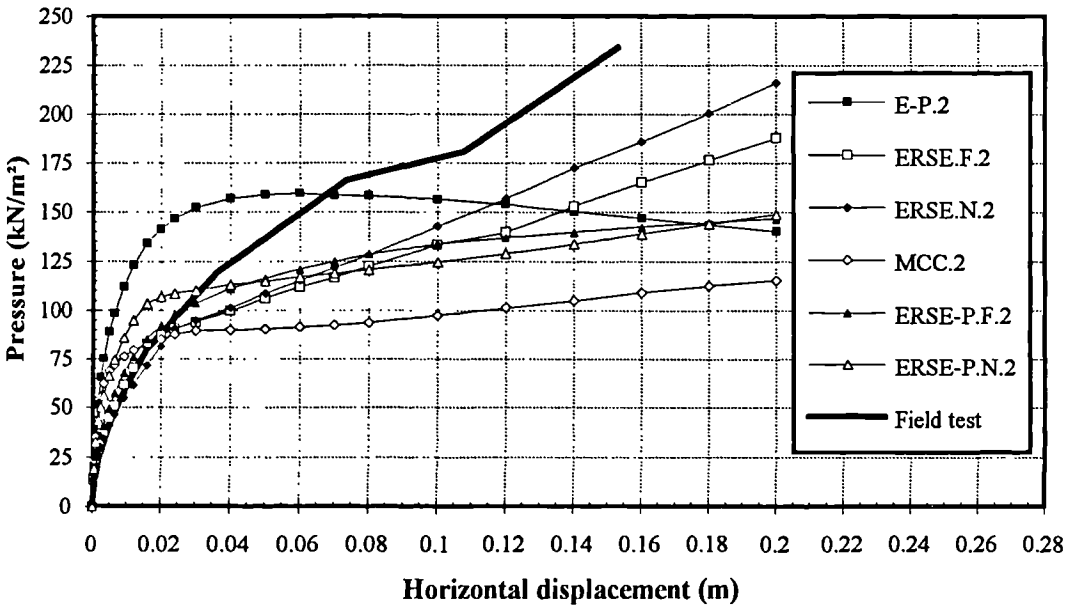

Fig. 7.11. The pressure-displacement relationships predicted by different analyses in the model with interface elements around the pipe (see Table 7.1 for the description of analysis names in the legend).

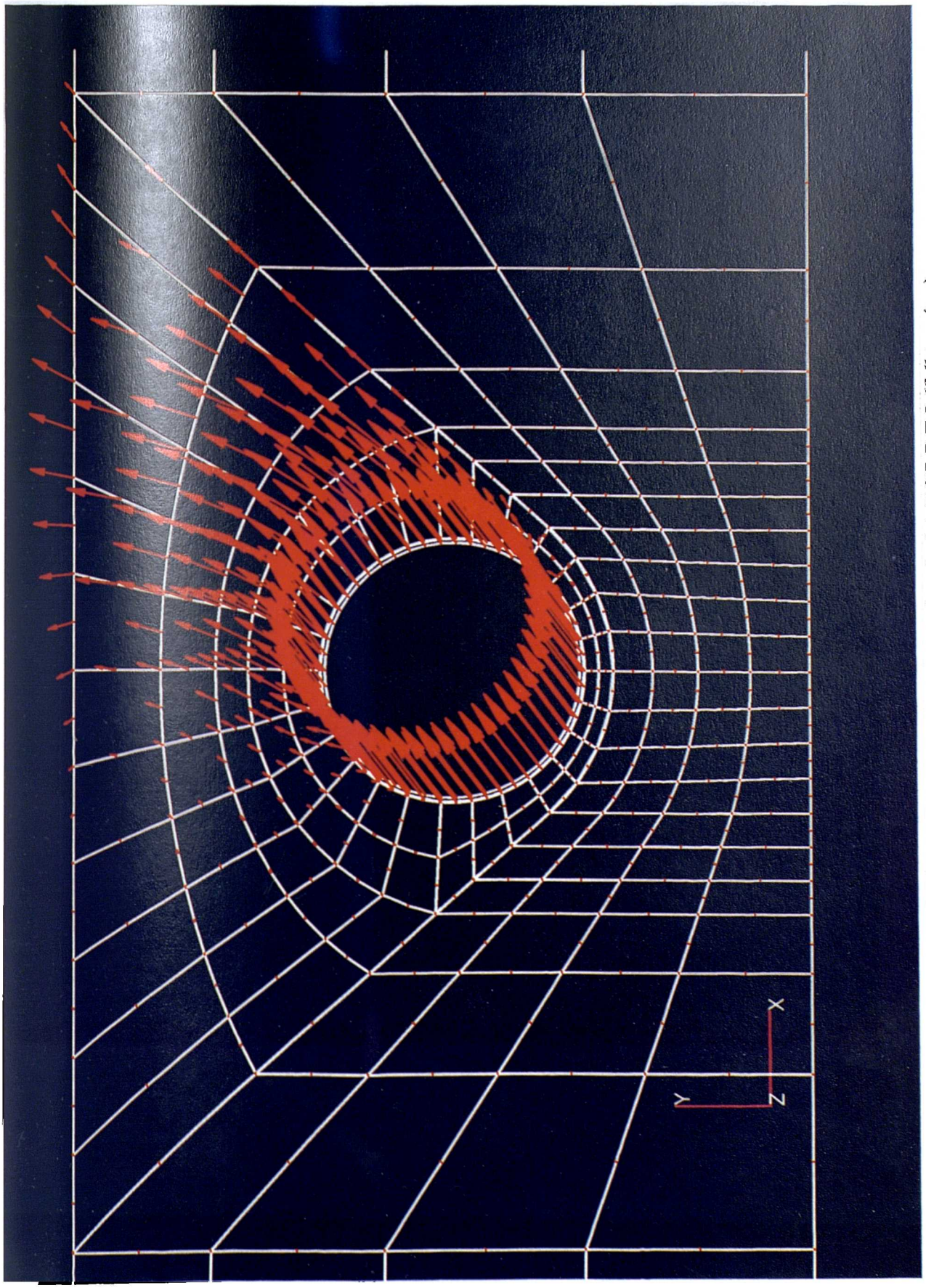

Fig. 7.12 (a). Displacement vectors of analysis ERSE-P.F.3 (full tension).

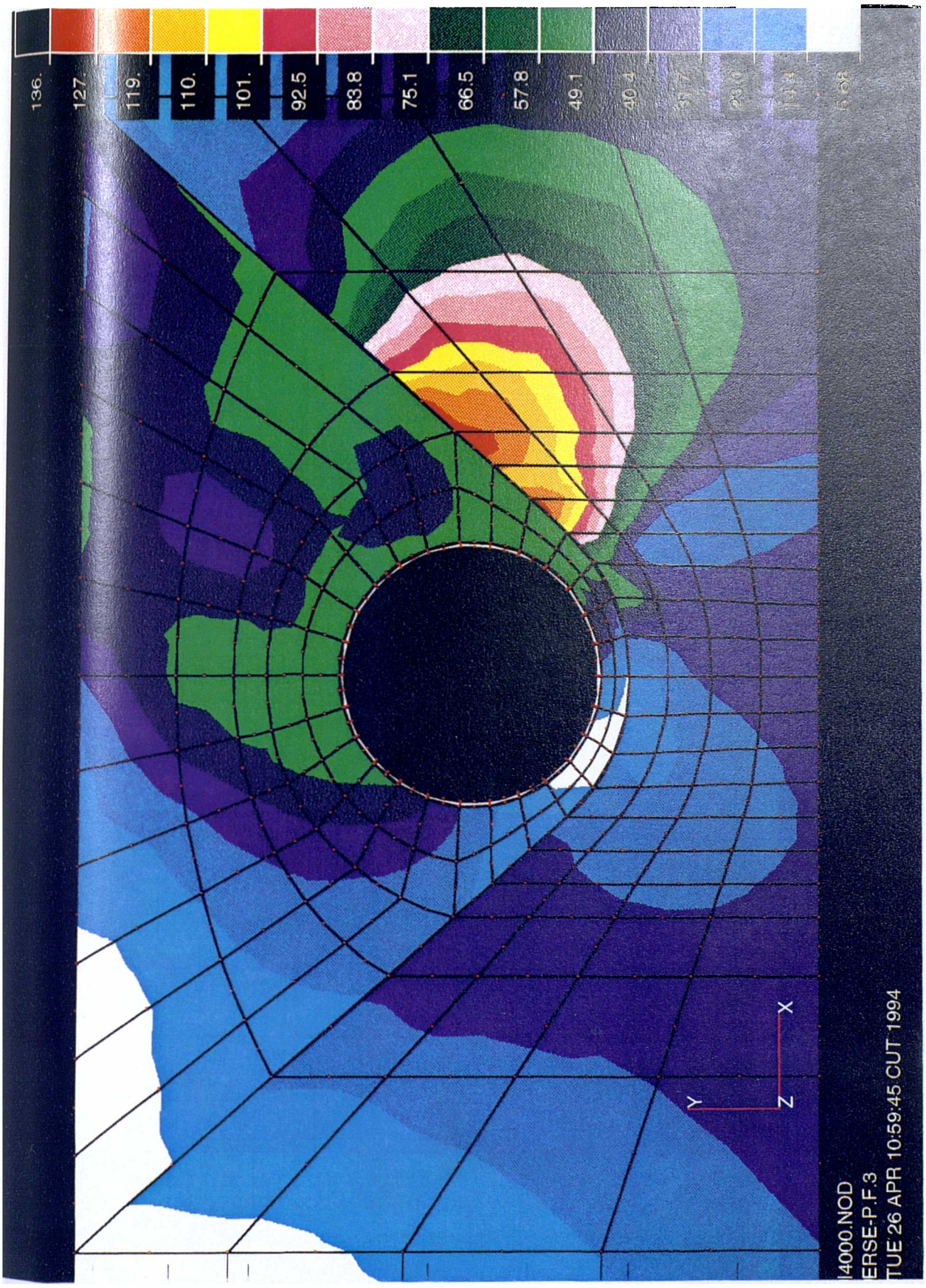

Fig. 7.12 (b). Deviator stress contour of analysis ERSE-P.F.3 (full tension).

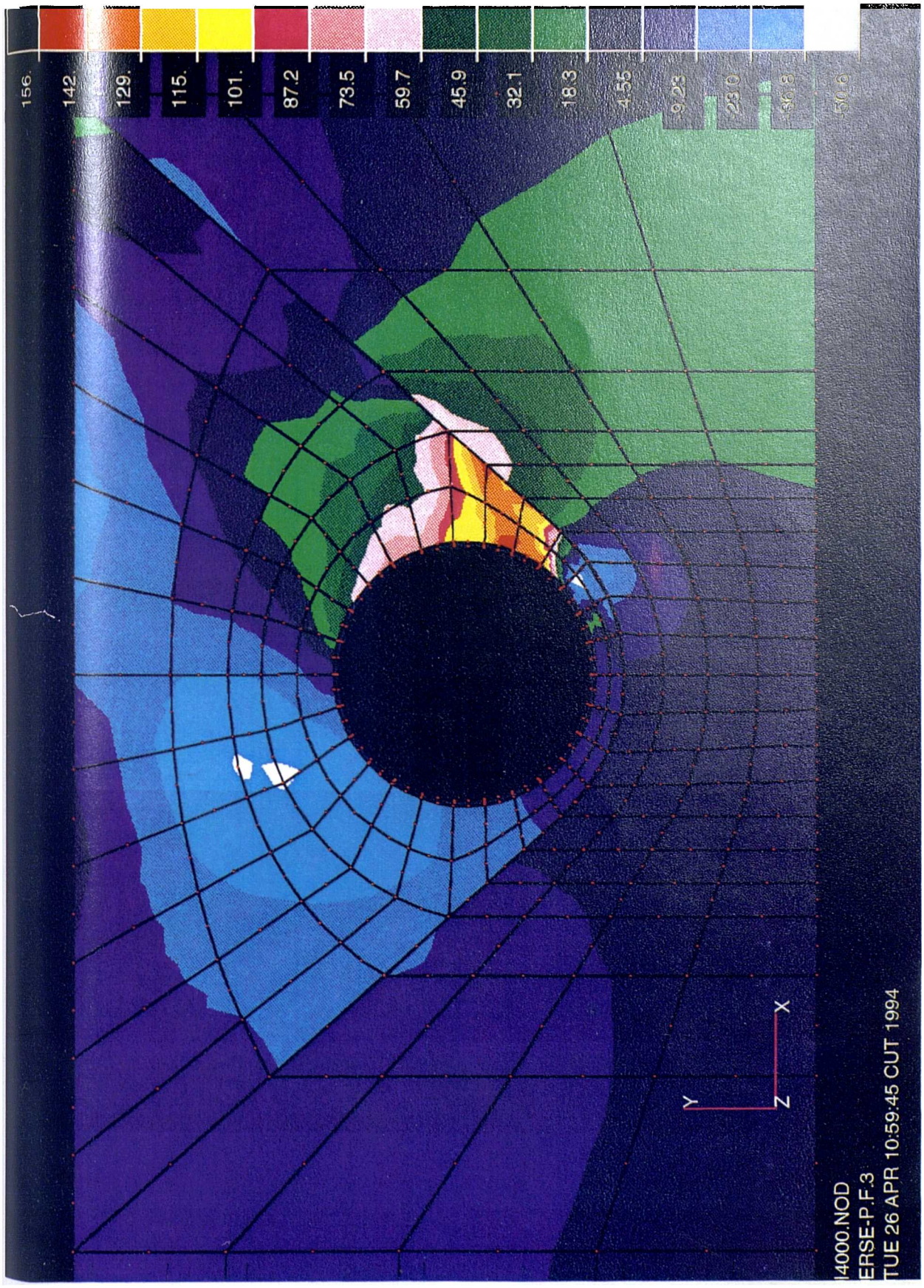

Fig. 7.12 (c). Mean total stress contour of analysis ERSE-P.F.3 (full tension).

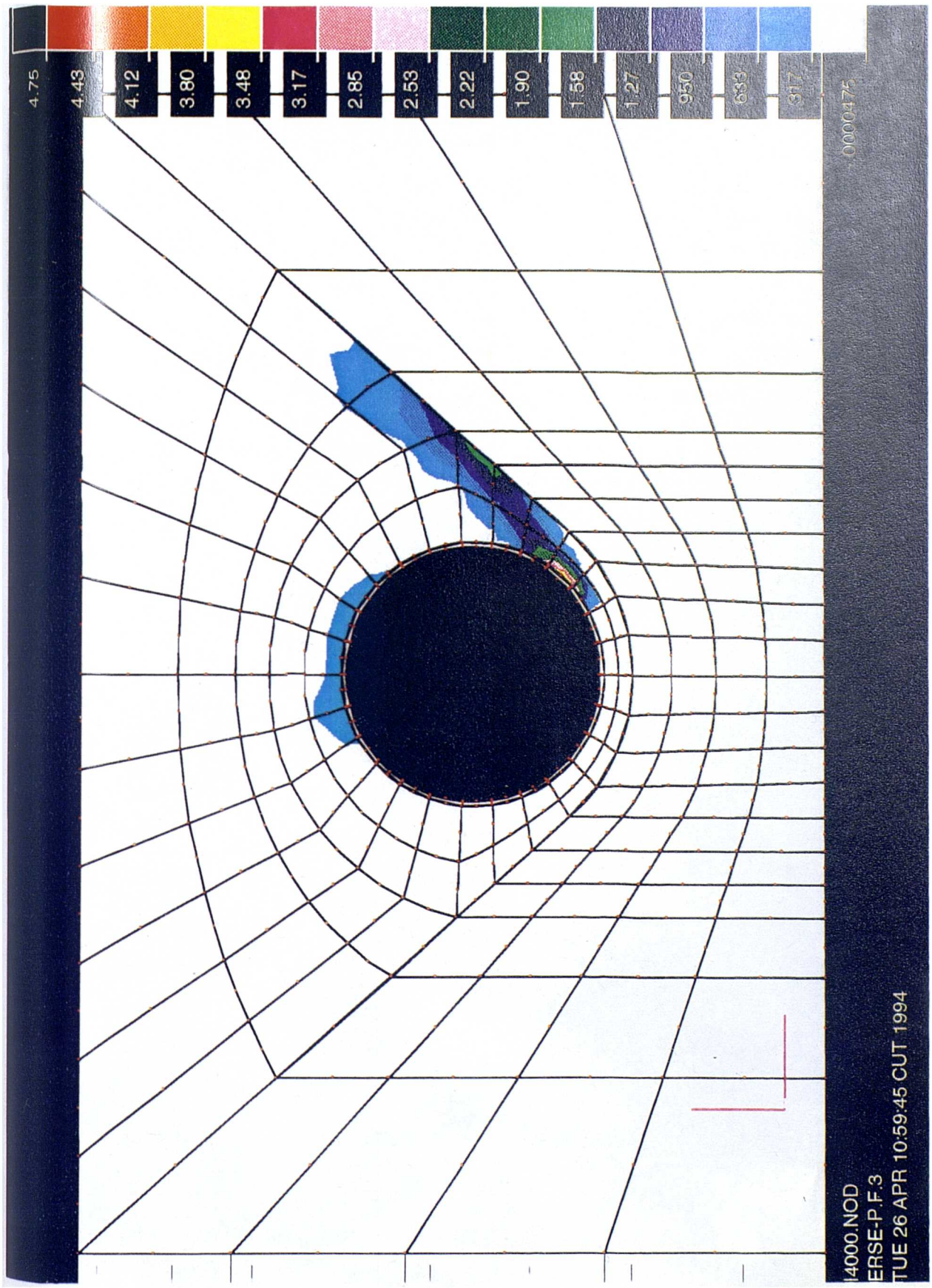

Fig. 7.12 (d). Shear strain contour of analysis ERSE-P.F.3 (full tension).

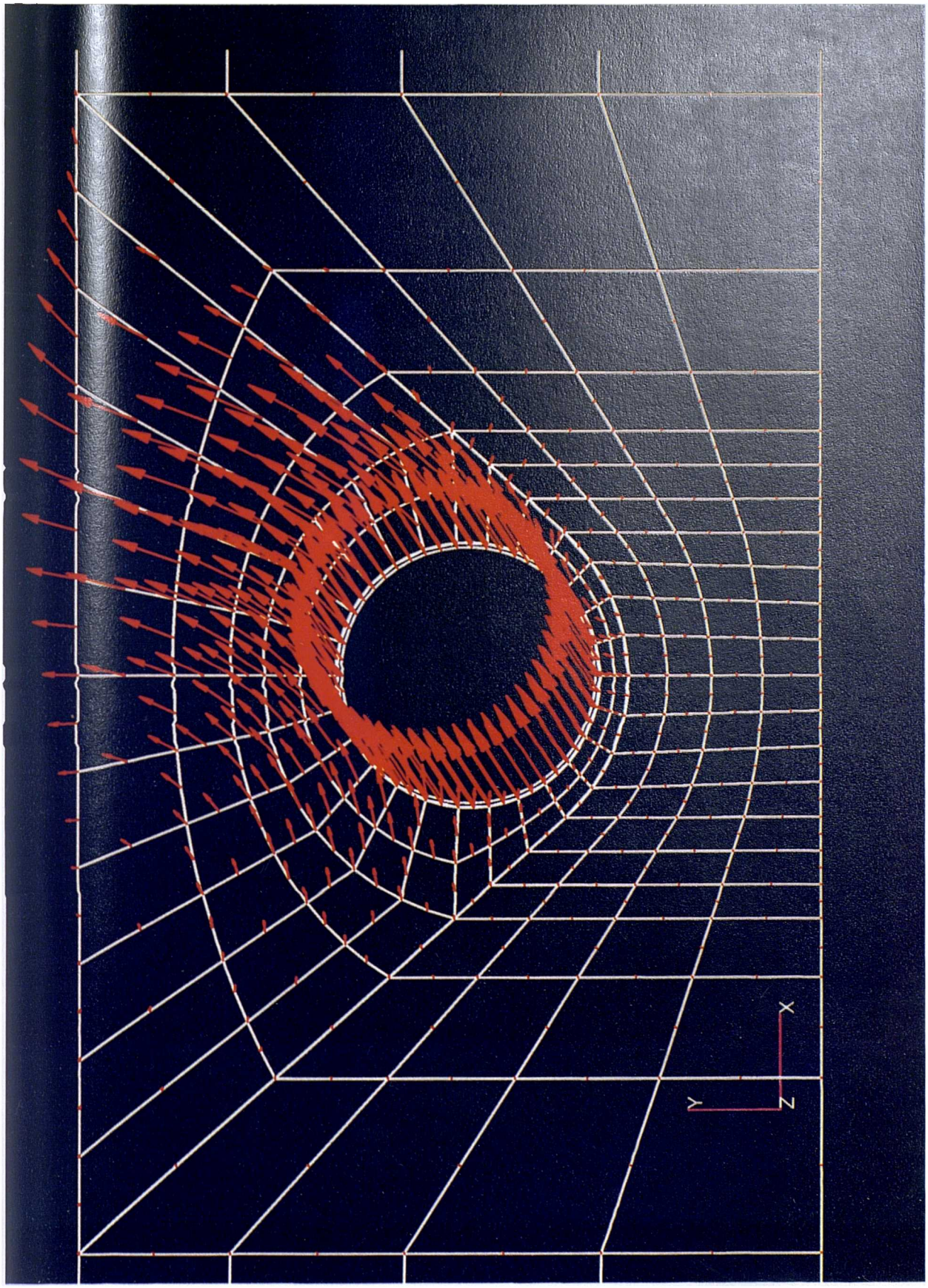

Fig. 7.13 (a). Displacement vectors of analysis ERSE-P.N.3 (no tension).

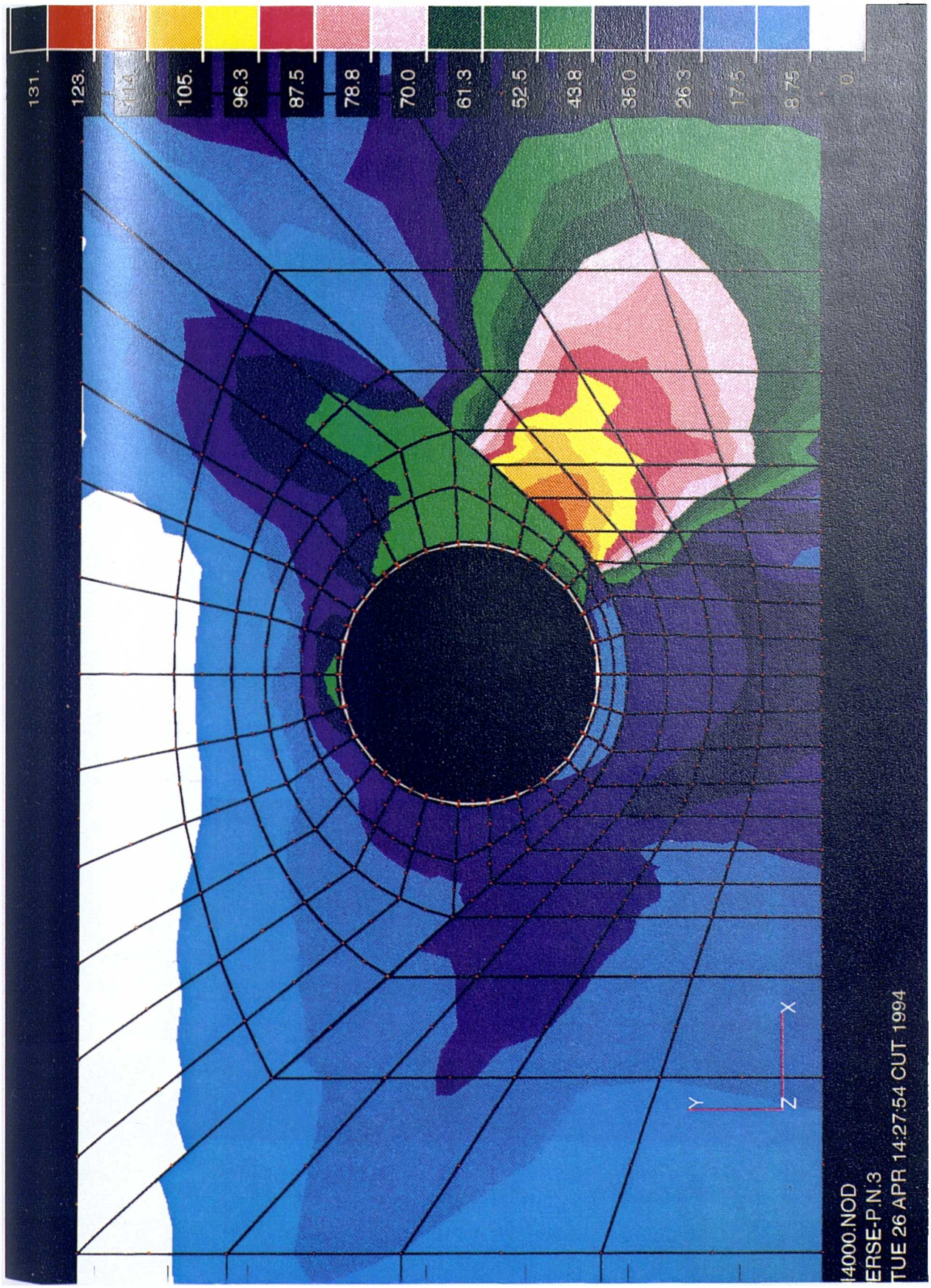

Fig. 7.13 (b). Deviator stress contour of analysis ERSE-P.N.3 (no tension).

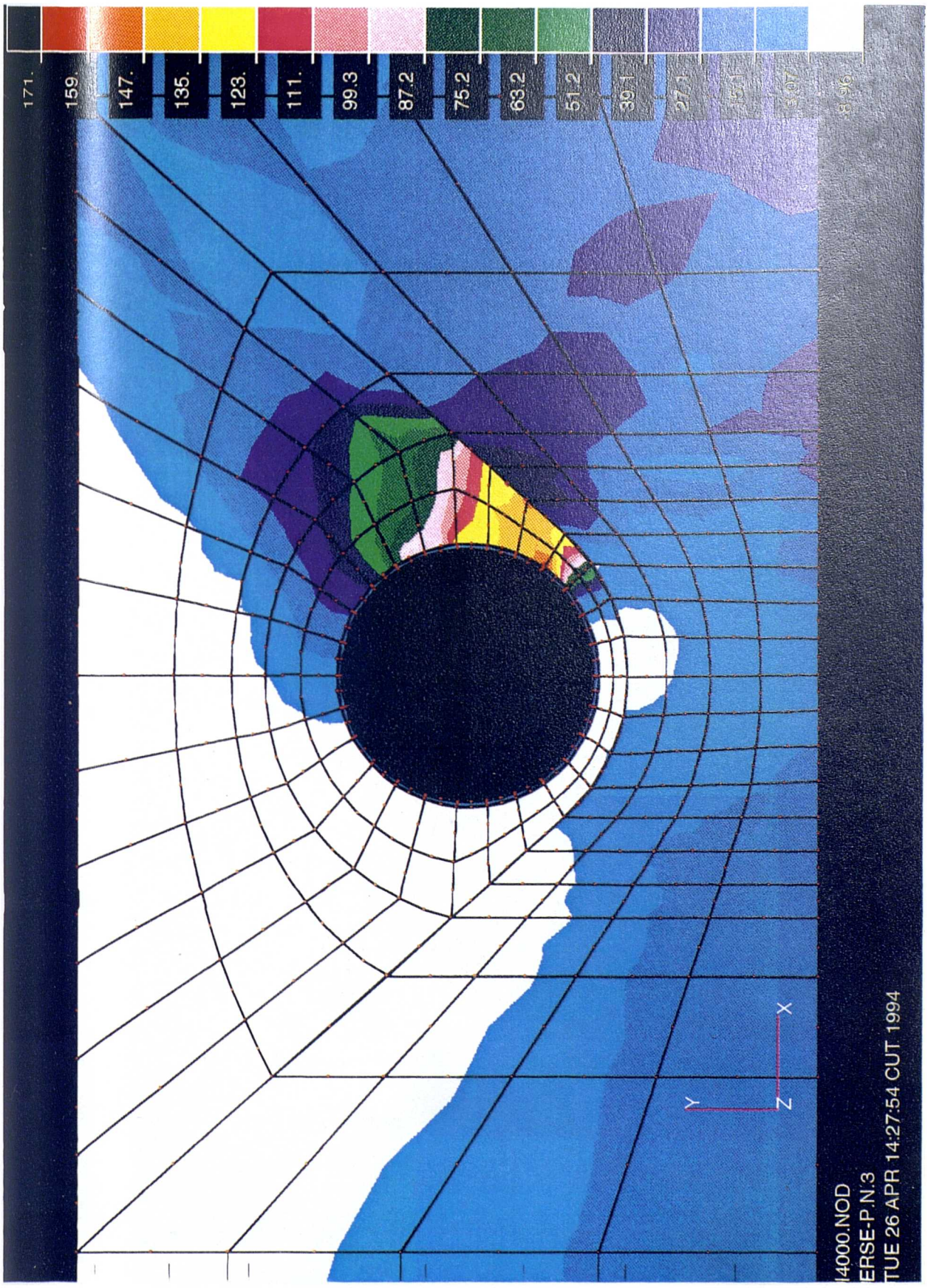

Fig. 7.13 (c). Mean total stress contour of analysis ERSE-P.N.3 (no tension).

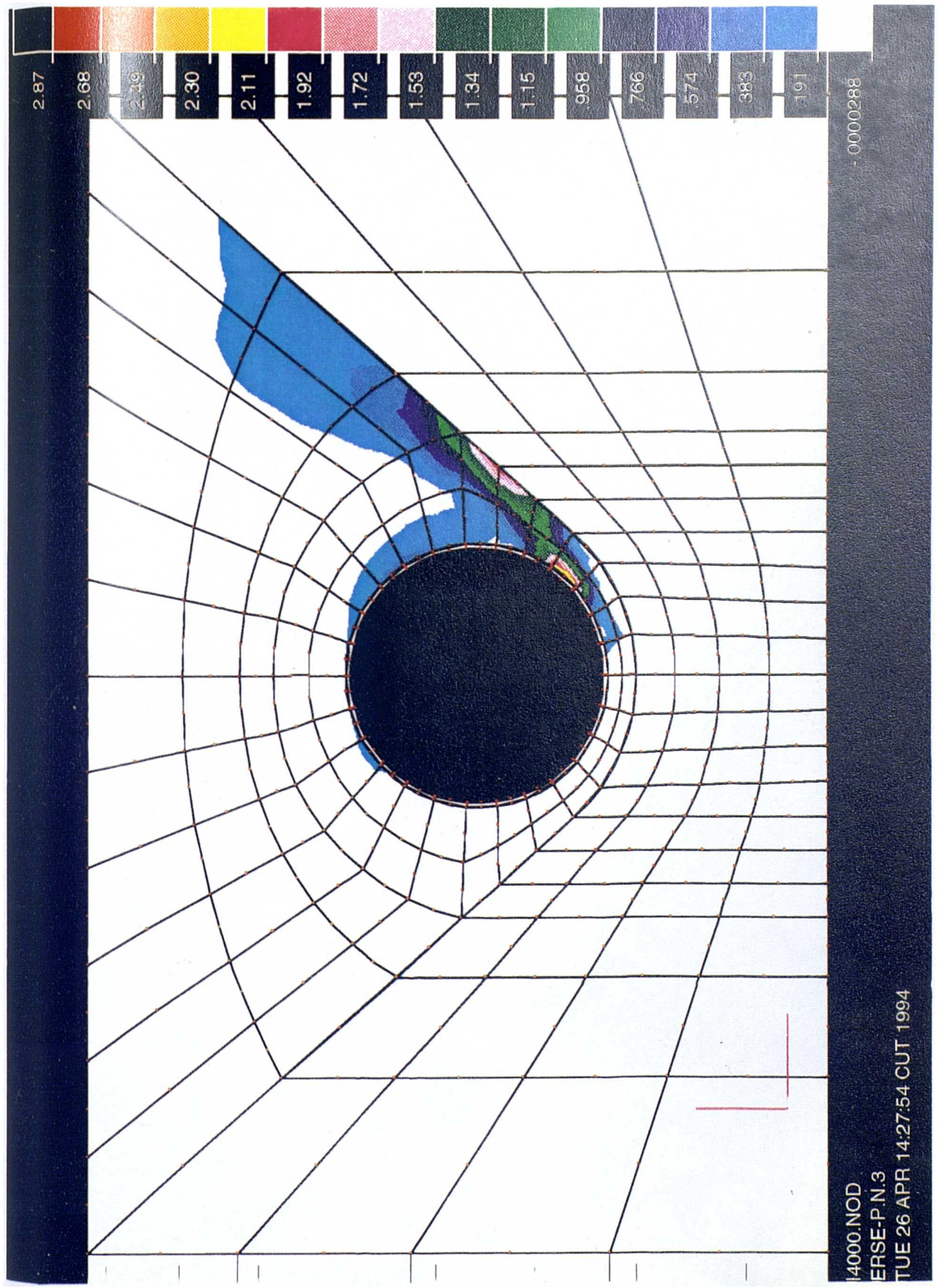

Fig. 7.13 (d). Shear strain contour of analysis ERSE-P.N.3 (no tension).

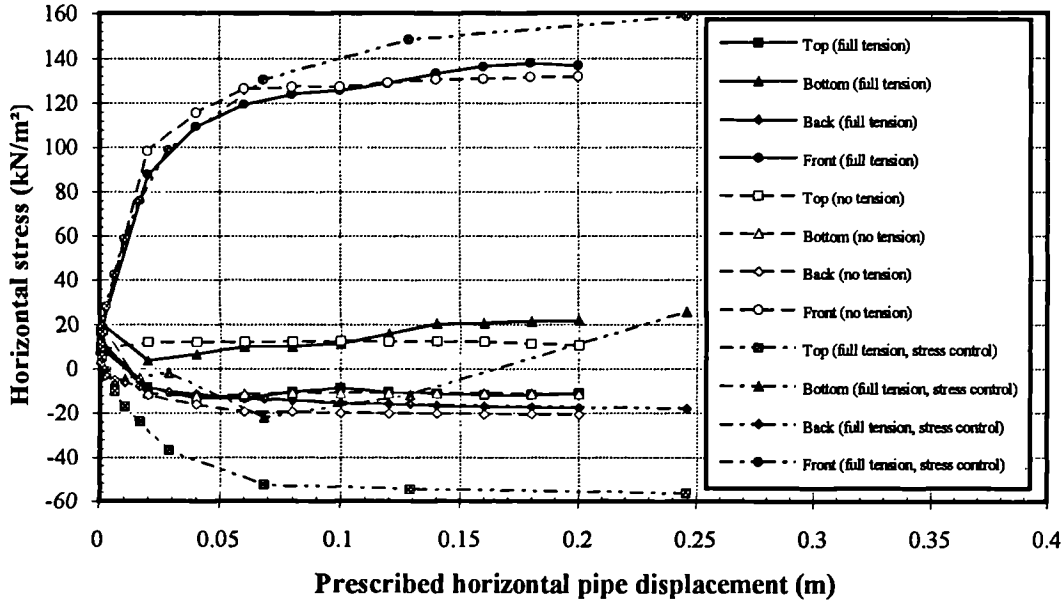

(a)

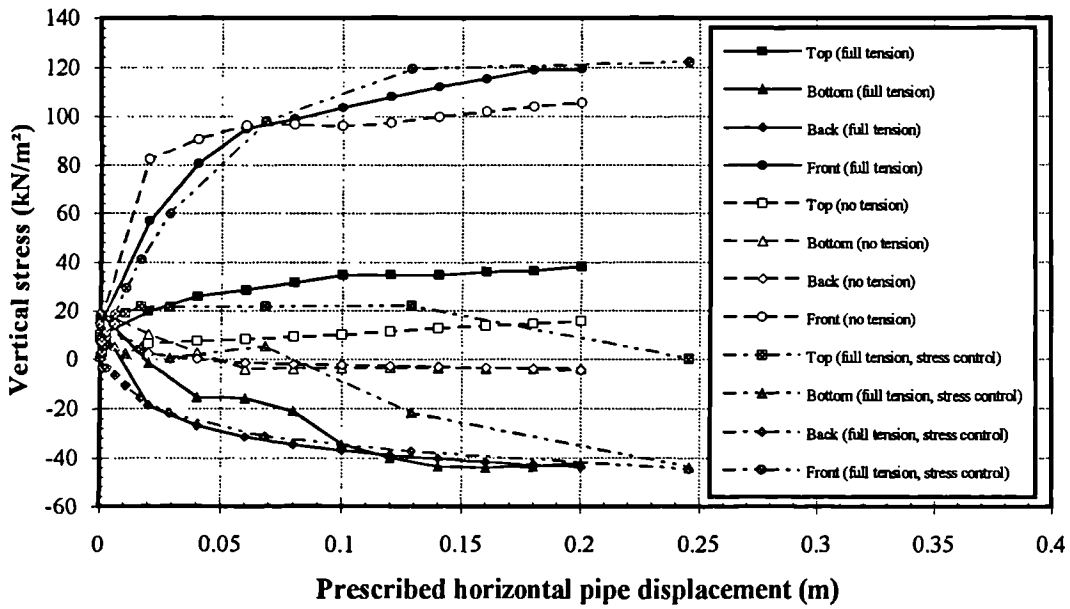

(b)

Fig. 7.14. Total stress paths at the top, bottom, back and the front of the pipe for the Elasto-plastic models with and without tension in the model with interface elements around the pipe and along the trench (a) horizontal stress, (b) vertical stress.

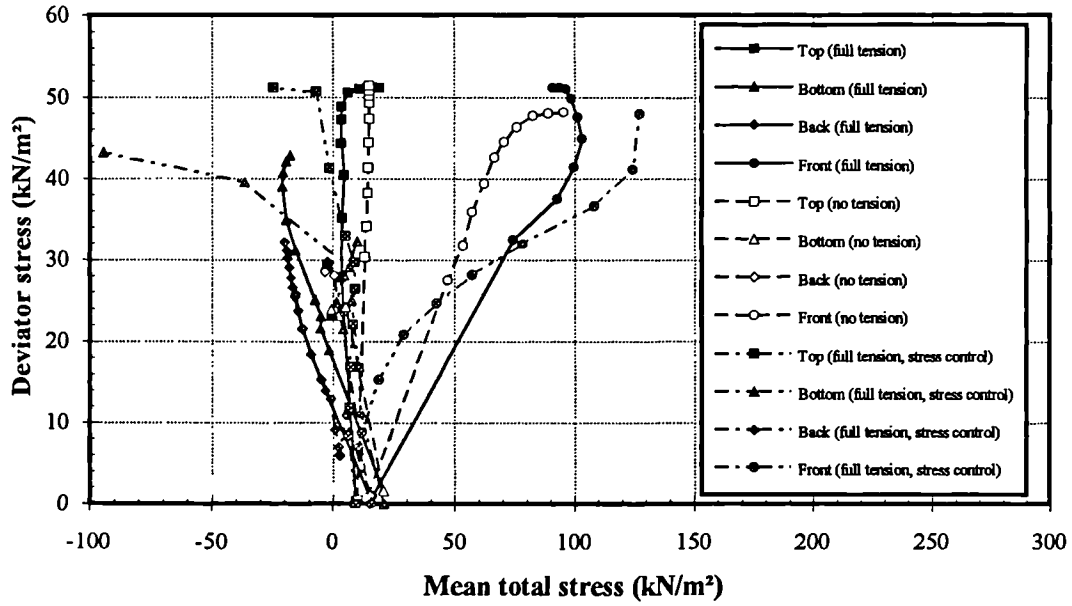

(c)

Fig. 7.14. Total stress paths at the top, bottom, back and the front of the pipe for the Elasto-plastic models with and without tension in the model with interface elements around the pipe and along the trench (c) *q-p* path.

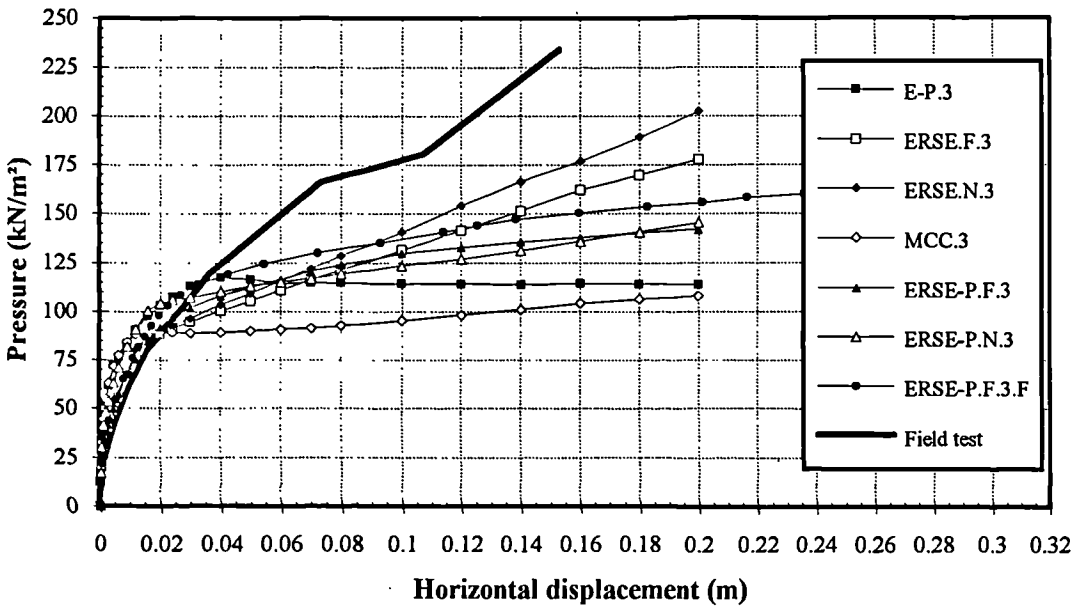

Fig. 7.15. The pressure-displacement relationships predicted by different analyses in the model with interface elements around the pipe and along the trench (ERSE-P.F.3.F is stress controlled analysis and the others are strain controlled, see Table 7.1 for the description of analysis names in the legend).

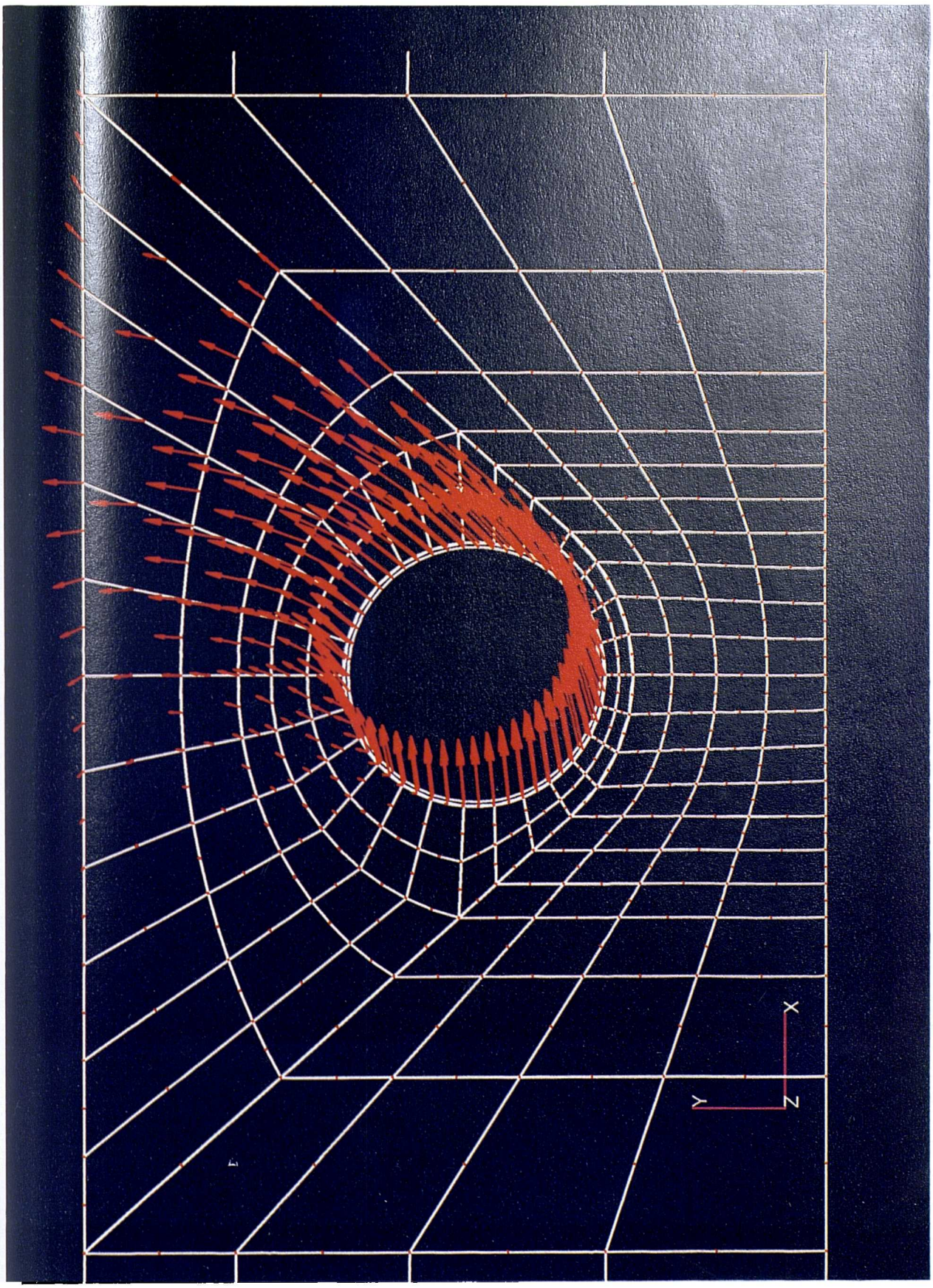

Fig. 7.16 (a). Displacement vectors of analysis ERSE-P.F.3.F (full tension, stress controlled).

Fig. 7.16 (b). Deviator stress contour of analysis ERSE-P.F.3.F (full tension, stress controlled).

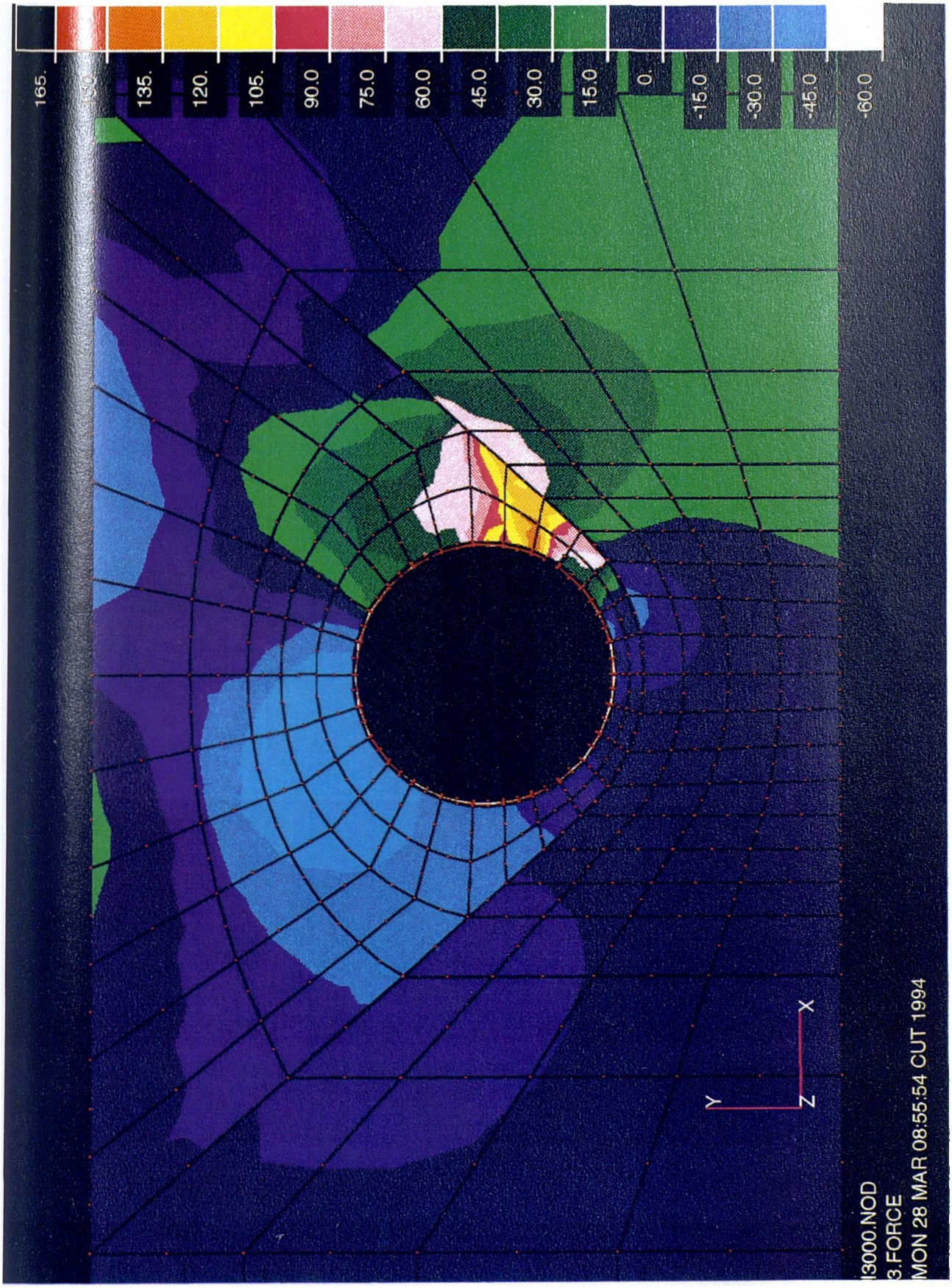

Fig. 7.16 (c). Mean total stress contour of analysis ERSE-P.F.3.F (full tension, stress controlled).

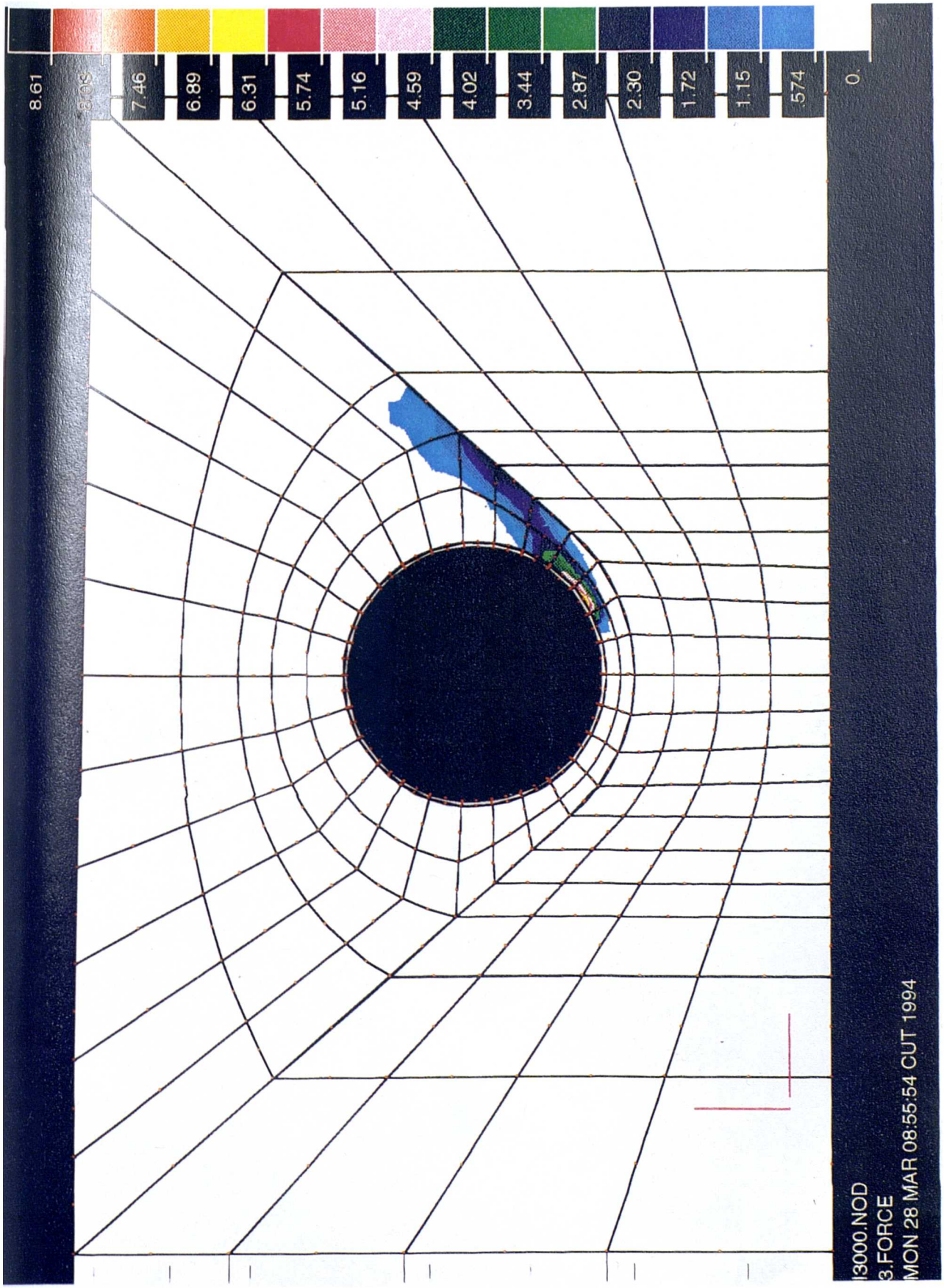

Fig. 7.16 (d). Shear strain contour of analysis ERSE-P.F.3.F (full tension, stress controlled).

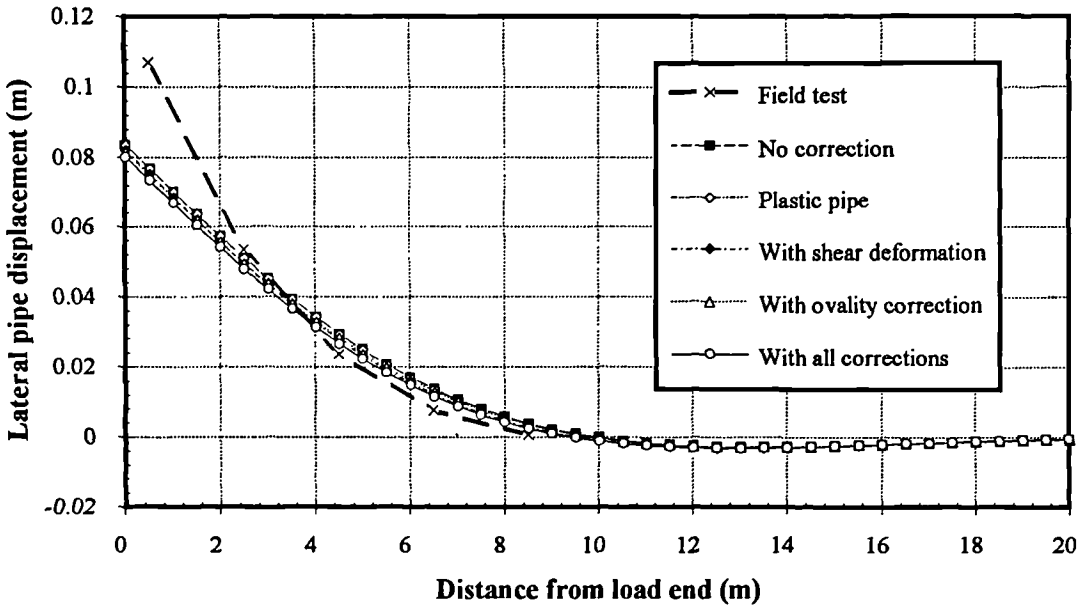

(a)

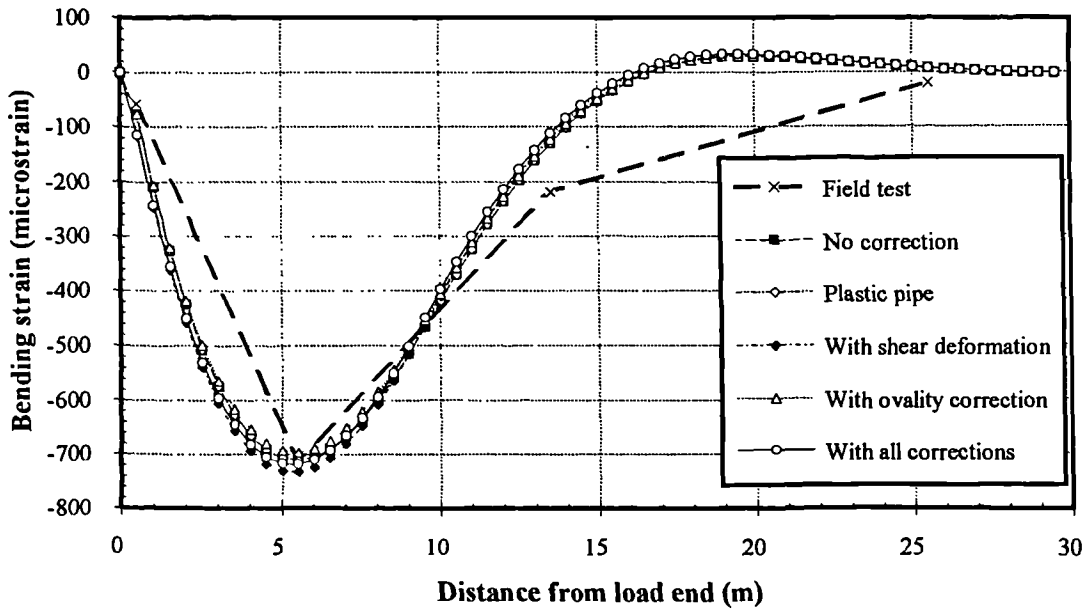

(b)

Fig. 7.17. Results of using different modifications in WOMOD at load = 592kN
(a) lateral pipe displacement, (b) bending strain.

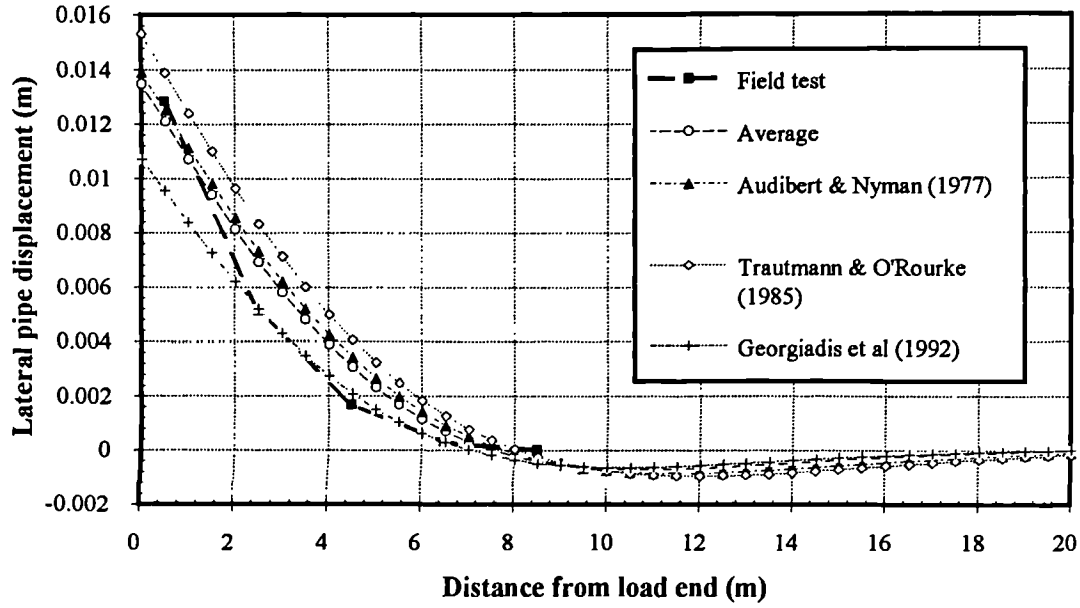

(a)

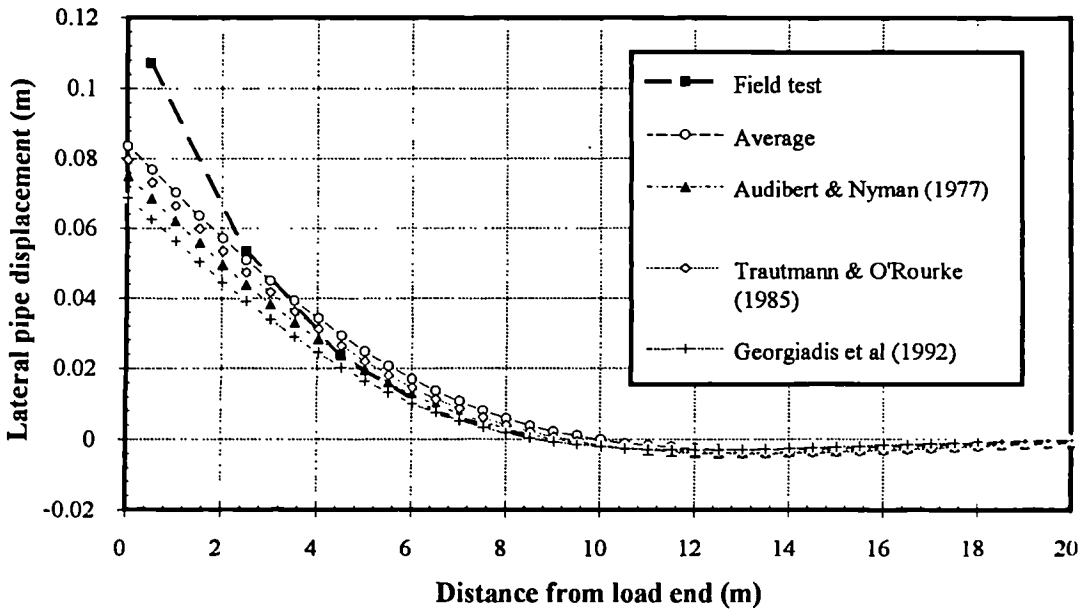

(b)

Fig. 7.18. Predicted distributions of lateral pipe displacement by WOMOD using the *P-y* curves back-calculated from field test (a) load = 181kN, (b) load = 592kN.

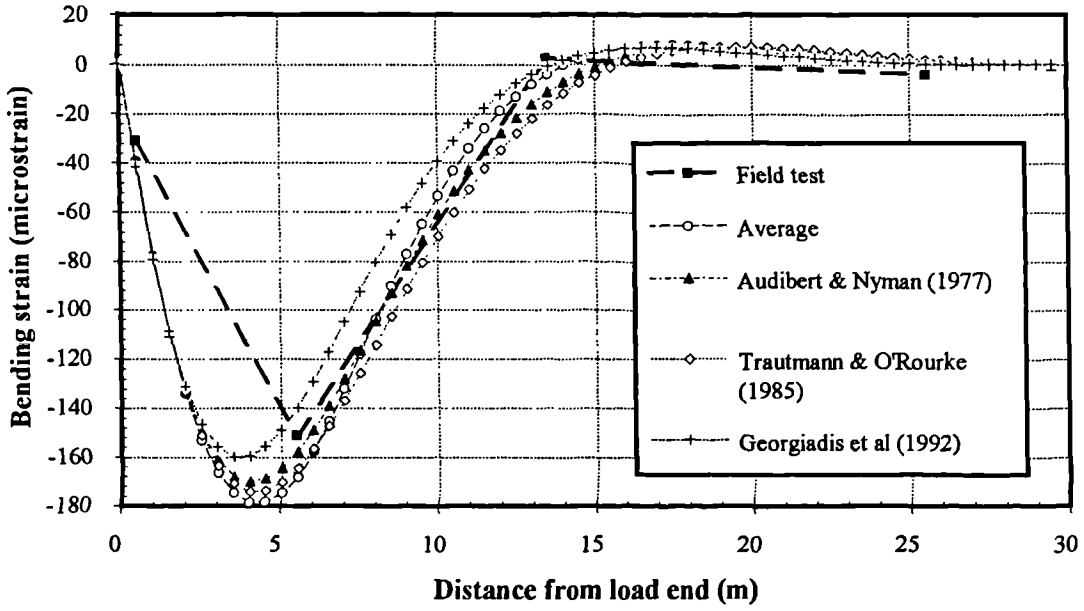

(a)

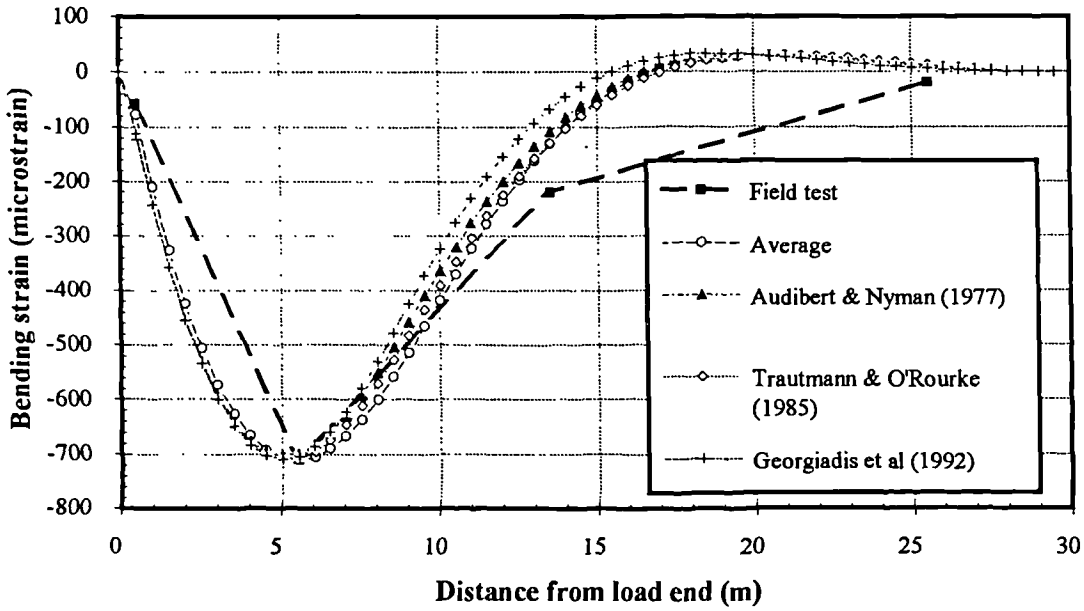

(b)

Fig. 7.19. Predicted distributions of bending strain by WOMOD using the *P-y* curves back-calculated from field test (a) load = 181kN, (b) load = 592kN.

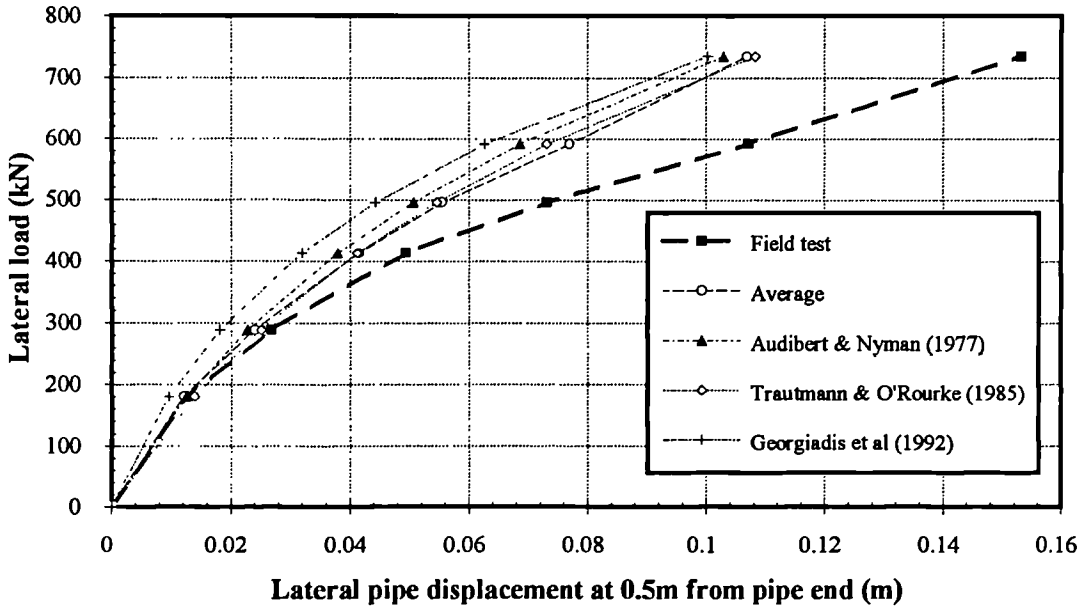

Fig. 7.20. Predicted maximum lateral pipe displacements by WOMOD using the *P-y* curves back-calculated from field test.

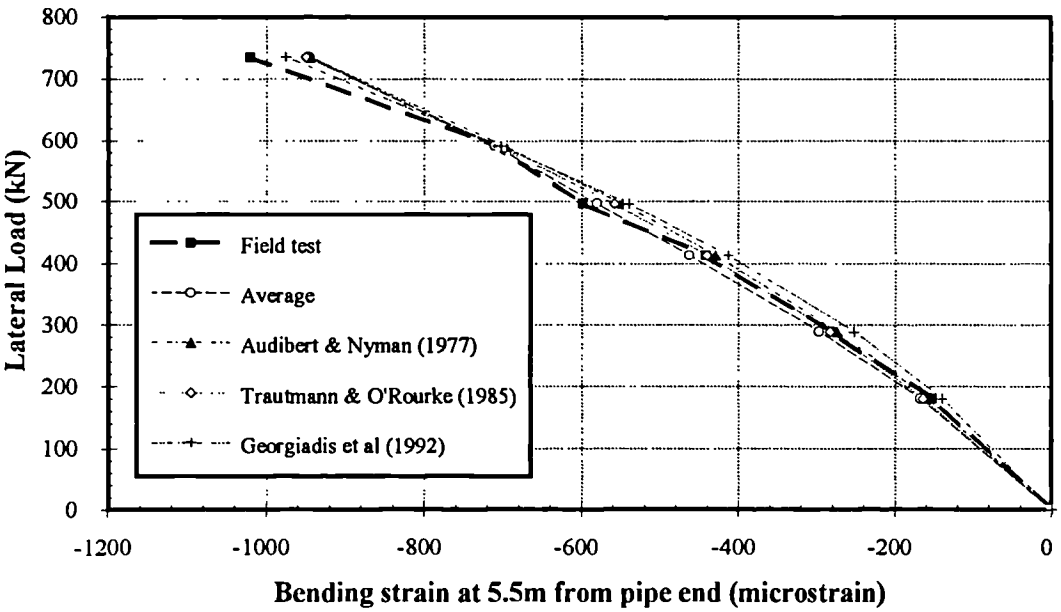

Fig. 7.21. Predicted maximum bending strains by WOMOD using the *P-y* curves back-calculated from field test.

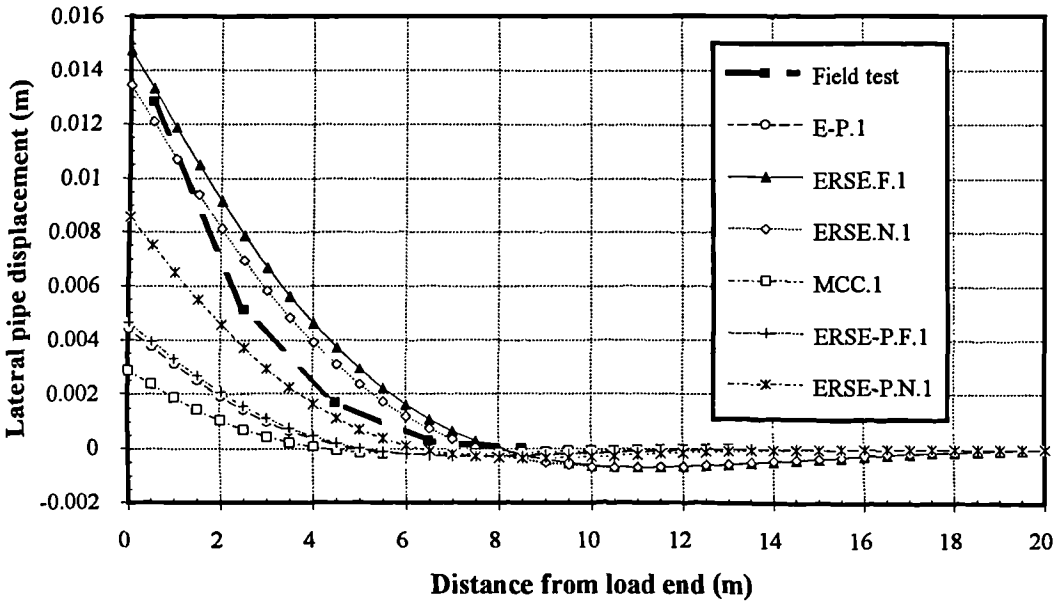

(a)

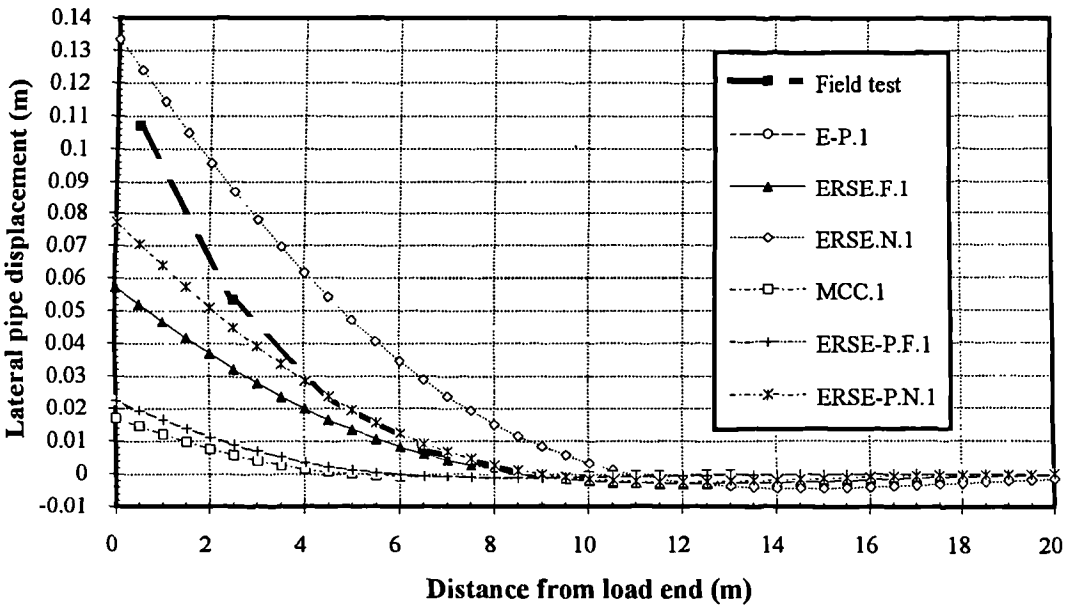

(b)

Fig. 7.22. Predicted distributions of lateral pipe displacement by WOMOD using the *P-y* curves from the rigid cavity model (a) load = 181kN, (b) load = 592kN.

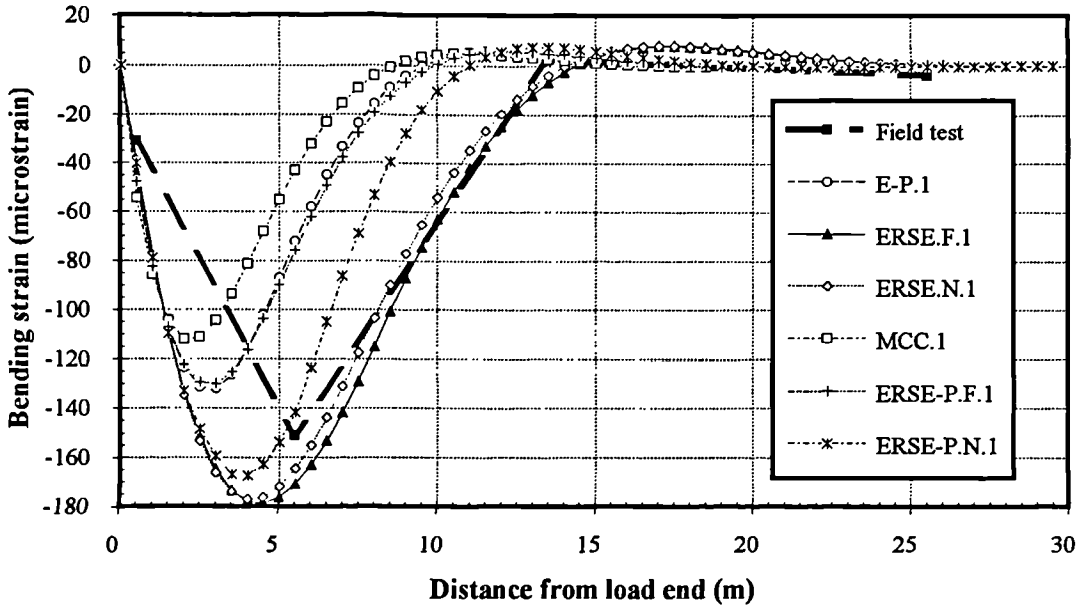

(a)

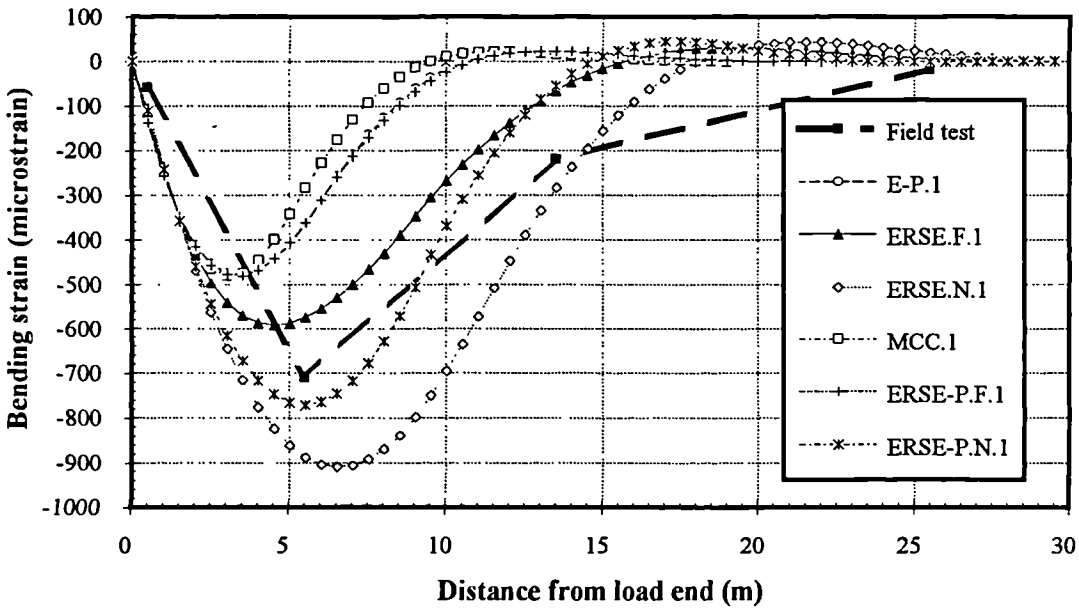

(b)

Fig. 7.23. Predicted distributions of bending strain by WOMOD using the *P-y* curves from the rigid cavity model (a) load = 181kN, (b) load = 592kN.

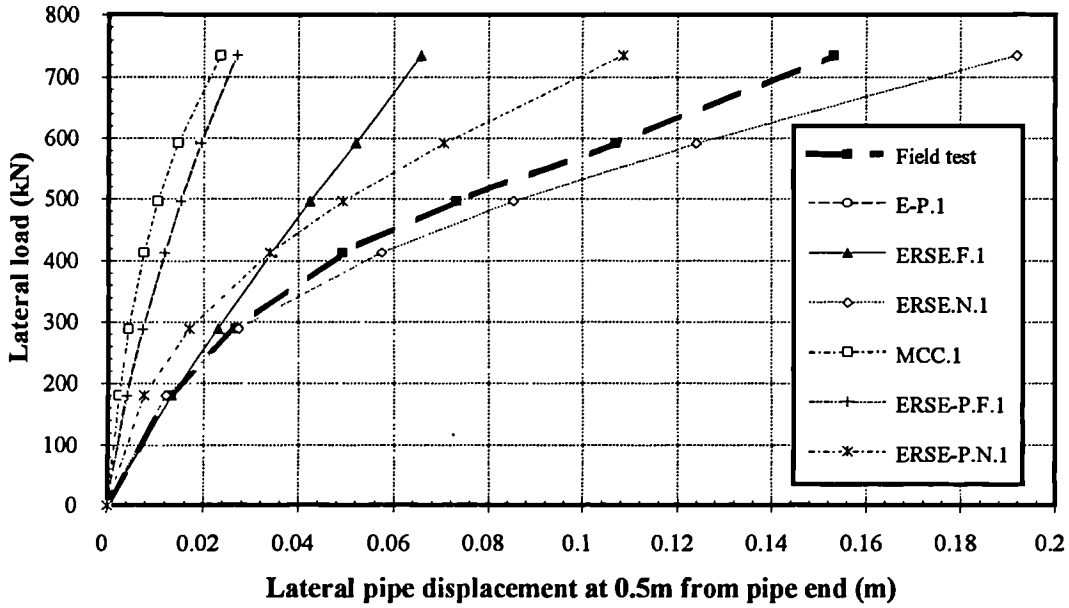

Fig. 7.24. Predicted maximum lateral pipe displacements by WOMOD using the *P-y* curves from the rigid cavity model.

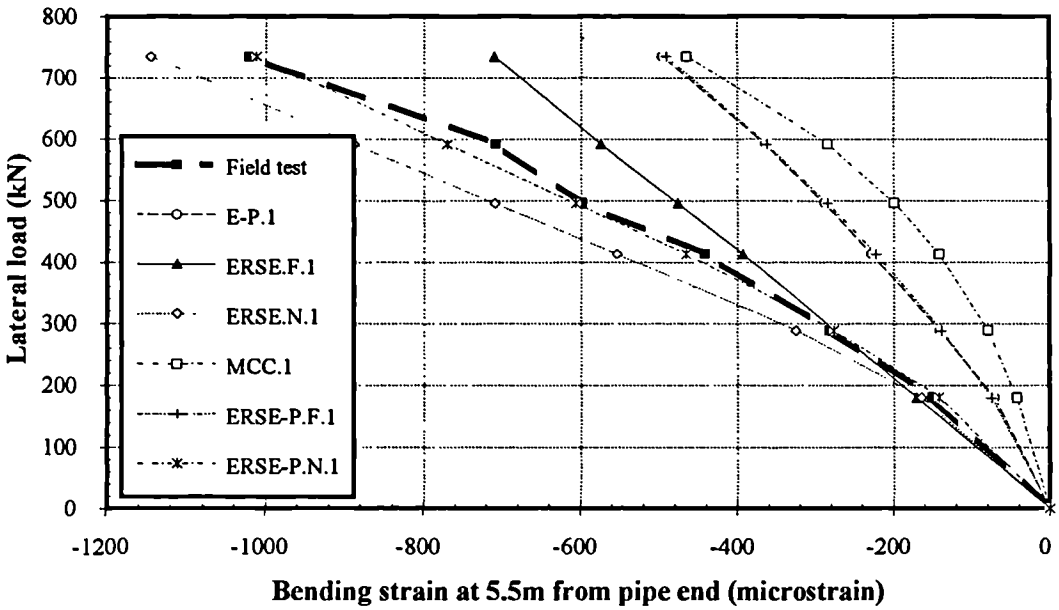

Fig. 7.25. Predicted maximum bending strains by WOMOD using the *P-y* curves from the rigid cavity model.

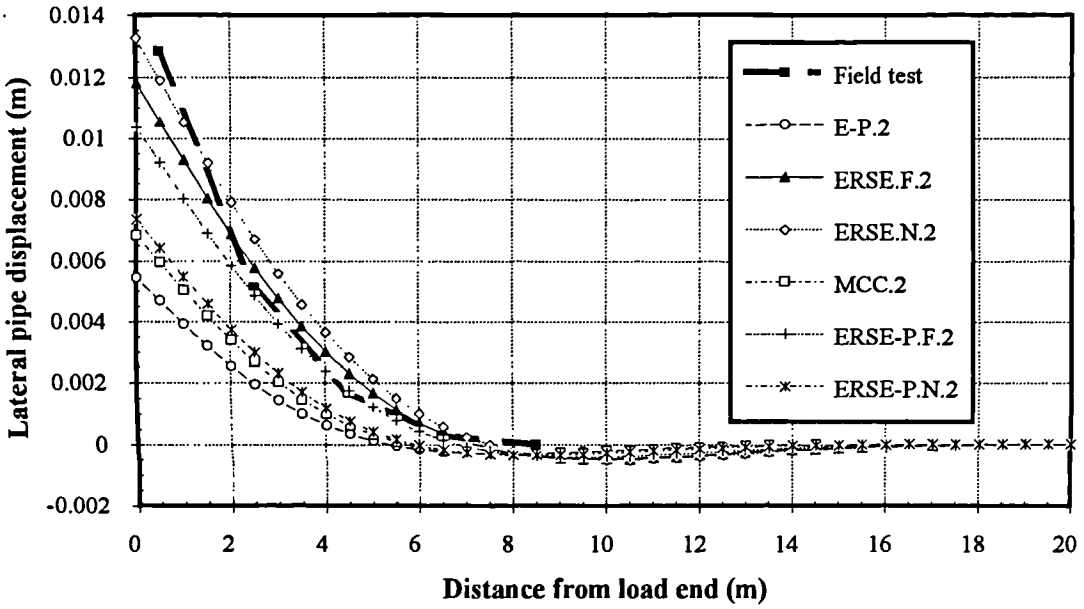

(a)

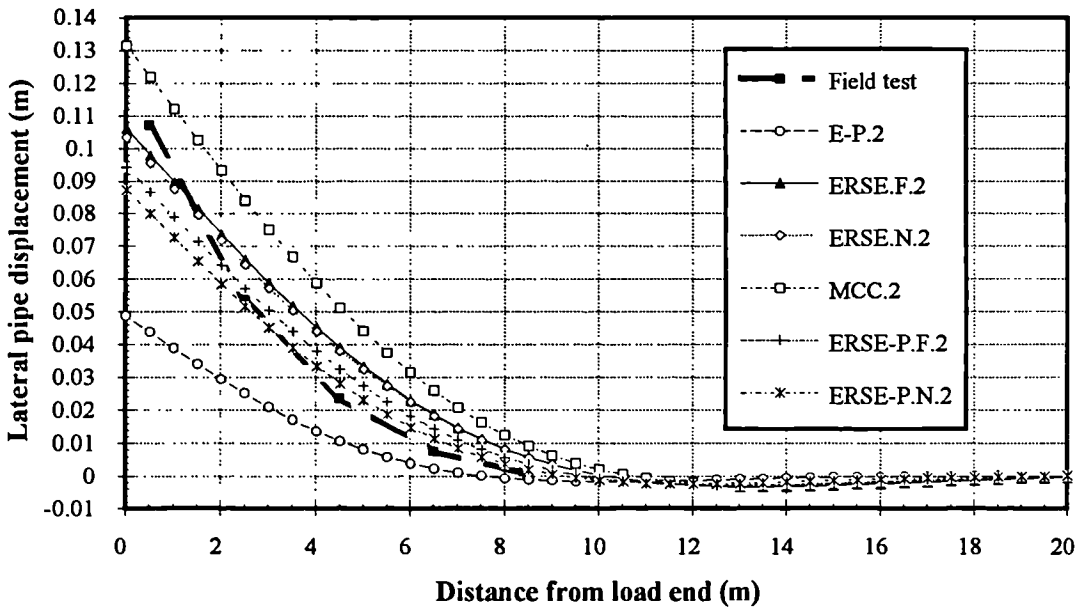

(b)

Fig. 7.26. Predicted distributions of lateral pipe displacement by WOMOD using the *P-y* curves from the model with interface elements around the pipe (a) load = 181kN, (b) load = 592kN.

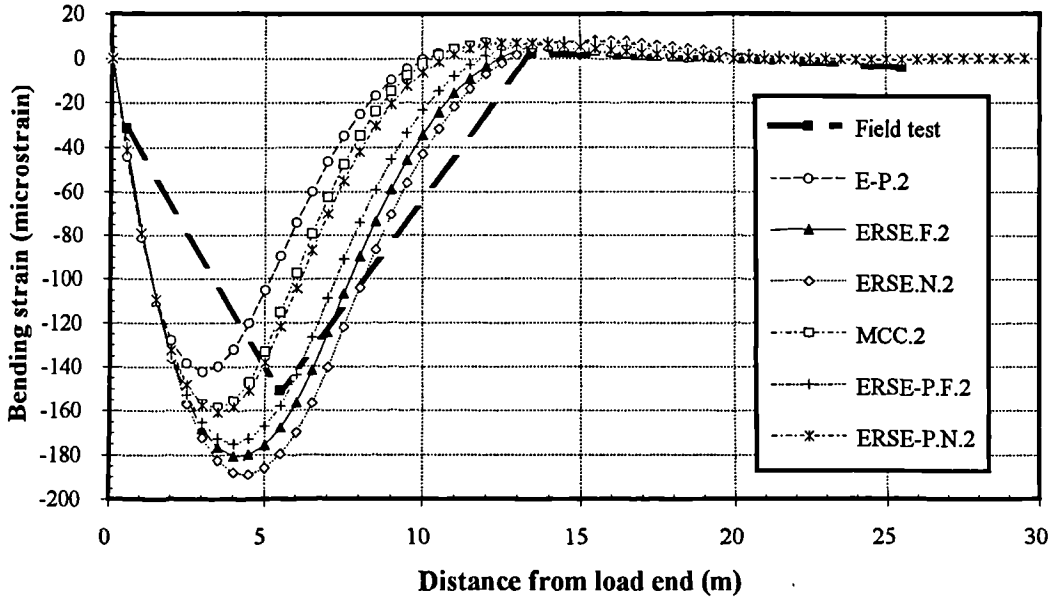

(a)

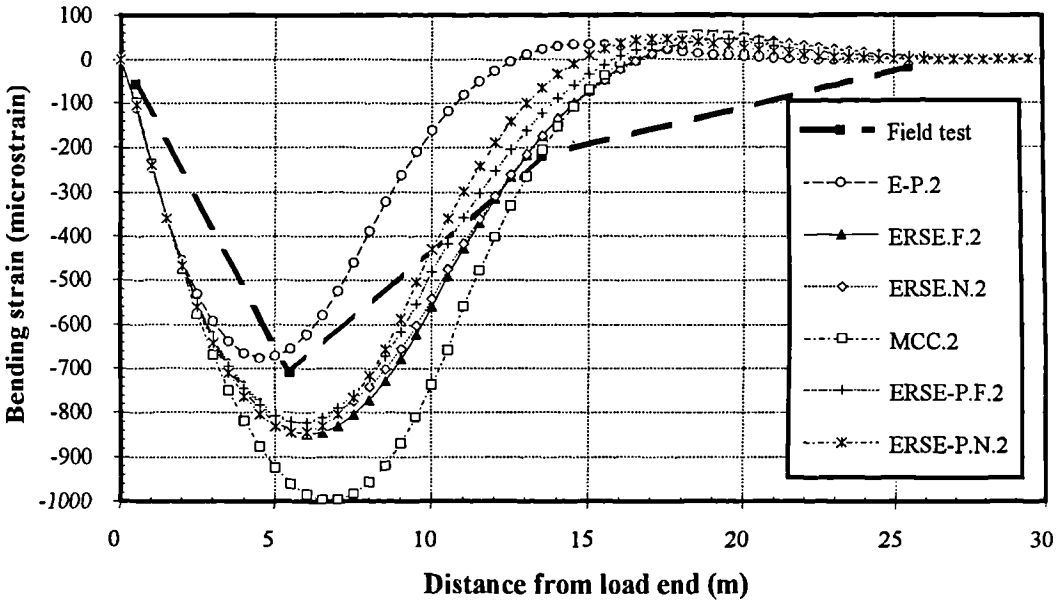

(b)

Fig. 7.27. Predicted distributions of bending strain by WOMOD using the *P-y* curves from the model with interface elements around the pipe (a) load = 181kN, (b) load = 592kN.

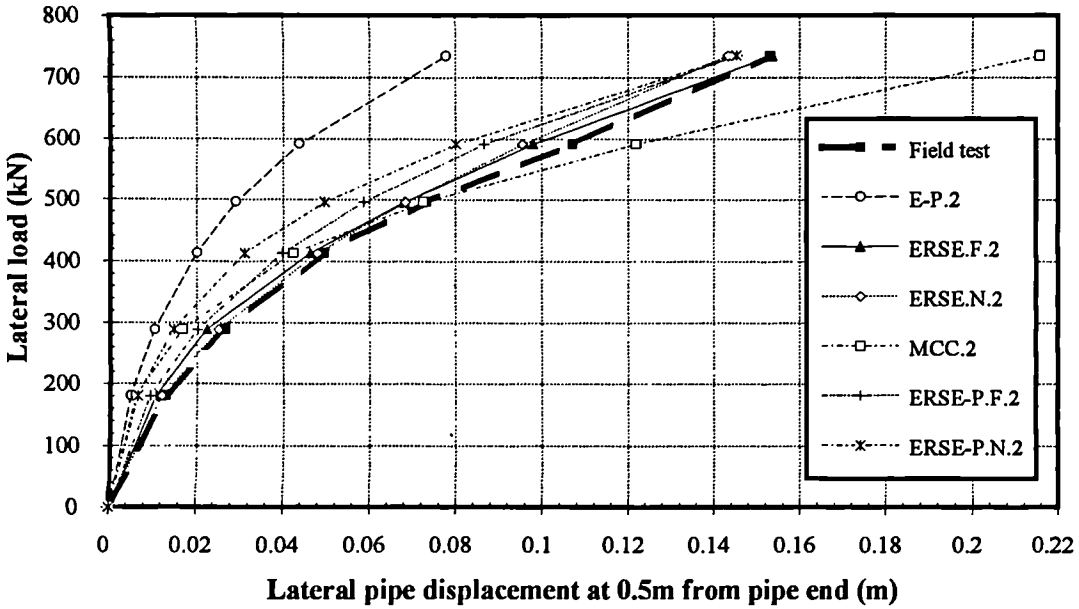

Fig. 7.28. Predicted maximum lateral pipe displacements by WOMOD using the *P-y* curves from the model with interface elements around the pipe.

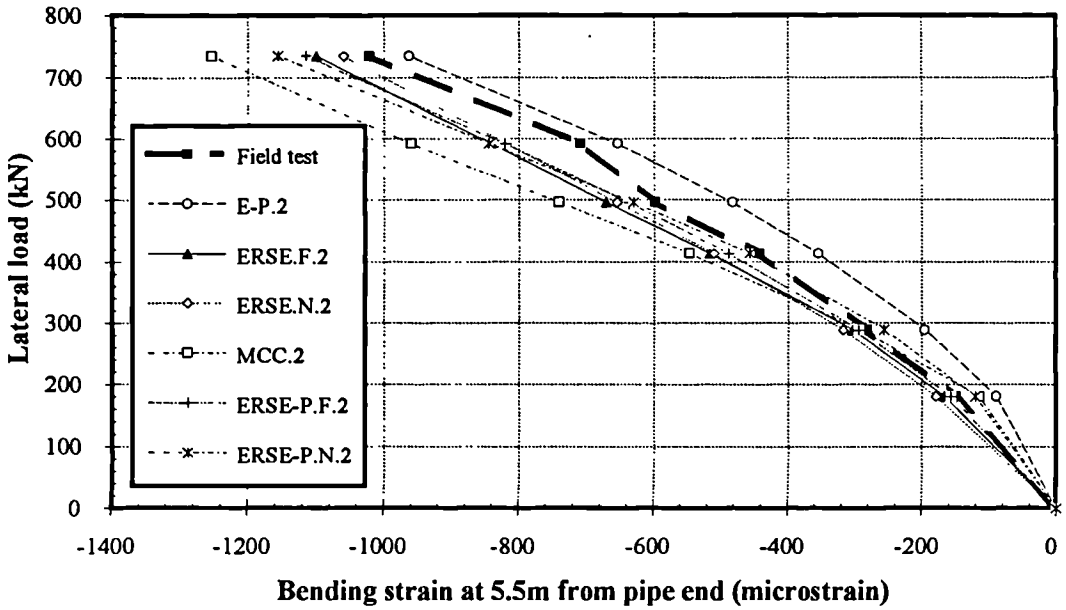

Fig. 7.29. Predicted maximum bending strains by WOMOD using the *P-y* curves from the model with interface elements around the pipe.

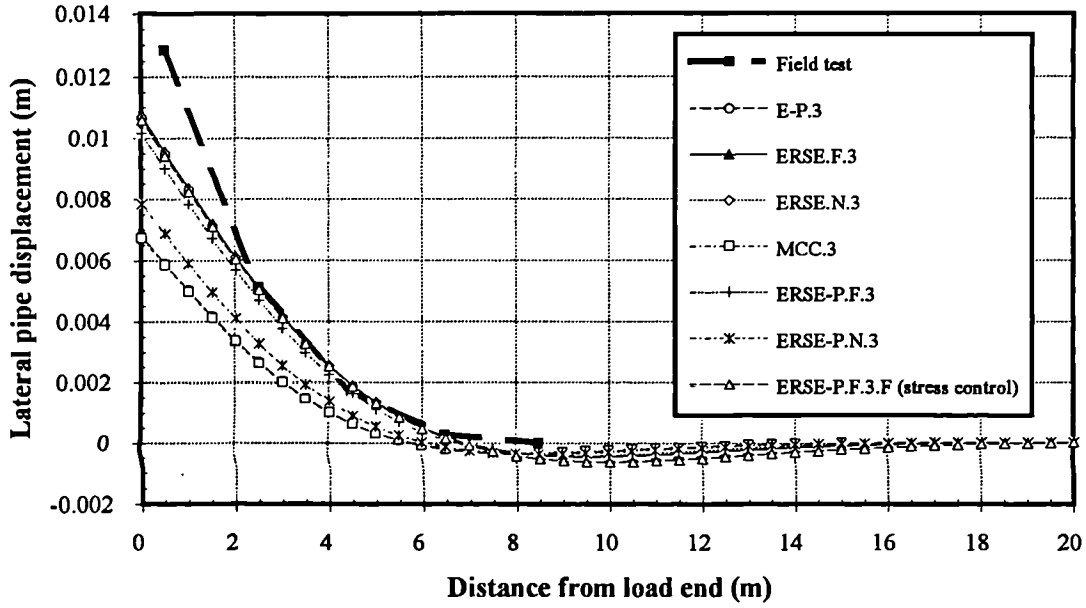

(a)

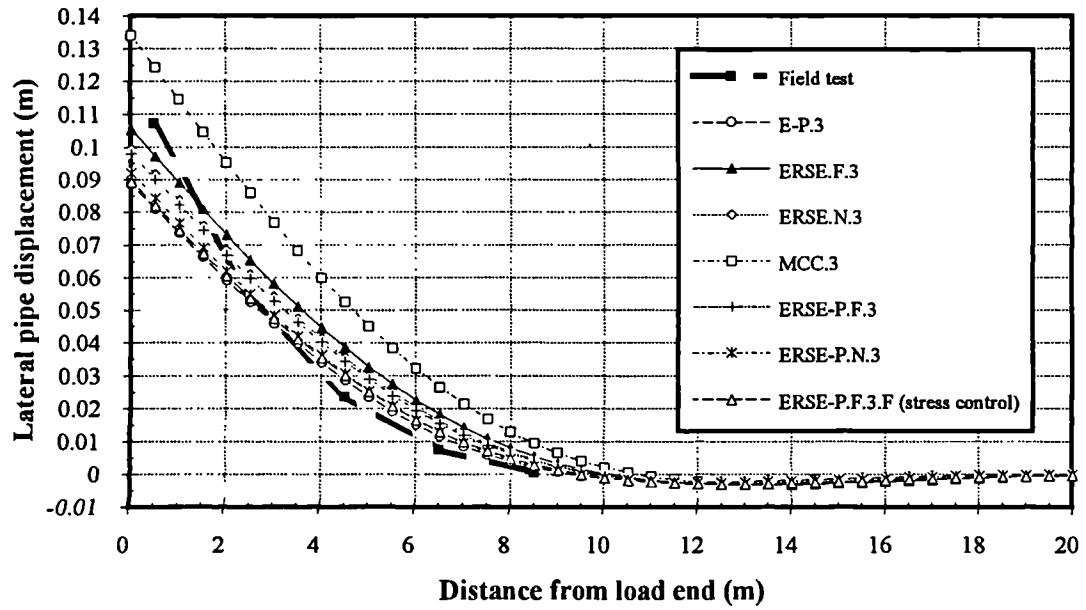

(b)

Fig. 7.30. Predicted distributions of lateral pipe displacement by WOMOD using the *P-y* curves from the model with interface elements around the pipe and along the trench (a) load = 181kN, (b) load = 592kN.

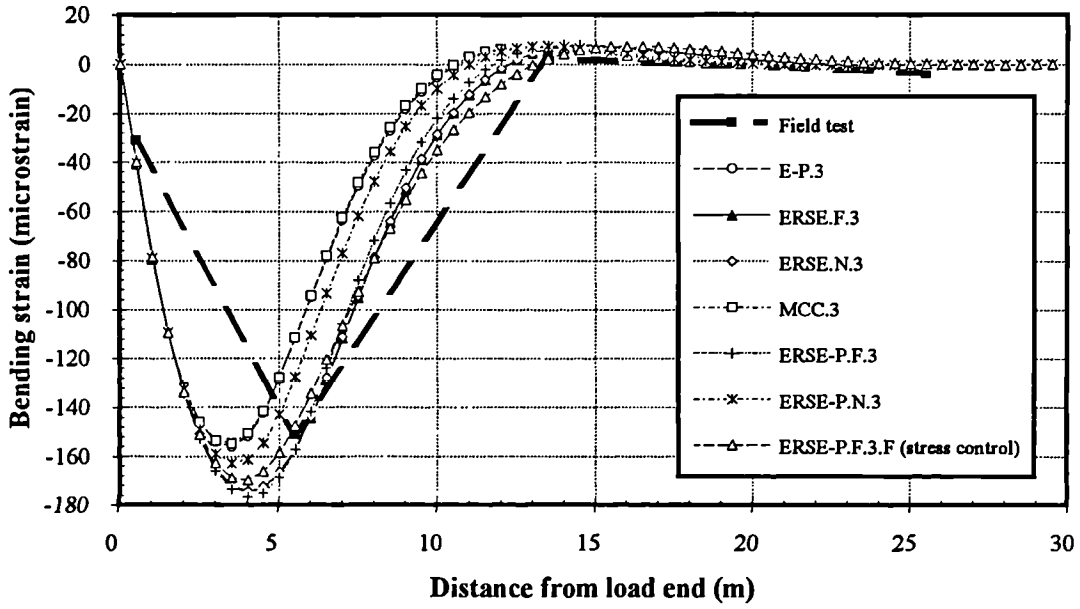

(a)

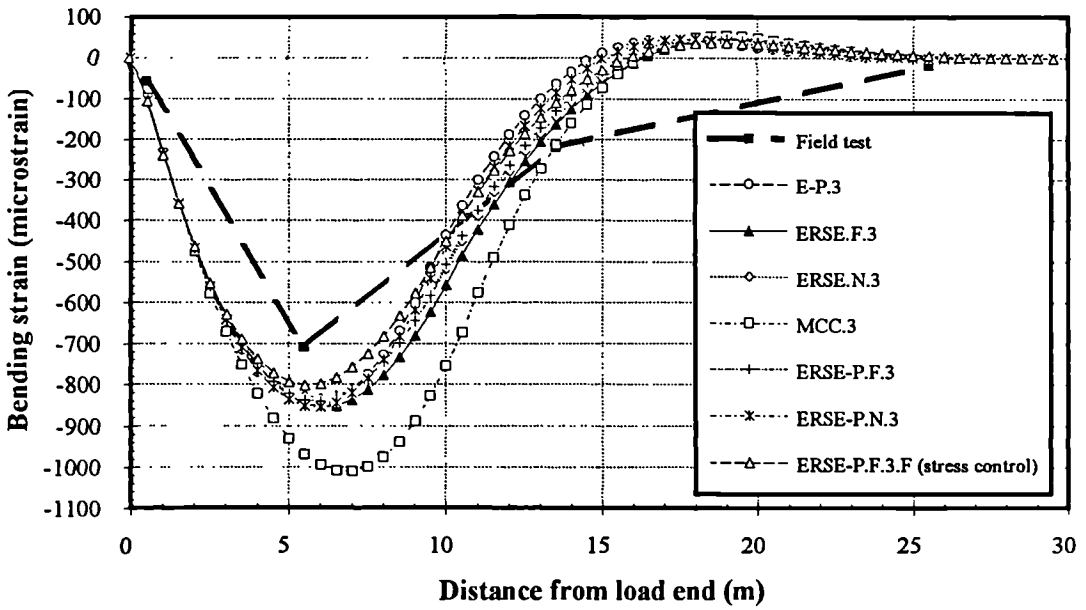

(b)

Fig. 7.31. Predicted distributions of bending strain by WOMOD using the *P-y* curves from the model with interface elements around the pipe and along the trench (a) load = 181kN, (b) load = 592kN.

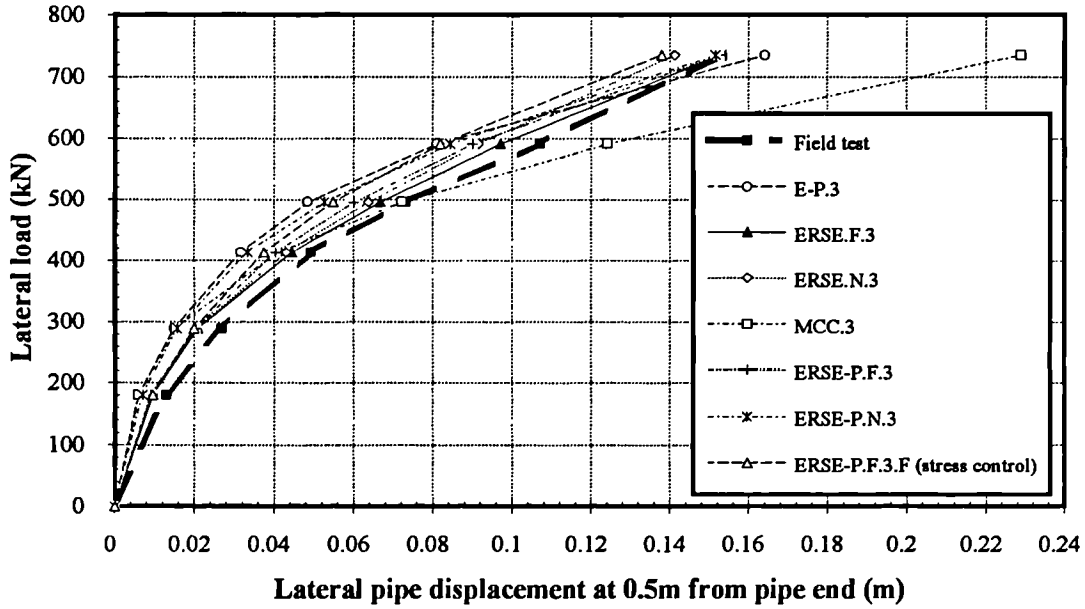

Fig. 7.32. Predicted maximum lateral pipe displacements by WOMOD using the *P-y* curves from the model with interface elements around the pipe and along the trench.

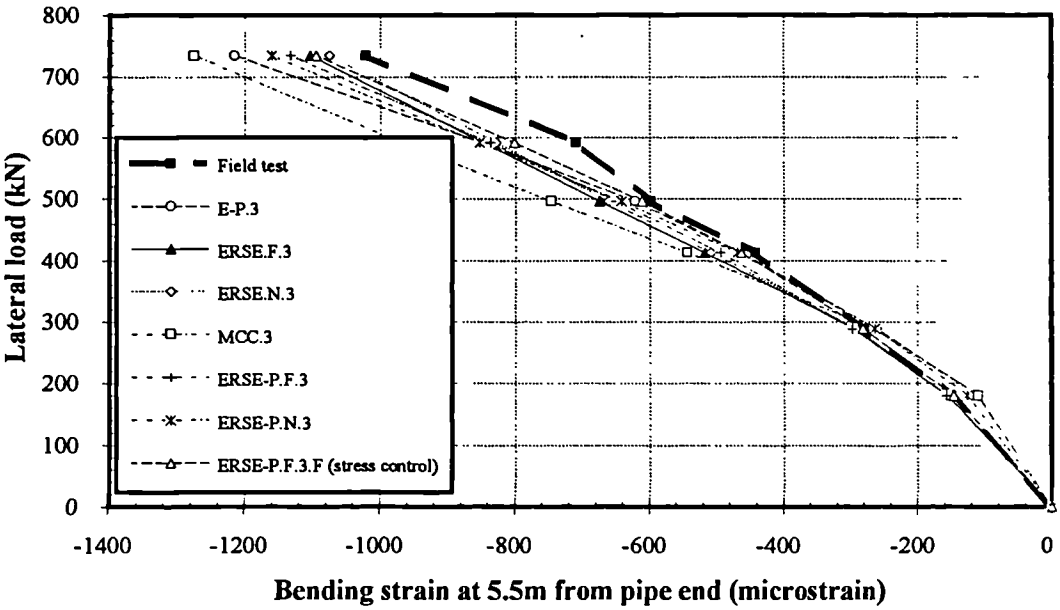

Fig. 7.33. Predicted maximum bending strains by WOMOD using the *P-y* curves from the model with interface elements around the pipe and along the trench.

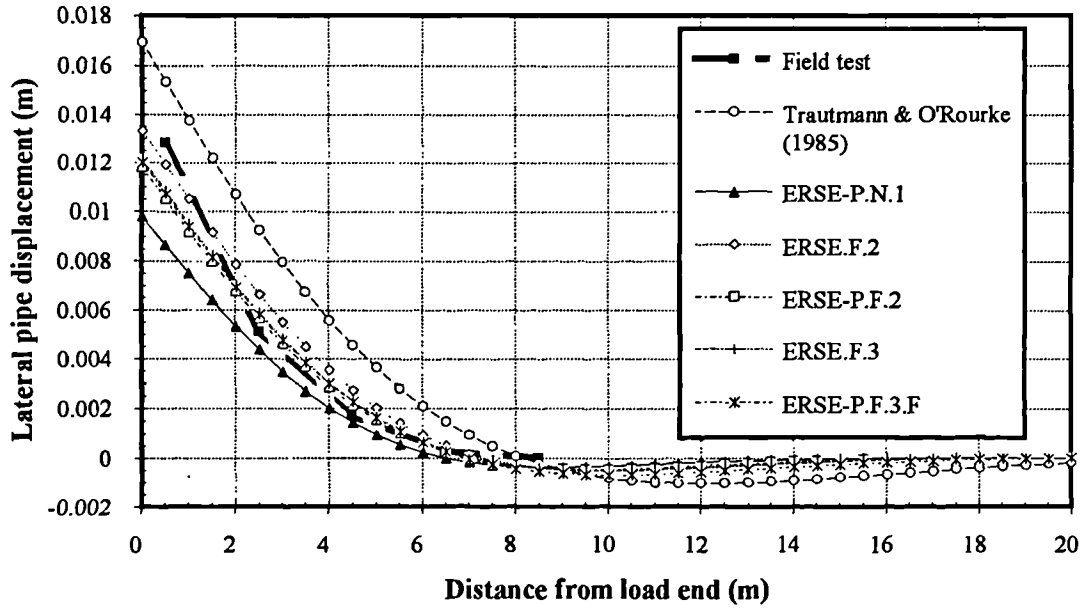

(a)

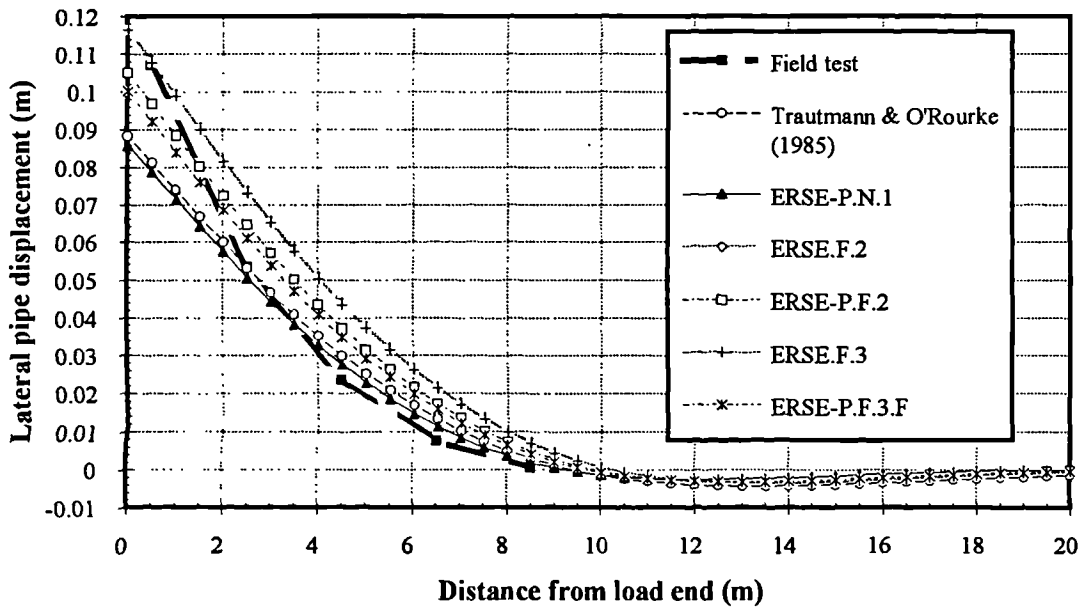

(b)

Fig. 7.34. Predicted distributions of lateral pipe displacement by WOMOD using reduced *P-y* curve near the loading end for six most promising *P-y* curves from Sections 7.3.1 to 7.3.4 (a) load = 181kN, (b) load = 592kN.

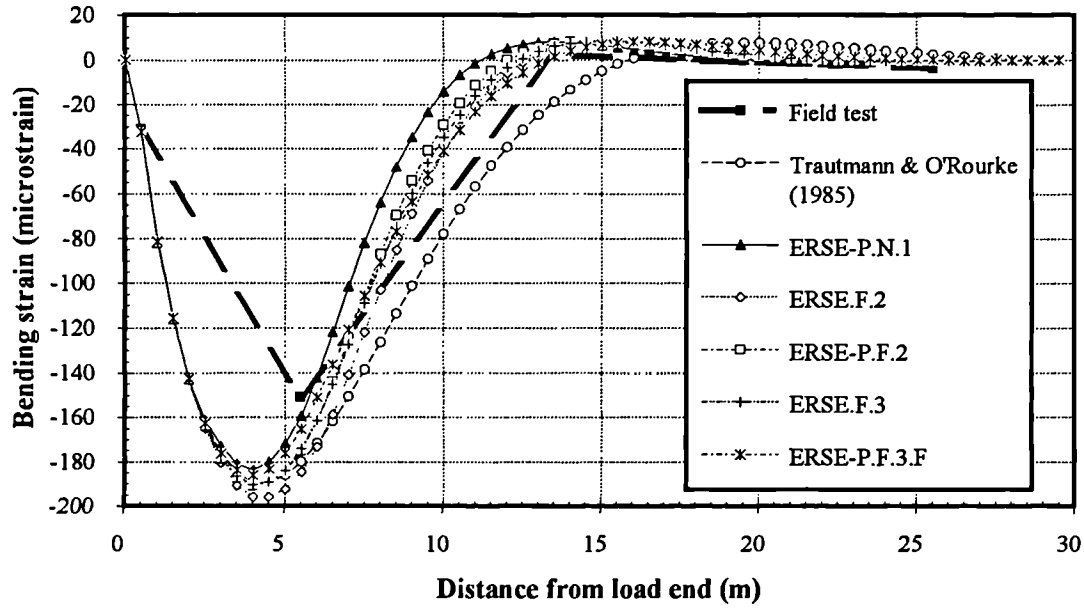

(a)

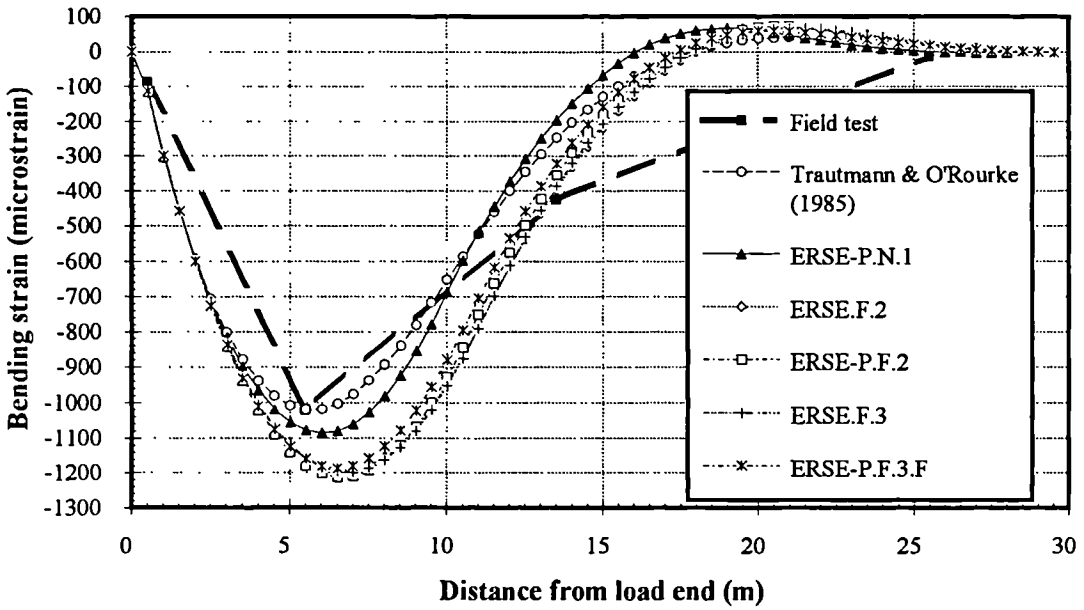

(b)

Fig. 7.35. Predicted distributions of bending strain by WOMOD using reduced *P-y* curve near the loading end for six most promising *P-y* curves from Sections 7.3.1 to 7.3.4 (a) load = 181kN, (b) load = 592kN.

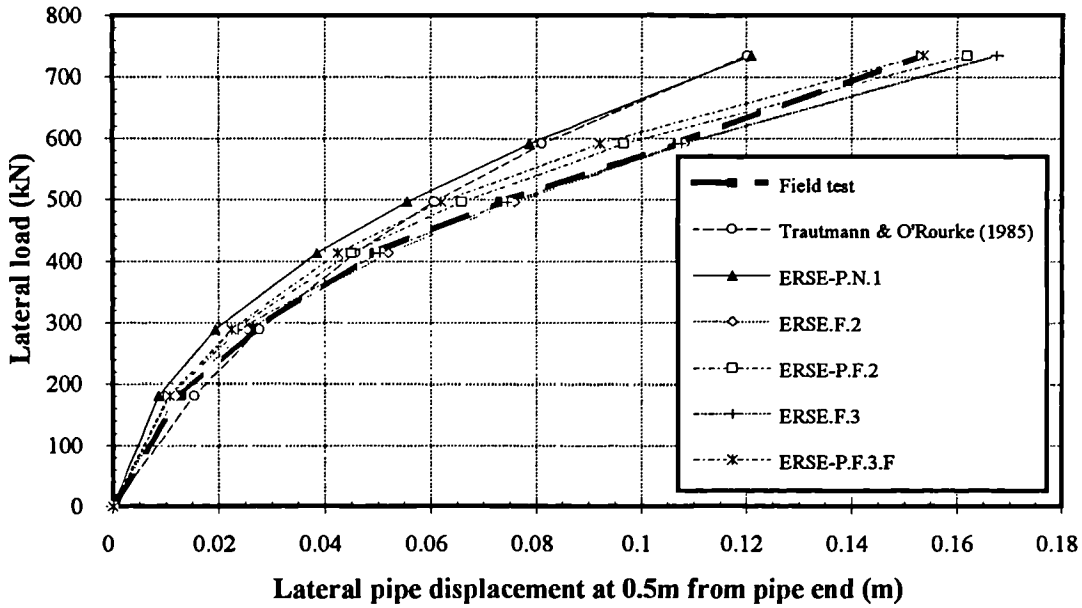

Fig. 7.36. Predicted maximum lateral pipe displacements by WOMOD using reduced *P-y* curve near the loading end for six most promising *P-y* curves from Sections 7.3.1 to 7.3.4.

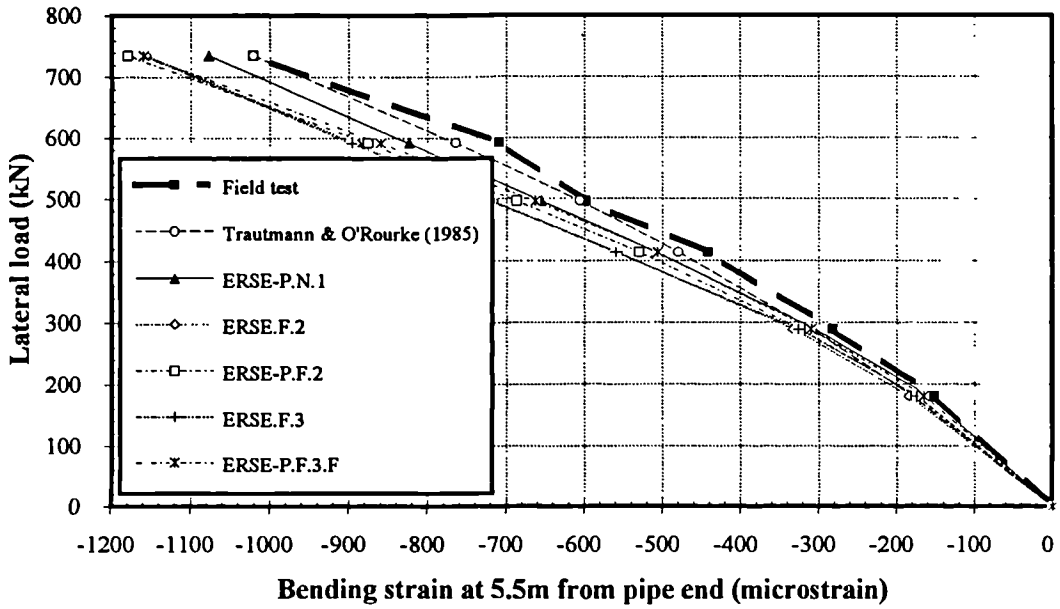

Fig. 7.37. Predicted maximum bending strains by WOMOD using reduced *P-y* curve near the loading end for six most promising *P-y* curves from Sections 7.3.1 to 7.3.4.

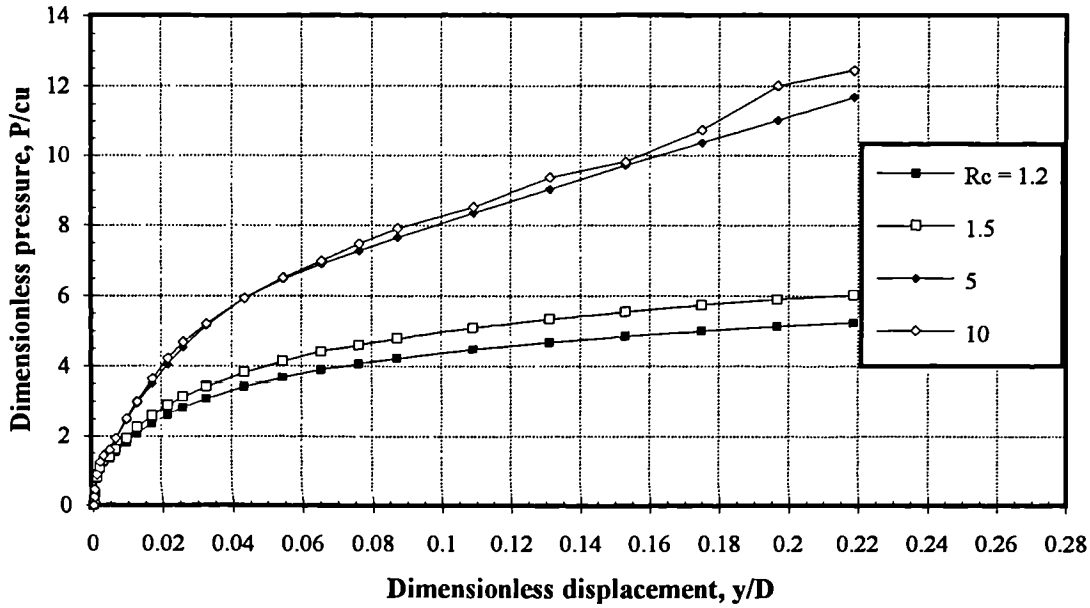

(a)

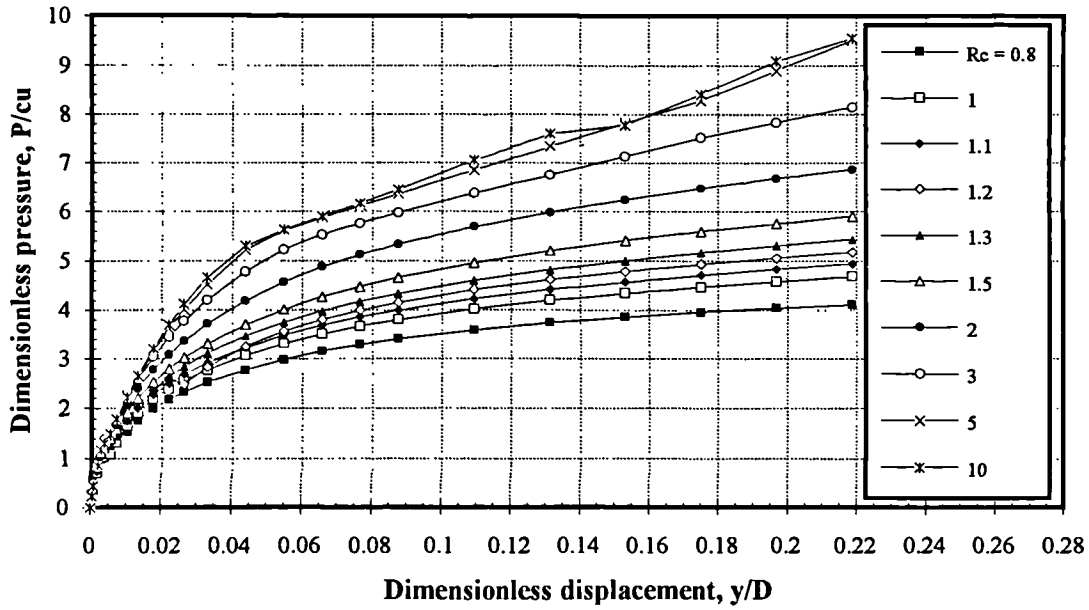

(b)

Fig. 7.38. Dimensionless pressure-displacement relationships of the parametric study for vertical trench sides with different width of trench (a) width = 1.2m, (b) width = 1.4m.

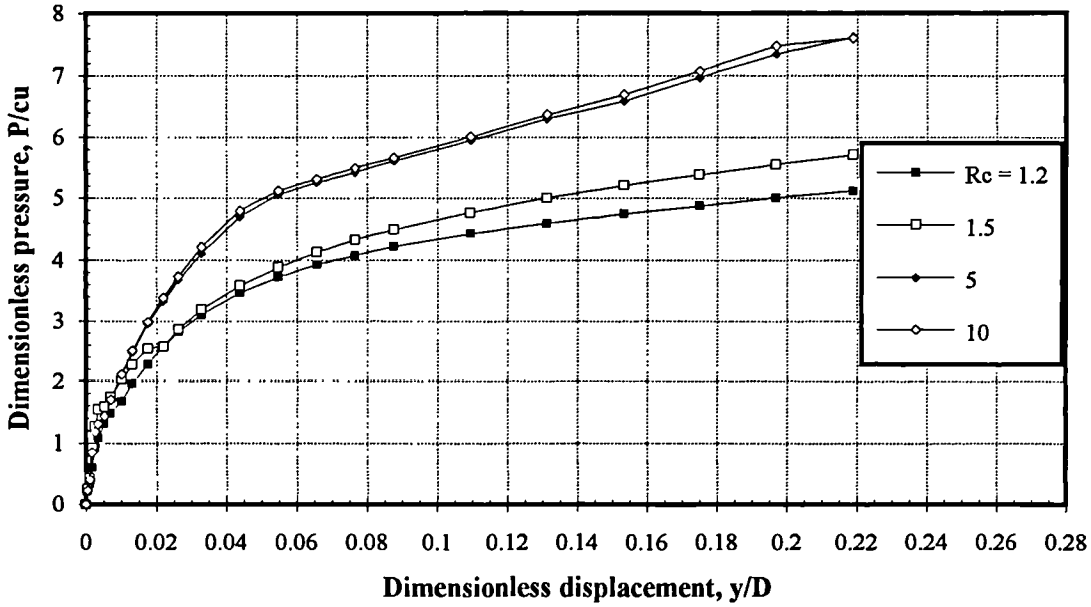

(c)

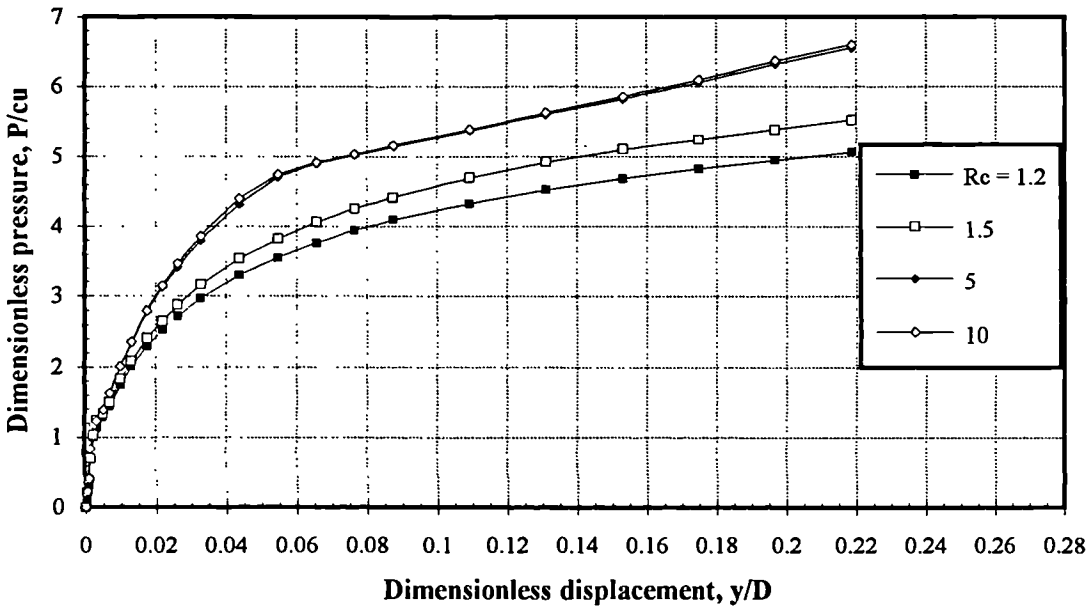

(d)

Fig. 7.38. Dimensionless pressure-displacement relationships of the parametric study for vertical trench sides with different width of trench (c) width = 1.6m, (d) width = 1.8m.

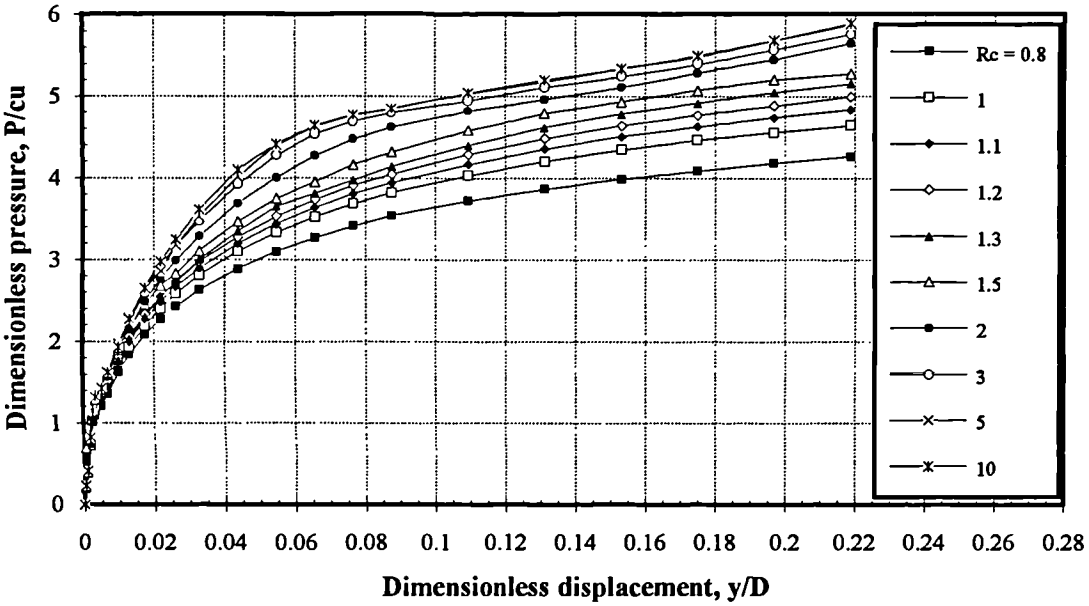

(e)

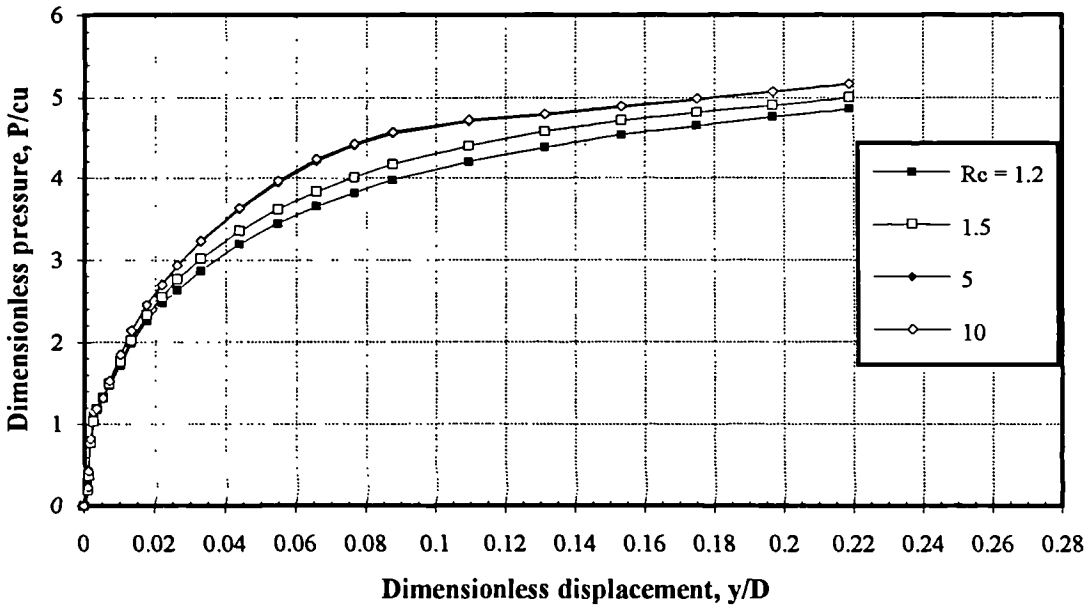

(f)

Fig. 7.38. Dimensionless pressure-displacement relationships of the parametric study for vertical trench sides with different width of trench (e) width = 2.0m, (f) width = 2.5m.

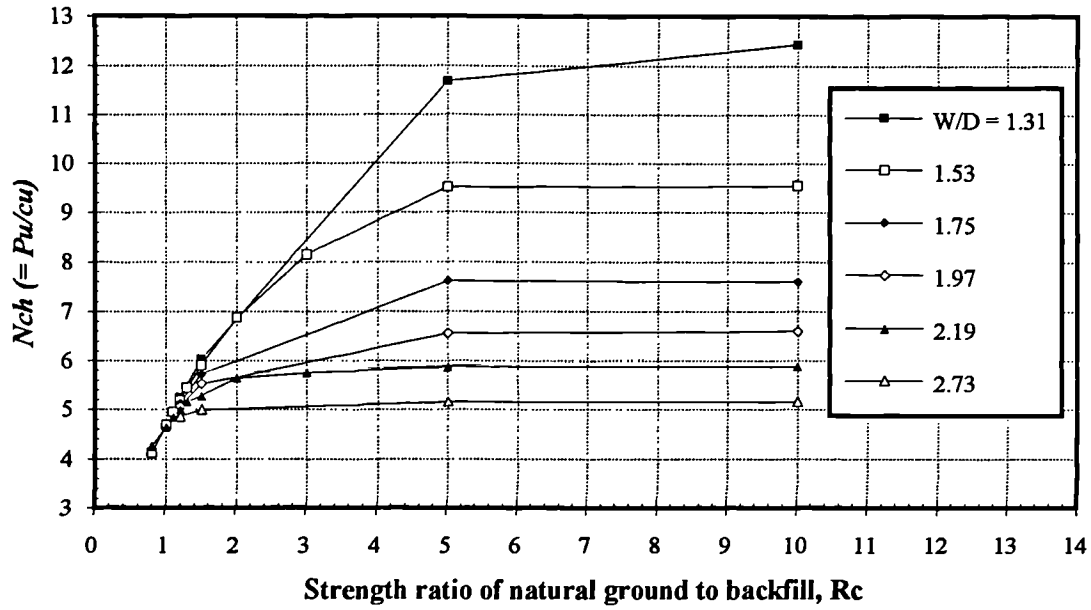

Fig. 7.39. The relationships of N_{ch} against R_c at different *W/D* ratios for trench with vertical sides.

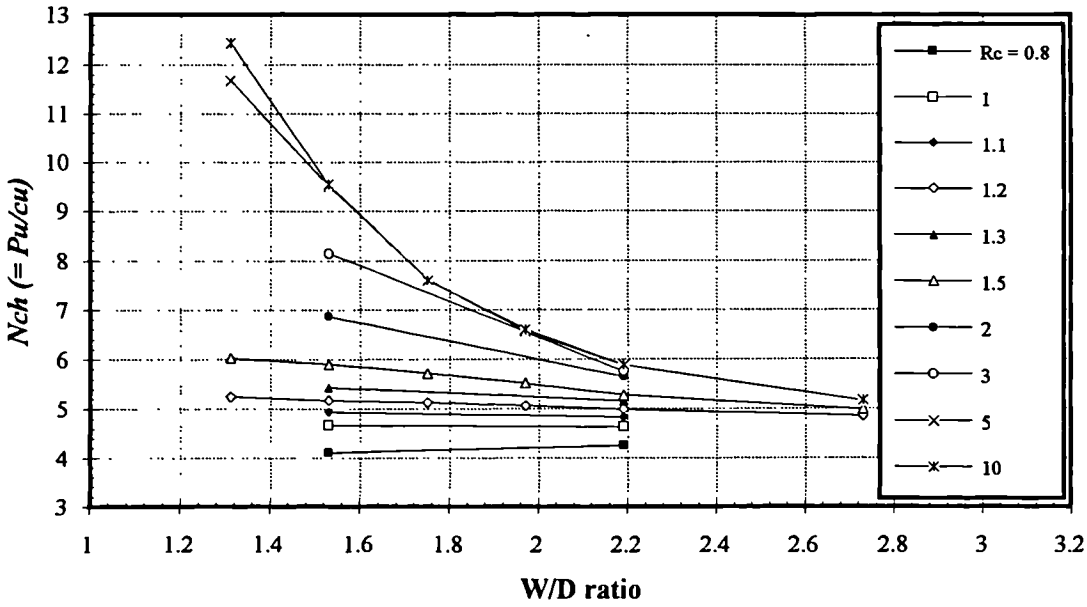

Fig. 7.40. The relationships of N_{ch} against *W/D* ratio at different R_c for trench with vertical sides.

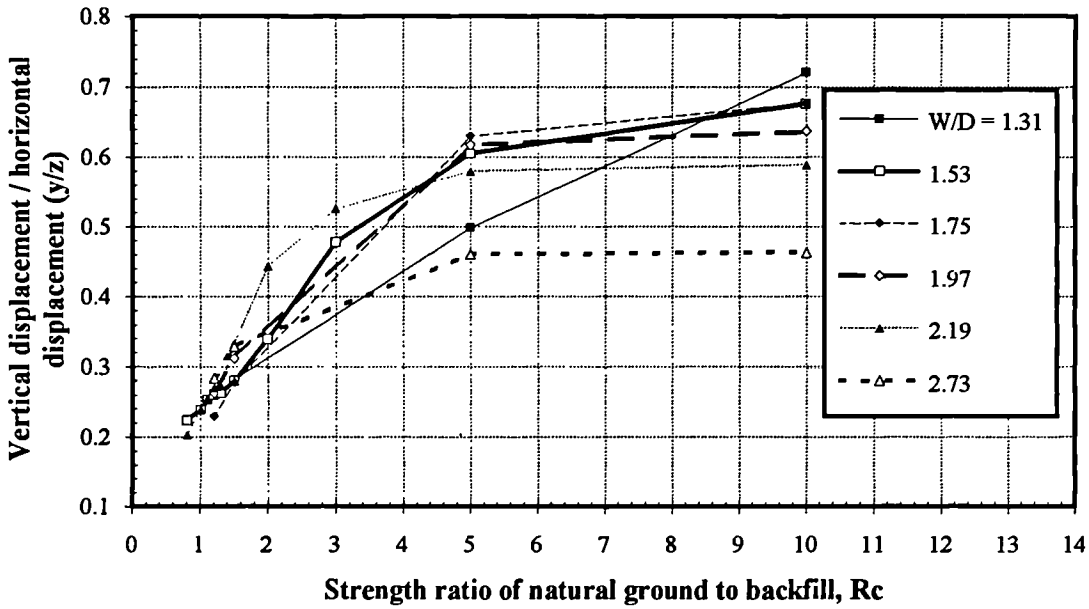

Fig. 7.41. The relationships of y/z against R_c at different W/D ratios for trench with vertical sides.

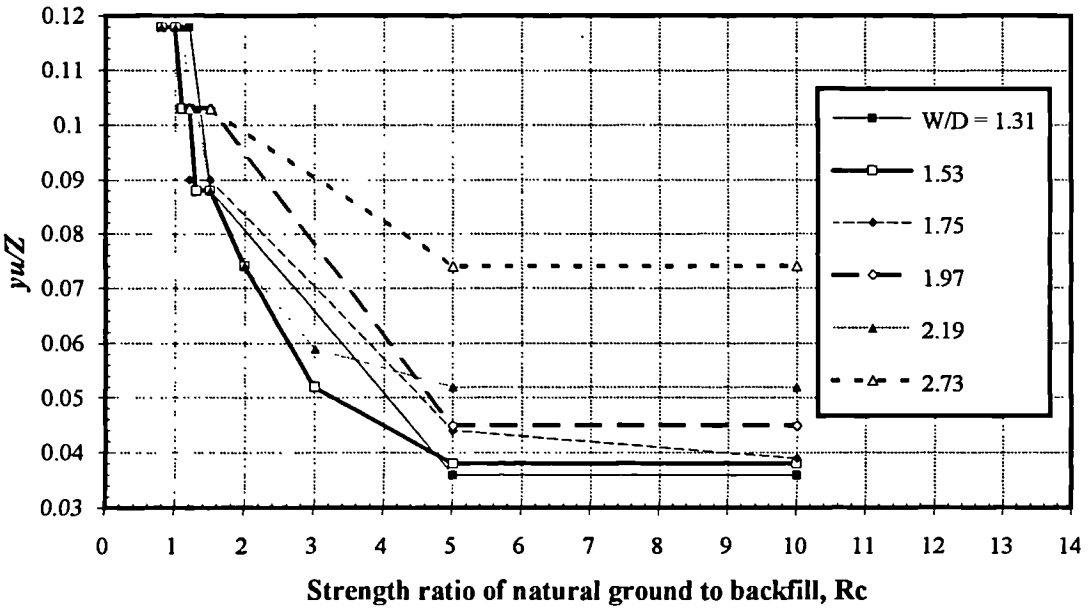

Fig. 7.42. The relationships of non-dimensional ultimate displacement y_u/Z against R_c at different W/D ratios for trench with vertical sides.

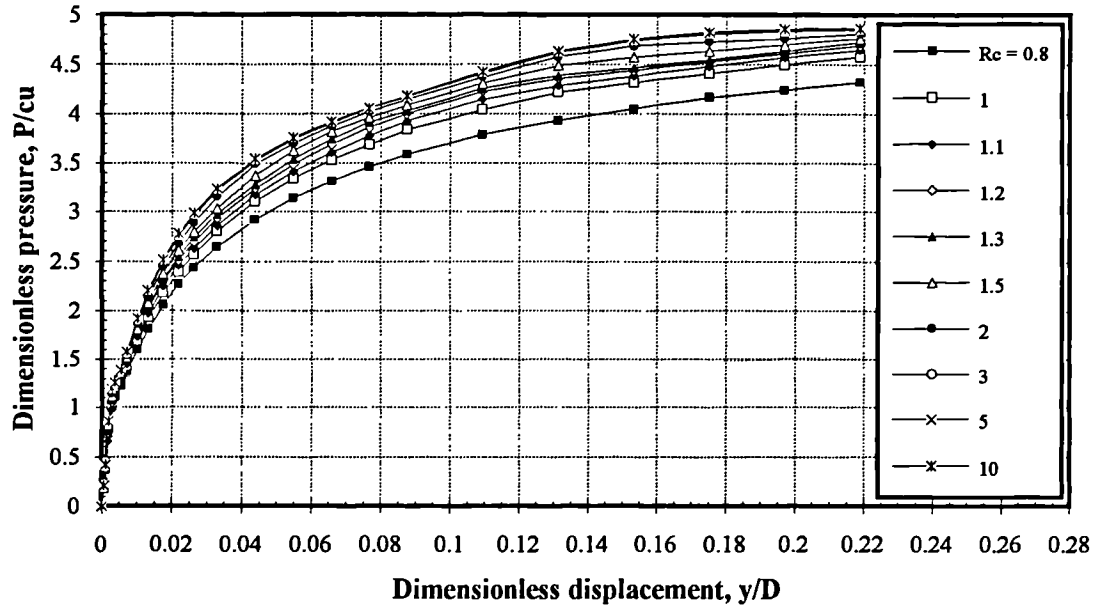

(a)

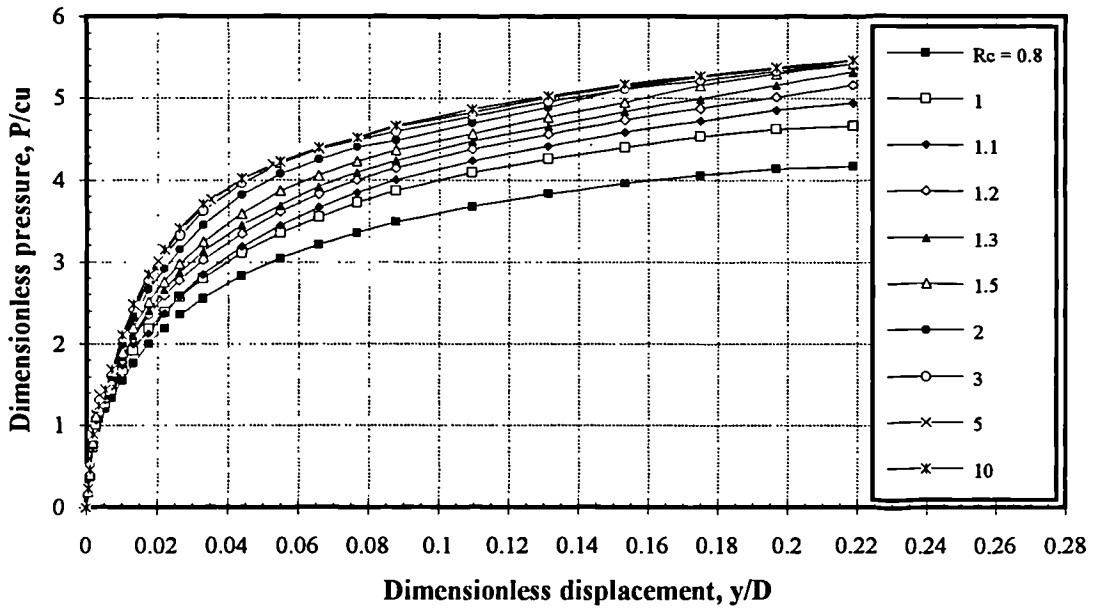

(b)

Fig. 7.43. Dimensionless pressure-displacement relationships of the parametric study for different angle of the trench sides (a) angle = 30°, (b) angle = 45°.

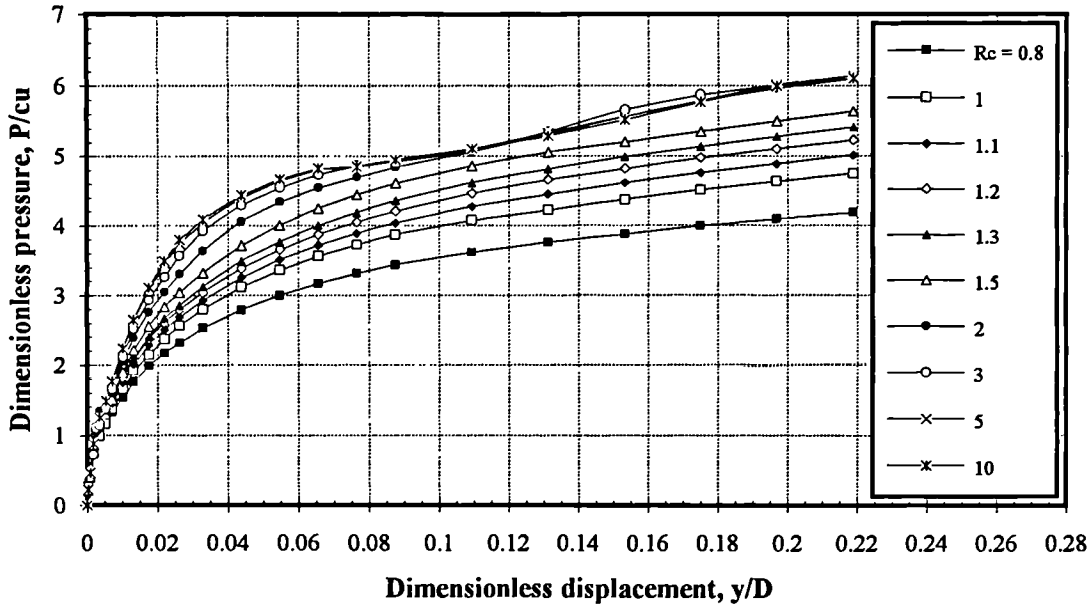

(c)

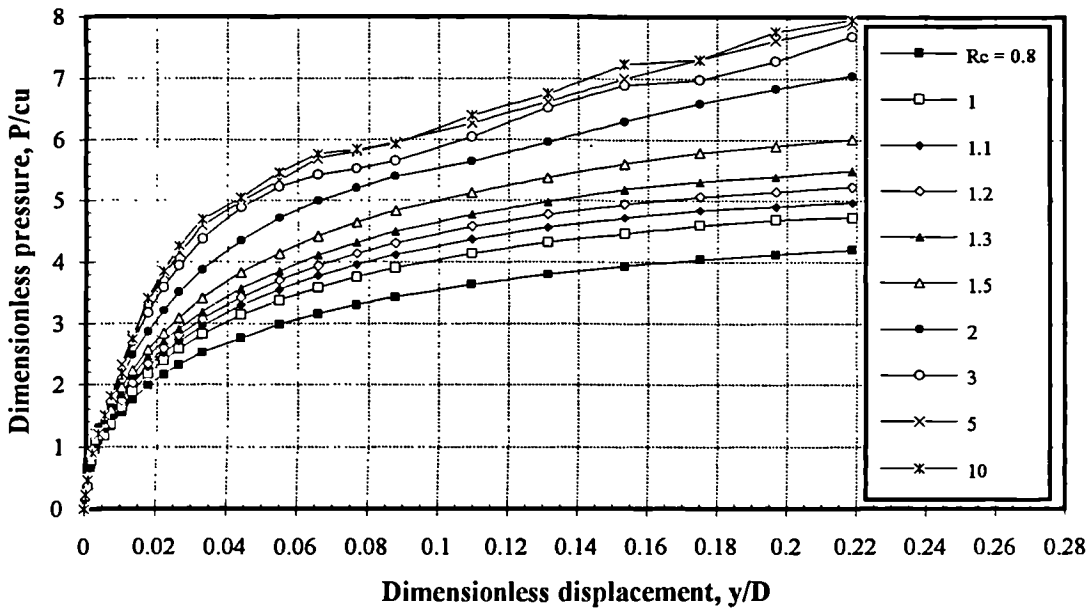

(d)

Fig. 7.43. Dimensionless pressure-displacement relationships of the parametric study for different angle of the trench sides (c) angle = 60°, (d) angle = 75°.

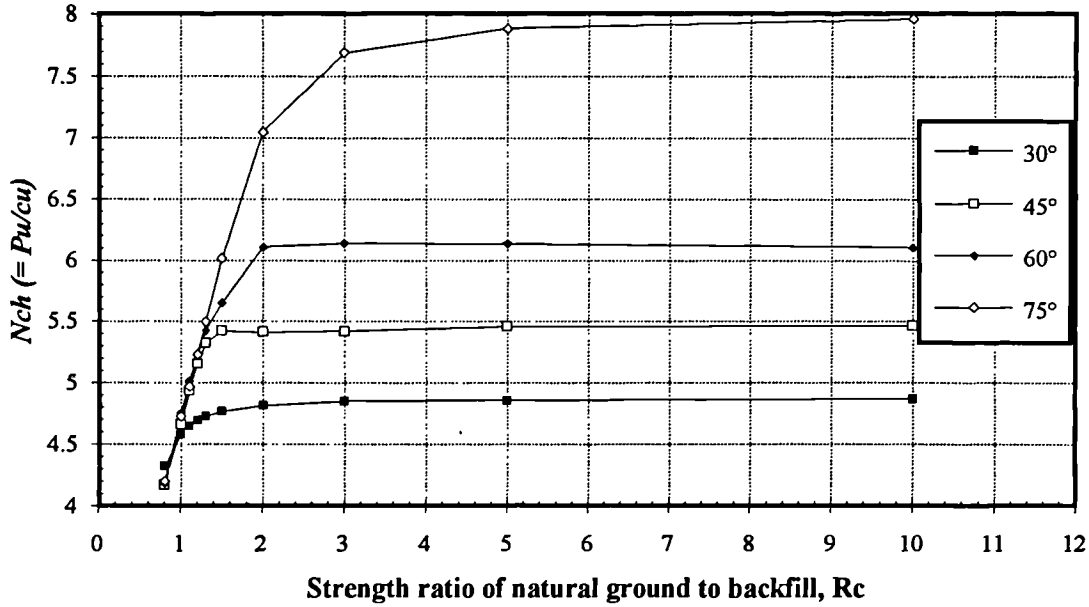

Fig. 7.44. The relationships of N_{ch} against R_c at different angle of trench sides.

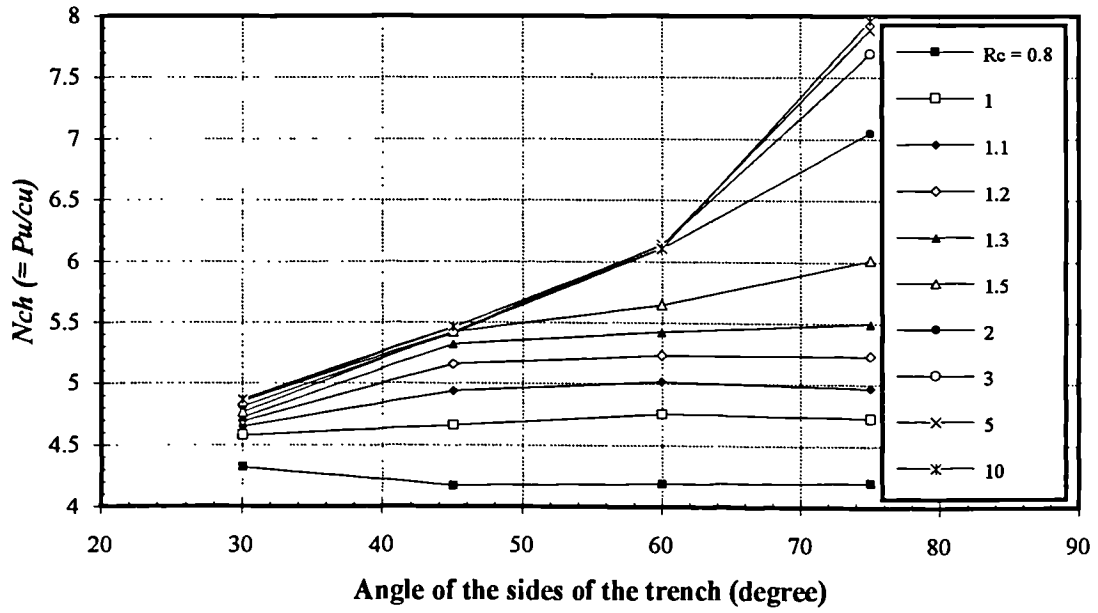

Fig. 7.45. The relationships of N_{ch} against angle of trench sides at different R_c.

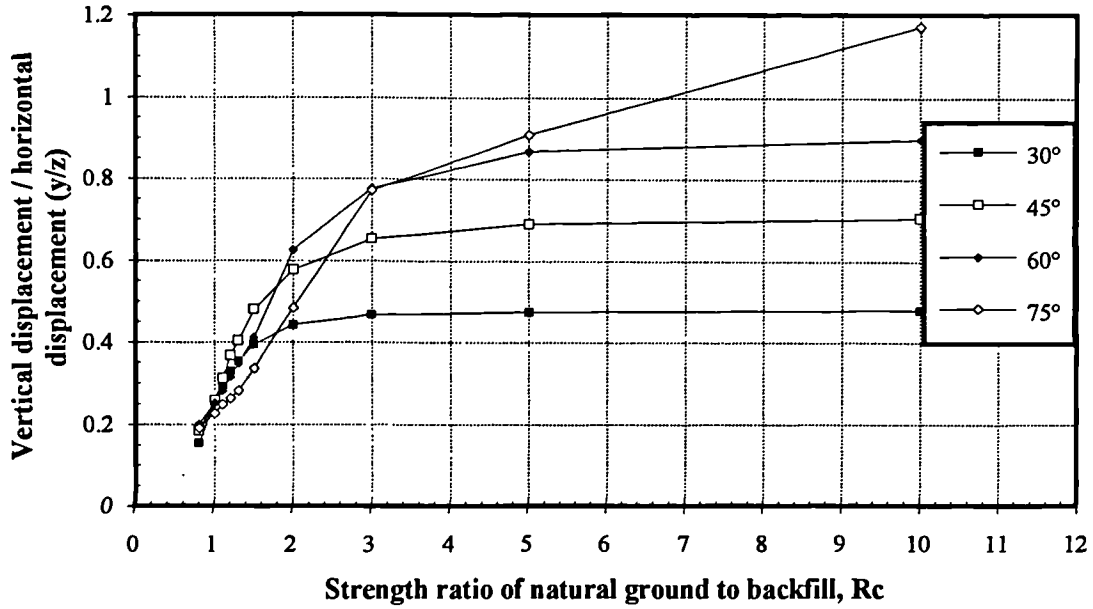

Fig. 7.46. The relationships of y/z against R_c at different angles of trench sides.

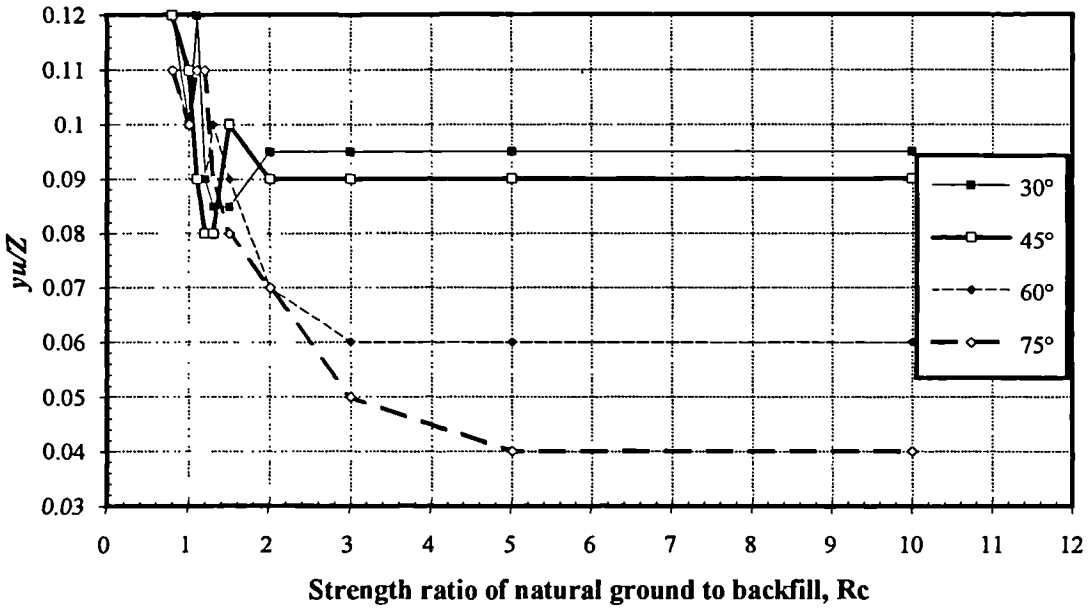

Fig. 7.47. The relationships of non-dimensional ultimate displacement y_u/Z against R_c at different angles of trench sides.

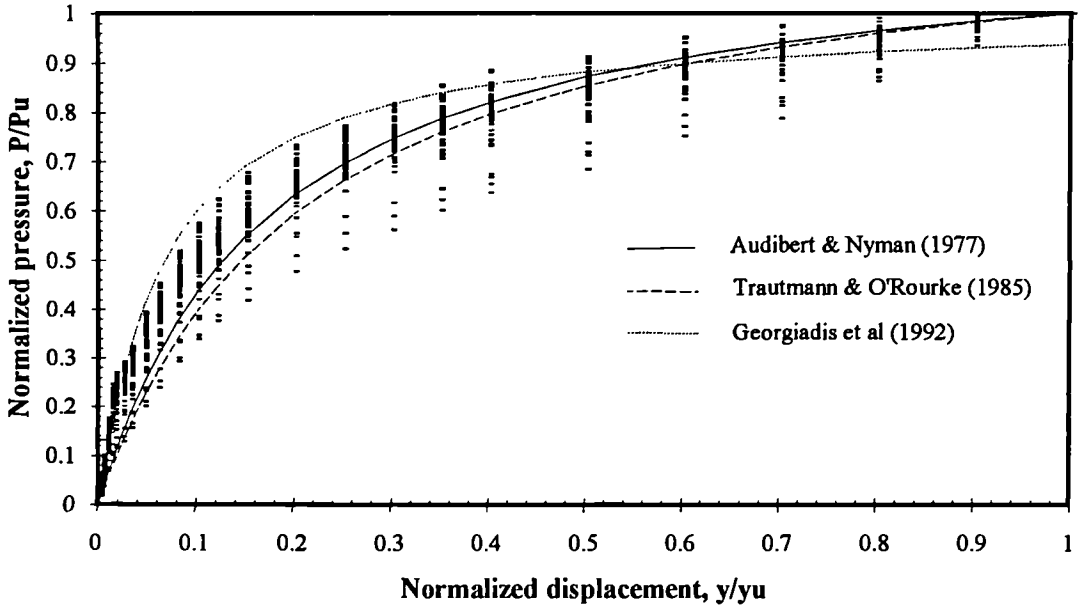

Fig. 7.48. Normalized pressure-displacement relationships of all the *P-y* curves predicted in the parametric study.

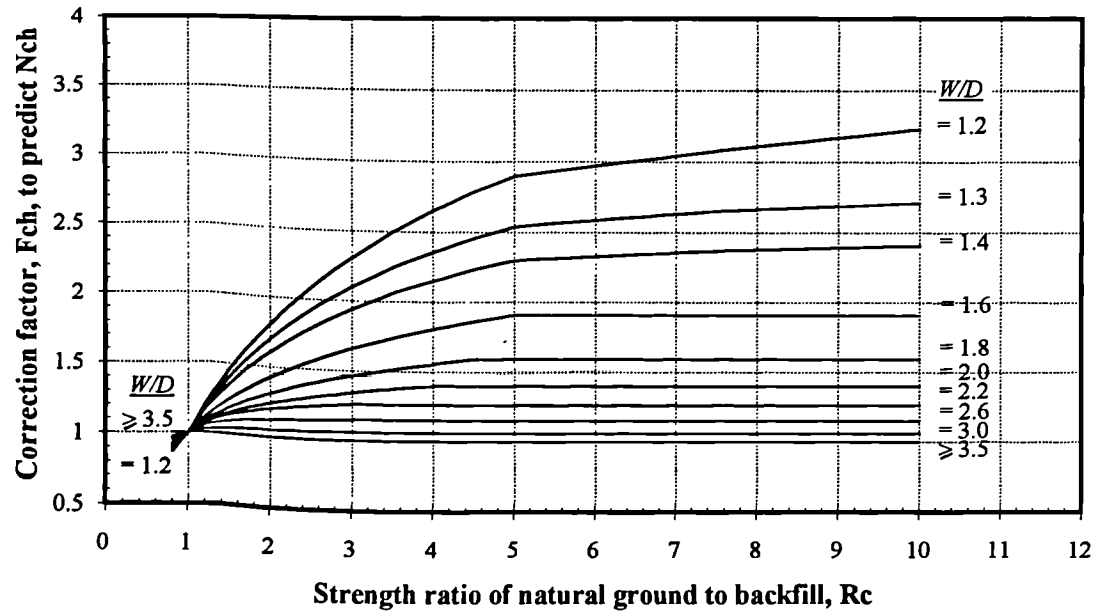

Fig. 7.49. The relationships of the correction factor F_{ch} against R_c at different *W/D* ratio for trench with vertical sides.

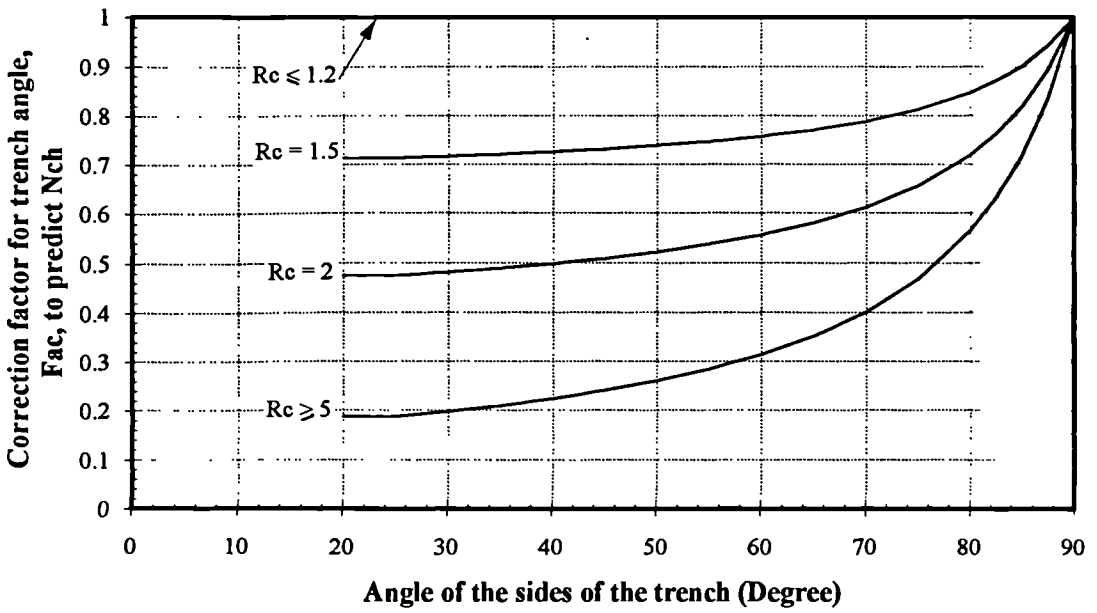

Fig. 7.50. The relationship of the correction factor F_{ac} against angle of trench sides.

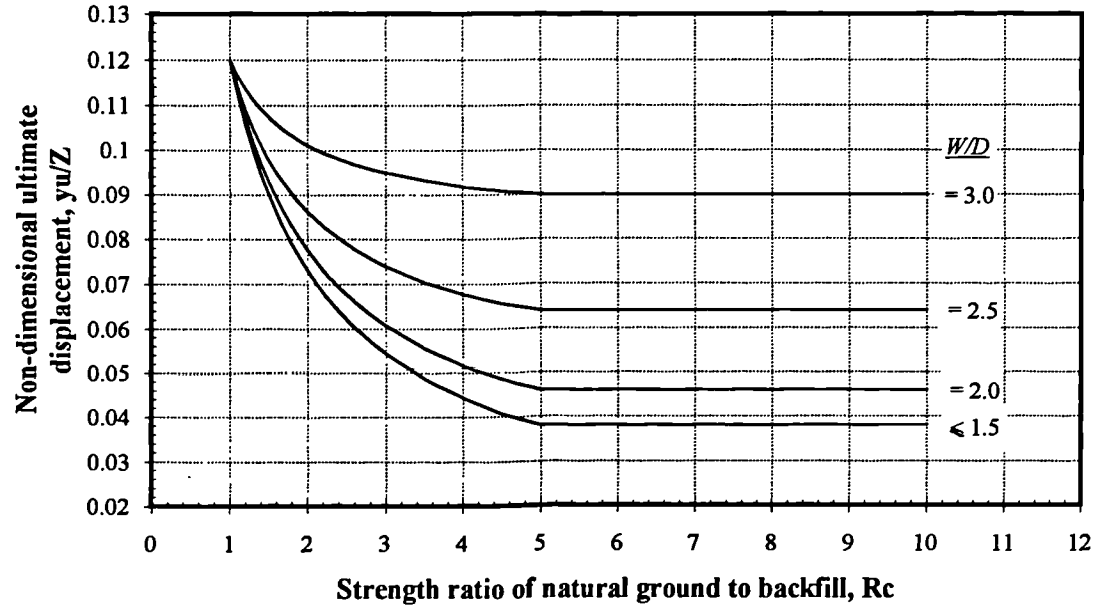

Fig. 7.51. The relationships of the non-dimensional ultimate displacement y_u/Z against R_c at different *W/D* ratio for trench with vertical sides.

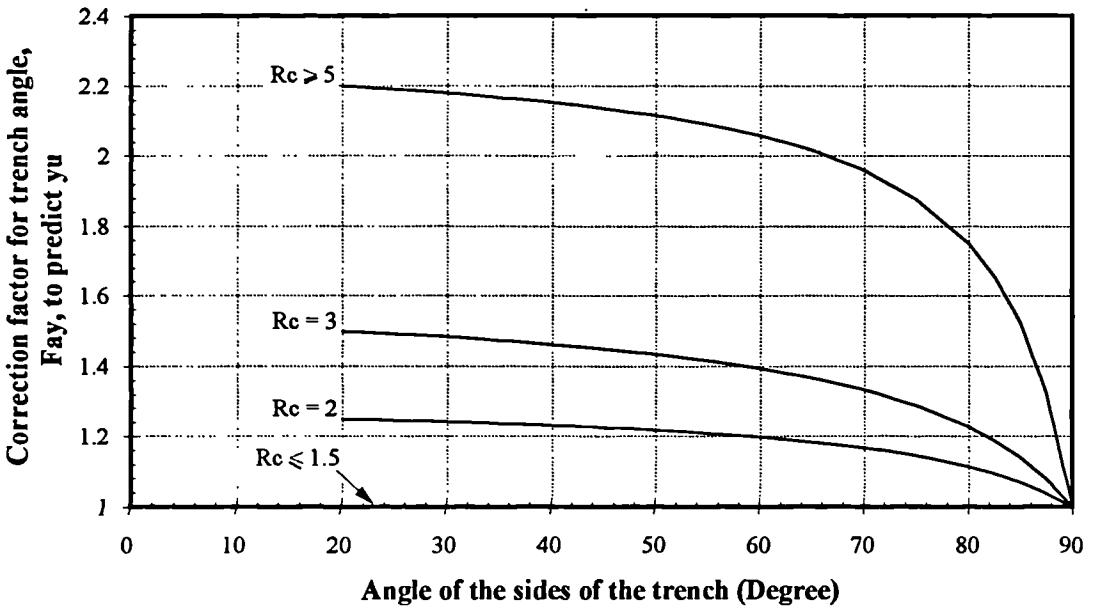

Fig. 7.52. The relationship of the correction factor F_{ay} against angle of trench sides.

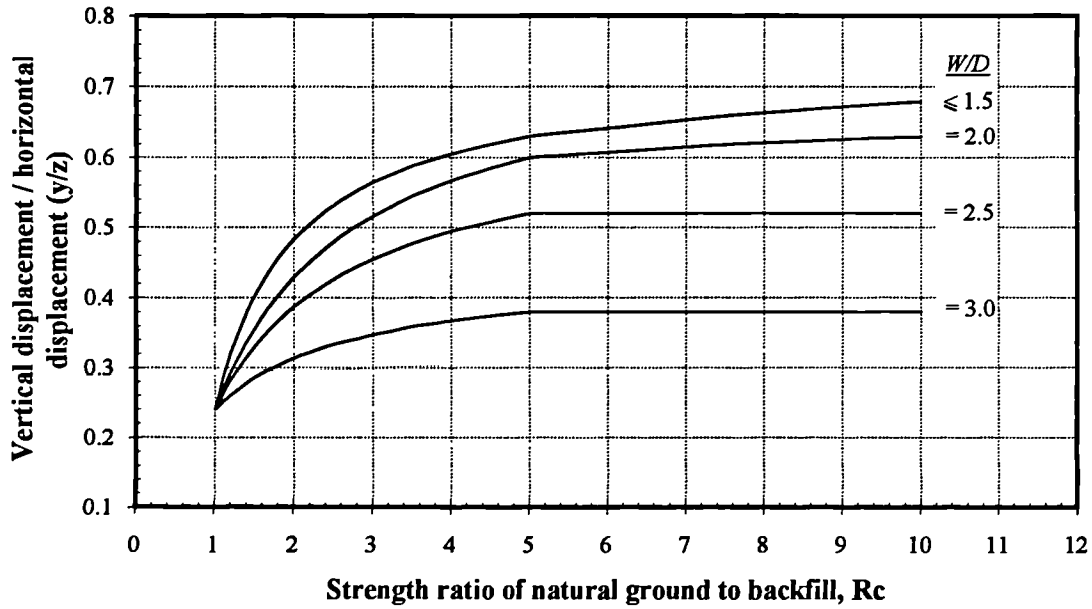

Fig. 7.53. The relationships of the ratio of vertical displacement and horizontal displacement against R_c at different *W/D* ratio for all angle of trench side.

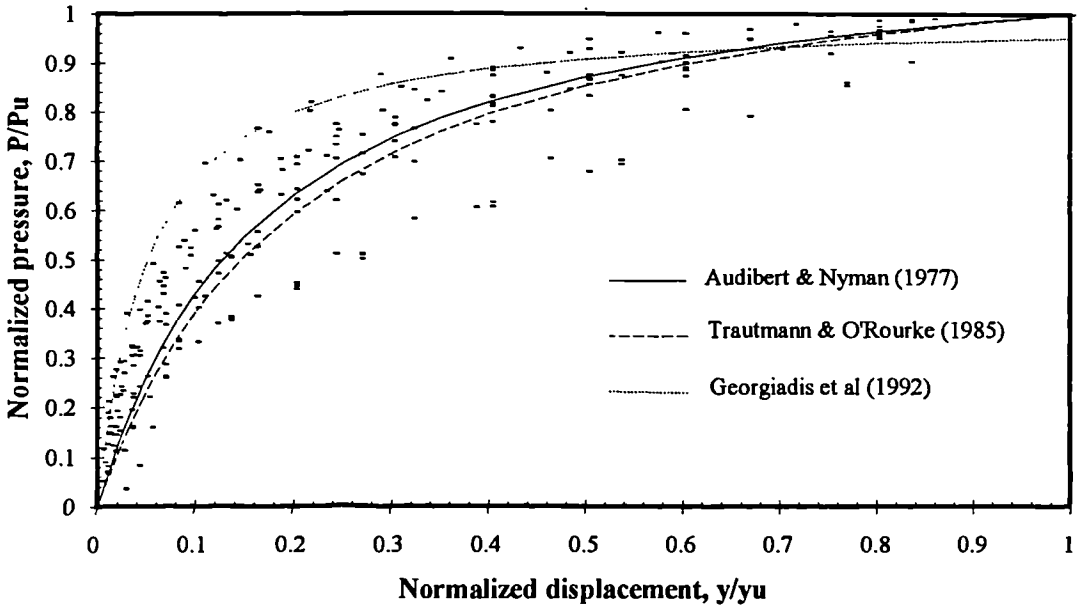

Fig. 7.54. Normalized pressure-displacement relationships of all the *P-y* curves predicted by 2-D FE analyses in Section 7.2.

CHAPTER 8

DISCUSSION

8.1. Summary of Discussions Presented in Previous Chapters

The following points of discussion have already been presented in the main text and will not be discussed further in this Chapter. For details of the discussion refer to the main text.

- Some of the methods that other researchers used in the modelling of soil/pipe interaction problem were discussed in Section 2.9.
- The processed results of the axial and lateral push tests were discussed in Sections 3.2.1 and 3.2.2 respectively.
- The work by Booth (1991) and Ng (1993) for modelling the lateral push test were discussed in Section 3.5.
- The results of single element tests for the three kinds of interface element were discussed in Section 4.3.
- The results of the benchmark tests to examine the behaviour of the interface elements were discussed in Section 4.5.
- The limitations of the modifications of WOMOD (plastic behaviour of the pipe, change in shape of the cross-section and shear deformation) and suggestions for further improvement of the program were discussed in Sections 6.6 and 6.7 respectively.

8.2. The Hilderstone Pipe Loading Tests

Although the test pipe was heavily instrumented to measure various results during the load tests, several important results are not available. In the axial push test, the relative displacements between the soil and the pipe were not measured. For the lateral push test, no upward movements of the pipe were measured. Also the number of strain gauges was insufficient to pick up the maximum bending moment of the pipe. Change of shape of the pipe cross-section was only crudely assessed. Improvements, particularly in the amount of data collected, have to be made if further *in situ* tests are to provide the information required for the validation of numerical methods to model the behaviour of buried pipeline. Improvements are also required in the way the test is carried out as the rigid cross-brace placed near the loading end (Fig. 3.8) has affected the behaviour of the pipe, such as the ovality of the cross-section and the bending stiffness of the pipe.

It should be noted that the axial and lateral push tests were performed on the same pipe section with the axial push test being carried out first. The disturbance of the surrounding soil and the breakage of bonding between the soil/pipe interface could influence the results of the subsequent lateral push test. The effect, however, is likely to be small. For ideal situation, the two tests should be carried out on different pipe sections, but the cost for the testing is also a major consideration.

8.3. The *P-y* Curve From Lateral Push Test

The method used to obtain a *P-y* relationship from the lateral pipe loading test was presented in Section 3.2.2. Due to the deficiency of the number of strain gauges fixed near the loading end of the pipe, however, the value of the maximum bending moment is uncertain, thus the polynomials that represented the bending moment profiles is not very accurate. The back-calculated *P-y* curve does not reach an ultimate pressure near the end

but shows a gradual increase in soil pressure. This may be due to the unloading/reloading cycle during the test and the transition of pipe from the backfill to the stronger natural ground, as discussed in Section 3.2.2. The reasons for this strain hardening behaviour and its influence on the elastic beam on elastic foundation analysis should be investigated by further research. Nevertheless, this hardening behaviour only affects the behaviour of the pipe at large deflection and has little influence in most practical cases. The results of the elastic beam on elastic foundation analysis in Section 7.3.1 for modelling the lateral push test showed that the results of the analyses using the back-calculated *P-y* curve gave very good agreement with the field data, indicating that the polynomials that represent the bending moment profiles were reasonably accurate.

The plot of three hyperbolic pressure-displacement relationships to fit the *P-y* curve from the field test, shown in Fig. 3.15, indicated that the formulations by Audibert & Nyman (1977) and Trautmann & O'Rourke (1985) both give a good fit to the field data and can be used for practical purposes. However, the formulation by Georgiadis *et al* (1992) fitted better at the initial part of the *P-y* curve, in which the other two formulations under-predicted the initial slope of the *P-y* curve. At low load, the *P-y* curve by Georgiadis *et al* (1992) give a slightly better prediction in the WOMOD analysis for the modelling of the lateral push test (Section 7.3.1). Thus the hyperbolic *P-y* relationships by Audibert & Nyman (1977) and Trautmann & O'Rourke (1985) should be improved in future research (see also Section 8.11).

8.4. Stress Path Tests

8.4.1. Soil Specimens

The soil specimens used for the stress path tests were recompacted using "disturbed" soil material recovered from the field. Comparing the test results in this research and in Leach & Row (1991), the strength of backfill material was very similar (Tables 3.1 and 3.3). For the natural ground, the recompacted specimen in this research was very stiff such that the stress-strain behaviour was virtually linear up to the limiting load of the testing apparatus. This large difference in the strength between the backfill and natural ground will influence the pressure-displacement response of the pipe at larger displacement.

8.4.2. Selected Stress Path

The selection of stress paths for the triaxial tests was based on a pipe moving horizontally. The stress paths of the corresponding elements were checked by a preliminary analysis in which the cavity was displaced horizontally and constrained in the vertical direction, and the agreement was satisfactory. In the final analyses, however, the pipe was not only moving horizontally, but also vertically to represent the true pipe movement. Examination of the stress path of a point in front of the pipe (element A in Fig. 3.17) in the final analysis indicated that the vertical stress increased significantly during the analysis although it was assumed to remain constant (Fig. 7.5). This was due to the vertical movement of the pipe which induced a vertical stress. In this situation, the stress path is difficult to predict accurately, but is likely to be increasing horizontal and vertical stresses, with the vertical stress between zero and the value of horizontal stress.

8.4.3. Drainage Condition During the Tests

During the stress path tests, drainage was not allowed at any stage, thus the samples were in an undrained condition. This was justified by the fact that duration of the pipe loading test was a few hours and the low permeability of the soil (typical permeability of the backfill is 1×10^{-9}m/s from Leach & Row, 1991) means a very slow rate of dissipation of the excess pore water pressure. Also, the time available did not allow fully drained tests to be carried out, which may be more appropriate in order to determine the parameters for the Modified Cam clay and the time-dependent behaviour of the soil.

8.4.4. Selection of Soil Models

From the results of the stress path tests in Table 3.3, the degree of saturation of the samples was between 82 – 90%, and the air voids between 3 – 5%, thus the soil samples were unsaturated. Both Modified Cam clay and Elastic-perfectly plastic models are only suitable for the modelling of fully saturated soil. Therefore the two soil models have poor agreement with the results of the stress path tests in the single element test (Fig. 3.23) On the other hand, the Non-linear elastic and Elasto-plastic models, which use directly the results of the stress path test, modelled the behaviour of the unsaturated soil satisfactorily However, the Non-linear elastic model is only suitable in conditions having monotonic loading, *i.e.* no unloading-reloading cycle of stress (see Section 2.4.4). In the case of any uncertainty, the Elasto-plastic model should be used. The British Gas Elasto-plastic model provides the strain hardening and/or strain softening observed in physical tests and includes the recording link between plastic volumetric and plastic shear strain. Its key success does not lie in any feature that is unique to the modelling of unsaturated soils. The weakness of the model is the lack of mean pressure influence. The advice of the author is to incorporate the mean pressure effect by the appropriate selection of stress paths for the identification of the stress-strain relationship.

Even so, these two soil models cannot be used in more complex loading conditions in unsaturated soils such as suction changes and time-dependent behaviour. A suitable unsaturated soil model should be used in these situations, for example the critical state model for unsaturated soil (Alonso, Gens & Josa, 1990).

8.5. Further Modifications to the CRISP90 Interface Element

Several modifications were made to the CRISP90 interface element especially in the re-bonding behaviour. However, the stress-strain relationships of the normal behaviour (linear elastic) and shear behaviour (bilinear elastic-perfectly plastic) are rather simple. Better stress-strain relationships may be implemented into the interface element to improve the behaviours. At the moment, the CRISP90 interface element is only suitable to describe the interface behaviour in a single separation-closure cycle. For dynamic/cyclic response of an interface, suitable cyclic stress-strain relationships for the normal and shear behaviour should be used.

8.6. Numerical Modelling of the Axial Push Test

The proposed two-dimensional finite element model in Chapter 5 for the modelling of the behaviour of a buried pipeline subjected to an axial load, is more realistic than a 1-D model. However, the idealized geometry of the surrounding soil in the 2-D model may influence the accuracy of the prediction. For the Hilderstone case, the cover depth to the pipe was 0.9m but the backfill beneath the pipe was only 0.1m thick, thus the thickness of the backfill soil surrounding the pipe cross-section was non-uniform (see Fig. 3.2). The non-uniform thickness of backfill surrounding the pipe, which was idealized as an even thickness in the

proposed 2-D model, may influence the prediction of the total displacement and stress distribution of the pipe. Additional analyses may need to be carried out using an average backfill thickness to examine the sensitivity of the idealization. The model may be improved by using two layers of interface elements, one at the top and one at the bottom of the pipe, with different thicknesses of backfill attached to it (for example, in the Hilderstone case, the thickness of the backfill at top of the pipe = 0.9m and at the bottom = 0.1m), which may be more accurate in describing the geometry of the surrounding soil.

The boundary condition at the ground surface was idealized as fixed, which is not strictly true. The restraints of the overburden soil were provided by the adjacent soil along the pipe which may allow a limited movement of the soil at the ground level. It is necessary to carry out a full 3-D FE analysis to examine the accuracy of the 2-D model. The absence of a 3-D interface element in CRISP90 may be substituted by a thin 20-noded brick element with elastic-perfectly plastic material properties to model the shear behaviour of the soil/pipe interface.

Although the proposed 2-D model predicted the axial push test reasonably well, a small disagreement between the predicted and measured results still existed. Apart from the above limitations of the 2-D model, the possible variation of soil properties over the length of the tested pipe section may be a major reason for the disagreement, as discussed in Section 5.2.

8.7. The Finite Difference Approach in WOMOD

The fourth order differential equation for bending of pipe is approximated numerically using the finite difference approach in the program WOMOD. The approach has the advantage of being easier to implement and manage, and cheaper to solve. However, it is very difficult to

incorporate other modifications to the basic differential equation such as the coupled shear deformation (Section 6.5.2) and the large displacement effect (Section 6.7.1).

Another method mentioned in Section 2.6.3.1, based on a 1-D 2-noded beam element with soil springs at each node, is easier to incorporate other modifications into the stiffness matrix. This method is also being widely used and available in many finite element programs. If further improvements such as the coupled shear deformation and large displacement effect are needed, this 2-noded beam element method is preferable.

8.8. Finite Element Analysis to Predict the *P-y* Curve

8.8.1. Upward Movement of Pipe

The upward movement of the pipe was mainly due to the geometry of the trench (the sloping sides of the trench), the difference in strength between the backfill and the natural ground and the rigid boundary at the bottom of the mesh. Less vertical movement should occur if the trench walls are vertical and if the backfill and the natural ground have approximately the same strength. This was demonstrated by the parametric study in Section 7.4 (Figs 7.41 and 7.46). Unfortunately, the upward movement has not been measured in the field tests, and a comparison of the results could not be made.

8.8.2. Prescribed Horizontal Displacement of Pipe

The initial expectation of Ng (1993) was that the pressure-displacement relationship of the pipe would flatten out within 25mm horizontal displacement in the FE analysis. However, the results of the analyses performed by Ng (1993) showed that this did not happen even at 50mm horizontal displacement and the pressures continued to increase. For this reason, all

the analyses carried out in this research involved a horizontal displacement of 200mm which covered the maximum pipe displacement experienced in the Hilderstone pipe loading test (160mm). The pressure-displacement relationships plotted in Figs 7.6, 7.11 and 7.15 show that most relationships have not flattened out even at 200mm displacement, excepting the Elastic-perfectly plastic model which exhibited a peak pressure at approximately 60mm horizontal displacement. The reasons for the strain hardening behaviour may be due to the transition of the pipe from the backfill to the stronger natural ground, thus giving a higher reaction onto the pipe and a different characteristic to the soil models.

8.8.3. Tensile Stress at the Back of the Pipe

It can be seen that, from the *P-y* curves in Figs 7.6, 7.11 and 7.15, the curve by the analysis ERSE-P.N.1 was in best agreement with the field test. The *P-y* curves by the Elasto-plastic model with interface elements also gave a reasonably good prediction. Moreover, the WOMOD analyses in Section 7.3.5 for the modelling of the lateral push test showed that the results of analysis ERSE-P.N.1 were marginally better than the analyses with interface elements. These *P-y* curves predicted by FE analysis, however, all under-predicted the *P-y* curve back-calculated from the field test. Despite the accuracy of the *P-y* curve from field test, the (unknown) amount of pore water pressure dissipated will have influenced the strength of the soil. This time-dependent behaviour of the soil should be investigated.

Although analysis ERSE-P.N.1, which used the no tension procedure, gave a better fit to the test data, photographs taken during the test show separation occurred between the soil and the back of the pipe. The no tension procedure, which is a simplification of the real behaviour, cannot model this separation nor any slip between the soil and the pipe surface which may occur. Therefore, a better option would be the use of interface elements to surround the pipe and between the backfill and natural ground to allow for any possible slip.

When the interface elements were used, the results of using "full tension" and "no tension" were very similar because the separation of interface elements that occurred behind the pipe has prevented the tensile stress being transferred to the soil. This is evident in the *P-y* relationships in Figs 7.11 and 7.15 and the WOMOD results in Sections 7.3.3 and 7.3.4.

The choice between using the no tension procedure and interface elements to tackle the problem of tensile stress behind the pipe is optional. Both of them give reasonably good predictions of the pipe behaviour in the WOMOD analysis. Although the results by the no tension procedure are slightly better compared with that using interface element, the use of interface elements is theoretically more sophisticated and potentially better than the no tension procedure.

8.8.4. Roughness and Limiting Adhesion of Soil / Pipe Interface

In Section 7.2.2.1, a parametric study was carried out to examine the effect of roughness and limiting adhesion of the soil/pipe interface in the 2-D FE analysis for predicting the *P-y* relationship. The results show that the roughness of the pipe could significantly affect the predicted *P-y* relationship. The limiting adhesion σ_{ntlim}, however, only affects the initial part of the *P-y* curve and once σ_{ntlim} is reached, the *P-y* curve behaves as the immediate breakaway condition. This suggests that σ_{ntlim} only affects the behaviour of the pipe at very small deflections and may be ignored, provided that σ_{ntlim} is small when compared with P_u.

8.8.5. Ovality of the Pipe

A change in the shape of the pipe was recorded during the field loading test; this will influence the stresses around it, the main effect in the 2-D FE analysis being the change in the projected area *A* used in the determination of the average soil pressure *P*. The area was found to increase during the analysis, and so the average pressure calculated assuming a

rigid pipe has been over-estimated (analyses in Sections 7.2.1, 7.2.2 and 7.2.3.1). On the other hand, the increased projected area attracted more soil reaction, thus the total soil reaction ΣR also increased (see Section 7.2.1). The net effect is dependent on the soil properties and the stiffness of the pipe cross-section. The stress controlled analyses carried out in Section 7.2.3.2, which allowed the shape of the cross-section of the pipe to change, predicted the maximum pressure being 9% greater than the displacement controlled analysis. The stress controlled analysis seems to be more realistic and makes a better prediction of the *P-y* relationship than displacement controlled analysis.

However, the stress controlled analysis is more difficult to carry out because the horizontal pressure needs to be converted into nodal forces beforehand. Moreover, all the post-processing programs to obtain the *P-y* relationship were developed based on displacement controlled analysis. It requires a lot of work to obtain the *P-y* relationship from stress controlled analysis at this moment. New post-processing programs are needed if stress controlled analysis is to be used regularly.

8.9. Elastic Beam on Elastic Foundation Analysis

From the results presented in Section 7.3.5, the agreement between the analytical and experimental results was very good for the Elasto-plastic model with the no tension procedure or interface elements and the Non-linear elastic model with interface elements. However, the pipe deflections were under-predicted at the end of the pipe even with reduced soil strength to represent a weaker soil zone. This may be due to the presence of a rigid cross-brace near the loading end which influenced the behaviour of the pipe. Experiences of other researchers at ERS show that the predictions of displacement profile by WOMOD in other cases were much better, so this may be a unique problem that occurred in the Hilderstone case only.

The WOMOD analyses carried out in this research only concerned the bending behaviour of the pipe. This assumption is true in the Hilderstone case because the lateral displacement was small compared with the diameter of the pipe, and the applied loading was perpendicular to the longitudinal axis of the pipe. However, when a very large lateral load ia applied or when the loading is not perpendicular to the longitudinal axis of the pipe, the simultaneous axial and lateral loading effects described in Section 6.7.2 must be considered. Further modifications of WOMOD to include axial springs are needed.

The elastic beam on elastic foundation approach is simple to use and cheap to run for modelling pipelines subjected to lateral loading. However, a full 3-D finite element analysis should provide better modelling of this soil/pipe interaction problem as described in Section 2.6.3.2. A more powerful computer and parallel computing techniques should allow cheaper and faster 3-D FE analysis that can be used more regularly.

8.10. The Parametric Study

The parametric study carried out in Section 7.4 has investigated the influence of three factors in the prediction of a *P-y* relationship, including the relative strength between the natural ground and the backfill, the width of the trench and the angle of the sides of the trench. The results show that P_u increases as R_c and the angle of the trench sides increases, but decreases as *W/D* increases for $R_c > 1$. On the basis of the results of the parametric study, two correction factors were suggested in Section 7.5 which can be included in the general equation (Eq. 2.19) to determine P_u, as shown in Eq. (7.2). The two correction factors F_{ch} and F_{ac}, presented as design charts, are the first attempt to include the influence of R_c, *W/D* ratio and the angle of the trench sides in the determination of P_u. Similar design charts were also suggested for the determination of y_u and vertical pipe movement.

However, several factors have not been examined in the parametric study:

i. Diameter of the pipe — while one of the main controlling parameters in the study is the *Z/D* ratio, the pipe diameter itself as an individual parameter is not directly relevant to the numerical analysis. However, in the field, there is expected to be some effect due to scaling effect (*e.g.* particle size). For a different diameter of pipe, especially small diameter pipe, the behaviour may be different, but the effect is likely to be small.

ii. Burial depth to pipe diameter ratio (*Z/D*)— the parametric study was based on the Hilderstone case in which the pipe has a diameter of 0.9144m (36 inches) and a burial depth of 1.3572m. The study was therefore based on one *Z/D* ratio only. The applicability of the correction factors to different *Z/D* ratios should be investigated, but the existing results are accurate enough for practical purposes. Moreover, it is desirable to carry out a set of parametric studies with $R_c = 1$ and angle of trench sides = 90° but with different *Z/D* ratios to determine a relationship of the basic capacity factor, which can be used to compare with other empirical methods for obtaining N_{ch} (*e.g.* Figs 2.27 and 2.30).

iii. Depth of the lower boundary of the FE mesh — due to the existence of a stiff clay stratum in the Hilderstone case, the lower boundary of the FE mesh was fixed at a relatively shallow depth. Generally, the lower boundary should be placed as far as possible to reduce the boundary effect. This shallow lower boundary can influence the vertical pipe movement, thus P_u and y_u, but the effect should be very small.

iv. Frictional soil — the parametric study was based on cohesive soil and undrained conditions, and another set of correction factors would be needed for frictional (granular) soil and drained conditions.

v. Stiffness of the soil — similar to (i), the parametric study was based on one soil stiffness only. Different stiffnesses will influence the initial slope of the predicted *P-y* curves, but not the value of P_u. Stiffer soils should have smaller y_u, and softer soils have larger y_u.

The above factors should be investigated by further parametric studies with more general site conditions to refine the method.

8.11. The Empirical Methods to Predict *P-y* Curve

The construction of a non-linear *P-y* curve requires three pieces of information: the value of P_u, y_u and a non-linear function to describe the locus of the *P-y* relationship. In Section 7.5, comparisons were made with several empirical methods to obtain the three components.

The empirical methods for obtaining P_u, however, all failed to take into account the existence of the backfill trench. The correction factors presented in Section 7.5 have to be used in conjunction with the empirical methods in order to account for the backfill trench. It can be seen that, from Fig. 7.49, a P_u value predicted by the original empirical methods can be three times less than the present extended method, depending on the geometry of the trench and the strength of the soils. It has been shown that the Hansen bearing capacity factor (Fig. 2.27), together with Eq. (7.2) give the best agreement with the P_u value from the field test (Table 7.3). However, it may be useful to carry out the parametric study described in the previous section to check the validity of the Hansen bearing capacity factor for different *Z/D* ratios.

The empirical methods under-predicted the actual y_u in the Hilderstone case because they fail to take into account the existence of the backfill trench, as shown in Section 7.5. On the other hand, the prediction of y_u by the suggested relationships in Figs 7.51 and 7.52, based on the parametric study in Section 7.4, gave much better agreement with the field test and should be used instead of the empirical methods.

The hyperbolic formulations by Audibert & Nyman (1977) and Trautmann & O'Rourke (1985) gave reasonably good fits to the field data (Fig. 3.15), the results of the parametric

study (Fig. 7.48) and the results of the 2-D FE analyses in Section 7.2 (Fig. 7.54). The *P-y* curves by the two formulations are very similar, both of them or the mean curve of the two (Eq. 7.3) can be used in practice. However, Figs 3.15, 7.48 and 7.54 all show that the two hyperbolic formulations under-predicted the initial slope of the data. Attempts were made to adjust the two constants in Eq. (7.3) to fit the data better at the initial part of Fig. 7.48, but then the middle and final parts of the curve gave poor agreement to the data. From experience, when a pipeline is close to failure, the adjacent soil can be expected to be close to failure, *i.e.* at the final part of the *P-y* curve. Therefore, it is more sensible to have accurate middle and final parts of the *P-y* curve rather than the initial part. Another type of non-linear formulation is needed to fit the data better, especially at the initial part.

8.12. Practical Implications of the Research

The present research ties in with the on going research of soil/pipe interaction within the gas industry. The numerical methods presented can be used by researchers to improve the understanding of pipeline response to lateral and axial ground loading, and will assist in the prediction of the behaviour of pipelines due to external loading in a more rigorous manner. The extended empirical methods for predicting the *P-y* curve in Section 7.5 can be used by practising engineers in routine design work on steel pipes and other metallic pipes (*e.g.* cast iron). Applicability of the results to non-metallic pipes (*e.g.* plastic) needs support by further research. It should be noted that this research work has concentrated on the undrained behaviour of clay soils. The findings are therefore applicable to fairly short term loading problems. The results of this research could help engineers to achieve a better design of pipeline and more accurate risk analysis to avoid distortion or failure of pipelines, thus to assist in achieving optimum integrity and safe operation of the present and future buried pipeline system.

CHAPTER 9

CONCLUSIONS AND SUGGESTIONS FOR FUTURE WORK

9.1. Conclusions

This research study deals with the behaviour of buried pipelines subjected to external loading. Numerical methods have been developed to model the response of pipeline under axial and lateral loadings. Based on the parametric study using a 2-D FE model, a set of design charts has been developed for practising engineers to predict the pressure-displacement relationship of a laterally loaded pipeline.

From the work presented in the previous Chapters, the following main conclusions are drawn:

i. The two stage method of analysis used in this research has been shown to be valid and gives good results for predicting the behaviour of buried pipes subjected to external loading such as differential ground movement.

ii. Soil restraint to a buried pipeline can be predicted by suitable modelling with the finite element method.

iii. The results of analyses using the British Gas Elasto-plastic models, and incorporating interface elements or the no tension procedure, give closest agreement with the experimental results.

iv. The modified interface element can be used to model the separation and slip between the soil and the pipe surface. It is theoretically more sophisticated than the no tension procedure in tackling the problem of tensile stress behind the pipe, although the results using the no tension procedure were closer to the field results then those produced using the interface element.

v. The change in the shape of the pipe cross-section during the FE analysis can affect the prediction of the pressure-displacement relationship of the pipe. A stress controlled analysis can be used instead of a displacement controlled analysis to take into account this factor but post-processing programs will have to be developed to obtain a *P-y* relationship from stress controlled analysis.

vi. The Elastic-perfectly plastic and Modified Cam clay models are only suitable for modelling fully saturated soil. For unsaturated soil, the British Gas Elasto-plastic model or the British Gas Non-linear elastic model should be used.

vii. The elastic beam on elastic foundation program has been modified to improve the modelling of the pipe in which plastic behaviour of the pipe, change in shape of the cross-section and shear deformation have been implemented. Results show that these effects did not significantly affect the bending behaviour of the Hilderstone pipeline.

viii. A 2-D FE model, capable of modelling the axial behaviour of a pipeline subjected to axial loading, has been developed and shown to give good prediction of the axial push test.

ix. A parametric study has investigated the influence of several factors in the prediction of the *P-y* relationship, including the relative strength between the natural ground and the backfill, the width of the trench and the angle of the sides of the trench. Extended empirical methods based on this parametric study can be used by practising engineers in routine design work to predict a *P-y* relationship quickly. Design charts relating

the ultimate horizontal pressure, ultimate horizontal displacement and vertical upward displacement of a laterally loaded pipeline to the relative strength between the natural ground and the backfill, the width of the trench and the angle of the sides of the trench were presented. These are relevant to undrained behaviour of soil and the vertical displacement of the pipe is only constrained by the soil.

9.2. Suggestions for Future Work

This thesis provides data which for practical purposes are sufficiently accurate to be used directly in the solution of engineering problems. However, from a research perspective, there are several matters which require further research, namely:

i. The stress-strain relationships to describe the behaviour of the CRISP90 interface element (linear elastic for normal behaviour and bilinear elastic-perfectly plastic for shear behaviour) should be improved by using more sophisticated non-linear stress-strain relationships.

ii. Improve the proposed 2-D model for the modelling of the axial push test by using an average backfill thickness and two layers of interface element as described in Section 8.6, and carry out a full 3-D finite element analysis to examine the accuracy of the proposed 2-D model.

iii. The elastic beam on elastic foundation program WOMOD should be improved by implementing the post-yield behaviour of the pipe, the coupled shear deformation and large displacement effect. The axial springs should be added into the program to model combined axial and lateral loadings.

iv. A post-processing program should be developed for obtaining *P-y* relationships from stress controlled analysis.

v. The time-dependent behaviour of the soil should be investigated in the 2-D FE analysis for predicting the *P-y* relationship.

vi. A more detailed parametric study should be carried out to investigate the influence of the following factors in the prediction of *P-y* relationship by 2-D finite element analysis:

- Diameter of the pipe
- Burial depth of the pipe
- Width of the trench
- Relative strength between the natural ground and the backfill
- Initial stiffness of the soils
- Angle of the sides of the trench
- Depth of the lower rigid boundary

These factors should be investigated systematically to examine whether the design charts for determining P_u, y_u and vertical pipe movement presented in Section 7 5 are valid for the different site conditions stated above. If necessary, based on the new parametric study, the relationships to predict the *P-y* curve should be revised

vii. Carry out a programme of full scale pipe loading tests in controlled conditions, including (according to priority) relative strengths between the natural ground and the backfill, trench widths, burial depths, different pipe diameters, initial stiffness of the soils, angles of the trench sides and depths of the lower rigid boundary, to act as benchmarks to examine the validity of the suggested design charts in Section 7.5 in the prediction of ultimate horizontal pressure, ultimate horizontal displacement, vertical upward displacement and the shape of the non-linear load-displacement curve of laterally loaded pipelines. The instrumentation for these tests should be better than in the Hilderstone case, *i.e.* more strain gauges near the loading area, measurement of vertical displacement and ovality of the pipe cross-section.

viii. Carry out full 3-D FE analyses to investigate the effects of the existence of a backfill trench on the behaviour of laterally loaded pipeline and act as a benchmark, similar to the above mentioned full scale pipe loading tests, to examine the effectiveness of the two stage analysis technique.

REFERENCES

Ali, S. R. (1993a). *Numerical Modelling of Unsaturated Soils at Low Stress Levels*, PhD Thesis, University of Sheffield.

Ali, S. R. (1993b). *A Stress-Strain Model for Loose Granular Soil*, British Gas Engineering Research Station, internal report R.5042 (confidential and restricted to British Gas).

Allgood, J. R., Ciani, J. B. & Lew, T. K. (1968). The influence of soil modulus on the behaviour of cylinders in sand. Paper at *47th Annual Meeting Highway Research Board*, Washington, DC. Also Tech. report R-582 Naval Civil Engineering Lab., Port Hueneme, California, USA.

Alonso, E. E., Gens, A. & Josa, A. (1990). A constitutive model for partially saturated soils. *Géotechnique*, Vol. 40, No. 3, pp. 405–430.

Anagnostopoulous, C. & Georgiadis, M. (1993). Interaction of axial and lateral pile responses. *Journal of Geotechnical Engineering*, ASCE, Vol. 119, No. 4, pp. 793–799.

Atkinson, J. H. & Bransby, P. L. (1978) *The Mechanics of Soils, An Introduction to Critical State Soil Mechanics*, McGraw-Hill.

Attwell, P. B. & Woodman, J. P. (1982). Predicting the dynamic of ground settlement and its derivatives caused by tunnelling in soil. *Ground Engineering*, Vol. 15, No. 8, November, pp. 13–23, 36.

Audibert, J. M. E. & Nyman, K. J. (1977). Soil restraint against horizontal motion of pipes. *Journal of Geotechnical Engineering*, ASCE, Vol. 103, No. GT10, pp. 1119–1142.

ASCE (1984). *Guidelines for the Seismic Design of Oil and Gas Pipeline Systems*, Committee on Gas and Liquid Fuel Lifelines, ASCE.

Barenberg, M. (1988). Correlation of pipeline damage with ground motions. *Journal of Geotechnical Engineering*, ASCE, Vol. 114, No. 6, pp. 706–711.

Beer, G. (1985). An isoparametric joint/interface element for finite element analysis. *Int. J. Num. Methods Eng.*, Vol. 21, pp. 585–600.

Bickel, J. O. & Kuesel, T. R. (Editors) (1982). *Tunnel Engineering Handbook*, Van Nostrand Reinhold Company.

Bolzoni, G., Cuscunà, S. & Perego, U. (1993). Physical and mathematical modelling of pipeline behaviour in landslide areas. *9th PRC/EPRG Biennial Joint Technical Meeting on Line Pipe Research*, 11–14 May, Houston, Texas, paper No. 5.

Booth, J. (1991). *Numerical Prediction of Soil Restraint to Pipe Movement*, BEng project report, Dept. of Mechanical Eng., Newcastle-upon-Tyne Polytechnic.

British Gas (1994). *Soil/Pipe Interaction Relationships*, British Gas Engineering Research Station, ERSM89.

Britto, A. M. & Gunn, M. J. (1990). *CRISP90, User's and Programmer's Guide*, Vol. 1, Cambridge University.

Brown, D. A. & Shie, C. F. (1990). Three dimensional finite element model of laterally loaded piles. *Computer and Geotechnics*, Vol. 10, No. 1, pp. 59–79.

Brown, D. A. & Shie, C. F. (1991). Some numerical experiments with a three dimensional finite element model of laterally loaded piles. *Computer and Geotechnics*, Vol. 12, No. 2, pp. 149–162.

Carder, D. R. & Taylor, M. E. (1983). *Response of a Pipeline to Nearby Deep Trenching in Boulder Clay*, Department of the Environment, Department of Transport, Transport and Road Research Laboratory, report LR1099.

Carder, D. R., Taylor, M. E. & Pocock, R. G. (1982). *Response of a Pipeline to Ground Movements Caused by Trenching in Compressible Alluvium*, Department of the Environment, Department of Transport, Transport and Road Research Laboratory, report LR1047.

Chard, B. M. & Symons, I. F. (1982). *Trial Trench Construction in London Clay: A Ground Movement Study at Bracknell*, Department of the Environment, Department of Transport, Transport and Road Research Laboratory, report LR1051.

Chard, B. M., Symons, I. F., Toombs, A. F. & Nagarkatti, A. S. (1983). *Trial Trench Construction in Alluvium: A Ground Movement Study at Avonmouth*, Department of the Environment, Department of Transport, Transport and Road Research Laboratory, report LR1077.

Chen, L. & Poulos, H. G. (1993). Analysis of pile-soil interaction under lateral loading using infinite and finite element. *Computer and Geotechnics*, Vol. 15, No. 4, pp. 189–220.

Cheney, J. A. (1976). *Buckling of Thin-Walled Cylindrical Shells in Soil*, Department of the Environment, Department of Transport, Transport and Road Research Laboratory, TRRL Supplementary report 204.

Cheney, J. A. (1991). Local buckling of tubes in elastic continuum. *Journal of Engineering Mechanics*, ASCE, Vol. 117, No. 1, pp. 205–217.

Cheung, Y. K., Lee, P. K. K. & Zhao, W. B. (1991). Elastoplastic analysis of soil-pile interaction. *Computer and Geotechnics*, Vol. 12, No. 2, pp. 115–132.

Chua, K. M. & Lytton, R. L. (1989). Viscoelastic approach to modelling performance of buried pipes. *Journal of Transportation Engineering*, ASCE, Vol. 115, No. 3, pp. 253–269.

Clough, G. W. & Duncan, J. M. (1971). Finite element analysis of retaining wall behaviour. *Journal of the Soil Mechanics and Foundations Division*, ASCE, Vol. 97, No. SM12, pp. 1657–1673.

Craig, R. F. (1992). *Soil Mechanics*, 5th edition, Chapman & Hall.

Crofts, J. E., Menzies, B. K. & Tarzi, A. I. (1977). Lateral displacement of shallow buried pipelines due to adjacent deep trench excavations. *Géotechnique*, Vol. 27, No. 2, pp. 161–179.

Desai, C. S. (1977). Soil-structure interaction and simulation problems. In *Finite Element in Geomechanics*, ed. Gudehus, G., Ch. 7, pp. 209–250, Wiley, Chichester.

Desai, C. S. (1982). Constitutive modelling and soil-structure interaction. In *Numerical Methods in Geomechanics*, ed. Martins, J. B., pp. 103–143, D. Reidel Publishing Company.

Desai, C. S. & Nagaraj, B. K. (1988). Modelling for cyclic normal and shear behaviour of interfaces. *Journal of Engineering Mechanics*, ASCE, Vol. 114, No. 7, pp. 1198–1217.

Desai, C. S., Drumm, E. C. & Zaman, M. M. (1985). Cyclic testing and modelling of interfaces. *Journal of Geotechnical Engineering*, ASCE, Vol. 111, No. 6, pp. 793–815.

Desai, C. S., Zaman, M. M., Lightner, J. G. & Siriwardane, H. J. (1984). Thin-layer element for interfaces and joints. *International Journal for Numerical and Analytical Methods in Geomechanics*, Vol. 8, No. 1, pp. 19–43.

Dickin, E. A. (1988). Stress-displacement of buried plates and pipes. *Centrifuge 88*, ed. Corté J. F., Balkema Press, Rotterdam, pp. 205–214.

Dunnavant, T. W. & O'Neill, M. W. (1989). Experimental *p-y* model for submerged stiff clay. *Journal of Geotechnical Engineering*, ASCE, Vol. 115, No. 1, pp. 95–114.

Fearnehough, G. & Middleton, E. (1992). Pipelines take the strain. *R&D Digest*, Issue No. 11, pp. 26–29, British Gas plc, Research and Technology.

Ford, H. & Alexander, J. M. (1977). *Advanced Mechanics of Materials*, 2nd edition, Ellis Horwood.

Gabr, M. A., Lunne, T. & Powell, J. J. (1994). *P-y* analysis of laterally loaded piles in clay using DMT. *Journal of Geotechnical Engineering*, ASCE, Vol. 120, No. 5, pp. 816–837.

Georgiadis, M., Anagnostopoulous, C. & Saflekon, S. (1992). Centrifugal testing of laterally loaded piles in sand. *Canadian Geotechnical Journal*, Vol. 29, No. 2, pp. 208–216.

Georgiadis, M. & Butterfield, R. (1982). Laterally loaded pile behaviour. *Journal of Geotechnical Engineering*, ASCE, Vol. 108, No. 1, pp. 155–165.

Gere, J. M. & Timoshenko, S. P. (1990). *Mechanics of Materials*, 3rd edition, PWS-KENT Publishing Company.

Ghaboussi, J., Wilson, E. L. & Isenberg, J. (1973). Finite element for rock joints and interfaces. *Journal of the Soil Mechanics and Foundations Division,* ASCE, Vol. 99, No. SM10, pp. 833–848.

Gilpin, R. R. (1980). A model for the prediction of ice lensing and frost heave in soils. *Water Resources Research,* Vol. 16, No. 5, pp. 918–930.

Goodman R. E., Taylor, R. L. & Brekke, T. L. (1968). A model for the mechanics of jointed rock. *Journal of the Soil Mechanics and Foundations Division,* ASCE, Vol. 94, No. SM3, pp. 637–659.

Goodwin, A. K. (1991). *One Dimensional Compression Behaviour of Unsaturated Granular Soil at Low Stress Levels*, PhD Thesis, University of Sheffield.

Griffiths, D. V. (1985). Numerical modelling of interfaces using conventional finite elements. *5th International Conference on Numerical Methods in Geomechanics,* Nagoya, Vol. 2, pp. 873–844.

Griffiths, D. V. (1987). Numerical studies of soil-structure interaction using a simple interface model. *Canadian Geotechnical Journal*, Vol. 25, No. 1, pp. 158–162.

Gumbel, J. E. & Wilson, J. (1981). Interactive design of buried flexible pipes – a fresh approach from basic principles, *Ground Engineering*, Vol. 14, No. 4, pp. 158–162.

Habibagahi, K. & Langer, J. A. (1984). Horizontal subgrade modulus of granular soils. *Laterally Loaded Deep Foundations: Analysis and Performance*, ASTM STP835, Langer, J. A., Mosley, E. T. & Thompson, C. D. Eds., ASTM, pp. 21–34.

Hansen, J. B. (1961). The ultimate resistance of rigid piles against transversal forces. *Bulletin 12*, Danish Geotechnical Institute, Copenhagen, Denmark.

Hetényi, M. (1946). *Beams on Elastic Foundation*, Ann Arbor: The University of Michigan Press.

Herbert, R. & Leach, G. (1990). *Damage Control Procedures for Distribution Mains.* Presented at the 56th Autumn meeting of The Institution of Gas Engineers, London, 27 November 1990. IGE Communication No. 1437, British Gas plc, E748.

Hird, C. C. & Russell, D. (1990). A benchmark for soil-structure interface elements. *Computer and Geotechnics*, Vol. 10, No. 2, pp. 139–147.

Hohberg, J. M. & Bachmann, H. (1988). A macro joint element for non-linear arch dam analysis. *Proc. of the 6th International Conference on Numerical Method in Geomechanics,* Innsbruck, ed. Swobda, G., Vol. 2, pp. 829–834.

Hucka, V. J., Blair, C. K. & Kimball, E. P. (1986). Mine subsidence effects on a pressurized natural gas pipeline. *American Institute of Mining, Metallurgical and Petroleum Engineers, Transactions*, Vol. 280, Part A, pp. 980–984.

Janbu, N., Bjerrum, L. & Kjaernsli, B. (1956). *Veiledning Ved Losning av Fundamenteringsoppgaver*, NGI Publication No. 16.

Jewell, R. A. (1991). Application of revised design charts for steep reinforced slopes. *Geotextiles and Geomembranes*, Vol. 10, No. 3, pp. 203–233.

Kennedy, R. P., Chow, A. W. & Williamson, R. A. (1977). Fault movement effects on buried oil pipeline. *Transportation Engineering Journal*, ASCE, Vol. 103, No. TE5, pp. 617–633.

King, P. J., Clegg, G. T. & Walters, W. J. (1977). *Report of the Inquiry into Serious Gas Explosions*, Department of Engergy, HMSO.

Koike, T., Imai, T. & Kaneko, T. (1992). Large deformation analysis of buried pipelines. *Proceedings of the Tenth World Conference on Earthquake Engineering*, 19–24 July, Madrid, Spain, Vol. 9, pp. 5443–5448.

Kooijman, A. P. & Vermeer, P. A. (1988). Elastoplastic analysis of laterally loaded piles. *Proc. of the 6th International Conference on Numerical Method in Geomechanics*, Innsbruck, ed. Swobda, G., Vol. 2, pp. 1033–1042.

Kwok, C. M. (1987). *Reinforced Embankments on Soft Ground*. PhD Thesis, University of Sheffield.

Kyrou, K. & Kalteziotis, N. A. (1985). The effect of trenching on adjacent pipelines. *Proceedings of the 11th International Conference on Soil Mechanics and Foundation Engineering*, San Francisco, Vol. 3, pp. 1657–1660.

Lambe, T. W. (1967). Stress path method. *Journal of the Soil Mechanics and Foundations Division*, ASCE, Vol. 93, No. SM6, pp. 309–331.

Lane, P. A. & Griffiths, D. V. (1988). Computation of the ultimate pressure of a laterally loaded circular pile in frictional soil. *Proc. of the 6th International Conference on Numerical Method in Geomechanics*, Innsbruck, ed. Swobda, G., Vol. 2, pp. 1025–1031.

Leach, G. (1986). *Soil Testing for Stress Analysis of Backfill Materials*, British Gas Engineering Research Station, internal report R.3418 (confidential and restricted to British Gas).

Leach, G. & Row, S. A. (1991). *Geotechnical Site Investigation on Alrewas-Audley Pipeline Near Hilderstone, Staffordshire*, British Gas Engineering Research Station, internal report R.4258 (confidential and restricted to British Gas).

Lee, K. M., Rowe, R. K. & Lo, K. Y. (1992). Subsidence owing to tunnelling, I. Estimating the gap parameter. *Canadian Geotechnical Journal*, Vol. 29, No. 6, pp. 924–940.

Marshall, W. T. & Nelson, H. M. (1990). *Structures*, 3rd edition, revised by Bhatt, P. & Nelson, H. M., Longman.

Matlock, H. (1970). Correlation for design of laterally loaded piles in soft clay. *Proc. 2nd Annu. Offshore Technol. Conf.*, Am. Inst. of Min., Metallurgy, and Pet. Eng., Houston, Tex., pp. 577–594.

Mercer, W. L. (1987). *Soil/Pipe Interaction Research at the Engineering Research Station*, Note on the major policy review of fundamental and speculative work, British Gas plc (confidential and restricted to British Gas).

Middleton, E., Carvill, H. C. & Johnson, G. M. (1990). *Permissible Stress Level in a Transmission Pipeline to Withstand Localised Buckling Resulting from Mining Subsidence*. British Gas Engineering Research Station, internal report R.4318 (confidential and restricted to British Gas).

Middleton, E. & Henderson, M. J. (1994). *A Tale of Two Faults*. Presented at the Pembroke Room, Helmont House, 20 October 1994. British Gas Wales.

Moore, I. D. (1988). Buckling of buried flexible structures of noncircular shape. *Proc. of the 6th International Conference on Numerical Method in Geomechanics*, Innsbruck, ed. Swobda, G., Vol. 2, pp. 1079–1084.

Nath, P. (1983). Trench excavation effects on adjacent buried pipes: finite element study. *Journal of Geotechnical Engineering*, ASCE, Vol. 109, No. 11, pp. 1399–1415.

Nath, P. (1987). *Analysis and Design of Buried Pipelines: a New Approach*. British Gas Engineering Research Station, internal report R.3790 (confidential and restricted to British Gas).

National Coal Board, (1975). *Subsidence Engineer's Handbook*, NCB, Mining Department, London.

Needham, D. & Leach, G. (1987). *Soil/Pipe Interaction*. British Gas Engineering Research Station, internal report R.3735 (confidential and restricted to British Gas).

Newmark, N. M. & Hall, W. J. (1975). Pipeline design to resist large fault displacements. *Proceedings of the US National Conference on Earthquake Engineering*, Ann Arbor, Michigan. Published by Earthquake Engineering Research Institute.

Ng, C. F. (1993). *Soil Restraint Calculation for Alrewas-Audley Pipeline at Hilderstone*. British Gas Engineering Research Station, internal report R.5072 (confidential and restricted to British Gas).

Ng, C. F. (1994). *Modification and Testing of the Standard Interface Element in CRISP90*. British Gas Engineering Research Station, internal report R.5271, May 1994 (confidential and restricted to British Gas).

Ng, C. F., Pyrah, I. C. & Anderson, W. F. (1994). Lateral soil restraint of a buried pipeline. *Proceedings of the Third European Conference on Numerical Methods in Geotechnical Engineering*, 7–9 September, Manchester, UK, ed. Smith, I. M., pp. 215–220.

Nixon, J. F. (1987). Ground freezing and frost heave. A review. *Northern Engineer*, Vol. 19, No. 3 and 4, pp. 8–18.

Nixon, J. F. (1992). Discrete ice lens theory for frost heave beneath pipelines. *Canadian Geotechnical Journal*, Vol. 29, No. 3, pp. 489–497.

Nyman, K. J. (1982). Soil response against the horizontal-vertical motion of pipes. Preprint 82-534, presented at ASCE National Convention, New Orleans, Louisiana, USA.

Nyman, K. J. (1984). Soil response against oblique motion of pipes. *Journal of Transportation Engineering*, ASCE, Vol. 110, No. 2, pp. 190–202.

O'Reilly, M. P. & New, B. M. (1982). Settlements above tunnels in the United Kingdom – their magnitude and prediction. *Proc. of Tunnelling '82*, Inst. of Mining and Metallurgy, London, pp. 173–181.

O'Rourke, M. & Ayala, G. (1993). Pipeline damage due to wave propagation. *Journal of Geotechnical Engineering*, ASCE, Vol. 119, No. 9, pp. 1490–1498.

O'Rourke, M. & Nordberg, C. (1992). Behaviour of buried pipelines subjected to permanent ground deformation. *Proceedings of the Tenth World Conference on Earthquake Engineering*, 19–24 July, Madrid, Spain, Vol. 9, pp. 5411–5416.

O'Rourke, T. D. (1978). Discussion of lateral displacement of shallow buried pipelines due to adjacent deep trench excavations (Crofts, J. E., Menzies, B. K. & Tarzi, A. I., 1977). *Géotechnique*, Vol. 28, No. 2, pp. 214–216.

O'Rourke, T. D. & Tawfik, M. S. (1987). *Large Ground Movement Effects On High Pressure Pipelines.* Geotechnical engineering report 87-1, Cornell University, Ithaca, New York, USA. Prepared for Consolidated Edison Company of New York, Inc.

Ovesen, N. K. & Stromann, H. (1972). Design method for vertical anchor slabs in sand. *Proc. Spec. Conf. on Performance of Earth and Earth Supported Structures*, USA, Vol. 1-2, pp. 1418–1500.

Palmer, L. A. & Thompson, J. B. (1948). The earth pressure and deflection along the embedded lengths of piles subjected to lateral thrusts. *Proceedings of the 2nd International Conference on Soil Mechanics and Foundation Engineering*, Rotterdam, Vol. 5, pp. 156–161.

Pande, G. N. & Sharma, K. G. (1979). On joint/interface elements and associated problems of numerical ill-conditioning. *International Journal for Numerical and Analytical Methods in Geomechanics*, Vol. 3, No. 1, pp. 293–300.

PDA Engineering (1989). *Patran Plus User Manuals*, Volumes 1 and 2 , PDA Engineering.

Poulos, H. G. & Davis, E. H. (1980). *Pile Foundation Analysis and Design*, John Wiley & Sons.

Prinja, N. K. & Clegg, R. A. (1993). Assembly benchmark tests for 3-D beams and shells exhibiting geometric non-linear behaviour. *Benchmark*, June 1993, pp. 16–22, NAFEMS.

Puswewala, U. G. A., Rajapakse, R. K. N. D., Domaschuk, L. & Shields, D. H. (1993). Creep response of laterally loaded piles in ice and permafrost. *Géotechnique*, Vol. 43, No. 2, pp. 223–240.

Pyke, R. & Beikae, M. (1984). A new solution for the resistance of single piles to lateral loading. *Laterally Loaded Deep Foundations: Analysis and Performance*, ASTM STP835, Langer, J. A., Mosley, E. T. & Thompson, C. D. Eds., ASTM, pp. 3–20.

Rajani, B. & Morgenstern, N. (1992). Behaviour of a semi-infinite beam in a creeping medium. *Canadian Geotechnical Journal*, Vol. 29, No. 5, pp. 779–788.

Rajani, B. & Morgenstern, N. (1993). Pipelines and laterally loaded piles in elastoplastic medium. *Journal of Geotechnical Engineering*, ASCE, Vol. 119, No. 9, pp. 1431–1448.

Rajani, B. B., Robertson, P. K. & Morgenstern, N. R. (1993). A simplified design method for pipelines subject to transverse soil movements. *Proceedings of the 12th International Conference on Offshore Mechanics and Arctic Engineering*, Vol. 5, pp. 157–165.

Randolph, M. F. & Houlsby, G. T. (1984). The limiting pressure on a circular pile loaded laterally in cohesive soil. *Géotechnique*, Vol. 34, No. 4, pp. 613–623.

Reese, L. C. (1958). Discussion of Soil modulus for laterally loaded piles by McClelland, B. & Focht, J. A. *Transactions*, ASCE, Vol. 123, Part VII, pp. 1071–1074.

Regan, T. (1982). *Fractures in Water Mains – The Effect of Longitudinal Bending*. PhD Thesis, City University, London.

Rizkalla, M., Poorooshasb, F. & Clark, J. I. (1992). Centrifuge modelling of lateral pipeline/soil interaction. *11th Offshore Mechanics and Arctic Engineering Conference (OMAE)*, 7–11 June, Calgary, Alberta, Canada.

Rogers, C. D. F. & O'Reilly, M. P. (1991). Ground movements associated with pipe installation and tunnelling. Proceedings of the *10th European Conference on Soil Mechanics and Foundation Engineering*, 26–30 May 1991, Florence, Italy, Vol. 2, pp. 907–910.

Roscoe, K. H. & Burland, J. B. (1968). On the generalised stress-strain behaviour of 'wet' clay, in *Engineering Plasticity*, eds. Heyman, J. & Leckie, F. A., Cambridge University Press, pp. 535–609.

Rowe, R. K. & Davis, E. H. (1982a). The behaviour of anchor plates in clay. *Géotechnique*, Vol. 32, No. 1, pp. 9–23.

Rowe, R. K. & Davis, E. H. (1982b). The behaviour of anchor plates in sand. *Géotechnique*, Vol. 32, No. 1, pp. 25–41.

Rowe, R. K. & Lee, K. M. (1992). Subsidence owing to tunnelling, II. Evaluation of a prediction technique. *Canadian Geotechnical Journal*, Vol. 29, No. 6, pp. 941–954.

Rowe, R. K., Lo, K. Y. & Kack, G. J. (1983). A method of estimating surface settlement above tunnels constructed in soft ground. *Canadian Geotechnical Journal*, Vol. 20, No. 1, pp. 11–22.

Ruffier, A. P. & Mahler, C. F. (1988). Finite element analysis of deep foundations subjected to uplift loading. *Proc. of the 6th International Conference on Numerical Method in Geomechanics*, Innsbruck, ed. Swobda, G., Vol. 2, pp. 1115–1120.

Russell, D. (1992a). *Finite Element Analysis of Embankments on Soft Ground Incorporating Reinforcement and Drains*, PhD Thesis, University of Sheffield.

Russell, D. (1992b). *DRCRISP User's Manual*, internal report, University of Sheffield.

Sagaseta, C. (1987). Analysis of undrained soil deformation due to ground loss. *Géotechnique*, Vol. 37, pp. 301–320.

Schofield, A. N. & Wroth, C. P. (1968). *Critical State Soil Mechanics*, McGraw-Hill.

Schweiger, H. F. & Hass, W. (1988). Application of the thin-layer interface element to geotechnical problems. *Proc. of the 6th International Conference on Numerical Method in Geomechanics*, Innsbruck, ed. Swobda, G., Vol. 2, pp. 907–912.

Sekiguchi, K., Rowe, R. K., Lo, K. Y. & Ogawa, T. (1992). Hoop tension analysis of a steel cell using optimization method for psendo-viscoplastic parameters. *Soil and Foundations*, JSSMFE, Vol. 32, No. 3, pp. 1–4.

Selvadurai, A. P. S. (1988). Mechanics of soil-pipeline interaction. *Proc. of the Annual Conference of The Canadian Society for Civil Engineering*, Vol. 3, pp. 151–173.

Selvadurai, A. P. S. & Pang, S. (1988). Non-linear effects in soil-pipeline interaction in a ground subsidence zone. *Proc. of the 6th International Conference on Numerical Method in Geomechanics*, Innsbruck, ed. Swobda, G., Vol. 2, pp. 1085–1094.

Spangler, M. G. (1956). Stresses in pressure pipelines and protective casing pipes. *Journal of Structural Division*, ASCE, Vol. 82, No. ST5, Proc. paper 1054.

Symons, I. F. (1978). Discussion of lateral displacement of shallow buried pipelines due to adjacent deep trench excavations (Crofts, J. E., Menzies, B. K. & Tarzi, A. I., 1977). *Géotechnique*, Vol. 28, No. 2, pp. 212–214.

Symons, I. F. (1980). Ground movements and their influence on shallow buried pipes. *The Public Health Engineer*, Vol. 8, No. 4, October 1980, pp. 149–153, 172.

Symons, I. F., Chard, B. & Carder, D. R. (1981). Ground movements caused by deep trench excavation. *Repair of Sewerage Systems*, ICE, London, pp. 73–100.

Terzaghi, K. (1955). Evaluation of the coefficients of subgrade reaction. *Géotechnique*, Vol. 4, pp. 287–326.

Thomas, H. O. (1978). Discussion of Soil restraint against horizontal motion of pipes (Audibert, J. M. E. & Nyman, K. J., 1977). *Journal of Geotechnical Engineering,* ASCE, Vol. 104, No. GT9, pp. 1214–1216.

Timoshenko, S. P. (1955). *Strength of Materials,* Part I, 3rd edition, D. Van Nostrand Company.

Timoshenko, S. P. & Goodier, J. N. (1970). *Theory of Elasticity,* 3rd edition, McGraw-Hill.

Tomlinson, M. J. (1957). The adhesion of piles driven into clay soils. *Proc. of the 4th International Conference on Soil Mechanics and Foundation Engineering,* London, UK, Vol. 2, pp. 66–71.

Toombs, A. F., McCaul, C. & Symons, I. F. (1982). *Ground Movement Caused by Deep Trench Construction in an Urban Area,* Department of the Environment, Department of Transport, Transport and Road Research Laboratory, report LR1040.

Trautmann, C. H. & O'Rourke, T. D. (1985). Lateral force-displacement response of buried pipe. *Journal of Geotechnical Engineering,* ASCE, Vol. 111, No. 9, pp. 1077–1092.

Trautmann, C. H., O'Rourke, T. D. & Kulhawy, F. H. (1985). Uplift force-displacement response of buried pipe. *Journal of Geotechnical Engineering,* ASCE, Vol. 111, No. 9, pp. 1061–1076.

Trigg, A. & Rizkalla, M. (1994). Development and application of a closed form technique for the preliminary assessment of pipeline integrity in unstable slopes. *Proceedings of the 13th International Conference on Offshore Mechanics and Arctic Engineering,* Vol. 5, pp. 127–139.

Vesic, A. B. (1961). Beams on elastic subgrade and Winkler's hypothesis. *Proc. of the 5th International Conference on Soil Mechanics and Foundation Engineering,* Paris, pp. 845–850.

Vougioukas, E. A. & Carydis, P. G. (1992). Performance of buried pipelines, subjected to fault movement. *Proceedings of the Tenth World Conference on Earthquake Engineering,* 19–24 July, Madrid, Spain, Vol. 9, pp. 5449–5452.

Wang, B. & Garga, V. K. (1993). A numerical method for modelling large displacements of jointed rocks. I. Fundamentals. *Canadian Geotechnical Journal,* Vol. 30, No 1, pp. 96–108.

Wang, L. R. L. & Yeh, Y. H. (1985). A refined seismic analysis and design of buried pipeline for fault movement. *Earthquake Engineering and Structural Dynamics,* Vol. 13, pp. 75–96.

Werner, H., Bellmann, J., Niedermeyer, S., Bauer, H. & Rahn, W. (1988). A comprehensive numerical model of rock joints and it implementation in a finite element model. *Proc. of the 6th International Conference on Numerical Method in Geomechanics,* Innsbruck, ed. Swobda, G., Vol. 2, pp. 841–848.

Williams, P. J. (1986). *Pipelines and Permafrost: Science in a Cold Climate*, Carleton University Press.

Wilson, E. L. (1977). Finite elements for foundations, joint and fluids. In *Finite Element in Geomechanics*, ed. Gudehus, G., Ch. 10, pp. 319–350, Wiley, Chichester.

Wilson-Fahmy, R. F., Koerner, R. M. & Sansone, L. J. (1994). Experimental behaviour of polymeric geogrids in pullout. *Journal of Geotechnical Engineering*, ASCE, Vol. 120, No. 4, pp. 661–677.

Winkler, E. (1867). *Die Lehre von der Elastizität and Festigkeit (On Elasticity and Flexibility)* Prague, Czechoslovakia.

Wood, D. M. (1990). *Soil Behaviour and Critical State Soil Mechanics*, Cambridge University Press.

Woodward, R. J., Lundgren, R. & Boitano, J. D.. (1961). Pile loading tests in stiff clays. *Proceedings of the 5th International Conference on Soil Mechanics and Foundation Engineering*, Vol. 2, pp. 177–184.

Yan, L. & Byrne, P. M. (1992). Lateral pile response to monotonic pile head loading. *Canadian Geotechnical Journal*, Vol. 29, No. 6, pp. 955–970.

Yeh, Y. H. (1988). Landslide effects to buried pipelines. *Proc. of the 6th International Conference on Numerical Method in Geomechanics*, Innsbruck, ed. Swobda, G., Vol. 2, pp. 901–905.

Yin, J. H., Paulin, M. J., Clark, J. I. & Poorooshasb, F. (1993). Preliminary finite element analysis of lateral pipeline/soil interaction and comparison to centrifuge model test results. *12th Offshore Mechanics and Arctic Engineering Conference (OMAE)*, 20–24 June, Glasgow, Scotland, UK.

Young, W. C. (1989). *Roark's formulas for Stress and Strain*, 6th edition, McGraw-Hill.

Zaman, M. M. (1985). Evaluation of "Thin-layer element" and modelling of interface behaviour in soil-structure interaction. *5th International Conference on Numerical Methods in Geomechanics*, Nagoya, Vol. 4, pp. 1797–1803.

Zienkiewicz, O. C., Best, B., Dullage, C. & Stagg, K. C. (1970). Analysis of non-linear problems in rock mechanics with particular reference to jointed rock systems. *Proc. 2nd Int. Conf. Society of Rock Mech.*, Belgrade, pp. 8–14.

Zienkiewicz, O. C. & Taylor, R. L. (1989). *The Finite Element Method*, Vol. 1, 4th edition, McGraw-Hill.

APPENDIX A

DERIVATION OF THE MATERIAL PARAMETERS FOR INTERFACE ELEMENT

The stress-strain behaviour of an ideal isotropic elastic material is given by the generalized form of Hooke's Law:

$$\left.\begin{aligned}
\delta\varepsilon_1 &= \frac{1}{E}(\delta\sigma_1 - \nu\delta\sigma_2 - \nu\delta\sigma_3)\\
\delta\varepsilon_2 &= \frac{1}{E}(\delta\sigma_2 - \nu\delta\sigma_3 - \nu\delta\sigma_1)\\
\delta\varepsilon_3 &= \frac{1}{E}(\delta\sigma_3 - \nu\delta\sigma_1 - \nu\delta\sigma_2)\\
\delta\gamma_{12} &= \frac{2}{E}(1+\nu)\delta\tau_{12}\\
\delta\gamma_{23} &= \frac{2}{E}(1+\nu)\delta\tau_{23}\\
\delta\gamma_{31} &= \frac{2}{E}(1+\nu)\delta\tau_{31}
\end{aligned}\right\} \quad \text{(A1)}$$

For plane strain conditions where $\varepsilon_2 = 0$, Eq. (A1) can be rewritten as:

$$\delta\varepsilon_1 = \frac{1}{E}\left[\delta\sigma_1(1-\nu^2) - \delta\sigma_3(\nu+\nu^2)\right] \quad \text{(A2)}$$

$$\delta\sigma_2 = \nu(\delta\sigma_1 + \delta\sigma_3) \quad \text{(A3)}$$

$$\delta\varepsilon_3 = \frac{1}{E}\left[\delta\sigma_3(1-\nu^2) - \delta\sigma_1(\nu+\nu^2)\right] \quad \text{(A4)}$$

For interface element, strain is only 1-D in the normal direction, $\therefore \varepsilon_3 = 0$; from Eq. (A1):

$$\delta\sigma_3 = \nu(\delta\sigma_1 + \delta\sigma_2) \quad \text{(A5)}$$

From Eqs (A3) and (A5), $\delta\sigma_2 = \delta\sigma_3$. Substitute $\delta\sigma_2$ for $\delta\sigma_3$, Eq. (A3) become:

$$\delta\sigma_3 = \frac{\nu\delta\sigma_1}{(1+\nu)} \quad \text{(A6)}$$

Substitute Eq. (A6) into Eq. (A2):

$$\delta\varepsilon_1 = \frac{(1+\nu)(1-2\nu)}{E(1-\nu)}\delta\sigma_1 \tag{A7}$$

By definition, the normal modulus $K_n = \frac{\delta\sigma_1}{\delta\varepsilon_1}$, $\therefore$ Eq. (A7) can be rewrite as:

$$\underline{\underline{K_n = \frac{E(1-\nu)}{(1+\nu)(1-2\nu)}}} \tag{A8}$$

Also from Eq. (A1):

$$\delta\gamma_{12} = \frac{2}{E}(1+\nu)\delta\tau_{12} \tag{A9}$$

By definition, shear modulus $K_s = \frac{\delta\tau_{12}}{\delta\gamma_{12}}$, $\therefore$ Eq. (A9) can be rewritten as:

$$\underline{\underline{K_s = \frac{E}{2(1+\nu)}}} \tag{A10}$$

From Eq. (A10):

$$E = 2K_s(1+\nu) \tag{A11}$$

Substitute Eq. (A11) into Eq. (A8):

$$K_n = \frac{2K_s(1+\nu)(1-\nu)}{(1+\nu)(1-2\nu)} \tag{A12}$$

Rearrange Eq. (A12) and collect all ν terms into left hand side:

$$\underline{\underline{\nu = \frac{K_n - 2K_s}{2(K_n - K_s)}}} \tag{A13}$$

Substitute back Eq. (A13) into Eq. (A11):

$$E = 2K_s + \frac{2K_s(K_n - 2K_s)}{2(K_n - K_s)} \tag{A14}$$

Rearrange Eq. (A14) and collect all E terms into left hand side:

$$\underline{\underline{E = \frac{(3K_n - 4K_s)K_s}{(K_n - K_s)}}} \tag{A15}$$

APPENDIX B

DERIVATION OF THE FINITE DIFFERENCE APPROXIMATION FOR ELASTIC BENDING OF A STRAIGHT BEAM INCLUDING SHEAR DEFORMATION (COUPLED SOLUTION)

Timoshenko (1955) presented an equation for bending of a straight beam including shear deformation:

$$\frac{d^2y}{dx^2} = -\frac{1}{E_pI_p}\left(M + \frac{E_pI_p}{G_pA_s}p\right) \tag{B1}$$

Rewriting Eq. (B1) in terms of pipe displacement u_p gives:

$$\frac{d^4u_p}{dx^4} + \frac{d^2p}{dx^2} \times \frac{1}{G_pA_s} = \frac{p}{E_pI_p} \tag{B2}$$

Finite difference approximation of the differential quantities in Eq. (B2) for a typical element i (Fig. 2.24):

$$\frac{d^4u_p(i)}{dx^4} = \frac{u_p(i-2) - 4u_p(i-1) + 6u_p(i) - 4u_p(i+1) + u_p(i+2)}{l^4} \tag{B3}$$

$$\frac{d^2p(i)}{dx^2} = \frac{p(i-1) - 2p(i) + p(i+1)}{l^2} \tag{B4}$$

For the case of the loading intensity p produced by soil displacement u_s:

$$p = k_hD(u_s - u_p) \tag{B5}$$

Substitute Eq. (B5) into (B4):

$$\frac{d^2p(i)}{dx^2} = \frac{k_hD(u_s-u_p)(i-1) - 2k_hD(u_s-u_p)(i) + k_hD(u_s-u_p)(i+1)}{l^2} \tag{B6}$$

Substitute Eqs (B3), (B5) and (B6) into Eq. (B2):

$$E_pI_p\left[\frac{u_p(i-2)-4u_p(i-1)+6u_p(i)-4u_p(i+1)+u_p(i+2)}{l^4}\right]+$$
$$k_hD\frac{E_pI_p}{G_pA_s}\left[\frac{u_s(i-1)-2u_s(i)+u_s(i+1)}{l^2}\right]-$$
$$k_hD\frac{E_pI_p}{G_pA_s}\left[\frac{u_p(i-1)-2u_p(i)+u_p(i+1)}{l^2}\right] = k_hD(u_s-u_p) \tag{B7}$$

Equation (B7) is for a typical element in the pipeline, and it can be applied to every elements in the pipe. Expressing Eq. (B7) in a matrix form for the complete pipeline:

$$\frac{E_pI_p}{l^4}\begin{bmatrix} & & & & & \text{zero} \\ & & & & & \\ & 1 & -4 & 6 & -4 & 1 \\ & & & & & \\ \text{zero} & & & & & \end{bmatrix}\begin{bmatrix} 1 \\ \vdots \\ \vdots \\ u_p(i-1) \\ u_p(i) \\ u_p(i+1) \\ \vdots \\ \vdots \\ n \end{bmatrix} + \frac{E_pI_p}{G_pA_sl^2}\begin{bmatrix} & & & & & \text{zero} \\ & & & & & \\ & 1 & -2 & 1 & & \\ & & & & & \\ \text{zero} & & & & & \end{bmatrix}\begin{bmatrix} 1 \\ \vdots \\ \vdots \\ k_h(i-1)Du_s(i-1) \\ k_h(i)Du_s(i) \\ k_h(i+1)Du_s(i+1) \\ \vdots \\ \vdots \\ n \end{bmatrix} -$$
$$\frac{E_pI_p}{G_pA_sl^2}\begin{bmatrix} & & & & & \text{zero} \\ & & & & & \\ & 1 & -2 & 1 & & \\ & & & & & \\ \text{zero} & & & & & \end{bmatrix}\begin{bmatrix} 1 \\ \vdots \\ \vdots \\ k_h(i-1)Du_p(i-1) \\ k_h(i)Du_p(i) \\ k_h(i+1)Du_p(i+1) \\ \vdots \\ \vdots \\ n \end{bmatrix} = \begin{bmatrix} 1 \\ \vdots \\ \vdots \\ k_h(i-1)Du_s(i-1) \\ k_h(i)Du_s(i) \\ k_h(i+1)Du_s(i+1) \\ \vdots \\ \vdots \\ n \end{bmatrix} - \begin{bmatrix} 1 \\ \vdots \\ \vdots \\ k_h(i-1)Du_p(i-1) \\ k_h(i)Du_p(i) \\ k_h(i+1)Du_p(i+1) \\ \vdots \\ \vdots \\ n \end{bmatrix}$$

(B8)

Rearrange Eq. (B8) to collect the unknown pipe displacement u_p on the right hand side of the equation:

$$\begin{bmatrix} 1 \\ \vdots \\ \vdots \\ k_h(i-1)Du_s(i-1) \\ k_h(i)Du_s(i) \\ k_h(i+1)Du_s(i+1) \\ \vdots \\ \vdots \\ n \end{bmatrix} - \frac{E_pI_p}{G_pA_sl^2} \begin{bmatrix} & & & & \text{zero} & & \\ & & 1 & -2 & 1 & & \\ \text{zero} & & & & & & \end{bmatrix} \begin{bmatrix} 1 \\ \vdots \\ \vdots \\ k_h(i-1)Du_s(i-1) \\ k_h(i)Du_s(i) \\ k_h(i+1)Du_s(i+1) \\ \vdots \\ \vdots \\ n \end{bmatrix} =$$

$$\begin{bmatrix} 1 \\ \vdots \\ \vdots \\ k_h(i-1)Du_p(i-1) \\ k_h(i)Du_p(i) \\ k_h(i+1)Du_p(i+1) \\ \vdots \\ \vdots \\ n \end{bmatrix} + \frac{E_pI_p}{l^4} \begin{bmatrix} & & & & & \text{zero} & & \\ & & 1 & -4 & 6 & -4 & 1 & \\ \text{zero} & & & & & & & \end{bmatrix} \begin{bmatrix} 1 \\ \vdots \\ \vdots \\ u_p(i-1) \\ u_p(i) \\ u_p(i+1) \\ \vdots \\ \vdots \\ n \end{bmatrix} -$$

$$\frac{E_pI_p}{G_pA_sl^2} \begin{bmatrix} & & & & \text{zero} & & \\ & & 1 & -2 & 1 & & \\ \text{zero} & & & & & & \end{bmatrix} \begin{bmatrix} 1 \\ \vdots \\ \vdots \\ k_h(i-1)Du_p(i-1) \\ k_h(i)Du_p(i) \\ k_h(i+1)Du_p(i+1) \\ \vdots \\ \vdots \\ n \end{bmatrix} \tag{B9}$$

The finite difference terms need to be modified for the first three and last three elements to suit the boundary conditions of the pipe ends.